

AD-A088 439

LOCKHEED-CALIFORNIA CO BURBANK RYE CANYON RESEARCH LAB

F/6 11/4

EFFECT OF LOAD HISTORY ON FATIGUE LIFE.(U)

JUN 80 J T RYDER

F33615-78-C-5090

UNCLASSIFIED

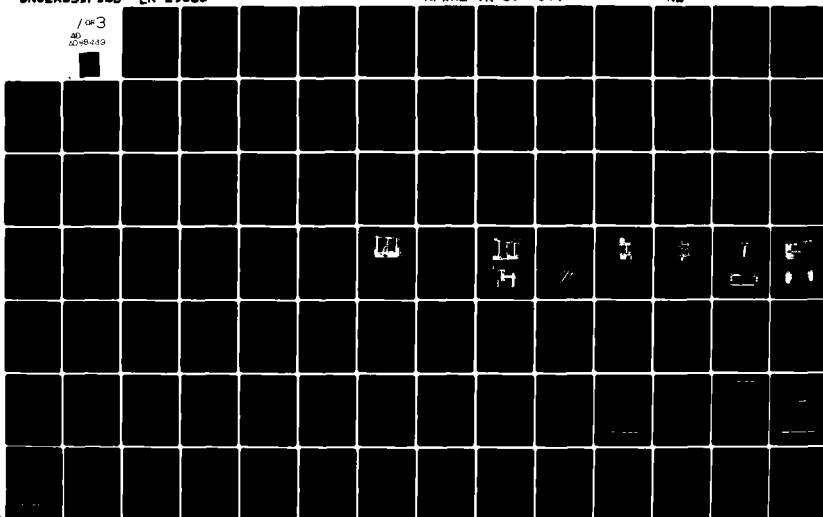
LR-29586

AFWAL-TR-80-4044

NL

/ OF 3

20-8449



AFWAL-TR-80-4044

LEVEL II

2

AD A088439

EFFECT OF LOAD HISTORY ON FATIGUE LIFE

J. T. RYDER

LOCKHEED-CALIFORNIA COMPANY
RYE CANYON RESEARCH LABORATORY
BURBANK, CALIFORNIA 91520

JUNE 1980

DTIC
SELECTED
AUG 18 1980

E

TECHNICAL REPORT AFML-TR-80-4044
Task I Final Report August 1978 — December 1979

Approved for public release; distribution unlimited.

AIR FORCE MATERIALS LABORATORY
AIR FORCE WRIGHT AERONAUTICAL LABORATORIES
AIR FORCE SYSTEMS COMMAND
WRIGHT-PATTERSON AIR FORCE BASE, OHIO 45433

11 JUL 1980 FILE

80 8 13 930

NOTICE

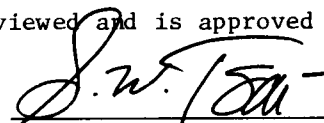
When Government drawings, specifications, or other data are used for any purpose other than in connection with a definitely related Government procurement operation, the United States Government thereby incurs no responsibility nor any obligation whatsoever; and the fact that the government may have formulated, furnished, or in any way supplied the said drawings, specifications, or other data, is not to be regarded by implication or otherwise as in any manner licensing the holder or any other person or corporations, or conveying any rights or permission to manufacture, use, or sell any patented invention that may in any way be related thereto.

This report has been reviewed by the Office of Public Affairs (PA) and is releasable to the National Technical Information Service (NTIS). At NTIS, it will be available to the general public, including foreign nations.

This technical report has been reviewed and is approved for publication.

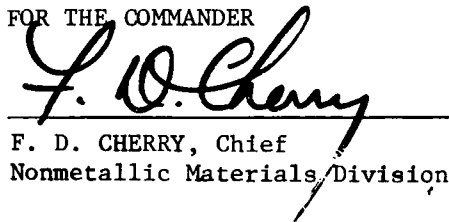


J.M. WHITNEY, Project Engineer
Mechanics & Surface Interactions Br.
Nonmetallic Materials Division



S.W. TSAI, Chief
Mechanics & Surface Interactions Br.
Nonmetallic Materials Division

FOR THE COMMANDER



F. D. CHERRY, Chief
Nonmetallic Materials Division

"If your address has changed, if you wish to be removed from our mailing list, or if the addressee is no longer employed by your organization, please notify AFWAL/MLBM, W-PAFB, OH 45433 to help us maintain a current mailing list."

Copies of this report should not be returned unless return is required by security considerations, contractual obligations, or notice on a specific document.

SECURITY CLASSIFICATION OF THIS PAGE (When Data Entered)

REPORT DOCUMENTATION PAGE		READ INSTRUCTIONS BEFORE COMPLETING FORM	
1. REPORT NUMBER AFWL-TR-80-4044 ✓	2. GOVT ACCESSION NO. AD-A088	3. RECIPIENT'S CATALOG NUMBER 439	
4. TITLE (and Subtitle) Effect of Load History on Fatigue Life	5. TYPE OF REPORT & PERIOD COVERED Final-Technical Task I- 30 August 1978-31 Dec. 1979	6. PERFORMING ORG. REPORT NUMBER LR 29166729586 ✓	
7. AUTHOR(s) J.T./Ryder	8. CONTRACT OR GRANT NUMBER(s) F33615-78-C-5090		
9. PERFORMING ORGANIZATION NAME AND ADDRESS Lockheed-California Company Division of Lockheed Corporation Burbank, California 91520	10. PROGRAM ELEMENT, PROJECT, TASK AREA & WORK UNIT NUMBERS 24190309		
11. CONTROLLING OFFICE NAME AND ADDRESS Materials Laboratory (MLBM) Air Force Wright Aeronautics Laboratory, Air Force Systems Command, Wright-Patterson AFB, OH 45433	12. REPORT DATE June 1980	13. NUMBER OF PAGES 260	
14. MONITORING AGENCY NAME & ADDRESS (if different from Controlling Office)	15. SECURITY CLASS. (of this report) Unclassified	15a. DECLASSIFICATION/DOWNGRADING SCHEDULE	
16. DISTRIBUTION STATEMENT (of this Report) Approved for public release; distribution unlimited			
17. DISTRIBUTION STATEMENT (of the abstract entered in Block 20, if different from Report)			
18. SUPPLEMENTARY NOTES			
19. KEY WORDS (Continue on reverse side if necessary and identify by block number) Composites, Graphite/Epoxy, Fatigue, NDI			
20. ABSTRACT (Continue on reverse side if necessary and identify by block number) The primary objectives of this program are to: 1) study in detail how mechanical loading parameters affect the fatigue life of graphite/epoxy laminates; 2) determine the effects of environmental and geometrical perturbations on the effects studied in objective 1; 3) analyze the results in a manner such that an expanded foundation is laid for formulating fatigue life			

DD FORM 1 JAN 73 1473 EDITION OF 1 NOV 65 IS OBSOLETE

SECURITY CLASSIFICATION OF THIS PAGE (When Data Entered)

420347

models based on knowledge of failure mechanisms. The research investigation is divided into four tasks: Task I, Diagnostic Experimentation; Task II, Effects of Loading Parameters; Task III, Effects of Environment and Geometry; Task IV, Data Analysis and Reporting. Tasks I, II and III are conducted sequentially while Task IV is conducted simultaneously with all three tasks. This report describes the analytical and experimental work undertaken in Task I.

In Task I, the laminate of interest was selected as a quasi-isotropic layup of T300/5208 graphite/epoxy material. The unidirectional properties of the material were characterized at room temperature, at 82.2°C (180°F), and at 82.2°C (180°F) in a high moisture content condition. Moisture and thermal properties were obtained. Static tension and compression properties of the quasi-isotropic laminate as well as those for unidirectional laminates were determined. The effect of strain rate was investigated. Baseline fatigue data were obtained at four stress ratios: +0.5, 0.0, -0.5, -0.0. An evaluation of NDI techniques was conducted to select procedures for use in Tasks II and III. A conceptual context for evaluating and analyzing the results of Tasks II and III was established.

NTIS GRA&I		<input checked="checked" type="checkbox"/>
DDC TAB		<input type="checkbox"/>
Unannounced		<input type="checkbox"/>
Justification		
By		
Distribution/		
Availability Codes		
Dist	Avail and/or special	
A		

FOREWORD

This report describes the results of the first part of an investigation of the effects of load history on the fatigue response of a graphite/epoxy laminate. Included are the results of Task I: Diagnostic experimentation which included baseline material, static, and fatigue properties and comparison and subsequent selection of NDI procedures. The research investigation was conducted by the Lockheed-California Company under Air Force Contract No. F33615-78-C-5090, Project/Task Number 24190309. The Air Force Project Engineer was Dr. S.W. Tsai and, subsequently, Dr. J. M. Whitney, both of the Mechanics and Surface Interactions Branch, Nonmetallic Materials Division, Air Force Wright Aeronautical Laboratory Materials Laboratory, Wright-Patterson Air Force Base, Ohio. Dr. J.T. Ryder was the Principal Investigator.

The program was conducted through the Structures and Materials Laboratory Department of the Lockheed-California Company. The support and contributions of W. E. Krupp and Y. A. Tajima, of the Materials Laboratory and of D.E. Pettit, F.M. Pickel, and J.P. Sandifer of the Fatigue and Fracture Mechanics Laboratory, and J. R. Crocker, Jr., of the Nondestructive Test and Research Inspection Department are gratefully acknowledged. To D.R. Diggs, also of the Fatigue and Fracture Mechanics Laboratory, goes my gratitude for his careful experimentation. In addition, the work of A. Denny, of the same laboratory, in the area of NDI is most appreciated for forcing the author to clarify ideas. Lastly, but actually foremost, I acknowledge and thank K.N. Lauraitis for her conceptual contributions formulated between us during many discussions throughout the program.

Section

FOREWORD

1 INTRODUCTION

- 1.1 Development of Program
- 1.2 Analytical Approach
- 1.3 Summary of Design Features

2 EXPERIMENTAL PROGRAM

- 2.1 Material and Laminate Selection
- 2.3 Fabrication and Quality Assurance
- 2.3 Experimental Program
- 2.4 Experimental Procedures
 - 2.4.1 Static tension and compression experiments and procedures
 - 2.4.2 Fatigue test procedures
- 2.5 Data Analysis
 - 2.5.1 General discussion of weibull function
 - 2.5.2 Weibull analysis procedures
 - 2.5.3 Description of selected analysis procedure
 - 2.5.4 Alternative procedures

3 MATERIAL CHARACTERIZATION

- 3.1 Prepreg Properties
- 3.2 Panel Properties
- 3.3 Environmental Conditioning
- 3.4 Moisture and Thermal Diffusivity and Thermal Expansion Properties
 - 3.4.1 Moisture diffusivity
 - 3.4.2 Thermal properties

TABLE OF CONTENTS (Continued)

Section	Page
4	109
STATIC TENSION AND COMPRESSION RESULTS	
4.1	109
Lamina Properties	
4.2	115
Laminate Properties	
4.2.1	115
Static tension	
4.2.2	122
Static compression	
5	125
FATIGUE RESULTS	
5.1	127
Fatigue Test Results	
5.2	138
Residual Strength Results	
6	141
EVALUATION AND SELECTION OF NDI METHODS FOR DAMAGE MONITORING	
6.1	142
Selection of Techniques	
6.2	148
NDI: Experimental Procedures	
6.3	154
NDI Experimental Test Matrix	
6.4	156
NDI Experimental Results	
6.4.1	156
DIB enhanced x-ray radiography	
6.4.2	166
Ultrasonic inspection	
6.4.3	166
Acoustic emission	
6.4.4	176
Edge replication	
6.4.5	177
Stiffness monitoring	
6.4.6	179
Temperature monitoring	
6.5	181
Selection of NDI Techniques for Tasks II and III	
7	183
SUMMARY AND CONCLUSIONS	
REFERENCES	189
APPENDIX A — T300/5208 GRAPHITE/EPOXY LAMINATE AND TEST SPECIMEN FABRICATION QUALITY CONTROL PLAN	199
APPENDIX B — SUMMARY OF STATIC TEST RESULTS	219
APPENDIX C — SUMMARY OF FATIGUE TEST RESULTS	243

LIST OF FIGURES

Figure		Page
1	Unnotched composite test specimen	23
2	Notched composite specimen	24
3	Location of thickness and width measurements	26
4	Overall view of composite compression test apparatus, with acrylic enclosure and warm air supply	31
5	Installation of modified hydraulic grips in universal testing machine	33
6	Specimen positioning device	33
7	"Full-fixity" apparatus, showing auxilliary platens	34
8	Specimen and restraint fixture installed in grips	35
9	Installation of Lockheed extensometer	36
10	Fatigue grip	37
11	Tension-tension fatigue test showing failed quasi-isotropic laminate coupon.	37
12	Compression fatigue restraint fixture.	38
13	Influence of shape parameter k on probability of survival	42
14	Locations of three specimens from each panel used for specific gravity and acid digestion tests	60
15	Longitudinal cross section of (0) ₁₆ unidirectional panel, 2VX1394 (100x)	62
16	Transverse cross section of (0) ₁₆ unidirectional panel, 2VX1394 (100X)	63
17	Longitudinal cross section of (±45) _{4S} panel, 1VX1386 (100X)	64
18	Transverse cross section of (±45) _{4S} panel, 1VX1386 (100X)	65
19	Longitudinal cross section of (0/45/90-45 ₂ /90/45/0) _S panel, 1VX1392 (100X)	66
20	Transverse cross section of (0/45/90-45 ₂ /90/45/0) _S panel, 1VX1392 (100X)	67

LIST OF FIGURES (Continued)

Figure		Page
11	Initial moisture distribution in 0° unidirectional lamina coupons	69
12	Initial moisture distribution in 90° unidirectional lamina coupons	70
23	Initial moisture distribution in $\pm 45^{\circ}$ lamina coupons	71
24	Initial moisture distribution in quasi-isotropic laminate coupon	72
25	Moisture weight gain in representative lamina coupons	73
26	Final moisture distribution in 0° lamina coupon	75
27	Final moisture distribution in 90° lamina coupon	75
28	Final moisture distribution in $\pm 45^{\circ}$ lamina coupon	76
29	Preconditioning of 16-ply unidirectional laminate (1SV1136) for sorption and desorption studies	80
30	Moisture distributions in unidirectional test coupons following sorption at 66°C (150°F)/98% RH	82
31	Saturated concentrations, C_s , calculated from moisture distributions in sorption experiments.	84
32	Sorption-desorption kinetic curves at 66°C (150°F) of unidirectional laminate	85
33	Arrhenius relationships of D and $1/T$ for sorption in 98% RH at 49, 66, 82, and 93°C (120, 150, 180, and 200°F)	87
34	Moisture distributions in unidirectional test coupons after desorption in vacuo over Drierite at 66°C (150°F). Test coupons first saturated by immersion at 66°C (150°F)	90
35	Function $D(C)$ for unidirectional laminate calculated from the moisture distributions shown in Figure 11 (desorption at 66°C (150°F))	91
36	Moisture distributions in desorption of coupons first saturated by immersion at 93°C (200°F).	93
37	Sorption-desorption Kinetic curves at 66°C (150°F) (See Figure 32)	95

LIST OF Figures (Continued)

Figure		Page
38	Moisture distributions in unidirectional coupons during second sorption of Figure 37	96
39	Thermal expansion results for 0° unidirectional coupon 1VX1453-C9	99
40	Thermal expansion results for 90° unidirectional coupon 2XV1453-A11	100
41	Diagram of thermal conductivity experiment	102
42	Thermal conductivity on 0° directions of unidirectional panel	103
43	Thermal diffusivity in thickness direction unidirectional panel	104
44	Thermal conductivity in thickness direction of unidirectional panel	105
45	Specific heat of unidirectional panel, 1VX1453	107
46	Representative 0° unidirectional coupons which failed in static tension at room temperature in laboratory air	112
47	Representative 0° unidirectional coupons which failed in static compression at room temperature in laboratory air	113
48	Representation 90° unidirectional coupons which failed in static tension at room temperature in laboratory air	113
49	Representative 90° unidirectional coupons which failed in static compression at room temperature in laboratory air	114
50	Representative ±45 coupons which failed in static tension at room temperature in laboratory air	114
51	Representative quasi-isotropic laminate coupons which failed in static tension at low strain rate in room temperature, laboratory air	116
52	Compression, shock wave, rebound failure of tensile, quasi-isotropic coupon 2VX1391-B13 tested in room temperature, laboratory air	120
53	Photograph of coupon 2VX1390-C5 with representative squiggles and subsequently sectioned top layers of specimen showing non-overlap of squiggles	121

LIST OF FIGURES (Continued)

Figure		Page
54	Representative quasi-isotropic laminate coupons which failed in static compression at low strain rate in room temperature, laboratory air	123
55	Schematic diagram of tension - compression fatigue restraint system	128
56	Quasi-isotropic, fatigue stress-life scan results at $R = +0.5$ (room temperature, laboratory air)	129
57	Quasi-isotropic, fatigue stress-life scan results at $R = 0.0$ (room temperature, laboratory air)	130
58	Quasi-isotropic, fatigue stress-life scan results at $R = -0.5$ (room temperature, laboratory air)	131
59	Quasi-isotropic, fatigue stress-life scan results at $R = 1.0$ (room temperature, laboratory air)	132
60	Delamination of "squiggle" defect during initial fatigue cycling	133
61	Face and edge views of coupons fatigue tested at $R = +0.5$ (top, 2VX1391-B26, 414 MPa (60 ksi), $N_F = 267,700$; bottom, 2VX1391-B1, 379 MPa (55 ksi), N_F at (2×10^6))	134
62	Face and edge views of coupons fatigue tested at $R = 0.0$ (Top, 1VX1396-AS, 379 MPa (55 ksi), $N_F = 18740$; bottom 2VX1391-D20 310 MPa (45 ksi), $N_F = 476,020$)	135
63	Face and edge views of coupons fatigue tested at $R = -0.5$ (top, 1VX1392-B12, 379 MPa (55 ksi), $N_F = 13937$; bottom 1VX1392-B5, 414 MPa (60 ksi), $N_F = 26,350$)	136
64	Face and edge views of coupons fatigue tested at $R = -1.0$ (top, 2VX1391-B14, 276 MPa (40 ksi) $N_F = 18400$; bottom 2VX1391-A26, 207 MPa (30 ksi), $N_F = 802,709$)	137
65	Comparison of tension-tension fatigue data of laminated composites of T300/5208 and T300/934 in room temperature, laboratory at $R = 0.0$	139
66	Schematic of acoustic emission event	151
67	Schematic diagram of acoustic emission system	152
68	Cross section in the 0° direction of a coupon loaded statically to 60% of the Average Ultimate Tensile Strength	158
69	Enhanced x-ray photographs of coupons fatigue cycled at 310 MPa (45 ksi), $R = 0.0$, showing 90° and -45° ply matrix cracking	159

LIST OF FIGURES (Continued)

Figure		Page
70	Enhanced x-ray photographs of coupons fatigue cycled at 310 MPa (45 ksi), R = 0.0, showing +45° cracking and delamination and 0° longitudinal cracking	160
71	Enhanced x-ray photographs of coupons fatigue cycled at 379 MPa (55 ksi), R = 0.0 showing 90° and -45° ply matrix cracking	162
72	Enhanced x-ray photographs of coupons fatigue cycled at 379 MPa (55 ksi), R = 0.0, showing +45° ply cracks, delamination initiation and growth, and 0° ply cracks	163
73	Differential amplitude distribution, 0-40,000 cycles	169
74	Differential amplitude distribution, 40,000-63,000 cycles	169
75	Differential amplitude distribution, 117,000-125,000 cycles	170
76	Differential amplitude distribution, 82,000-92,000 cycles	170
77	Count rate vs load, static tension test	171
78	Amplitude distribution diagram for static tension test to failure	172
79	Amplitude distribution diagram for static tension test, 0 to 60% average ultimate stress	172
80	Acoustic emission event	173
81	Amplitude distribution diagram for static tension test to failure conducted at 6 mm/mm/min	175
82	Plastic-cast replications of quasi-isotropic laminate coupon loaded in static tension to approximately 60% of the average ultimate strength	176
83	Matrix cracking revealed on a coupon edge by using chalk and standard photography. Coupon loaded in static tension to approximately 85% of average ultimate strength	178
84	Layup of laminate U1 16 Ply (0°) ₁₆	205
85	Layup of laminate U2 16 Ply (±45°) ₄₅	207
86	Layup of laminate L1 16 Ply (0/45/90/-45 ₂ /90/45/0) _S	208
87	Sample autoclave record	209
88	Un-notched composite test specimen	210
89	Notched composite test specimen	212

LIST OF TABLES

Table		Page
1	Interlaminar Normal Stresses at Free Edges of Test Coupon	19
2	Quality Assurance Testing Outline	20
3	Task I Experimental Test Matrix	28
4	Properties of T300 Fibers Used in Various Lockheed Programs	54
5	Summary of Lockheed Quality Control Tests For NARMCO RIGIDITE 5208-T300 Material Batch #1283	55
6	Summary of NARMCO Quality Control Tests for RIGIDITE 5208/T300, NARMCO Certified Test Report No. 35990	57
7	Identification Numbers of Panels Used In Experimental Program	58
8	Resin, Fiber, and Void Analysis Results	59
9	Comparison Between Initial Moisture Content Obtained From Distribution Analysis and by Drying	72
10	Moisture Gain in Traveler Coupons Conditioned at 82.2°C (180°F), 90% R.H. in Laboratory Air	74
11	Initial and Final Moisture Contents of Lamina and Laminate Coupons Determined by Drying of Coupons	76
12	Percent Weight Loss of Lamina Coupons During Static Tests at 82.2°C (180°F): Test Time Approximately 5 Minutes	78
13	Estimated Percent Moisture Content Within Coupons Tested in Task I	78
14	Test Schedule - Unidirectional Laminate (1SV1136)	81
15	Diffusion Coefficient, D, and Saturated Concentration, C_s : Unidirectional Panel 1SV1136	86
16	Activation Energies for Various Composites	88
17	Saturated Concentration, C_s , of Moisture in T300/5208 unidirectional laminate	89
18	Comparison of 0° Unidirectional Lamina Static Test Results	110

LIST OF TABLES (Continued)

Table		Page
19	Summary of Weibull Parameters for 0° Unidirectional Lamina Static Test Data	110
20	Comparison of 90° Unidirectional Lamina Static Test Results	111
21	Summary of Weibull Parameters for 90° Unidirectional Lamina Static Test Data	111
22	Comparison of ±45° Unidirectional Lamina Static Tension Test Results	112
23	Summary of Quasi-Isotropic Static Tension Test Results at Room Temperature	117
24	Summary of Weibull Parameters for Quasi-Isotropic Static Tension Results at Room Temperature	117
25	Effect of "Squiggle" Defect on Static Tensile Strength	123
26	Summary of Quasi-Isotropic Static Compression Test Results at Room Temperature	124
27	Summary of Weibull Parameters for Quasi-Isotropic Static Compression Results at Room Temperature	124
28	Tension Residual Strength Tests of Unfailed Fatigue Coupons	140
29	Compression Residual Strength Test Results of Un-failed Fatigue Coupons	140
30	NDI Test Matrix for Static Tension Tests Strain Rate = 0.01 mm/mm/min	155
31	NDI Test Matrix for Tension-Tension Fatigue Tests $\sigma_{max} = 310$ MPa (45 ksi), R = 0.0	155
32	NDI Test Matrix for Tension-Tension Fatigue Tests $\sigma_{max} = 55$ MPa (55 ksi), R = 0.0	156
33	Effect of Fatigue Life on Tensile Stiffness at 310 MPa (45 ksi) at R = 0.0	180
34	Thermal Temperature Data for Coupons Fatigue Cycled at 310 MPa (45 ksi) at R = 0.0	181
35	Damage Detection Capabilities of Evaluated NDI Techniques	182
36	Summary of NDI Technique Evaluation Process	182
37	Material Control	203
38	Cure Cycle	206
39	Test Requirements	207

LIST OF TABLES (Continued)

Table		Page
40	Tension Test Results of Lamina U1, 0° Unidirectional Coupons at Room Temperature in Laboratory Air	220
41	Tension Test Results of Lamina U1, 0° Unidirectional Coupons at 82.2°C (180°F), Dry, in Laboratory Air	221
42	Tension Test Results of Lamina U1-1, 0° Unidirectional Coupons at 82.2°C (180°F), Wet, in Laboratory Air	222
43	Compression Test Results of Lamina U1, 0° Unidirectional Coupons at Room Temperature in Laboratory Air	223
44	Compression Test Results of Lamina U1, 0° Unidirectional Coupons at 82.2°C (180°F), Dry, in Laboratory Air	224
45	Compression Test Results of Lamina U1, 0° Unidirectional Coupons at 82.2°C (180°F), Wet, in Laboratory Air	225
46	Tension Test Results of Lamina U1, 90° Unidirectional Coupons at Room Temperature in Laboratory Air	226
47	Tension Test Results of Lamina U1, 90° Unidirectional Coupons at 82.2°C (180°F), Dry, in Laboratory Air	227
48	Tension Test Results of Lamina U1, 90° Unidirectional Coupons at 82.2°C (180°F), Wet, in Laboratory Air	228
49	Compression Test Results of Lamina U1, 90° Unidirectional Coupons at Room Temperature in Laboratory Air	229
50	Compression Test Results of Lamina U1, 90° Unidirectional Coupons at 82.2°C (180°C), Dry, in Laboratory Air	230
51	Compression Test Results of Lamina U1, 90° Unidirectional Coupons at 82.2°C (180°F), Wet, at Room Temperature	231
52	Tension Test Results of Lamina U2, ±45° Lamina Coupons at Room Temperature in Laboratory Air	232
53	Tension Test Results of Lamina U2, ±45° Lamina Coupons at 82.2°C (180°F), Dry, in Laboratory Air	233
54	Tension Test Results of Lamina U2, ±45° Lamina Coupons at 82.2°C (180°F), Wet, in Laboratory Air	234
55	Results of Tension Tests of Quasi-Isotropic Laminate Conducted at ~0.01 in./in./min Environment: Room Temperature Laboratory Air	235
56	Results of Static Tension Tests of Quasi-Isotropic Laminate Conducted at ~6 in./in./min Loading Rate Environment: Room Temperature, Laboratory Air	236

LIST OF TABLES (Continued)

Table		Page
57	Results of Tension Tests of Quasi-Isotropic Laminate Panel Containing Minimal Amount of "Squiggle" Defects, Conducted at ~0.01 in./in./min Loading Rate Environment Room Temperature, Laboratory Air	237
58	Results of Tension Tests of Quasi-Isotropic Laminate Panel Containing Major Amount of "Squiggle" Defects, Conducted at ~0.01 in./in./min Loading Rate Environment, Room Temperature, Laboratory Air	238
59	Results of Static Tension Tests of Quasi-Isotropic Laminate Panel Containing "Squiggle" Defect, Conducted at ~6 in./in./min Loading Rate	239
60	Results of Compression Tests of Quasi-Isotropic Laminate Conducted at ~0.01 in./in./min Loading Rate Environment: Room Temperature Laboratory Air	240
61	Results of Tension Tests of Quasi-Isotropic Laminate Conducted at ~6 in./in./min Loading Rate Environment: Room Temperature, Laboratory Air	241
62	Stress-Life Scan Results of Fatigue Tests at $S = +0.5$ for Un-Notched Quasi-Isotropic Laminate Environment: Room Temperature, Laboratory Air	244
63	Stress-Life Scan Results of Fatigue Tests at $R = 0.0$ for Un-Notched Quasi-Isotropic Laminate Environment: Room Temperature, Laboratory Air $f = 10$ Hz	245
64	Stress-Life Scan Results of Fatigue Tests at $R = -0.5$ for Un-Notched Quasi-Isotropic Laminate Environment: Room Temperature, Laboratory Air $f = 10$ Hz	247
65	Stress-Life Scan Results of Fatigue Tests at $R = -1.0$ for Un-Notched Quasi-Isotropic Laminate Environment: Room Temperature, Laboratory Air $f = 10$ Hz	248

SECTION 1

INTRODUCTION

During the past decade the increased use of composite materials in aircraft and their proposed use for primary structural applications has introduced a greater need for development of predictive capability for fatigue life and strength changes. To accomplish this goal, an understanding of the effects of various load histories on the fatigue life of composites is essential. The achievement of this understanding necessitates an awareness of damage mechanisms and a comprehension of their relationship in order that at least a qualitative prediction of load history effects can be formulated.

Fundamentally the cause of damage for both metals and composites is the same, namely: the extension or breakage of atomic bonds or both. The physical structure of most materials formed of metallic elements allows them to be considered homogeneous, continuous, and isotropic at small dimensions (generally at any dimension greater than 1 or 2 mm). Thus, the fundamental damage mechanism manifests principally as the processes termed slip, twinning, cleavage, and microcracking. These microscopic processes are the most important ones of concern for explaining most macroscopic effects. In many cases of interest, they result in macroscopic size flaws which dominate the microscopic damage.

The macroscopic expression of damage and failure mechanisms exhibited by laminated composite materials are not normally encountered in similar studies of metals except in the case of bonded bimetallics. Although laminated composites are made up of at least two material phases of quite different properties, this is not unique since the same fact is true for many metallic materials. Laminated composite materials differ from most other materials in the fact that their method of formation results in a state where conditions of homogeneity, continuity, and isotropy occur at macroscopic levels (at least

centimeters if not meters). In fact, for most practical applications of laminated composites, such a state is not actually ever reached in a direction perpendicular to the plies. Therefore, for qualitative understanding of laminated composites up to the onset of 0° fiber breakage, the underlying damage mechanism which needs to be considered is matrix cracking influenced by the anisotropic nature of the material (inter and intralamina cracking). The same type of consideration is involved in the attempt to understand anisotropic metals and, especially, bimetallics. Thus, in formulating life and strength prediction techniques, attention must center upon gaining an understanding of the cause of and driving mechanism behind crack initiation and extension. This understanding may need to be combined, for certain applications, with a detailed study of fiber breakage in 0° plies.

Associated with the difficulties in defining the nature of damage growth and the ascertainment of associated failure modes for laminated composites, are the added considerations of: 1) developing and selecting adequate inspection methods to detect and monitor damage; 2) developing analysis methods to define the severity of damage; 3) developing adequate terms and methods for classifying failure modes; 4) determining the state of the stress/strain/energy field within the material. This program necessarily addresses these problems in the course of determining some of the effects of load history on the fatigue life of a graphite/epoxy composite laminate.

The primary objectives of the program are to: 1) study in detail how mechanical loading parameters affect the life of graphite/epoxy laminates; 2) determine the effects of environmental and geometrical perturbations on the effects studied under objective 1; and 3) analyze the results in a manner which gives at least a qualitative understanding of the experimental results. The analysis must be conducted in a manner such that a foundation is laid for formulating fatigue life models based on knowledge of failure mechanisms. This report explains how the experimental program helps meet the need of understanding load history effects; gives a general description of the analytical approach which will be taken; gives a detailed overview of the experimental program; and gives the results of the experimental work conducted in Task I.

1.1 DEVELOPMENT OF APPROACH

To interpret the results of the experiments to be conducted, the relationship between program objectives and the selected experiments must be established. Based upon the concepts raised in the opening paragraphs of this introduction, a comprehensive, descriptive analysis of how crack formation and growth is influenced by load history is required. A mathematical formulation of the process will result in a quantitative description, the accuracy of which is dependent upon the previous analysis, and the practical difficulties of obtaining appropriate input data and the human labor required for achieving a desired level of accuracy.

For laminated composites, the damage mechanism of crack extension, whether inter or intralamina, is the dominant one of interest. Qualitative analysis of what influences crack formation, location, and growth will result in an understanding of macroscopic phenomena. Consider, as an example, the case of an unnotched multidirectional laminated composite subjected to steadily increasing tension load. The location of crack formation (intramatrix cracks, interlamina delamination) and their saturation numbers in transverse plies can be approximated by mathematical analysis.^{1,2} An energy approach prediction may be the most fruitful since stress has the same units as energy (stress times strain is energy per unit volume) and thus an energy concept will allow for volumetric effects. This approach has been pursued by Wang and Crossman.^{2,3} Crack formation and extension is caused by the increase in load (energy input). Final fracture is due to localized transfer of load into the 0° plies, localized fracture of 0° fibers which in turn influence the breakage of the 0° plies, and further transfiber crack extension followed by coupon fracture at a region where a critical number of such fiber breakages interact. For this static tension case, the mechanism which can be identified as the cause of crack extension is that due to increasing load (energy).

For the case of constant amplitude tension-tension fatigue, transverse cracks are formed on the first load cycle because of the increasing load, as in static tension. Each additional input of energy (cycle) extends the crack (damage), however minutely, due to the mechanisms which are classified, for ease of mathematical analysis, into the processes termed creep and fatigue

crack growth. The mechanism of creep can be idealistically considered to occur only at or near the maximum load and be described as crack extension under constant load due to a stable rate of breakage and partial reformation of atomic bonds. The mechanism of fatigue crack growth can be termed cyclic crack extension. Such extension is due to breakage and complete or partial reformation of atomic bonds during each energy (load) input cycle in such a manner that the original state is changed slightly on each cycle. Thus in the case of fatigue, the single mechanism of crack formation and growth can be divided, for analytical convenience, into the three manifesting mechanisms of initial loading, creep, and cyclic cracking. Final fracture occurs for similar reasons as in the static tension case, namely: transfer of load to 0° plies, fracture of 0° fibers at various locations, and final coupon fracture in a region where the 0° fiber breakages sufficiently interact. Similar to the static tension case, the location, type, and number of, at least, initial cracks, can be approximated by an appropriate laminate analysis.¹⁻³

The above general description leads to the conclusion that for the cases of static tension and tension-tension fatigue, three different ways of dividing the mechanism of damage, crack extension, can be conveniently identified: increasing load, creep, cyclic cracking. Further, one can conclude that the final damage state of the coupon at fracture can be, at least in theory, deterministically related to the initial state if the loading path is known. However, the final damage state prior to fracture can not automatically be assumed to be path dependent.

The question of path independence or dependence appears to be a key consideration. There is experimental and analytical evidence that some layups, loaded in an unnotched configuration, reach a "characteristic damage state" of transverse cracking and interrelated intralamina delamination.¹ Other layups do not appear to reach such a state prior to coupon fracture.³ The existence of a characteristic damage state for all possible layups is, therefore, not clear. Those layups where such a state does exist can be said to be path independent because both static tension or tension-tension fatigue loading lead to the same state. However, if fracture into two pieces is defined as failure, static tension and tension-tension fatigue loading may result in

path dependent failure states. The reason for this is that for some layups after a characteristic damage state has been reached, if one exists, delamination under fatigue loading prior to fracture can be significantly greater than that which occurs under static tension loading.⁴ The transfer of load into the 0° plys will be different for the two loading paths and thus the damage state is path dependent.

A descriptive analysis similar to that just given for tension loading could be done for static compression loading and for tension-compression or compression-compression fatigue. As before, incipient crack locations could be, at least theoretically, determined mathematically. In this case, the three different ways of dividing the mechanism of damage (increasing load, creep, cyclic cracking) are believed to still be convenient. The path dependent character of the final fracture event is also believed to exist. Therefore, an attitude as to the nature of damage initiation and growth for laminated composites may be formulated as follows:

- The dominant type of damage of analytical concern for descriptive and mathematical analysis is matrix cracking.
- Matrix cracking can be intralamina (transverse) or interlamina (delamination).
- The mechanism of crack extension (atomic debonding) can be conveniently classified (for mathematical formulation purposes) as being due to: load increase, creep, and cyclic cracking.
- The damage state at any time is deterministically related to the initial state.
- The definition of failure can influence whether the damage state at failure is or is not dependent on the loading path

This attitude can lead to several deductions, among which are:

- The laminate stacking sequence determines the inter and intralaminar normal and shear stresses which, in turn, determine: location and eventual density of intralamina cracks; location and propagation path of delaminations. These characteristics can be calculated, at least approximately, by known mathematical procedures.
- Final fracture must be ascertained by determining the manner in which load is transferred to the 0° plys. This requires analysis of the influence of local delamination on the fracture of 0° fibers and

analysis of the effect of such fiber fractures on 0° ply integrity and coupon failure behavior.

- Temperature, width, length, and notches affect both static strength and fatigue life because they alter either matrix properties or stress state or both.
- Stiffness changes with time during fatigue cycling.
- Fatigue life depends on the definition of failure. If failure is defined as an amount of stiffness change, fatigue life will be much different than if defined as the number of cycles to a characteristic damage state or as fracture of the specimen into two or more pieces.

The attitude outlined above allows the results of the planned experiments to be related to the program objectives. The formulated attitude is based upon a qualitative analysis of the nature of damage initiation and growth in laminated composites. The effect of a general loading history depends upon the three identified mechanisms of crack extension. Hence, the relative dominance of these mechanisms must be assessed to understand the effect of any general load history. The relative importance of the three mechanisms and how they influence the damage accumulation and failure process needs to be assessed. The experiments planned in Tasks II and III of this program will discriminate among these mechanisms. In Task II, five different load histories will be evaluated: progressive loading, time under load, block fatigue, pre-load, overload.

In Task II, coupons will be fatigue cycled at constant frequency and at an increasing amplitude on each cycle, called progressive loading, such that failure occurs in a specific preselected period of time. If the distribution of failure loads for progressive loading is the same as for the initial static strength, the mechanism of increasing load causing crack extension is dominant and that due to cyclic cracking less important. Thus, the progressive loading experiments will differentiate between these two mechanisms. Similarly, time under load fatigue experiments will be conducted using a trapezoidal wave shape and thus will differentiate between the mechanisms of creep and cyclic cracking. If the trapezoidal data are similar to the sine wave data on the basis of time under load, the mechanism of creep may be considered to be dominant. If the data are not similar, the conclusion can be made that crack

extension is highly dependent on the cyclic cracking mechanism. Fatigue loading consisting of a block at one stress level followed by a block at another level to failure can not clearly differentiate among the creep and cyclic cracking mechanisms. However, the dependence of damage extension at one stress level upon the previous damage state can be determined.

The remaining types of Task II experiments, preload and overload, will be of most value in developing correct analytical life prediction formulations. The relationship between the overload or preload induced damage and subsequent fatigue induced damage is related to the dominance of the creep or cyclic cracking mechanism.

1.2 ANALYTICAL APPROACH

In this program, a relationship will be sought between the experimental data and the theoretical conceptions. This relationship will hopefully help in formulating fatigue life prediction methodologies. The objective requires definition of an analytical procedure for dividing the problem into parts as an aid in conceptualization. The problem of formulating fatigue life prediction methodology involves the further problem of establishing the damage state of a coupon or structure at any time. The relationship between the damage state and time is usually termed the rate of residual strength degradation. The reason for relating residual strength degradation and fatigue life prediction is because of the manner in which fatigue loading is accounted for in many structural designs.

Typically, a structural member is required to withstand some particular high load, applied at any time during a complex fatigue history. Attention is therefore focused upon ensuring that the member has sufficient strength at any time to withstand the design limit load. Therefore, consideration is given to the state of residual strength of the part throughout the load history. To meet design requirements, analytical procedures are needed which not only predict fatigue life, but also describe expected changes in residual strength. Successful analytical procedures are also often required which allow for formulation of methods which guarantee some minimum fatigue life. Such a method would avoid or reduce damage inspection requirements. These inspection

requirements are related to the residual strength question since inspection for damage is undertaken to estimate the remaining load carrying capability of components. Summarizing, to meet the objectives of many structural fatigue design considerations, analytical procedures are expected, in the ideal, to meet three requirements: 1) predict fatigue life; 2) predict the state of residual strength; and 3) define procedures for ensuring a minimum fatigue life.

Two analytical approaches have developed to meet the above requirements. These approaches may be called statistical and mechanistic. In the statistical approach, macroscopic phenomenon such as global stress, number of cycles, time, or tensile strength at any point in time are tabulated. Relationships among the parameters are sought by considering them as statistical variables and formulating statistical probability equations which describe observed rates of change. Physical mechanisms are postulated to explain hypothesized relationships among the variables and their rate of change. The mechanistic approach considers possible physical mechanisms of damage, formulates mathematical descriptions and, in theory, derives the expected macroscopic relationships from the microscopic phenomena. The starting points of the two analytical approaches are thus quite different. One leads from the macroscopic to the microscopic on the basis that the mechanisms of damage may be too complex for direct formulation. The other leads from the microscopic to the macroscopic on the basis that a broad spectrum of unsuspected macroscopic relationship can be derived.

The statistical procedures commonly found in the literature⁵⁻⁸, all have common elements in that the same four basic assumptions are stated. First, the distribution of observed phenomena can be represented by an exponential equation (this is usually chosen as a two parameter Weibull equation). Second, change in strength can be represented by a power law. Third, fatigue life and global stress are related by a power law. Fourth, there is a one-to-one relationship between residual strength and fatigue life. Implicit in these assumptions is the unexpressed assumption that the stress required to fracture a coupon into two pieces is path independent. The various proposed power laws have different mathematical exponents depending on the interpretation of the

form of the variable relationship. Hahn⁹ has put this statistical procedure on a more rigorous basis. Yang and Jones⁸ have shown how the various statistical approaches are related. In other approaches¹⁰ damage growth concepts have been postulated, but in a manner general enough and with the same four assumptions that they reduce to a statistical approach.⁸ Statistical approaches for life prediction and strength degradation require experimental data to be obtained for each layup under each type of loading and environment. Their accuracy is dependent upon the correctness of the assumption that fracture strength is path independent. One of the problems of using only a statistical approach is that generalized formulations are difficult to devise. For instance, some layups increase in static tensile residual strength due to fatigue loading if they contain a notch.^{4,11}

Mechanistic approaches^{1,2,12} attempt to follow crack initiation through growth and up to fracture. Except for the case of a dominant flaw at the scale of the laminate, the mathematics to describe fracture quantitatively are as yet undeveloped due to the complex state of cracking. Certain procedures give qualitative and even quantitative predictions of early damage states under both static and fatigue loading.^{1,2} The simplest procedures appear to be energy approaches.² Because of the complexities of the mechanistic approach, crack growth laws are often formulated¹³ after determining the mechanism of importance in a particular loading environment. Such approaches are only successful if a quasi-dominant flaw can be considered as being the most important damage mechanism. For many layups and loading conditions, this concept is probably too restrictive.

The analytical approach of this program is based upon a conception as to the needs of the designer, inspector, and customer. The designer needs to be able to determine, at least approximately, what the static and fatigue characteristics of a selected layup will be before the structure is fabricated. This will allow selection of a layup by analysis and subsequent experimental verification of the particular layup selected. In the ideal, changes in static and fatigue characteristics as the layup is changed would be implicitly included in the iterative layup selection procedure. The customer would like some reasonable assurance of the material's ability to survive a specified use

for a predetermined period of time. The inspector requires knowledge of what amount and type of damage is of concern. The analytical approach of this program is based upon an awareness of these diverse requirements. The general approach is based upon a synthesis of the experience and insights of statistically and mechanistically based concepts. Several examples of this interactional synthesis can be given.

If the lamina properties of a selected material are known under various environmental conditions, present mechanistic mathematical approaches can determine the following characteristics: expected static tensile strength, interlamina stresses (σ_z and τ_{xz}), transverse cracking densities, predilection of the first cracks within a layup being intra or interlaminar, and the characteristic saturated state of transverse cracking. From this knowledge, an approximate S-N curve could possibly be estimated. For example, for unnotched coupons subjected to tension-tension fatigue loading, the life at the ultimate strength is counted as one cycle. Hypothetically the life for these coupons may be greater than 10^6 cycles when the maximum fatigue stress is less than the stress at which maximum transverse cracking can occur in off axis plies under static load.^{4,14} The S-N curve is known to be concave with data scatter being approximately one order of magnitude for quasi-isotropic layups and two to three orders of magnitude for high 0° content layups. Stiffness changes can be calculated by stress analysis methods^{1,2} up to the maximum transverse cracking state. Using present statistical procedures, estimates of residual strength degradation could be made because the extent of scatter could be estimated.

Mathematical results could be compared to designer and customer requirements. If they did not correspond, a new layup would be selected and subjected to the same analysis. Correspondence of analytical properties and requirements would be verified by experimental evaluation of the selected laminate, after which the statistical parameters would be corrected to the experimental values. A similar synthesized mechanistic/statistical approach might be able to be used for notched coupons or for tension-compression fatigue. Spectrum fatigue could possibly be qualitatively accounted for by a cycle counting method such as that proposed by Yang and Jones⁸, although this may not be adequate.

The difficulty with the above suggested scheme is that the procedure needs to be integrated into the design interational process. Although an estimate of strength and fatigue characteristics could be made without testing any layups, characteristics would not be known until after the selection of a particular layup. To solve this problem, a class of layups needs to be represented by a simple parameter or set of parameters. Such a parameter could be integrated into the tentative design process, thus avoiding the post-facto mathematical analysis of a large number of laminates. The determination of such parameters is outside the scope of the present program because only one layup is being investigated. Tensile stiffness change has been suggested as such a parameter. However, some layups can withstand severe damage or even fail in fatigue without significantly affecting tensile stiffness.⁴

Another phenomenon which may possibly be best described by mechanistic/statistical approaches is the manner in which inter and intralamina matrix cracks coalesce. Mechanistic approaches can determine whether characteristic damage states^{1,2} exist for a particular layup and provide a description of such states. In addition, the approach can determine the order of inter or intralamina cracking and at what load the cracking will occur.^{2,3} However, the rate of crack growth and the manner of interaction may be dependent on so many factors that the best approach may be to combine the mechanistically derived information with a statistical description of the damage growth.

The fracture of 0° plies may also possibly be accounted or by a combined statistical/mechanistic approach. If the cause of 0° ply fracture is due to extension of one fiber breakage region, mechanistic procedures may be adequate. If, however, a number of 0° fiber breakage regions interact critically to cause fracture, a statistical description of their mechanistically determined interaction would be fruitful for modeling damage growth. Such a concept could be made practical by combining the research of fiber composite investigators^{15,16} with certain mathematical formulations developed for metals.¹⁷

Conceptual Summarization

The experimental data of this program will be analyzed in such a manner as to aid in the formulation of predictive techniques for laminated composites

under complex spectrum loading. The analysis approach is predicated on the concept that fatigue life prediction is a dynamic process and thus is not restricted to a particular technique or set of mathematical equations. By this is meant that successful fatigue life prediction is the result of a dynamic interaction of the analyst with the problem resulting in a positive movement towards solution. This process is carried out without being bound by any one mathematical procedure. The process involves first, an analysis of the information needed for a particular situation, followed by selection of appropriate mathematical equations from the broad number available, and finally the delineation of required physical experiments.

If the problem of interest is one of simple constant amplitude loading, fatigue life can probably be fairly easily predicted. That this can be done at least for some layups is intended to be demonstrated. The more difficult process of predicting fatigue life, strength state, and cumulative damage under spectrum loading for complex geometry is not easily accomplished at present except by actual generation of test data. The solution of this problem is believed not to be one of determining whether proof testing works or of developing a particular cumulative damage rule. Instead, the solution rests upon our understanding of the fatigue process thus allowing definition of what is appropriate for a particular layup/load history/environment/ geometry state. In some situations this understanding may result in the use of a dominant flaw type damage growth rule. In others, proof testing may be employed.

This program is intended to improve our understanding of fatigue in laminated composites thus aiding in the delineation of the life prediction process. This will be accomplished by placing analytical attention on three related research areas. First, the usefulness of dividing the crack extension mechanism into three mechanisms (load increase, creep, cyclic growth), as commonly done, will be evaluated. Second, the nature of the failure process under various load histories will be established such that concepts related to path dependence or independence are clarified. This will be accomplished by comparisons among the experimental data and by documentation of the damage

initiation and growth process. Third, the importance of defining failure will be emphasized. The appropriate mathematical aids (stress and energy analysis, laminated plate theory) will be used, as necessary, in the investigation of these three research areas. The planned experiments will provide a basis for evaluating the concepts.

1.3 SUMMARY OF RESEARCH PROGRAM

The research program is divided into four Tasks. Under Task I, Diagnostic Experimentation, the baseline experimental data are obtained and diagnostic inspection techniques selected for detecting and monitoring damage. Task II, Effects of Loading Parameters, sequentially follows Task I and involves obtaining experimental data on the effects of various load histories on fatigue life. After Task II, Task III, Effects of Environment and Geometry, is undertaken to determine the effects of environmental and geometrical perturbations on the load history effects studied in Task II. Task IV, Data Analysis and Reporting, is being conducted simultaneously with Tasks I, II, and III.

TASK I - Diagnostic Experimentation

One laminate of T300/5208 graphite/epoxy material is being used in this program. The laminate is a 16-ply, quasi-isotropic layup of the following configuration: $(0/+45/90/-45_2/90/+45/0)_s$. This material and laminate were selected to provide maximum continuity in the formulation of a comprehensive data base since these are the same ones for which extensive fatigue and static test data are being developed under AFML Contracts F33615-77-C-5140 and AFFDL Contract F33615-77-C-3084.

Material lamina properties were determined under three environmental conditions: 1) room temperature, dry; 2) 82.2°C (180°F), dry; 3) 82.2°C (180°F), wet. Static tests to obtain lamina strength and modulus properties were conducted at each of these conditions using five different loading conditions of 16-ply laminates: 1) 0° unidirectional tension; 2) 90° unidirectional tension; 3) ±45° tension; 4) 0° unidirectional compression; and 5) 90° unidirectional compression. In addition, thermal and moisture diffusivities, equilibrium moisture contents, and expansional strains due to temperature were obtained.

The static tension strength and compression strength distributions of the quasi-isotropic laminate were determined at a typical static loading rate and at the loading rate used in 10 Hz fatigue tests. Selected coupons were non-destructively inspected for damage growth. Techniques used were: acoustic emission; edge replication; acoustic holoscan, B-scan and C-scan; and enhanced X-ray radiography.

Laminate fatigue properties were obtained under constant amplitude loading at a frequency of 10 Hz. A stress-life scan consisting of tests at four load ratios ($R = +0.5, 0.0, -0.5, -1.0$) was conducted. One-half of all fatigue runouts were tested in tension and one-half in compression. In addition to temperature and modulus monitoring, the NDI procedures used in the static tests were used to monitor the fatigue tests. Based on the NDI test results, diagnostic procedures were selected for use in Tasks II and III for detecting and monitoring damage initiation and growth.

TASK II - Effects of Loading Parameters (1980 - 1981)

The stress-life relations will be obtained in detail at stress levels selected on the basis of Task I results in addition to testing additional residual strength coupons. Tests will be conducted at R ratios of 0.0 and -1.0. One-half of the fatigue runouts (defined as 1×10^6 cycles) will be tested in static tension and one-half in static compression to determine residual strengths. These data will form the reference baseline. A number of different loading histories will be investigated to determine their effects on constant amplitude fatigue properties of the selected laminate and material.

The concept of summation of fatigue damage at different stress levels for prediction of fatigue life will be investigated at two of the maximum stress levels studied in the stress life scan of Tasks I and II, one above the fatigue limit and one at or near the fatigue limit. Specimens will be tested at four different combinations of high-low and low-high constant amplitude fatigue stress levels. The effect of progressive (increasing amplitude) fatigue loading on static strength will be determined. The effect of time under load will be investigated by introducing a trapezoidal fatigue loading wave form. Fatigue tests using a trapezoidal wave form will be conducted

at one maximum stress level, selected on the basis of previous test results, and at each of the two R ratios. The effect of overloads on constant amplitude fatigue life and damage will be investigated using six different loading conditions. The effect of preload will be studied to ascertain the possible relationship between the static strength and subsequent fatigue life. Coupons will be preloaded, followed by constant amplitude fatigue cycling, at two different maximum stress levels. The preload stress level and subsequent fatigue stress levels will be determined by the static strength and stress-life scan results of Tasks I and II. Selected stress-life and fatigue loading parameter coupons will be monitored for damage initiation and growth.

TASK III - Effects of Environment and Geometry (1981 - 1982)

The environmental conditions selected for this task are: 82.2°C (180°F), dry condition (coupon moisture content as manufactured); 82.2°C (180°F), 95 ± 5% R.H. equilibrium moisture conditioning (≈1.1% by weight); and a two and eight week exposure to thermal spiking. All coupons to be used in this task are machined from the same panels manufactured under Task I so that commonality of material is maintained. Before mechanical testing all specimens will be conditioned in their appropriate environments until equilibrium is obtained. Environmental conditions will be maintained throughout the fatigue tests. The static tension and compression strength properties of the laminate will be determined for dry and wet coupons at 82.2°C (180°F) and after exposure to the two thermal spiking durations. In addition, the same static properties will be obtained at room temperature using coupons which contain a hole.

A constant amplitude fatigue stress-life scan will be conducted at two R ratios (0.0 and -1.0) for four different environmental conditions: 1) 82.2°C (180°F) dry; 2) 82.2°C (180°F) wet; and 3) and 4) two conditions of repeated thermal spiking. The stress life scan will also be conducted on the hole geometry specimen. Stress levels for these tests will be based upon previous test results of Tasks I and II. A limited study of the viscoelastic effects on the laminate fatigue properties will be conducted. This study will be undertaken at elevated temperature, in both the dry and wet environmental conditions, and will explore the different viscoelastic effects as evidenced

under different fatigue test frequencies and those due to time under load. The effect of frequency will be explored at one stress level (selected based upon previous test results) using constant amplitude sinusoidal wave forms at frequencies of 1 and 10 Hz. The modifying effect of a hole upon the previously determined load history results will be obtained at $R = 0$ and -1 under four fatigue loading conditions: high-low stress, low-high stress, overload, and preload. These tests will all be conducted at a room temperature, laboratory air test condition. For all fatigue testing conducted in this task, one-half of all fatigue runout (1×10^6 cycles) coupons will be tested in static tension and one-half in static compression. Selected coupons tested in this task will be inspected for damage initiation and growth. The damage monitoring and inspection procedures will be the same as used in Task II.

TASK IV - Data Analysis and Reporting

In this task, a statistical analysis is being performed on each data set. The analysis includes determination of mean, and standard deviation and the Weibull distribution parameters. Comparison and correlation studies of the static and fatigue results with failure modes and fatigue life are being conducted to serve as a basis for formulating fatigue life models based on knowledge of failure mechanisms.

SECTION 2

EXPERIMENTAL OVERVIEW

This section presents a discussion of the rationale for material and laminate selection, outlines the Task I experimental test matrix, and describes the test procedures.

2.1 MATERIAL AND LAMINATE SELECTION

The selected fiber/resin system was Narmco's Rigidite T300/5208. The reasons for selection of this material were:

- The consistent quality of the T300 fiber
- There is an extensive database at Lockheed-California Company and at other companies on this material. Much of the data is directly related to that which is being obtained in this program. The most pertinent data will be from AFFDL Contract F33615-77-3084, "Advanced Residual Strength Degradation Rate Modeling for Advanced Composite Structures;" AFML Contract F33615-77-C-5140, "Effect of Environment on Compressive Strengths of Laminated Epoxy Matrix Composites;" and NASA/Langley Contract NAS1-14000, "Flight Service Evaluation of an Advanced Composite Empennage Component on a Commercial Transport Aircraft." All three of these contracts use the T300/5208 system.
- The Air Force had a greater interest in this material than other materials at the time of contract award.

The laminates used in this program are a unidirectional 0° layup, $(0)_{16}$, designated U1 from which 0° and 90° unidirectional coupons were obtained; a $\pm 45^\circ$ layup, $(\pm 45)_{4s}$, designated U2; and a quasi-isotropic layup, $(0/45/90/-45/90/45/0)_s$ designated L1. The U1 and U2 unidirectional laminates were used in Task I to obtain lamina properties. Only one laminate, L1, was selected for evaluating load history effects as per the original Air Force

request. The selection of laminate L1 for Tasks I, II, and III was based on the following considerations:

- a. The laminate must be representative of those commonly used in aircraft structures.
- b. Interlaminar shear and tensile normal stresses should be minimized to prevent premature edge delamination.
- c. Symmetry about the mid-plane should be maintained to avoid warping under load or due to fabrication stresses.
- d. Laminate thickness must be such that adequate bond strength can be obtained.

Laminates for aircraft structures are typically selected from the $0_i/\pm 45_j/90_k$ or $0_i/\pm 45_j$ orientation families. The 0° direction is generally oriented parallel to the principal axial loading direction; $\pm 45^\circ$ plies provide shear strength and stiffness or buckling resistance, and when needed, 90° plies provide additional strength in the transverse direction, reduce the Poisson's ratio, and can be used to mitigate some of the free-edge stresses.

The selection of laminate stacking sequence was governed by three considerations: symmetry, tab bond strength requirements, and free-edge effects. Laminates of sixteen or more plies impose severe strength requirements on the tab bond, so surface plies were oriented at 0° . This choice was selected although many laminate designs for aircraft skin covers have 45° fiber orientations on the outside surface. Angle plies terminating at a free edge induce interlaminar shear and normal stresses due to differences in Poisson ratios. The magnitude and sign of these stresses are functions of the lamina orientations, thicknesses, stacking sequence, and external and thermal stresses. Interlaminar normal tension stresses of sufficient magnitude can cause edge delamination that reduces both static and fatigue strengths. Stacking the laminate so that the normal stresses are compressive generally increases the fatigue strength over that of a laminate with tensile normal stresses. However, cyclically applied loading with reversing direction, as in this program, results in reversal of the sign of the normal stress. Consequently, for fatigue coupons subjected to compressive loading, laminae must be stacked to minimize normal stresses and thus their effects on fatigue strength. Another

point of consideration was that matrix dominated layups (low number of 0° plies) would be generally expected to be more susceptible to load history than fiber dominated layups (high number of 0° plies). This conclusion is supported by the literature^{4,18}.

The above considerations were combined with the objectives of the RFP, (restriction to one laminate configuration) and used to arrive at the selected laminate, L1. This type of laminate is often said to have matrix dominated failure modes. Data on a laminate subject to fiber dominated failure modes would be desirable, but some of that data will be available on the same material from the results of AFML Contracts F33615-77-C-3084 and 5140, and on the T300/934 system from AFML Contracts F33615-75-C-5118 and F33615-77-C-5045. The proposed laminate has the distinct advantage of having a definite stress-life curve not displayed by laminates containing a higher percentage of 0° plies^{18,19}. A Lockheed computer program, ISGMZ, based on the method of Pagano and Pipes²⁰, which approximates the interlaminar stresses, was used as an aid in selecting the stacking sequence. Laminate ultimate strengths were calculated using the Lockheed program HYBRID. The results for tensile and compressive loading of the selected laminate are given in Table 1.

TABLE 1. - INTERLAMINAR NORMAL STRESSES AT FREE EDGES OF TEST COUPON

σ_x^a MPa(ksi)	(0/45/90/-45/-45/90/45/0) _s			
	Tension 84.1(12.2)		Compression -84.1(12.2)	
$\Delta T, ^\circ C (^\circ F)$	0 (0)	111 (200)	0 (0)	111 (200)
σ_y^0 , MPa(psi)	1.43 (-208)	27.3 (3960)	1.33 (193)	9.94 (1442)
σ_y^{45} , MPa(psi)	32.3 (4985)	34.4 (4985)	-32.2 (-4669)	-32.8 (-4754)
σ_y^{90} , MPa(psi)	-63.2 (-9175)	-94.4 (-13700)	63.1 (9150)	53.7 (7794)
σ_z^{max} , MPa(psi)	0.32 (46)	1.70 (246)	0.006 (9)	0.38 (55)
σ_z^{min} , MPa(psi)	-0.069 (-10)	0.28 41	-0.32 (-46)	-0.34 (-49)

a - $\sigma = 84.1$ MPa (12.2 ksi) is the limiting stress for the first ply failure, σ_{90}^{tu} , when ΔT is assumed to be $111^\circ C$ ($200^\circ F$) and $\sigma_x = 538$ MPa (78 ksi)

2.3 FABRICATION AND QUALITY ASSURANCE

Essentially, fabrication and quality assurance procedures followed those used previously in Contract F33615-77-C-5045⁴. The procedures are outlined in this section. Appendix A contains the detailed quality assurance and fabrication procedure used in this study. Table 2 outlines the steps taken to assure test panel quality and uniformity.

Prepeg Quality Assurance - A single batch of 305 mm (12 in.) wide prepeg was used for all test laminates thus preventing the possibility of the data being affected by batch-to-batch variations. The assumption was made (and was supported by previously obtained results^{4,18}) that after coupons have been manufactured, no significant change in their properties would occur during shelf storage at room temperature, $40 \pm 10\%$ R.H. Although this assumption was not expected to be perfectly true over the three year testing period of this contract, the variation in properties due to long-term storage was expected to be less than that due to batch-to-batch variations. This assumption will be checked during Task III.

TABLE 2. - QUALITY ASSURANCE TESTING OUTLINE

Material Form	Test
Prepeg (receiving inspection)	<ul style="list-style-type: none">- Visual examination (fiber uniformity, fiber alignment)- Volatiles content- Uncured resin content- Control of shelf life
Layup (prior to cure)	<ul style="list-style-type: none">- Visual examination of excess section for proper orientation of each ply
Curing	<ul style="list-style-type: none">- Automated autoclave programming for control of cure parameters- Permanent records of cure temperature and pressure maintained for each autoclave run
Cured Laminates	<ul style="list-style-type: none">- Visual examination (resin starvation, fiber wash-out, pinholes, etc.)- Thickness per ply- Cured resin content- Density- Void content (calculated)- Examination of cross-section under magnification- Nondestructive inspection of each test laminate by ultrasonic "C" scan

Resin content, volatiles content, and flow of the prepeg were inspected for conformance to specified tolerances upon receipt. Prepeg material was also inspected for flaws such as fiber misalignment, breakage, gaps, excess resin, and starved areas, and any portions of the batch containing these flaws was rejected.

Storage of Prepeg Materials - All prepeg materials were stored in sealed moisture proof bags in refrigerators at -17.8°C (0°F) to assure adequate shelf-life. Materials which exceeded specified storage periods were not used.

Layup of Laminates - Before layup, all materials, when removed from refrigerators, were allowed to come to room temperature before unsealing bags to prevent water condensation on prepeg surfaces. Layup of laminates was performed in a semi-clean room with temperature controlled to $21 \pm 2^{\circ}\text{C}$ ($70 \pm 5^{\circ}\text{F}$). This reduced contamination with dust or foreign matter. Controlled temperature assured proper tack and drapé of prepregs and prevented water condensation problems. Fiber orientation in a layup was accomplished by use of suitable templates to meet the required angle tolerances of $\pm 1/2^{\circ}$.

Curing of Laminates - Test laminates were fabricated in an autoclave using vacuum pressure augmented by autoclave pressure. The autoclave incorporated automatic programming instrumentation to control dwell time and heating rates. In the autoclave, pressure was not dependent upon tool or platen quality. These factors minimized the variation between separate cure operations. Test laminate fabrication required more than one autoclave cycle, but close controls reduced the possibility of significant test panel variations.

Bleeding was accomplished by use of a perforated, releasable membrane placed in contact with the laminates and backed with an absorbent material. This permitted escape of air and volatiles as well as bleeding of resin to reduce resin content of the laminates to specified levels. Pressure bags of suitable heat resistant plastic film were sealed in place over the layup.

Prior to cure, an excess section of the layup was examined to ensure proper filament orientation in each ply. During the cure cycle, a complete

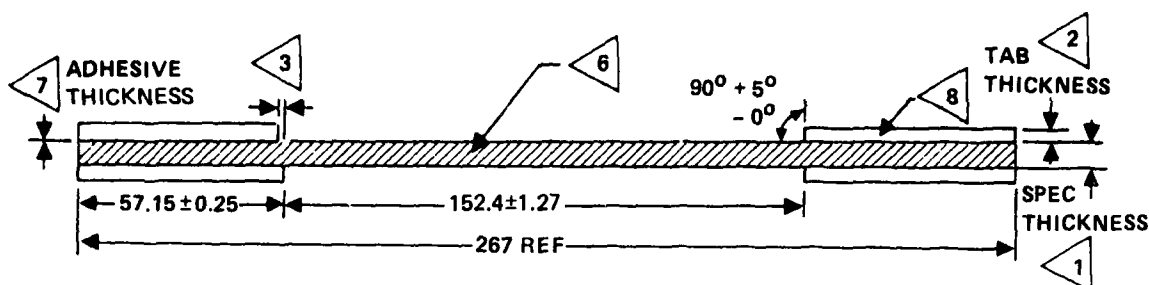
permanent record was maintained of temperature, vacuum pressure, and autoclave pressure. This record included heat-up rates and times of pressure application and release.

Test laminates were visually examined for defects such as resin starvation, fiber wash-out, pinholes, and voids. Thickness per ply, cured resin content, and density were determined. Weight percent fiber and resin were measured on each panel by replicate determinations using the acid digestion method. Density was measured by the water displacement method. From the known fiber and resin densities, fiber volume fraction and void volume fraction were calculated. All panels were fabricated such that a 25.4 mm (1.0 in.) wide edge could be trimmed off on all sides.

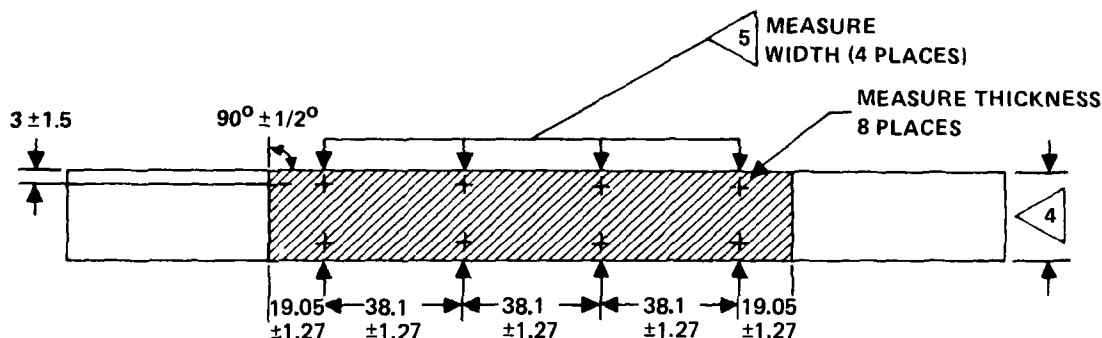
Each test laminate panel was nondestructively inspected by ultrasonic C-scan procedure for voids, delaminations, and other defects. NDI standard references were incorporated into each panel which consisted of three Teflon 0.05 mm (0.002 in.) thick film pads 3.2 to 12.7 mm (0.125 to 0.5 in.) diameter placed in the upper right hand corner. The references in each panel were compared to standard panels fabricated identical to the panels used in the test program except that 0.05 mm (0.002 in.) thick Teflon film pads of 3.2 to 12.7 mm (0.125 to 0.5 in.) diameter were placed at eight locations in the upper and lower halves of the standard panel.

The panel and coupon fabrication procedure used in this program is described in Appendix A. For laminate U1, two panels were fabricated of approximate dimensions, 610 by 1219 mm (24 by 48 in.); for laminate U2, two panels of approximate dimensions, 610 by 635 mm (24 by 25 in.), and for laminate L1, 19 panels of approximate dimensions 914 by 1219 mm (36 by 48 in.).

Specimen Design - Figure 1 shows the specimen design for the unnotched coupons machined from laminates U1, U2, and L1 used in this task and for the L1 panels of Tasks II and III. Figure 2 shows the notched coupon design to be used in Task III. This geometry for the notched coupon was selected in order to make a direct comparison between unnotched and notched data. A research study¹⁹ conducted to investigate systematically the effect of geometry on the fatigue properties of graphite/epoxy laminate strongly



ALL DIMENSIONS IN MILLIMETERS



- ◁9 SPECIMENS TO BE FLAT OVER THE ENTIRE 267 mm (10.5 in.) LENGTH WITHIN 0.25 mm (0.01 in.)
- ◁8 TAB EDGES TO BE PARALLEL TO SIDES OF SPECIMEN WITHIN 0.025 mm (0.001 in.) OVERHANG NOT TO EXCEED 3.8 mm (0.003 in.)
- ◁7 THE TAB AND SPECIMEN BONDING SURFACES TO BE THOROUGHLY SOLVENT CLEANED USING METHYL-ETHYL-KETONE PRIOR TO BONDING. A 177°C (350°F) CURING ADHESIVE IS TO BE USED AND MUST COVER ENTIRE SURFACE UNIFORMLY.
- ◁6 SPECIMENS TO BE CUT DRY. MACHINED SURFACES TO BE r_{ms} 50 OR BETTER. NO EDGE DAMAGE OR FIBER SEPARATION SHOULD BE VISIBLE UNDER 10X MAGNIFICATION.
- ◁5 MEASURE SPECIMEN WIDTH 4 PLACES. WIDTH MUST NOT VARY BY MORE THAN 0.102 mm (0.004 in.)
- ◁4 SPECIMEN WIDTH TO BE 22.225 ± 0.127 mm (0.875 ± 0.005 in.)
- ◁3 MISMATCH OF TABS FROM SIDE TO SIDE NOT TO EXCEED 0.25 mm (0.01 in.)
- ◁2 TABS TO BE CUT FROM AN 6 PLY LAMINATE FABRICATED FROM PREPREG OF 1581 GLASS FABRIC IN A 177°C (350°F) CURING EPOXY.
- ◁1 SPECIMEN THICKNESS TO BE WITHIN ± 0.08 mm (± 0.003 in.) OF THE AVERAGE OF 8 THICKNESS MEASUREMENTS.

Figure 1. - Unnotched composite test specimen

indicated that characteristic fatigue life is dependent on geometry. Details for the machining of these coupons are given in Appendix A. Features considered in the selection of this configuration are outlined below:

- The geometry can be used for static tension and compression tests as well as for either tension-tension or tension-compression fatigue tests.
- Adequate specimen length is important in composite specimens in order to obtain uniform stress conditions within the test section. Load introduction through the tabs must be transferred to the central plies by shear; the low shear modulus results in appreciable shear lag within the tabbed area. The resultant relative displacement of surface and centerline fibers must be accommodated within the specimen test length.
- Longer test specimens accommodate much more easily to small test misalignment and eccentricity. The 152 mm (6 in.) gage length selected here is considered important in minimizing stress variations which may be introduced by practical limitations in fabrication tolerances and test installation and thus in reducing test scatter.
- The relatively long length aids in minimizing end effects which could affect damage propagation behavior from a hole.
- The specimen size is sufficient to provide a good probability of including point-to-point variations in material and layup properties, as well as large enough to be more representative of aircraft structures.
- Variations in test results due to the discontinuity at the specimen edge will vary with laminate, material, and fabrication practice, but in general will diminish as width is increased. The 25 mm (1 in.) width was chosen to minimize the free edge effects which are usually on the order of a laminate thickness^{21,22} so that these do not unduly influence the damage propagation behavior.
- Dimensions are convenient for fabrication and machining; tolerances required to obtain the necessary precision in test results are achievable without extraordinary measures.

After fabrication and prior to testing, the thickness of all coupons was measured in eight places and the width in four places (see Figure 3 for these locations). The width of any one coupon varied at most ± 0.0127 mm (± 0.0005 in.), $\pm 0.06\%$, within the gage length. The width of all coupons varied by less than ± 0.10 mm (± 0.004 in.) within the gage lengths. The area of any one coupon was found to vary by less than $\pm 1.5\%$ from the average area of all coupons.

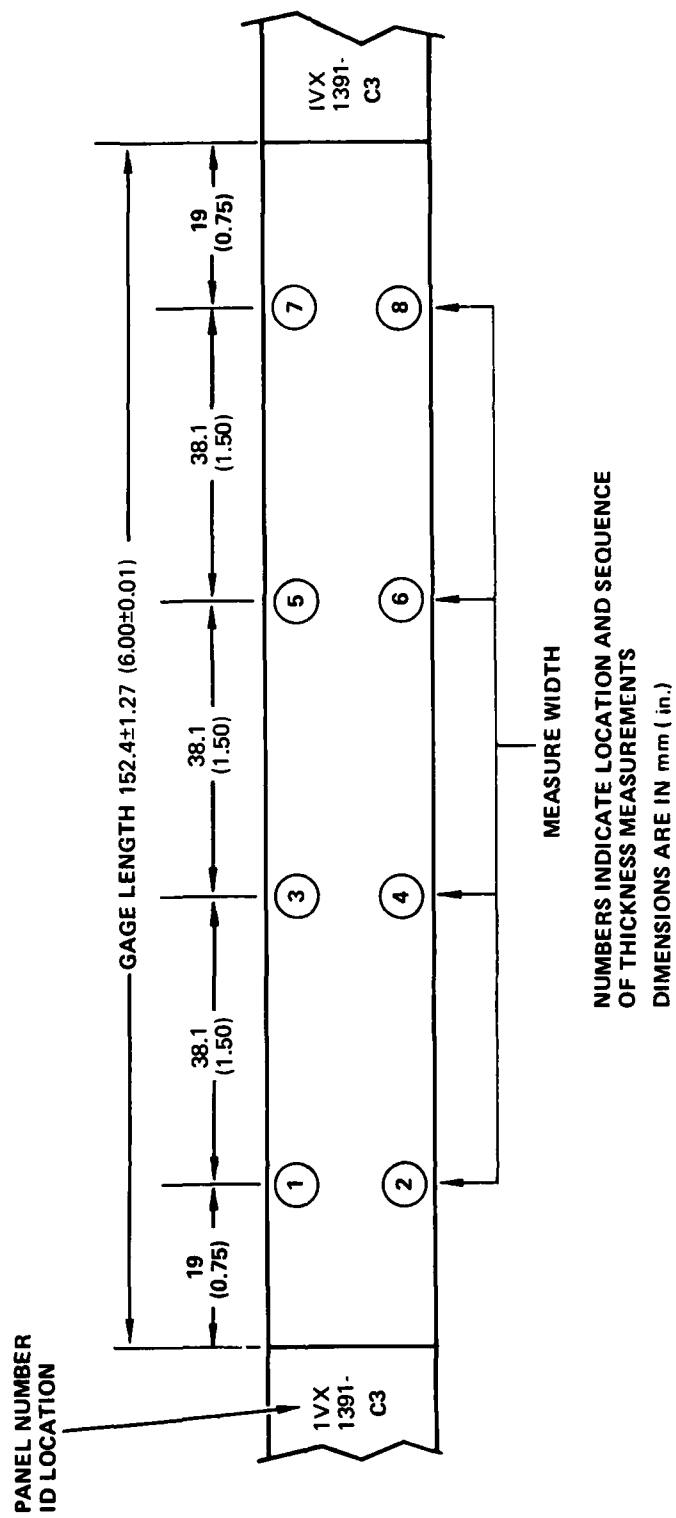
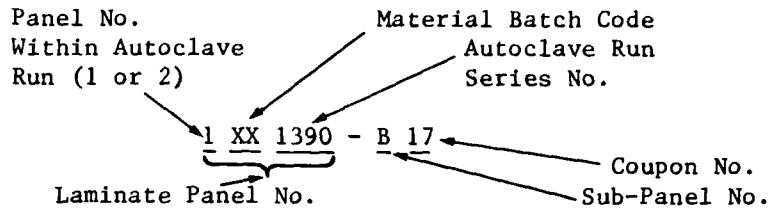


Figure 3. - Location of thickness and width measurements

All coupons were identified by the following system:



Autoclave and panel numbers are consecutive at Lockheed and are an internal reference number unique to each panel. The test panels were cut into sub-panels, and numbered as A, B, C, and D. This system of coupon identification allowed for traceability of each coupon to previous panel location and of each panel to fabrication history.

Panel layout was designed such that adjacent 90° and 0° direction tapes within a ply had their edges (line discontinuity) aligned with those of other plies of the same orientation. Thus, all 0° line discontinuities of one ply were directly lined up above those of other 0° plies within a total error of 0.1 mm (0.040 in.). The same alignment error occurred for the 90° line discontinuities. However, none of the line discontinuities of a $+45^\circ$ or -45° ply aligned with those of another ply of the same orientation. The layup pattern is shown in Appendix A.

This choice of line discontinuity pattern combined with the pattern of coupon location within a panel insured that 90° line discontinuities would lie within the coupon tabs, that all 0° line discontinuities would fall within two coupons of each subpanel (numbers 11 and 22) and that each coupon would be similarly influenced by $+45^\circ$ and -45° line discontinuities. Coupons 11 and 22 from each subpanel were eliminated from the experimental program. The care in panel and coupon manufacture resulted in coupons without 0° or 90° line discontinuities and similarly influenced by $+45^\circ$ and -45° line discontinuities. Thus the results of test program would not be influenced by line discontinuities. This influence was of concern since previous investigations have shown a significant effect of such discontinuities on distributions of static strength and fatigue life.^{4,23}

2.3 EXPERIMENTAL PROGRAM

The experimental program conducted in Task I is given in Table 3. Item 1 consisted of determination of 0° and 90° unidirectional lamina strength and modulus values under both transverse and longitudinal static tension and compression loading conditions as well as $\pm 45^\circ$ shear strength and modulus characteristics. In addition, the thermal and moisture properties were evaluated. In Item 2 the static tension and compression strength distributions of laminate L1 were determined at a common static testing strain rate as well as at the strain rate used in subsequent fatigue testing (equivalent to 10 Hz).

Item 3 consisted of monitoring static coupons for damage initiation and growth. Separate coupons were chosen for this study so that no bias could occur to the static strength distributions due to load interruption for NDI and the NDI procedures themselves. These coupons were inspected using four NDI procedures. The loading of coupons was interrupted at 20, 40, 60, and 80% of the average tensile strength. At each of these load interruptions,

TABLE 3. - TASK I EXPERIMENTAL TEST MATRIX

Item	Test Type	Stress Levels & Strain Rates	R Ratios	Replicates ^a	Data Required ^a	Minimum Total No. of Test Specimens
1.	Lamina Static Properties	Tension and Compression	-	10 at RT,D; 10 at 180°F,D, 10 at 180°F,W	0° Tension, 90° Tension, $\pm 45^\circ$ Tension, 0° Compression, 90° Compression	150
2.	Laminate Static Properties	Tension & Compression at 2-strain rates (0.01 mm/mm/min and equivalent to 10 Hz)	-	20	Static Tension & Compression Strength Distribution at RT,D Conditions	80
3.	Laminate Static Damage Growth Properties	Tension at 2-strain rates	-	3 to 5	Monitoring of damage initiation & growth under static loading	20
4.	Laminate Fatigue Properties	6 Stress Levels	-1,-0.5,0, +0.5	5	Stress-Life Scan	120

a - RT = Room Temperature, D = Dry, W = Wet

edge replication for cracks were conducted at maximum load; subsequently coupons were removed and inspected by the Holoscan acoustic inspection procedure and by TBE enhanced X-ray radiography. Throughout these tests and on selected coupons of the Item 2 tests, the acoustic emission counts, total count, count rate, and amplitude versus frequency signature were monitored.

Under Item 4, a fatigue stress-life scan of the laminate panels was conducted at six stress levels and four R ratios consisting of five replicates per stress level. Five coupons per stress level was adequate to define the average or characteristic life at each stress level. The R ratios were chosen to meet RFP requirements and to allow for comparison among the data sets for determination of the relative importance, if any, of stress range and maximum stress. Half of any coupons which reached fatigue runout were tested in static tension and half in static compression.

Included in Item 4 were the NDI procedures which constituted one of the primary purposes of this Task. Selected coupons tested in Item 4 had their temperature changes continuously monitored throughout the tests. These coupons were also strain gaged allowing determination of the dynamic modulus at the test start. At specific intervals, the fatigue test was interrupted and an extensometer used to determine the static stress-strain curve up to the maximum fatigue stress level of the particular coupon being tested. In addition, at each test interruption, the coupons were inspected after removal for damage initiation and growth by an acoustic Holoscan unit and by enhanced X-ray radiography. Damage initiation and growth were monitored at the test start and just prior to each test interruption by acoustic emission count, total count, and signature. The results of the NDI experimentation were not statistically meaningful, but allowed comparison of the four methods (edge replication, acoustic emission, acoustic Holoscan, and enhanced X-ray radiography) on a relative basis. After evaluation of all of the data, methods were selected for use in Tasks II and III as discussed in Section VI.

All of the laminate tests were conducted at room temperature in laboratory air. The lamina tests were performed at three different test conditions: room temperature dry; 82.2°C (180°F), dry; and 82.2°C (180°F) wet. The dry

condition was defined as the as manufactured moisture state while the wet condition was defined as the saturation moisture level at 82.2°C (180°F), $90 \pm 3\%$ R.H.

After fabrication, all coupons were kept in a chamber maintained at $22 \pm 1^{\circ}\text{C}$ ($72^{\circ} \pm 2^{\circ}\text{F}$) and $40 \pm 10\%$ relative humidity in a laboratory air environment. This environmental condition was called the standard room temperature, dry condition. Weight gain coupons were used to monitor moisture pickup in this environment. They were periodically measured to determine their percent weight gain. Coupons to be tested at high temperature were removed from the room temperature conditioning environment and conditioned at $82.2 \pm 1^{\circ}\text{C}$ ($180^{\circ} \pm 2^{\circ}\text{F}$) at $90 \pm 3\%$ R.H. until they reached equilibrium. Weight gain coupons accompanied the environmentally conditioned coupons and were used to monitor moisture pickup. Selected weight gain coupons were dried out after stabilization was reached and weight loss measured to establish the actual moisture content.

2.4 EXPERIMENTAL PROCEDURES

2.4.1 Static Tension and Compression Experimental Procedures

For both static tension and compression tests, load and deflection were continuously read out on an X-Y recorder so that stress-strain curves could be constructed. For the laminate tests, strain gauges were used to record strain, and stress-strain curves were displayed on a CRT screen by a computer after which hard copies were made. Ultimate strength, strain to failure, and the apparent modulus of elasticity were calculated. Stress was calculated using the coupon average area based on four locations equally spaced within the gauge length. An enclosure (metal or acrylic) surrounded the static test equipment for elevated temperature testing, Figure 4. The internal space was supplied with heated air. This arrangement provided specimen temperatures which were uniform throughout the gauge length and controlled to $\pm 1^{\circ}\text{C}$ ($\pm 2^{\circ}\text{F}$); the use of a convection heating or cooling ensured against local variations in specimen temperature such as may go undetected when radiant heating is used.

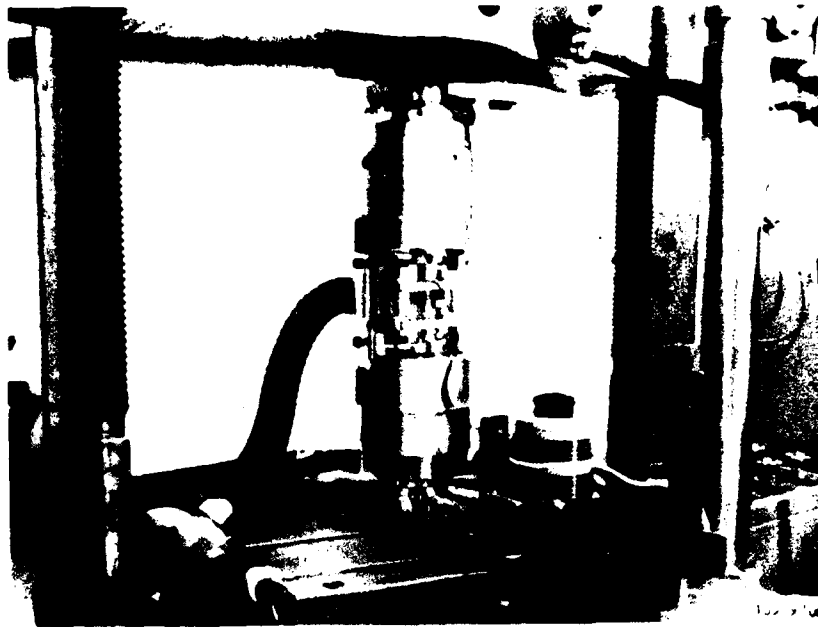


Figure 4. - Overall view of composite compression test apparatus, with acrylic enclosure and warm air supply

Static tension tests of laminates U1 and U2 were conducted in a 534 kN (120 kip) Baldwin static test machine while those for L1 were conducted in a 440 kN (100 kip) MTS machine. All testing was conducted similar to the procedures of ASTM D3039-74. Tests were conducted using MTS hydraulic self-aligning grips. Coupon alignment was assured by using a special exterior fixture attached to the grip assembly. Because coupon width varied only within ± 0.012 mm (± 0.0005 in.), the alignment procedure assured end-to-end coupon alignment within ± 0.076 mm (± 0.003 in.). A 50.8 mm (2 in.) extensometer was used to record deflection. Testing was conducted at a standard rate of ~ 0.01 mm/mm/min.

The experimental procedure selected for static compression strength consisted of testing the coupon in a fully constrained mode. This selected method enabled the same coupon geometry used in static tension and for fatigue testing to be used for static compression. The test results should be thought of in terms of column buckling under compression load in that the test condition consists of the state where the unsupported column length is

zero. Thus the test results correspond to an inelastic (fully constrained) failure mode.

In graphite/epoxy composites, compression failure is often assumed to be elastic and brittle, to correspond to the true compression strength, and to be essentially equivalent to the tensile strength. In practice, the composite responds inelastically in a manner not dissimilar to the macroscopic behavior of metals loaded in compression. Compression properties are dependent on test constraint and thus reflect the inelastic properties of the laminated structure formed of matrix and fibers which tend to buckle locally. Final fracture has a brittle-like appearance, but should be thought of as an inelastic phenomena. In this sense, an ultimate compression strength does not exist for composites similar to the situation for metals. These considerations are more fully discussed elsewhere²⁴.

Static compression tests were conducted using the same 534 kN (120 kip) Baldwin static and 440 kN (100 kip) MTS test machines used for the tension tests. Tests were run at a strain rate of ~ 0.01 mm/mm/min. A complete set of test fixtures was developed at Lockheed²⁴ which permit compression testing of composite laminate specimens under controlled conditions in either the fully-restrained mode, under column compression at various different pin-end lengths, or which can be used with fatigue buckling guides. The specimen-supporting fixtures are designed for use with MTS hydraulically-actuated grips.

Installation of the modified hydraulic test grips in a universal test machine is shown in Figure 5. A close-fitting steel shell surrounded each grip providing a mount for transverse adjustment screws that prevented destabilizing motion of the platens and specimen. The grips were rigidly mounted to the machine base and test head, alignment having first been achieved with the aid of spherically surfaced seats. Also shown in the photograph is a specimen positioning device, whose function is illustrated in Figure 6. The use of this device assured location of the specimen on the load axis of the grips to within 0.13 mm (0.005 in.).

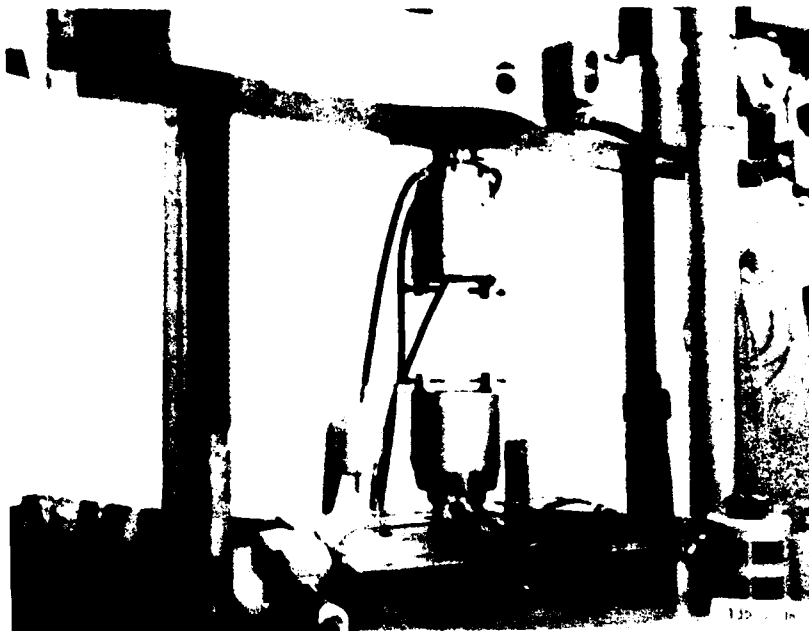


Figure 5. - Installation of modified hydraulic grips
in universal testing machine

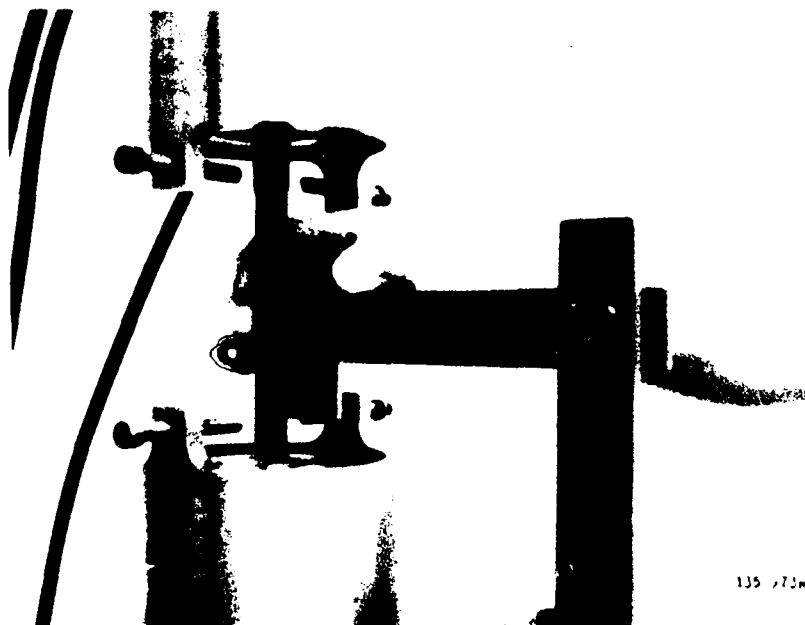


Figure 6. - Specimen positioning device

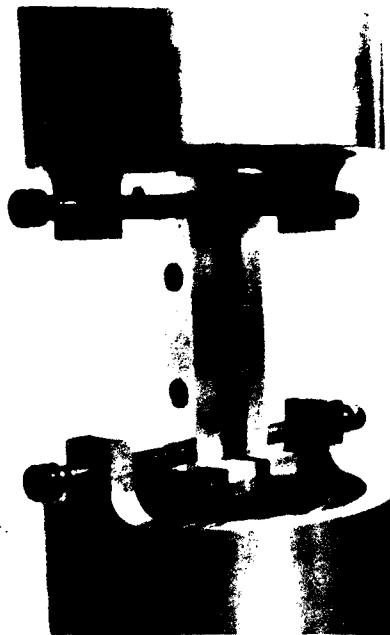
The fixture used to provide specimen support for testing to zero column length stress is shown disassembled in Figure 7. The fixture consists of two rigid guides or platens like those used by Ryder and Black²⁵ and similar in form to those of ASTM Test for Compressive Properties of Rigid Plastic (D 695-77) (Federal Test Standard 406). On the inner surfaces of the platens are located a set of extendable auxiliary platens which provide support over the full length of the test specimen. The auxiliary platens have a tapered overlap in the width dimension so that no critical length of the specimen is left unsupported. Access holes are provided for extensometer points of 50.8 mm (2.0 in.) gage length, or for electrical strain gages of 1.588 mm (0.0625 in.) length as were used in this program.

In Figure 8 the platens are shown assembled to a specimen which is installed in the grips. The four assembly screws were brought finger-tight providing light pressure between the platens and the specimen. Under these conditions, only a few pounds force was required to cause slippage of the entire platen assembly on the specimen. Exploratory tests have been conducted



135 996a

Figure 7. - "Full-fixity" apparatus, showing auxiliary platens



135 768K

Figure 8. - Specimen and restraint fixture installed in grips,

with the assembly screws tightened with a torque of as much as 1.13 N·m (10.0 in-lb), without producing detectable variation in the test results.²⁴ The installation was completed by bringing the large transverse restraining screws into light contact with the external platens. Figure 9 shows the installation of the extensometer used with this equipment. This instrument, which is of Lockheed-California Company design²⁶, utilizes a microformer sensor to provide a strain signal for conventional load-strain recording apparatus.

2.4.2 Fatigue Test Procedures

Fatigue testing was accomplished using closed-loop, electro-hydraulic, servo controlled, testing machines of 89 kN (20 kip) maximum allowable load. Each machine was equipped with a peak and valley load monitoring system which allowed continuous monitoring of the load signal maximum peak, maximum valley, and minimum peak and minimum valley such that load accuracy was



Figure 9. - Installation of Lockheed extensometer

maintained within $\pm 1.0\%$ of the full-scale reading. Fatigue grips were of the friction bolt type with integral alignment fixtures, see Figure 10. Coupon alignment was maintained within ± 0.0762 mm (± 0.003 in.) in any direction. All tests were conducted at 10 Hz. Figure 11 shows a typical tension-tension fatigue test set up and coupon failure. Minimum load in tension-tension (T-T) fatigue tests was approximately 200 N (50 lb).

Tension-compression (T-C) fatigue tests were conducted using the fixture shown in Figure 12. This fixture was designed to allow fully reversed compression up to the fully supported compression failure load. The openings on one side were designed to allow thermocouples and a strain gage to be attached. The other side had holes for attachment of acoustic emission transducers to the coupon surface.

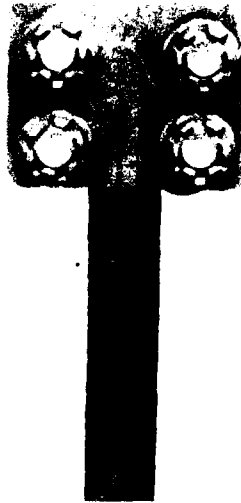


Figure 10. - Fatigue grip



Figure 11. - Tension-tension fatigue test showing failed quasi-isotropic laminate coupon.

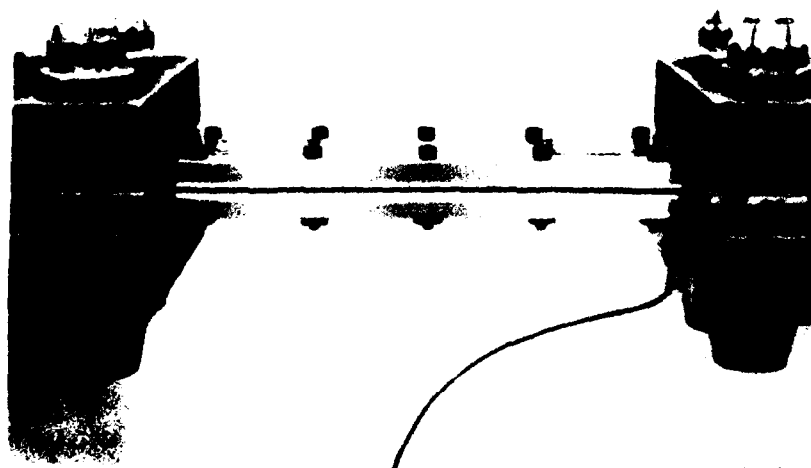
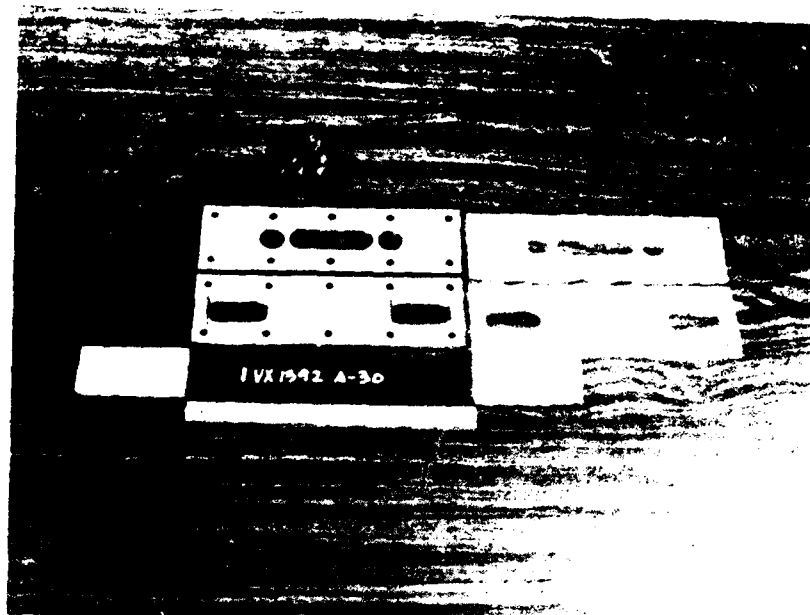


Figure 12. - Compression fatigue restraint fixture.

Fatigue tests were conducted by first dialing to the calculated mean load and setting the amplitude control such that the maximum load was approximately equal to 95% of the desired maximum load. Five or less cycles were then applied and the load time history recorded on high speed visicorders. This eliminated any possibility of a first cycle load overshoot and allowed the load at failure to be recorded for any first cycle failure coupon. The span control was subsequently increased such that minimum and maximum load were those desired. The peak and valley controls shutdown the fatigue loading and returned the load to the mean value if any load deviations beyond 0.5% were detected.

2.5 DATA ANALYSIS

For fatigue resistant design, one of the major questions concerning application of damage tolerance concepts is specification of percent levels of probability of survival. This question arises because of the need to translate reliability and confidence measures of data to parallel ones for design requirements²⁷. In fatigue, reliability can often be successfully defined in terms of the Weibull survivorship function. In Task IV of this program, all of the test data results were statistically analyzed and compared using a Weibull²⁸ distribution.

2.5.1 General Discussion of Weibull Function

In Weibull's representation of the statistics of fatigue, there are two random variates at each stress test condition. The first of these variates is the ordered sequence of the numbers of cycles to failure for each test result, n_i :

$$n_i: (n_1, n_2, n_3 \dots n_N).$$

The second random variate, x , is continuous and is the argument of the Weibull survivorship function, or probability of survival, expressed as

$$P(x) = \exp [-((x-e)/(v-e))^k], \quad (1)$$

where $x \geq e, v \geq e, k > 0, P(e) = 1, P(v) = 1/\exp(1).$

The connection between the random variates, n_i and x , is entirely empirical. In practice, numerical procedures are used to derive the three Weibull parameters k , e , and v by means of the approximation:

$$P(x) = 1 - i/N \text{ when } x = n_i, \quad (2)$$

$$\text{or } P(x) = 1 - i/(N + 1).$$

For equation (1), the mean of the sample set is given by²⁸:

$$\bar{x} = e + (v-e) \Gamma (1 + 1/k) \quad (3)$$

the median by:

$$x = e + (v-e) (\log_e 2)^{1/k} \quad (4)$$

and the mode by:

$$\tilde{x} = e + (v-e) (1 - 1/k)^{1/k} \quad (5)$$

where $\Gamma ()$ indicates the incomplete Gamma function.

During the past twenty-five years, a number of names have been applied to the parameters. In general, parameters e and v are considered as scale parameters or factors and the exponent k as a shape parameter. The term threshold parameter is usually applied to parameter e and the term

characteristic value to v . In analysis of composite data, k is frequently denoted by α and v by F . The scale parameter, e , is often referred to as the minimum life estimate. With this choice of words, e is suggested on physical grounds to be $e \geq 0$. Many authors have reasoned further that since $e \ll n_i$, $i = 1, 2, 3, \dots, N$, the Weibull survivorship function can be appropriately reduced to dependence on two parameters, k and v , with $e = 0$ arbitrarily. An argument against this practice will be described in this section.

The influence of the shape parameter k can be explained as follows. Define a reduced variate Z as:

$$Z = (x-e)/(v-e), \quad Z \geq 0, \text{ dimensionless,} \quad (6)$$

and express the probability of survival function as:

$$P(x) = \exp \left[-Z^k \right], \quad k > 0, \quad (7)$$

where $P(Z) = 1/\exp(1)$ when $Z = 1$,

and $P(Z) = 1$ when $Z = 0$, for all k .

If $k < 1$, this is sometimes interpreted as implying that the material develops resistance to fatigue as the number of load cycles is increased. If $k = 1$, the Weibull survivorship function reduces to the constant failure rate relation commonly used in reliability studies. If $k > 1$, one can inquire whether the test material experiences progressive damage as numbers of load cycles are increased.

Figure 13 illustrates the manner in which $P(Z)$ is dependent on the shape parameter k for the range of the reduced variate Z from zero to two. Empirical evidence does not support the interpretation that k might be a smoothly

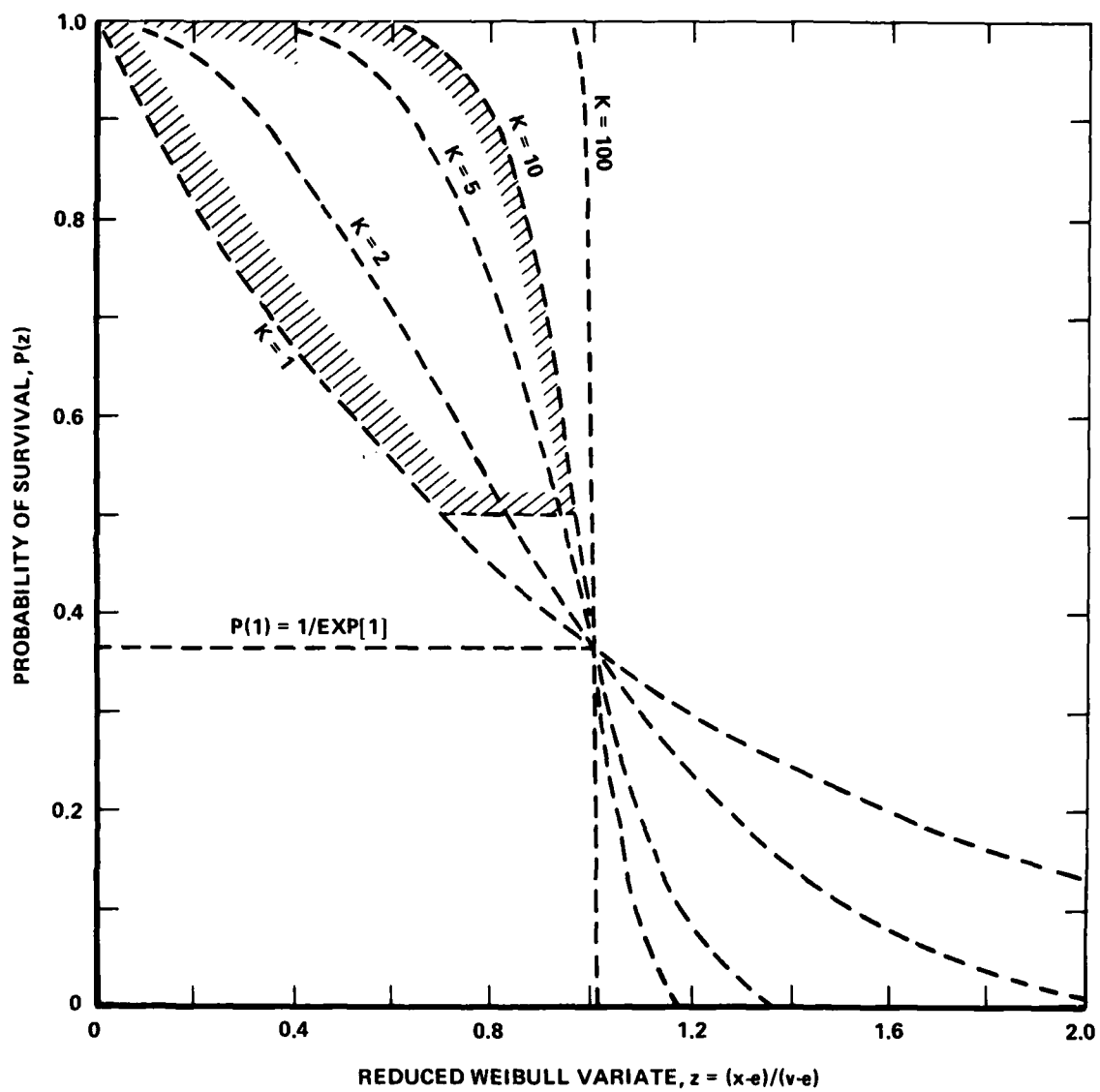


Figure 13. - Influence of shape parameter k on probability of survival

increasing function of stress amplitude. For practical purposes, in the case of structural fatigue, the region of Figure 13 of most interest to designers is bounded as follows:

- (a) Above by the limit $P(Z) = 1.0$
- (b) Below by the median $P(Z) = 0.5$
- (c) On the left by the curve $P(Z) = \exp [-Z]$
- (d) On the right by the curve $P(Z) = \exp [-Z^{-10}]$.

2.5.2 Weibull Analysis Procedures

There are three principal procedures which have been used to determine the Weibull parameters (k , e , and v) for a given data set. These are: the moment estimation (ME) method; the maximum likelihood estimation (MLE) procedure; and some form of the linear regression (LR) procedure. All three methods are also used to determine the unknown parameters of other types of fitting functions. The ME method principally consists of equating several population moments (equal to the number of unknown parameters) to the sample moments. The MLE method consists of setting the partial derivatives of the logarithm of $P(X)$, with respect to the parameters sought, equal to zero. In the LR procedure, the Weibull survivorship function is reduced to a linear equation. For the LR method, the solution for a two-parameter Weibull function is straightforward, but in the three-parameter case the solution is found by optimization of the correlation coefficient or by matching the sample skewness coefficient.

When one of the above described procedures was originally selected¹⁸ for analyzing graphite/epoxy composite strength and fatigue data, consideration was given to two thoughts. First, how well does the resultant Weibull survivorship function represent the original data set? Second, what, if any, extrapolative potential exists for the resultant function? Consideration of these two questions led to the selection of the LR procedure. The reasons for this selection will be described in detail along with references to recent work which supports the original choice. However, the data to be

generated in Tasks II and III will also be analyzed using the MLE procedure because of the frequency with which the procedure is presently used.

Both the ME and MLE methods require homogeneous samples. The reason for this requirement is that in the ME procedure the Weibull density function is integrated while in the MLE procedure, partial derivatives of the function are obtained. In this program, requirement of homogeneity was not assumed, a priori, to be necessarily met by sample information obtained from fracture data of composites. A procedure was desired which would be sensitive to the possible existence of multicomponent strength and fatigue life data. Such a requirement appears to be met by a LR procedure²⁹. The ME method can result in significant errors in estimation of k , e , and v ²⁹ and such errors increase as k increases. In the case of two-parameters, errors in estimation of k and v increase linearly with the true value of e (assumed to be zero) and can be greater than 100% when $e \geq v$ ²⁹. For the MLE procedure, three difficulties are encountered. First, the MLE solution of a data set is often a local maximum, but is not necessarily the maximum likelihood estimate²⁹⁻³³. Weibull and Weibull³⁰ found in a study of 300 random samples of 10 and 20 points each that approximately half of the estimates were not the maximum likelihood estimate, but were local maximums. Second, valid data sets can occur for which convergent solutions are not forthcoming, particularly for three parameter solutions³³. Third, if a given data set which actually belongs to a three-parameter Weibull population is assumed to be a two-parameter population ($e = 0$), the estimates of k and v can be significantly higher than their true values²⁹.

As previously alluded, in the analysis of graphite/epoxy composite data, the parameter e is often set equal zero. This practice greatly simplifies the mathematics especially for MLE procedures; however, there are strong objections against such a practice^{28,29,33}. These have already been discussed with reference to the ME and MLE procedures and are based upon the statistical error induced by the practice of setting $e = 0$. In summary, the three-parameter Weibull fit can be shown to fit the actual data set

better than the two-parameter.^{18,29,33} However, objections against the three-parameter Weibull fitting procedure are often raised upon the grounds that the parameter e may be found to have a negative value, particularly for a fatigue data set. The objection is thus raised that actual coupons can not have a finite probability of failure when the applied load is zero. Setting e equal to zero solves this problem. Setting e equal to zero is principally related to the question of the extrapolative capability of the Weibull function for graphite/epoxy composite fracture data.

Setting $e = 0$ results in the probability of survival, P_s , being equal to 1 when no load is applied to a coupon. While this is a reasonable expectation, the accuracy of fit in the range of the data is often sacrificed. At the same time, the resultant extrapolative estimates of strength and fatigue life at $P_s > 0.90$ may still be intolerably conservative. Therefore, in many cases by setting $e = 0$ little may be gained, and much lost. This problem is most critical for fatigue life data.

The problem of correctly extrapolating composite fatigue data is presently one of conjecture. This is due to three deficiencies: 1) large laboratory data sets for evaluating extrapolation from small subsets; 2) experimental data which correlates laboratory coupon results with structural test results; 3) field service experience. Therefore, while e should be greater than or equal to zero if it is truly a threshold parameter, correct values can not be determined at this time. Thus, setting $e = 0$ reduces the accuracy of our calculated fit to the data set but most likely results in extrapolative predictions being too conservative.

A possible solution to these problems has been suggested by Bowie, Besari, and Trapp³³ and will be discussed below. For the present, a three-parameter Weibull analysis procedure has been used throughout this report. The resultant analytical solutions closely fit the data and avoid the problems of ME and MLE solution procedures. The resultant functions are not of extrapolative value, but this is not considered to be pertinent for comparison

of data sets. Significant statistical analysis effort combined with extensive experimental investigations are needed before any extrapolative procedure can be developed and used with confidence. Hence, using a procedure which does not allow for extrapolation is not considered at the present time to be detrimental.

2.5.3 Description of Selected Analysis Procedure

The particular form of Weibull analysis used in this report has been discussed in detail elsewhere^{27,33}. Essentially, this procedure which consists of linear regression analysis in Z variate space, is similar to that used by Talreja.²⁹ The analysis procedure used is described in this section.

In the analytic procedure used in this program, an initial estimate was made of the probability of survival based directly on the test results, in a staircase manner, $P(n_i)$, $i = 1, 2, 3, \dots, N$,

where:

$$P(n_1) = 1 - 1/N$$

$$P(n_2) = 1 - 2/N$$

$$P(n_3) = 1 - 3/N$$

$$\begin{matrix} \cdot & \cdot \\ \cdot & \cdot \\ \cdot & \cdot \end{matrix}$$

$$P(n_N) = 1 - N/N = 0,$$

The function $P(n_i) = 1 - i/N$ was selected instead of the alternate function, $P'(n_i) = 1 - i/(N+1)$. The difference $(P'(n_i) - P(n_i))$ diminishes as N is increased. Thus for N equal to or greater than approximately 15, as in this investigation, the difference is undetectable. However, if extrapolations to probability of survival in the range above 90% are to be attempted, the choice of $P(n_i)$ rather than $P'(n_i)$ as initial distribution is the more conservative approach.²⁷ This is especially true for N less than 15.

With the above approach, the initial distribution is defined as:

$$P(n_i) = 1 - i/N$$

and $P(n_{i+1}) = 1 - i/N$ if $n_{i+1} = n_i$

otherwise $P(n_{i+1}) = 1 - (i+1)/N$

In most other analysis procedures, $p'(n_i) = 1 - i/(N+1)$ is selected as the initial description without regard to replication of the type: $n_{i+1} = n_i$. The choice of assigning the same initial probability to different coupons with the same n_i was considered appropriate because they do actually form a local mode, within the limits of testing accuracy, of the sample distribution obtained by experiment.

The appropriate variables of Equation 1 are found by forming N-1 relations:

$$\begin{aligned} P(n_1) &= 1-1/N = \exp \left[-((n_1-e)/(v-e))^k \right] \\ P(n_2) &= 1-2/N = \exp \left[-((n_2-e)/(v-e))^k \right] \\ &\vdots \\ P(n_N) &= 1-(N-1)/N = \exp \left[-((n_{N-1}-e)/(v-e))^k \right] \end{aligned} \quad (8)$$

The last relation for N is not used since $P(N) = 0$.

The parameters of Equation 1 were found by reducing the relationships of Equation 8 to the linear equation:

$$Y = bX+a. \quad (9)$$

The three-parameter Weibull linear equation is:

$$\left[-\ln P(X) \right]^{1/k} = bX + a, \quad (10)$$

where $e = -a/b$

and $v = (1+be)/b$.

For the two-parameter Weibull function ($e = 0$), the linear equation is:

$$\ln(-\ln(p(X))) = b \ln(X) + a, \quad (11)$$

where $k = b$

and $v = \exp(-a/b)$.

A linear regression method is used to determine k , e , and v . The initial order distribution is:

$$P(X_i) = 1 - i/N_p, \quad i = 1, 2, 3 \dots N_p. \quad (12)$$

Regression coefficients are found by least square analysis of $N_p - 1$ equations such as:

$$\left[-\ln(1 - i/N_p) \right]^{1/k} = bX_i + a, \quad i = 1, 2, 3 \dots N_p - 1. \quad (13)$$

The sample correlation coefficient, R, is calculated as:

$$R = \frac{\sum_{i=1}^M Y_i (aX_i = b) - \sum_{i=1}^M Y_i \sum_{i=1}^M (aX_i = b)}{\left[\left\{ M \sum_{i=1}^M Y_i^2 - \left(\sum_{i=1}^M Y_i \right)^2 \right\} \left\{ M \sum_{i=1}^M (aX_i = b)^2 - \left(\sum_{i=1}^M (aX_i = b) \right)^2 \right\} \right]^{1/2}} \quad (14)$$

where $M = N_p - 1$

The coefficients of linear regression and alternative correlation coefficient r are calculated by means of the following steps:

$$S_x = \left[\frac{M \sum_{i=1}^M X_i^2 - \left(\sum_{i=1}^M X_i \right)^2}{M(M-1)} \right]^{1/2}$$

$$S_y = \left[\frac{M \sum_{i=1}^M Y_i^2 - \left(\sum_{i=1}^M Y_i \right)^2}{M(M-1)} \right]^{1/2}$$

$$b = \frac{M \sum_{i=1}^M X_i Y_i - \left(\sum_{i=1}^M X_i \right) \left(\sum_{i=1}^M Y_i \right)}{M \sum_{i=1}^M X_i^2 - \left(\sum_{i=1}^M X_i \right)^2}$$

$$a = \left(\sum_{i=1}^M Y_i - b \sum_{i=1}^M X_i \right) / M$$

$$r = b S_x / S_y.$$

The standard deviation of the linear regression is calculated by means of the expression:

$$s = \left[\frac{(M-1)}{(M-2)} S_y^2 + (1 - r^2) \right]^{1/2}.$$

The values of k , e , and v are found by iterating on $1/k$ in Equation 13 and maximizing R in Equation 14. An alternative procedure would be to match the sample skewness to the Weibull function skewness by iteration of $1/k$. The coefficient of skewness is given by:

$$c.o.s. = \frac{\Gamma(1+3/k) - 3\Gamma(1+1/k)\Gamma(1+2/k) + 2\Gamma^3(1+1/k)}{(\Gamma(1+2/k) - \Gamma^2(1+1/k))^{3/2}}. \quad (15)$$

and recalling that $\Gamma(\)$ denotes the incomplete gamma function.

There are two primary difficulties with the method employed. First, the resultant Weibull functions could be used to imply that in some three-parameter cases and at a given extrapolation, high probability of survival ($P_s > 0.95$), fatigue life decreases as applied stress amplitude decreases. Second, in the case of two-parameter analysis, probability of survival functions tend to predict overly conservative extrapolated fatigue lives, particularly at low applied stress amplitudes. Both of these difficulties refer to the extrapolative capability of the resultant functions. This is not considered a problem for comparing the data sets, and as discussed in Section 2.5.2, extrapolation of the data does not appear to be presently feasible.

2.5.4 Alternative Procedures

Two other procedures are available for analyzing fracture data. They are the Standardized Variable Estimation (SVE) method²⁹ and the Modified Double Exponential Function (MDEF) method³³.

In the SVE method²⁹ the standardized variable Z is defined as in equation 6 for a Weibull survivorship function or as:

$$Z = \frac{X-e}{v} \quad (16)$$

for a Weibull probability of failure function. Thus, as mentioned in Section 2.5.1, the order statistics Z_i are independent of e and v and depend only on the shape parameter k . The expected value, EZ_i , median, MZ_i , and variance, VZ_i , of the order statistic Z_i have been derived by Lieblein³⁴. The characteristic values of Z_i depend only on the sample size, N , and the shape parameter, k .²⁹ From Equation 16, we obtain²⁹:

$$X_i = e + v EZ_i \quad (17)$$

$$\text{or} \quad X_i = e + v MA_i. \quad (18)$$

Equations 17 and 18 can be solved by linear regression. The shape parameter k is the value for which the correlation coefficient is a maximum²⁹. The parameters e and v are found as the X_i - intercept and slope of the best fit line.²⁹ If the sample data belong to different populations, this will result in the (X_i, EZ_i) and (X_i, MZ_i) scattering about different straight lines.²⁹

Talreja²⁹ found that the SVE method provided accurate estimates of k , e , and v for low values of k . At higher k values, the method often gives negative estimates of e . The procedure gave more accurate estimates of the parameters than the ME and MLE methods.²⁹

The MDEF is based upon the double exponential function of Gumbel.²⁸ In this procedure³³, for a set of sample fatigue lines, N_p , the initial distribution is defined by:

$$P(X_i) = 1 - i/(N_p + 1) \quad (19)$$

and $P(X)$ by:

$$P(X) = 1 - \text{Exp} [-\text{Exp} [-\alpha_o (X-u)]]. \quad (20)$$

For lives greater than u , the above function is used as described by Gumbel.²⁸ For lives less than u , α is a function of the life, X , where:

$$\alpha(X) = \alpha_o \left[\frac{\ln u - \ln X_o}{\ln X - \ln X_o} \right]. \quad (21)$$

The parameter X_o is defined as the threshold fatigue life. For $X \leq X_o$, P_s is defined as equal to unity. The modified double exponential function (MDEF) can be solved by ME, MLE, or LR procedures. The best procedure appeared to be linear regression.³³ The MDEF function was found to not only fit the sample data with high correlations, but to provide procedures for exploration of data extrapolation accuracy.³³

SECTION 3

MATERIAL CHARACTERIZATION

The characteristics of the graphite/epoxy material used in this program are described in this section. In addition, the environmental conditioning results for the various layups are reported.

3.1 PREPREG PROPERTIES

A single batch of Rigidite 5208/T300 305 mm (12 in.) wide graphite/epoxy tape was received the second week of November, 1978, from Narmco Materials, Inc. This batch was numbered 1283 and consisted of 11 rolls weighing a total of 1222 N (274,8 lb) with a 40 to 44% resin content. The fiber tensile strength and modulus of this batch is higher than previous batches received at Lockheed as shown in Table 4. The continuing change in fiber properties shown in Table 4 implies that any historical comparison of laminate properties is, at best, difficult to draw upon for determining future properties.

The required quality control tests on the material were conducted. The material was found to meet all requirements of the Quality Control Plan, and, therefore, was accepted. Material qualification tests were conducted by the Lockheed-California Company Quality Control Division and Narmco Materials, Inc. to assure material quality. The results of both sets of tests are presented in Tables 5 and 6.

3.2 PANEL PROPERTIES

From the received graphite/epoxy prepreg, two panels of 0° unidirectional laminate, two $\pm 45^{\circ}$ panels, and nineteen quasi-isotropic panels were manufactured. The panel numbers are listed in Table 7. Of the nineteen quasi-isotropic panels, only seventeen full panels and part of 1VX1392 are being used in the experimental program due to damage to two panels during manufacture into coupons.

TABLE 4
PROPERTIES OF T300 FIBERS USED IN VARIOUS LOCKHEED PROGRAMS

Manufacturer/ Batch No.	Date of Manufacture	Lockheed ID No.	Air Force Contract No. on which Material Used	Fiber Density g/cc	Fiber Tensile Strength MPa (ksi)	Fiber Modulus GPa (psi x 10 ⁶)
Fiberite/80-2 ^a	April, 1975	MJ	F33615-75-C-5118	1.76	2654 (385)	227.5 (33.0)
Fiberite/112-2 ^a	Oct. 1975	NH	F33615-75-C-5118	1.75	2537 (368)	233.0 (33.8)
Fiberite/6-C-73 ^b	July, 1977	SF	F33615-77-C-5045	1.76	2840 (412)	223.4 (32.4)
Narmco/1015 ^c	Nov. 1977	SY	F33615-77-C-5140	1.72	2840 (412)	226.2 (32.8)
Narmco/1079 ^c	Jan. 1978	TY	F33615-77-C-5140	1.74	3043 (441)	229.8 (33.3)
Narmco/1283 ^d	Oct. 1978	VX	F33615-78-C-5090	1.75	3284 (476)	237.4 (34.4)
Narmco/1295 ^e	Nov. 1978	WI	F33615-77-C-3084	1.75	3271 (474)	236.7 (34.3)

a - data reported in AFML-TR-76-241

b - data reported in AFML-TR-79-4128

c - data reported in AFML-TR-79-4179

d - material used on present contract

e - data reported in AFFDL-TR-79-3095

Resin, fiber, and void analysis results for the panels used in all three tasks are given in Table 8. The fiber volume testing was conducted by Delsen Testing Laboratories, Inc., Glendale, California, in accordance with ANSI/ASTM B-3171-73, Procedure A, entitled "Fiber Content of Reinforced Resin Composites" except as noted below:

- (a) Determinations for each strip of material were carried out in triplicate (see Figure 14 for location of test specimens).
- (b) Specimen size was approximately 1 gm rather than 0.3 gm.
- (c) The volume of Nitric Acid used for digestion was increased from 30 cm³ to 100 cm³ because of the larger specimen size.

The specific gravity testing was conducted in accordance with ANSI/ASTM D-792-66, Procedure A-1: "Specific Gravity and Density of Plastics by Displacement."

TABLE 5
SUMMARY OF LOCKHEED QUALITY CONTROL TESTS FOR NARMCO
RIGIDITE 5208-T300 MATERIAL BATCH #1283

Material Property	Specification Requirements C-22-1379A/111 (9/13/77)	Measured Property	Accepted
<u>UNCURED PROPERTIES</u>			
1. Areal Fiber Weight (4 req)	139 - 149 g/m ²	143 145 146 <u>141</u> Avg. 144 g/m ²	x ^a x x x
2. Infrared Spectrophotometric Anal. (1 req)	Conformance to file spectrogram	—	x
3. Volatiles (2 req) 60 ± 5 min at 350°F	3% Maximum	0.4% edge 0.35% center	x x
4. Dry resin content (4 req) (Sopplet)	38 - 44%	43.3% left 41.8% left center 41.9% right center 41.3% right Avg. 41.0%	x x x x
5. Resin Flow at 350°F and 85 psi (2 req)	15 - 29%	19.2% 19.4%	x x
6. Gel Time at 350°F (2 req)	For information only	19.0 minutes 19.5 minutes	— —
7. Fiber Orientation	0°	—	x
<u>CURED LAMINATES</u>			
1. Cured Fiber Volume, 16 ply panel (3 req)	60 - 68%	66.4 66.2 <u>66.0</u> Avg. 66.2%	x x x
2. Cured Fiber Volume, 8 ply panel (3 req)	60 - 68%	67.3 67.2 <u>67.5</u> Avg. 67.3%	x x x
3. Specific Gravity, 16 ply panel (3 req)	1.55 - 1.62	1.586 1.584 <u>1.588</u> Avg. 1.586	x x x
4. Specific Gravity, 16 ply panel (3 req)	1.55 - 1.62	1.592 1.590 <u>1.594</u> Avg. 1.592	x x x
5. Tensile Strength, longitudinal at 75°F (3 req)	170 ksi min.	242 235 <u>220</u> Avg. 232 ksi	x x x
6. Elastic Modulus, longitudinal at 75°F (3 req)	20·10 ⁶ psi min.	21.2·10 ⁶ 22.6·10 ⁶ <u>22.2·10⁶</u> Avg. 22.0·10 ⁶	x x x

TABLE 5
SUMMARY OF LOCKHEED QUALITY CONTROL TESTS FOR NARMCO
RIGIDITE 5208-T300 MATERIAL BATCH #1283 (Continued)

Material Property	Specification Requirements C-22-1379A/111 (9/13/77)	Measured Property	Accepted
7. Flexural Strength at 75°F (3 req)	210 ksi min.	289 280 <u>286</u> Avg. 285 ksi	x x x
8. Flexural Modulus at 75°F (3 req)	18·10 ⁶ spi min.	22.6 22.5 <u>22.7</u> Avg. 22.6·10 ⁶ psi	x x x
9. Flexural Strength at +180°F (3 req)	200 ksi min.	254 268 <u>261</u> Avg. 261 ksi	x x x
10. Flexural Modulus at +180°F (3 req)	16·10 ⁶ psi min.	21.8·10 ⁶ 22.8·10 ⁶ <u>22.5·10⁶</u> Avg. 22.4·10 ⁶ spi	x x x
11. Short Beam Shear Strength at 75° (3 req)	13 ksi min.	18.7 17.8 <u>18.4</u> Avg. 18.3 ksi	x x x
12. Short Beam Shear Strength at +180°F (3 req)	12 ksi min.	15.8 16.6 <u>14.8</u> Avg. 15.7 ksi	x x x
13. Thickness per ply, 16 ply panel (5 req)	0.0046 – 0.0056 inch	0.0049 0.0049 0.0048 0.0048 <u>0.0048</u> Avg. 0.0048 inch	x x x x x
14. Thickness per ply, 8 ply panel (5 req)	0.0046 – 0.0056 inch	0.0049 0.0046 0.0046 0.0049 <u>0.0049</u> Avg. 0.0048 inch	x x x x x
15. Ingestion: Acid, Temperature, Time		H ₂ SO ₄ /350°F/1.5 hrs.	
16. Resin Content	Information Only	8 Ply 26.4% Avg. 16 Ply 27.4% Avg.	
17. Water Absorption (24 hrs D.I.H ₂ O)	0.2% max.	8 Ply 0.15 16 Ply 0.17	
18. Liquid Chromatography		On file at Lockheed, Rye Canyon Research Laboratory	

a – an x indicates that the material passed this requirement

TABLE 6

SUMMARY OF NARMCO QUALITY CONTROL TESTS FOR RIGIDITE
5208/T300, NARMCO CERTIFIED TEST REPORT NO. 35990

MATERIAL: Rigidite 5208-T300-12"					
Batch No. 1283					
Roll	Amount	Resin Content	Areal Fiber Weight	Mfg. Date	Test Date
1	25.4 lb	42%	143 g/m ²	10-31-78	11-2-78
2	25.0	41	143		
3	21.1	41	144		
4	25.0	41	144		
5	25.6	42	144		
6	25.0	41	144		
7	24.8	40	144		
8	26.0	42	144		
9	25.2	41	144		
10	25.7	42	144		
11	26.0	44	143		
Volatiles:		0.6%			
Flow:		25%			
Gel Time:		27'25" min. @ 350°F.			
Tack:		Acceptable			
Specific Gravity:		1.58/1.58/1.58: 1.58 g/cc average (8 plies)			
		1.58/1.58/1.58: 1.58 g/cc average (16 plies)			
Fiber Volume:		65/65/65: 65% average (8 plies)			
		65/66/65: 65% average (16 plies)			
Cured Ply Thickness:		0.0051" (8 plies, Tensile panel)			
		0.0050" (16 plies, Flex and Shear panel)			
RT, 0° Flex:		261,550/307,120/329,390: 299,353 psi average			
RT, 0° Flex Modulus:		20.51/20.91/19.38: 19.38 x 10 ⁶ psi average			
RT, 0° Tensile:		237,530/257,280/212,470: 235,760 psi average			
RT, 0° Tensile Modulus:		20.99/20.62/20.28: 20.63 x 10 ⁶ psi average			
180°F., 0° Flex:		243,460/308,630/230,200: 260,760 psi average			
180°F., 0° Flex Modulus:		18.15/20.30/19.78: 19.41 x 10 ⁶ psi average			
RT Short Beam Shear:		18,820/20,200/19,710: 19,580 psi average			
180°F. Short Beam Shear:		17,520/18,150/17,400: 17,690 psi average			
Batch No. 1283					
RAW FIBER DATA					
Lot No.	Tensile Modulus	Tensile Strength	Yarn Density		
575-2	34.6 psi x 10 ⁶	471 psi x 10 ³	1.75 g/cm ³		
571-2	34.0	489	1.74		
577-2	34.3	457	1.76		
574-2	34.6	485	1.76		

TABLE 7
IDENTIFICATION NUMBERS OF PANELS USED
IN EXPERIMENTAL PROGRAM

Laminate U1 (0°) ₁₆ Unidirectional	Laminal U2 (±45°) ₄₅	Laminate L1 Quasi-isotropic (0/45/90/-45/90/45/0) ₈
2VX1394 1VX1453	1VX1386 1VX1471	2VX1390 1VX1391 2VX1391 1VX1392 2VX1392 1VX1395 2VX1395 1VX1396 2VX1396 1VX1403 2VX1403 1VX1413 2VX1413 1VX1414 2VX1414 1VX1425 2VX1425 1VX1442 2VX1442 1VX1458

Void content was determined in accordance with ANSI/ASTM D-2734-70 (Reapproved 1976). The void content results have an inherent error of $\pm 1.6\%$ in void content; i.e., a result of 2% voids can be between 0.4 and 3.6% voids. The error is due to uncertainty in original fiber and matrix density properties and in the amount of absorbed moisture which also affects density. This level of inherent error can result in physically impossible negative void content determinations. The chemical analysis void content determinations combined with the lack of any C-scan indications do imply that the void content of all panels is extremely low, $< 1\%$. Because no C-scan indications were observed in any of the panels, photographs of the C-scans are not included.

TABLE 8
RESIN, FIBER, AND VOID ANALYSIS RESULTS

Panel Production No.	Resin Content wt.%	Fiber Content vo.%	Void ^a Content, V _c %	Density gm/cc
2VX1394	26.0	67.1	0.34	1.588
1VX1453	25.8	67.5	-0.12	1.596
1VX1386	27.3	65.5	0.44	1.579
1VX1471	28.0	65.0	-0.05 ^b	1.579
1VX1394	26.2	66.7	0.45	1.585
2VX1390	27.9	64.8	0.42	1.576
1VX1391	26.8	66.2	0.38	1.583
2VX1391	26.4	66.5	0.42	1.584
1VX1392	26.8	66.0	0.49	1.581
2VX1392	27.3	65.6	0.39	1.580
1VX1395	26.4	66.5	0.43	1.584
2VX1395	26.4	66.5	0.44	1.584
1VX1396	26.5	66.3	0.52	1.582
2VX1396	26.6	66.2	0.48	1.582
1VX1403	26.5	66.4	0.33	1.585
2VX1403	26.1	66.8	0.47	1.585
1VX1413	26.5	66.4	0.34	1.585
2VX1413	26.4	66.6	0.30	1.586
1VX1414	26.9	66.0	0.26	1.584
2VX1414	26.6	66.3	0.30	1.585
1VX1425	27.3	65.6	0.26	1.582
2VX1425	26.8	66.1	0.37	1.583
1VX1442	27.6	65.3	0.22	1.584
2VX1442	27.2	65.8	0.16	1.584
1VX1458	27.3	65.7	0.14	1.584
Avg.		26.8	66.1	1.583
Std. Dev.		0.57	0.63	0.0037
Coeff. of Var. %		2.14	0.95	0.23
a - V _c void content determined by standard chemical analysis procedures, accuracy is $\pm 1.6\%$				
b - Artifact of chemical analysis procedure				

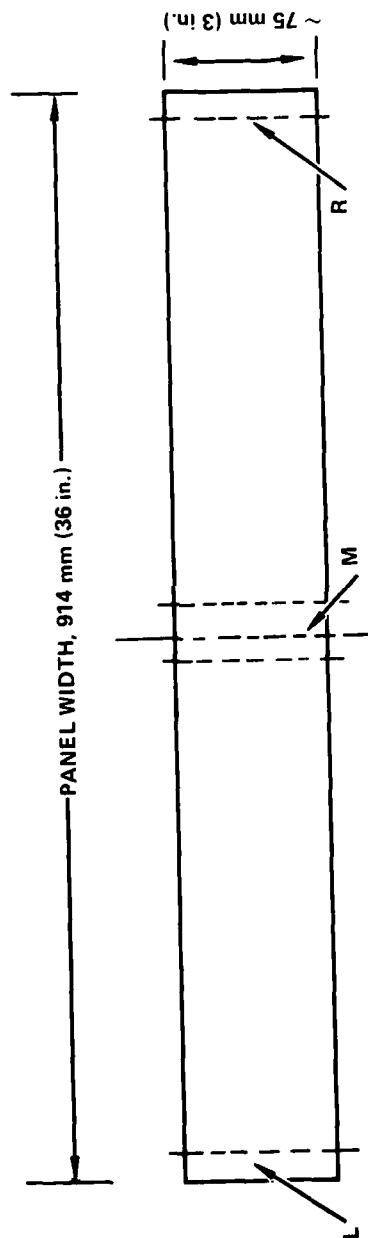


Figure 14. - Locations of three specimens from each panel used for specific gravity and acid digestion tests.

Microphotographs were taken of longitudinal and transverse cross-sections of panels representative of each different layup. Typical photomicrographic sections are shown in Figures 15 to 20. These photographs confirmed the low void content of the panels and displayed that no ply cracks existed after panel manufacture. Figure 19 shows a rare defect which occasionally occurs due to the presence of a small foreign particle.

3.3 ENVIRONMENTAL CONDITIONING

Some coupons used to determine lamina properties were conditioned at 82.2°C (180°F), 90 ±3% R.H, until an essentially equilibrium moisture content was obtained. These coupons were tested statically at 82.2°C (180°F). All other coupons were held at room temperature in laboratory air, 22°C (72°F), 40% R.H. Moisture distribution and weight gain was measured using 127 mm (5 in.) long by 25.4 mm (1.0 in.) wide traveler coupons cut from the gage section of typical test coupons. Traveler and moisture distribution coupons taken from the various laminates were used in four different groupings. They were:

- Group 1: Coupons used for determining initial moisture content and distribution prior to testing or to conditioning at 82.2°C (180°F), 90% R.H.
- Group 2: Coupons used to measure weight gain changes while being held in the room temperature, 45% R.H, holding chambers,
- Group 3: Coupons used for measuring weight gain during conditioning at 82.2°C (180°F) and 90% R.H. and for determining moisture distribution just prior to static and fatigue tests,
- Group 4: Coupons used for determining weight loss and moisture distribution changes which occurred due to static testing.

The results of each of these four groups will be discussed. The moisture distributions given in the following figures were experimentally determined using the procedure of Sandorff and Tajima.³⁵ All moisture distributions were determined using three samples cut from the traveler test coupon under investigation. The average weight loss values are those recorded during the dry out process used to determine the moisture distribution. The procedure used to determine the moisture distribution was

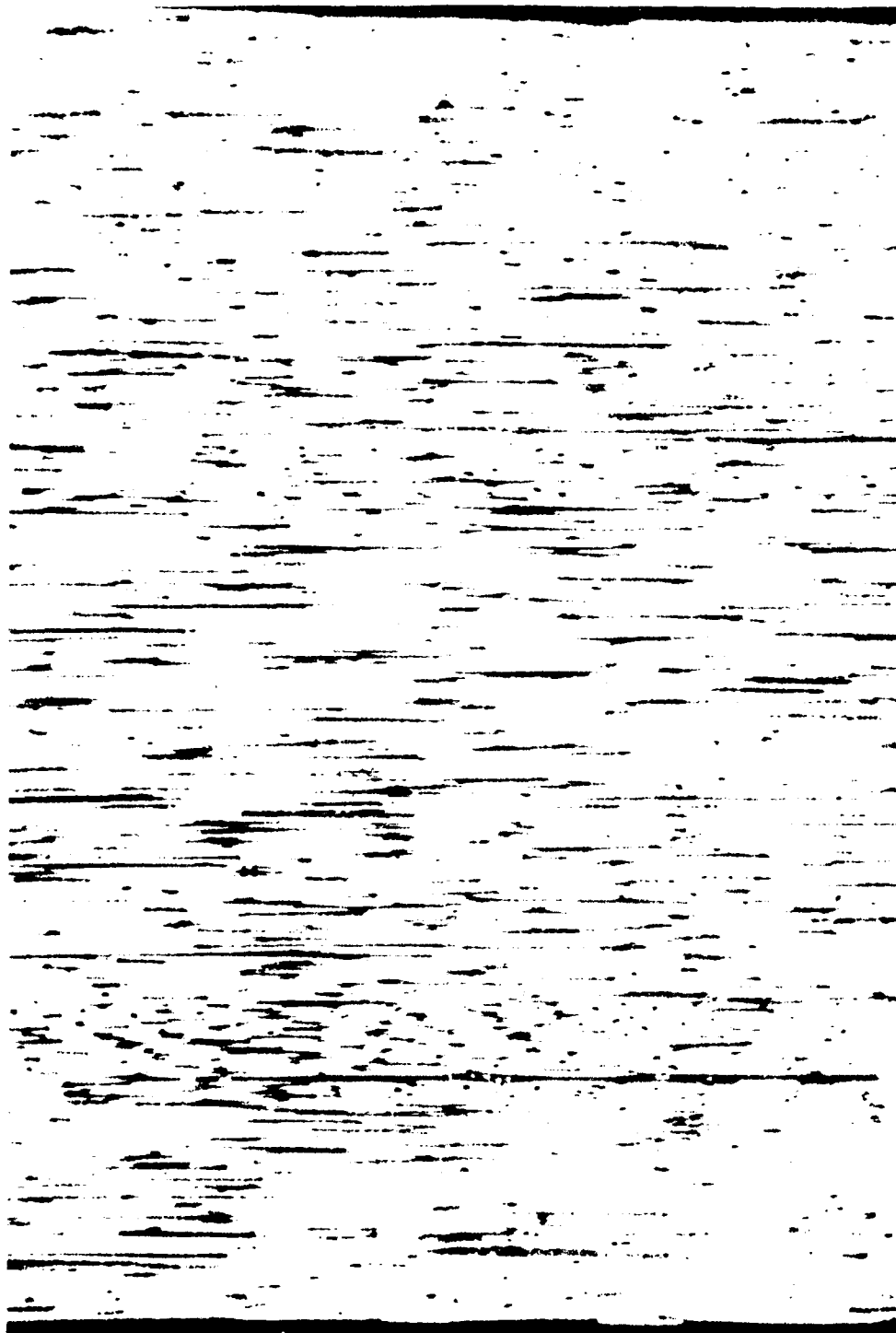


Figure 15. - Longitudinal cross-section of (0)₁₆ unidirectional panel, 2VX1394 (100X).



Figure 16. - Transverse cross-section of $(O)_{16}$ unidirectional panel, 2VX1394 (100X).

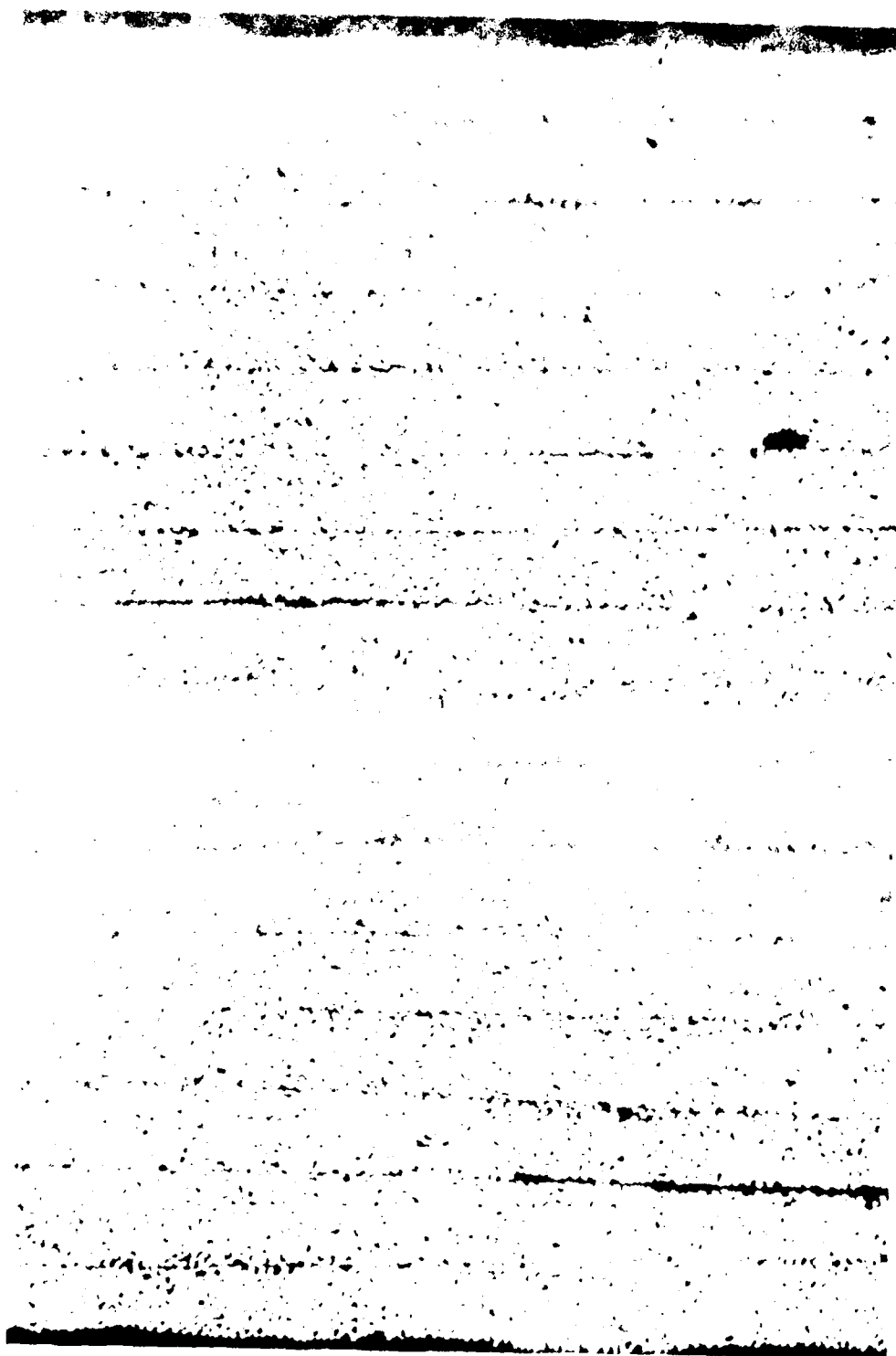


Figure 17. - Longitudinal cross-section of $(\pm 45)_{4S}$
panel, 1VX1386 (100X).

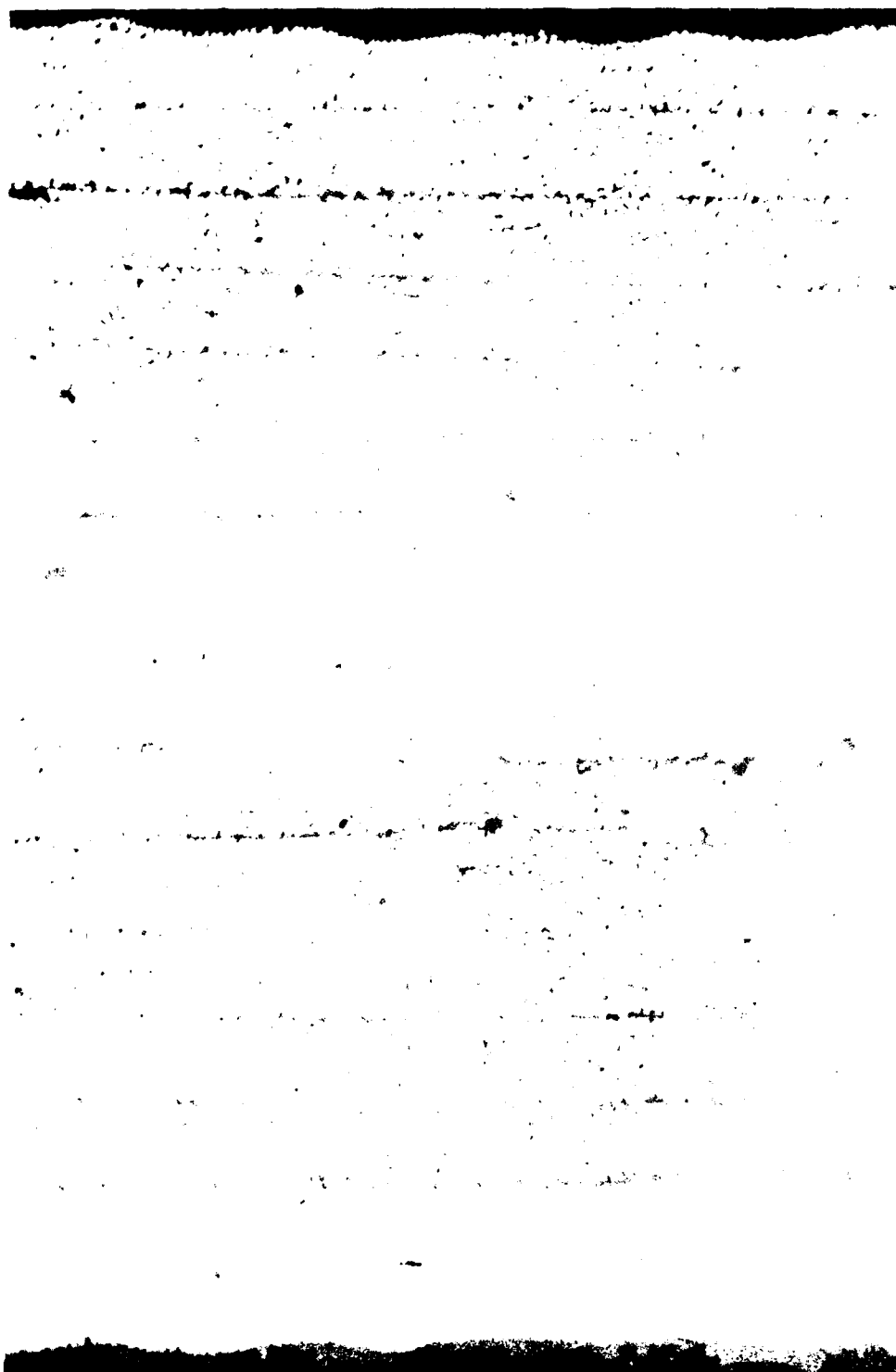


Figure 18. - Transverse cross-section of $(\pm 45)_{4S}$
panel, 1VX1386 (100X).



Figure 19. - Longitudinal cross-section of $(0/45/90/-45_2/90/45/0)_S$ panel, 1VX1392 (100X).

conducted in such a way to ensure that only moisture loss was being recorded during the drying process.³⁵ However, the weight loss obtained by any drying process is only that due to the release of unbound water. Thus, the amount of weight loss due to drying is not necessarily the same as the total weight gain from a zero condition since some of the water may be bound at the drying temperature.

Group 1: Initial Moisture Content and Distribution

The initial distribution of moisture within representative coupons after all manufacturing and machining operations were complete and before being placed in the room temperature, 45% R.H. holding chamber are shown in Figures 21 to 24 and summarized in Table 9. The results shown in Figures 21 to 24 show a greater initial moisture content for the quasi-isotropic laminate than for the unidirectional panels. The amount of moisture found in the quasi-isotropic laminate is essentially the same as that found for this layup made of T300/934 at the same state of manufacture.⁴ The initial moisture in the coupons after manufacturing and prior to conditioning was also determined by drying whole sections of the same coupons used for obtaining moisture distribution. Results are shown in Table 9 and compared to those determined by the moisture distribution process. The difference is apparently due to the continuous release of bound water during later drying.³⁶

Group 2: Weight Gain in Holding Chamber

Three traveler coupons were used to monitor weight gain due to moisture absorption of the laminate coupons held in the room temperature, 45% R.H. holding chamber. The results of the study showed that less than a 0.050% weight gain occurred in any one coupon over the five month experimental time period.

Group 3: Weight Gain and Moisture Distribution Changes due to Conditioning

Unidirectional coupons were conditioned at 82.2°C (180°F, 90 ±3% R.H. for 109 days. Figure 25 shows the weight gain history of typical coupons. The 0° coupons gained weight at the same rate as the 90° coupons. Table 10

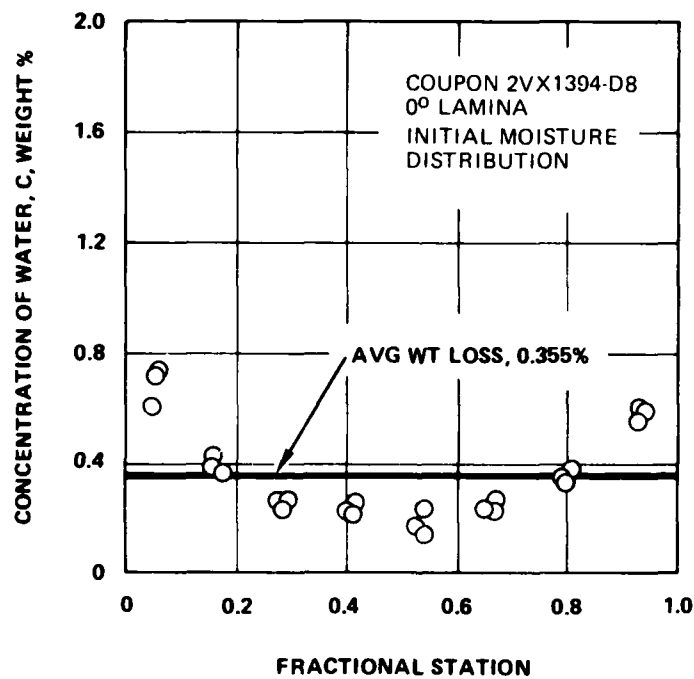
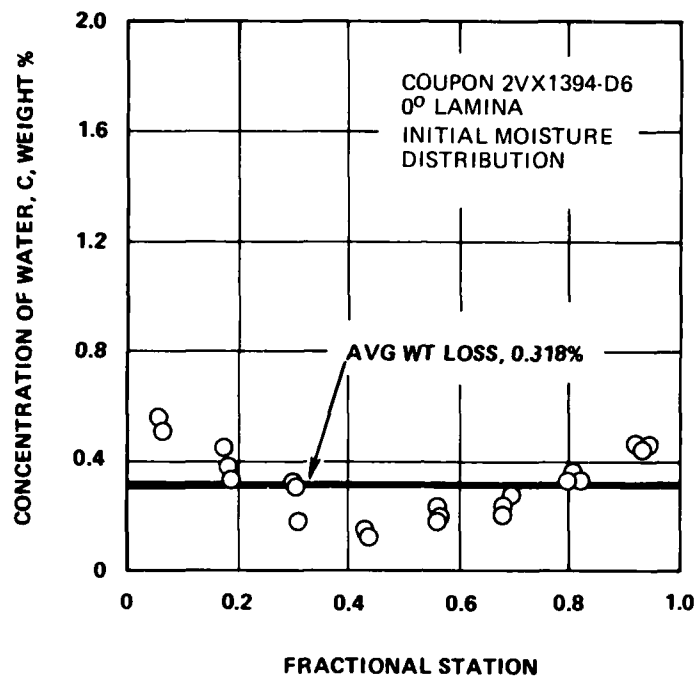


Figure 21.- Initial moisture distribution in 0° unidirectional lamina coupons.

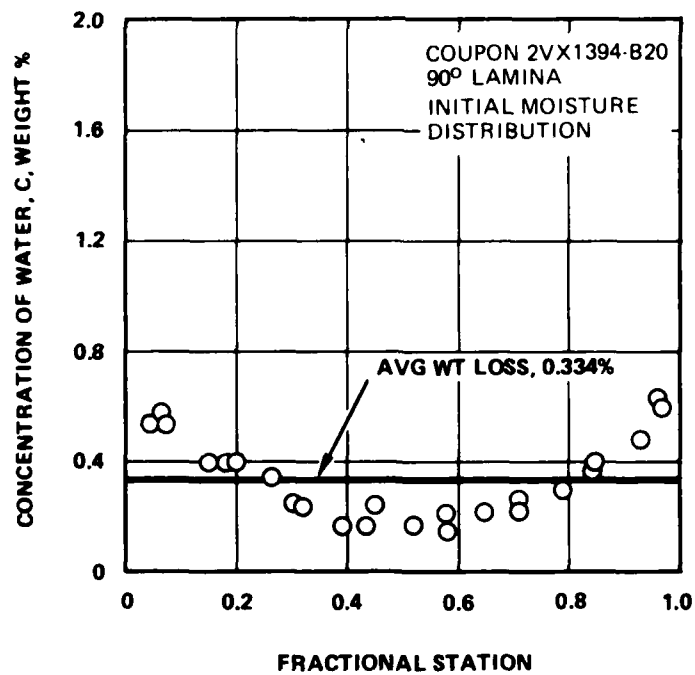
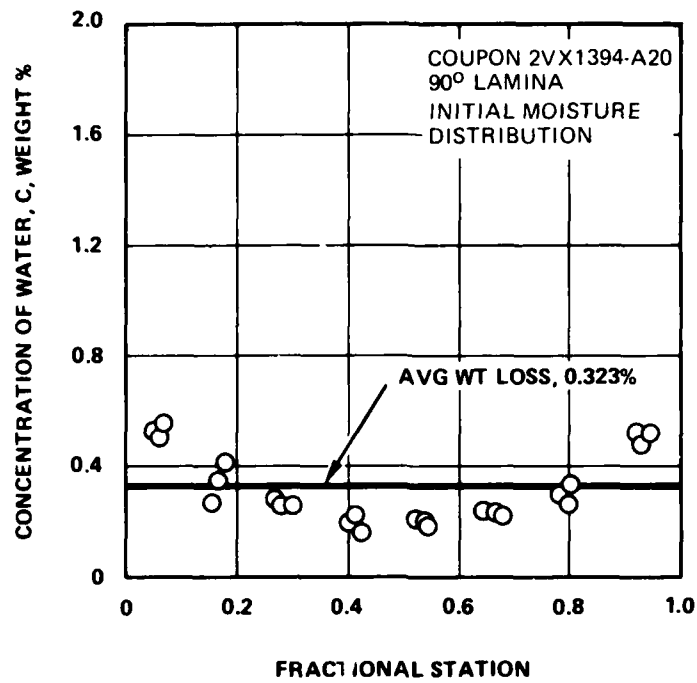


Figure 22. - Initial moisture distribution in 90° unidirectional lamina coupons.

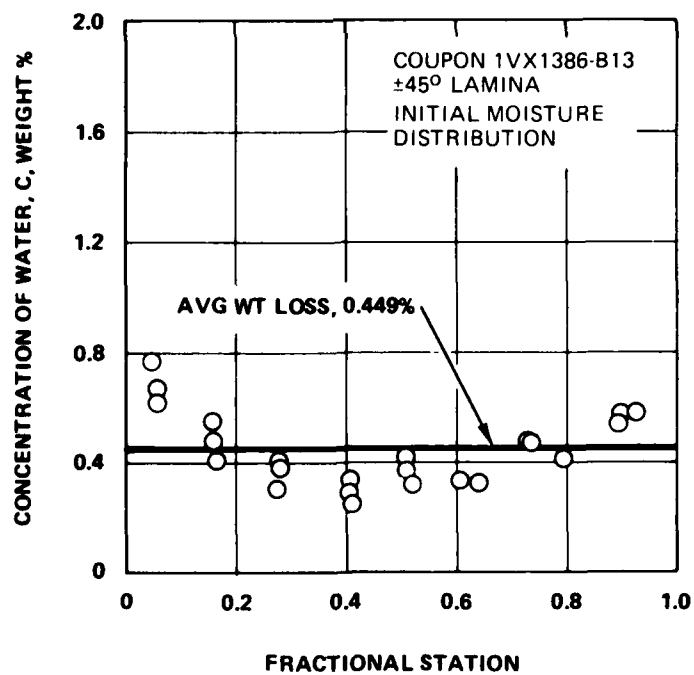
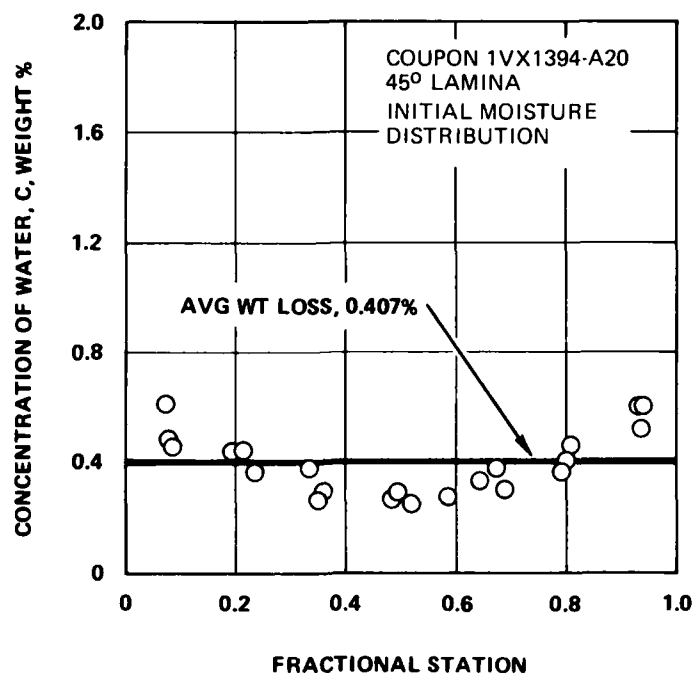


Figure 23. - Initial moisture distribution in ±45° lamina coupons.

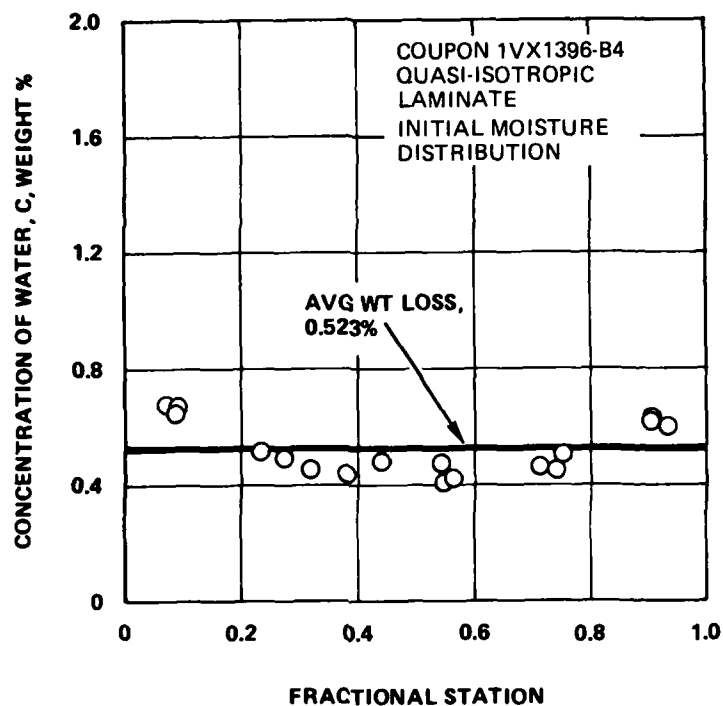


Figure 24. - Initial moisture distribution in quasi-isotropic laminate coupon.

TABLE 9
COMPARISON BETWEEN INITIAL MOISTURE CONTENT OBTAINED
FROM DISTRIBUTION ANALYSIS AND BY DRYING

Lamina Type	Coupon ID	Moisture Content ^a Obtained by Distribution Analysis, %	Moisture Content Obtained by Drying, %	
0°	2VX1394-D6	0.318	0.340 ^b	0.375 ^c
	2VX1394-D8	0.355	0.388	0.421
90°	2VX1394-A20	0.323	0.351	0.383
	2VX1394-B20	0.334	0.348	0.379
±45°	1VX1386-A20	0.407	0.482	0.512
	1VX1386-B13	0.449	0.505	0.535

a Individual sections dried for 72 hours at 93.3°C (200°F)

b Coupon section dried for 408 hours at 93.3°C (200°F)

c Coupon section dried for 2256 hours at 93.3°C (200°F)

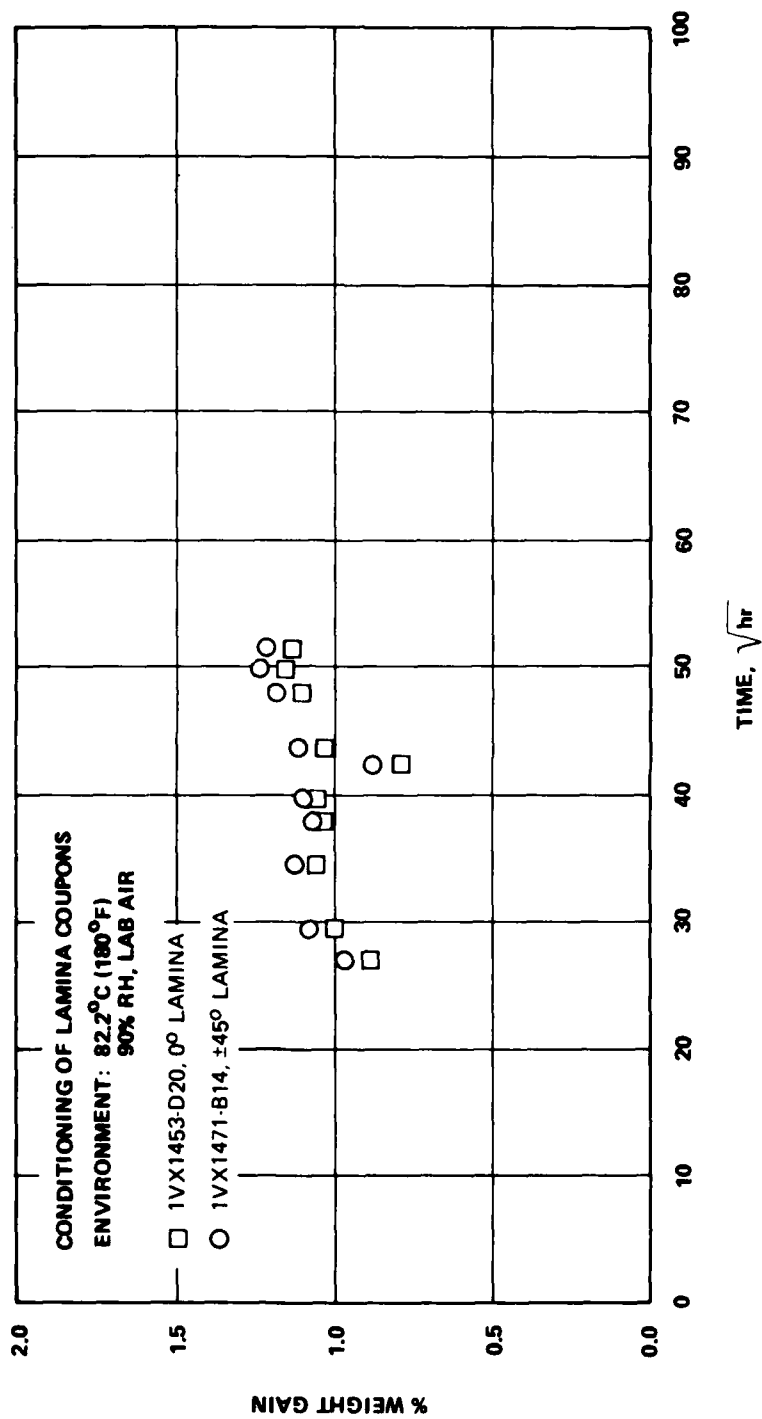


Figure 25, - Moisture weight gain in representative lamina coupons.

TABLE 10

MOISTURE GAIN IN TRAVELER COUPONS CONDITIONED AT 82.2°C (180°F), 90%
R.H. IN LABORATORY AIR

Values are in % Weight Gain

Days After Placement in Chamber	Lamina Type								
	0° Unidirectional			90° Unidirectional			±45°		
	Coupon ID			Coupon ID			Coupon ID		
	2VX1394 D20	1VX1453 D6	1VX1453 D20	2VX1394 A14	2VX1394 B15	1VX1453 A16	1VX1471 A9	1VX1471 B6	1VS1471 B14
0	0	0	0	0	0	0	0	0	0
2	0.060	0.075	0.067	0.059	0.063	0.077	0.101	0.104	0.104
8 ^a	0.057	0.077	0.067	0.054	0.051	0.076	—	—	—
10	—	—	—	—	—	—	0.125	0.139	0.125
30	0.785	0.918	0.895	0.795	0.783	0.911	0.996	1.001	0.967
36	0.915	1.039	1.006	0.926	0.906	1.033	1.113	1.118	1.077
49	0.951	1.134	1.081	0.976	0.962	1.085	1.155	1.154	1.136
59 ^a	0.902	1.052	1.041	0.953	0.954	1.048	1.090	1.110	1.071
65	0.942	1.085	1.065	0.970	1.199	1.072	—	1.125	1.095
74 ^b	0.683	0.799	0.801	0.699	0.699	0.787	0.901	0.888	0.878
79	0.942	1.061	1.031	0.953	0.954	1.047	1.138	1.133	1.116
95	1.017	1.119	1.116	1.023	0.984	1.112	1.197	1.196	1.186
102	1.055	1.164	1.158	1.037	0.986	1.106	1.253	1.256	1.236
109	1.026	1.144	1.139	1.052	1.028	1.143	1.245	1.229	1.233
Average		1.103			1.074			1.236	
Estimated Average Moisture Content		1.44			1.40			1.66	

a — Humidity system within the conditioning chamber malfunctioned for a few hours.

b — Humidity system within the conditioning chamber malfunctioned for two days.

shows the weight gain data in tabular form. Considering the zero day moisture content as a baseline, Table 10 shows that weight gain among the various traveler coupons was quite consistent within a lamina type. Final moisture distribution in representative coupons are shown in Figures 26 to 28 which show that each lamina had essentially reached an equilibrium moisture level. The difference between the final and initial moisture

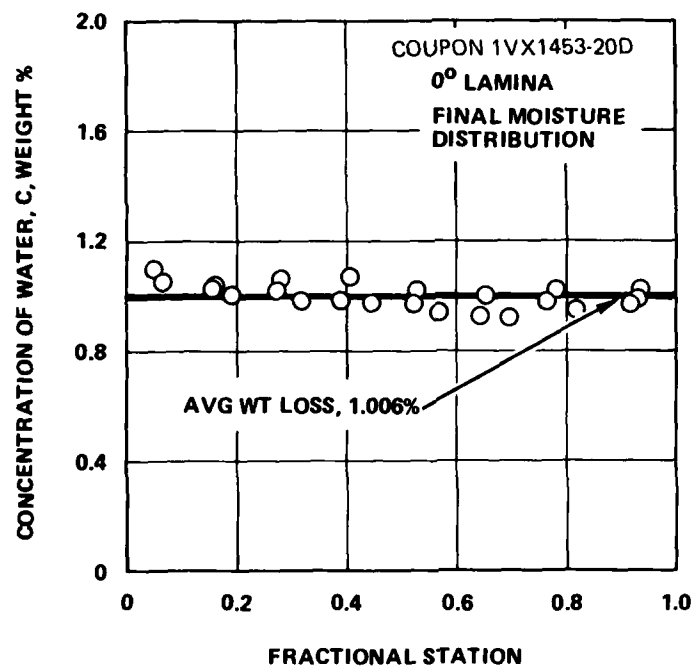


Figure 26. - Final moisture distribution in 0° lamina coupon.

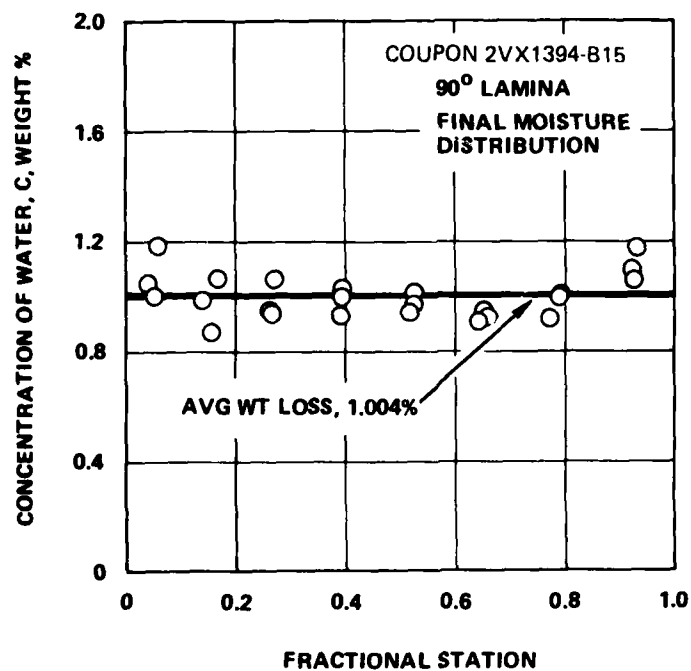


Figure 27. - Final moisture distribution in 90° lamina coupon.

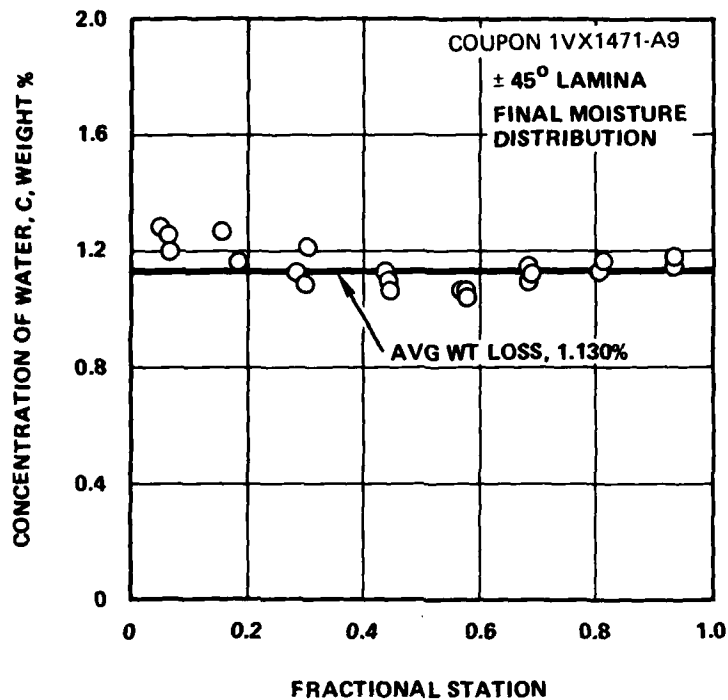


Figure 28. - Final moisture distribution in $\pm 45^\circ$ lamina coupon.

contents of these coupons as obtained by drying, did not agree with the weight gain found by weighing (compare Tables 10 and 11). The discrepancy of approximately 0.4 to 0.5 percent is believed to be due to absorbed bound water which occurs in the 5208 matrix but not in 934,³⁶

TABLE 11.

INITIAL AND FINAL MOISTURE CONTENTS OF LAMINA AND LAMINATE COUPONS DETERMINED BY DRYING OF COUPONS^a

Panel ID	Panel Type	Initial Moisture Content, Weight %	Final ^b Moisture Content, Weight %
2VX1394, 1VX1453	0°	0.336	1.006
2VX1394	90°	0.328	1.004
1VX1386, 1VX1471	±45°	0.428	1.145
1VX1392, 1VX1396	Q.-I.	0.522	

a Moisture content determined by averaging the individual contents of thin slabs obtained for determining moisture distribution.

b Moisture content after 109 days of conditioning at 82.2°C (180°F), 90% in Laboratory Air.

Group 4: Coupons Used for Determining Weight Loss and Moisture Distribution Changes Which Occurred During Static Testing.

Because of the experimental difficulties of statically testing coupons conditioned at 82.2°C (180°F), 90% R.H. in a 82.2°C (180°F), 90% R.H. environment, all of the high temperature static tests were conducted without adding humidity to the laboratory air environment. Therefore, an investigation was conducted to determine the effect on moisture content due to exposure of the specimens to the 82.2°C (180°F), laboratory air environment. Table 12 shows the experimentally measured weight loss for both conditioned and unconditioned coupons which went through the typical static test thermal cycle of five minutes duration (a 2-minute soak at temperature followed by a 3-minute static test). These results show that the time at temperature without high humidity reduced the moisture content by an acceptably low amount. Therefore, the static tests were conducted with a 2-minute soak, sufficient to obtain temperature equilibrium within the coupons, followed by a 3-minute test time.

Environmental Summary

The initial average moisture content within the traveler coupons ranged from 0.3% to 0.6%. Conditioning at 82.2°C (180°F), 90% R.H. for 90 days led to an essentially equilibrium moisture content of ~1.5% within the 0° and 90° unidirectional traveler coupons and ~1.7% in the ±45° coupons. The tests conducted and corresponding estimated average moisture levels are summarized in Table 13.

TABLE 12

PERCENT WEIGHT LOSS OF LAMINA COUPONS DURING STATIC TESTS AT
82.2°C (180°F): TEST TIME APPROXIMATELY 5 MINUTES

Coupon ID	Lamina Type	Test Condition	Wt. Before Test, g	Wt. After Test, g	% Wt. Loss
2VX1394-D9	0°	D ^a	10.9682	10.9623	0.054
2VX1394-D14	0°	D	10.9753	10.9735	0.016
2VX1394-CD	0°	W	11.5098	11.4950	0.129
2VX1394-D5	0°	W	11.3107	11.2971	0.120
2VX1394-A1	90°	D	9.6694	9.6677	0.018
2VX1394-A5	90°	D	10.2975	10.2962	0.013
1VX1453-A1	90°	W	9.5519	9.5489	0.031
1VX1453-A16	90°	W	11.8272	11.8138	0.113
1VX1471-A10	±45°	D	10.3054	10.3034	0.019
1VX1471-A21	±45°	D	10.1872	10.1784	0.086
1VX1386-B9	±45°	W	10.2855	10.2794	0.059

a - D indicates unconditioned coupon;

W indicates coupon conditioned at 82.2°C (180°F), 90% R.H. for 109 days.

TABLE 13

ESTIMATED PERCENT MOISTURE CONTENT WITHIN
COUPONS TESTED IN TASK I

Lamina or Laminate Type	Test Type	Test Environment	Estimated Average Moisture Content %
0°, 90°	Static	R.T. ^b , L.A. ^c	0.4
		82.2°C, Dry ^d	0.4
		82.2°C, Wet ^d	1.5
±45°	Static	R.T., L.A.	0.5
		82.2°C, Dry	0.5
		82.2°C, Wet	1.7
Q-1. ^a	Static & Fatigue	R.T., L.A.	0.6

a Q-1 - Quasi-Isotropic

b R.T. - Room Temperature

c L.A. - Laboratory Air

d Dry - as received moisture content

e Wet - moisture content after conditioning at 82.2°C (180°F), 90% R.H. for 109 days

3.4 MOISTURE AND THERMAL DIFFUSIVITY AND THERMAL EXPANSION PROPERTIES

3.4.1 Moisture Diffusivity

Moisture solubility and diffusivity in Narmco T300/5208 were investigated by Y. A. Tajima³⁷ for use on this contract and other external and internal Lockheed research program. Some of the results obtained by Tajima are given here. The remainder of this subsection is a paraphrase or a direct quote of his Lockheed report.³⁷

A 16-ply unidirectional laminate manufactured in the same manner as the panels used in this program was investigated. Sorption specimens were predried in vacuo over Drierite at 66° or 93°C (150° or 200°F). Desorption specimens were preconditioned to saturation by immersion in distilled water at 66° or 93°C (150 or 200°F), Figure 29. Immersion was selected in preference to a humidity cabinet for experimental expediency and because previous work and published reports indicated that immersion and saturated humidity were equivalent.^{38,39}

The edges of the 1.27 by 2.54 cm (0.5 x 1.0 in.) coupons were sealed with 3M lead foil-backed pressure sensitive tape, No. Y9053, just prior to a sorption or desorption experiment. Duplicate coupons were used in each test. After an exposure time estimated for a given moisture gain or loss (M_t), the coupons were sectioned and the moisture distribution and moisture content (M_t) determined.^{35,40,41} The test schedule is shown in Table 14. All moisture distributions were determined in duplicate. Forty-six moisture distributions in these unidirectional coupons were determined.

The moisture distributions were analyzed assuming either Fickian diffusion with constant diffusion coefficient, D , or concentration dependent diffusion coefficient, $D(C)$.³⁷ The diffusion of moisture in the lamina was followed through one and one-half cycles of sorption-desorption-sorption starting with predried samples.

First Sorption

Typical moisture distributions in coupons determined after sorption at 66°C (150°F)/98% RH are shown in Figure 30. The sorption experiments were

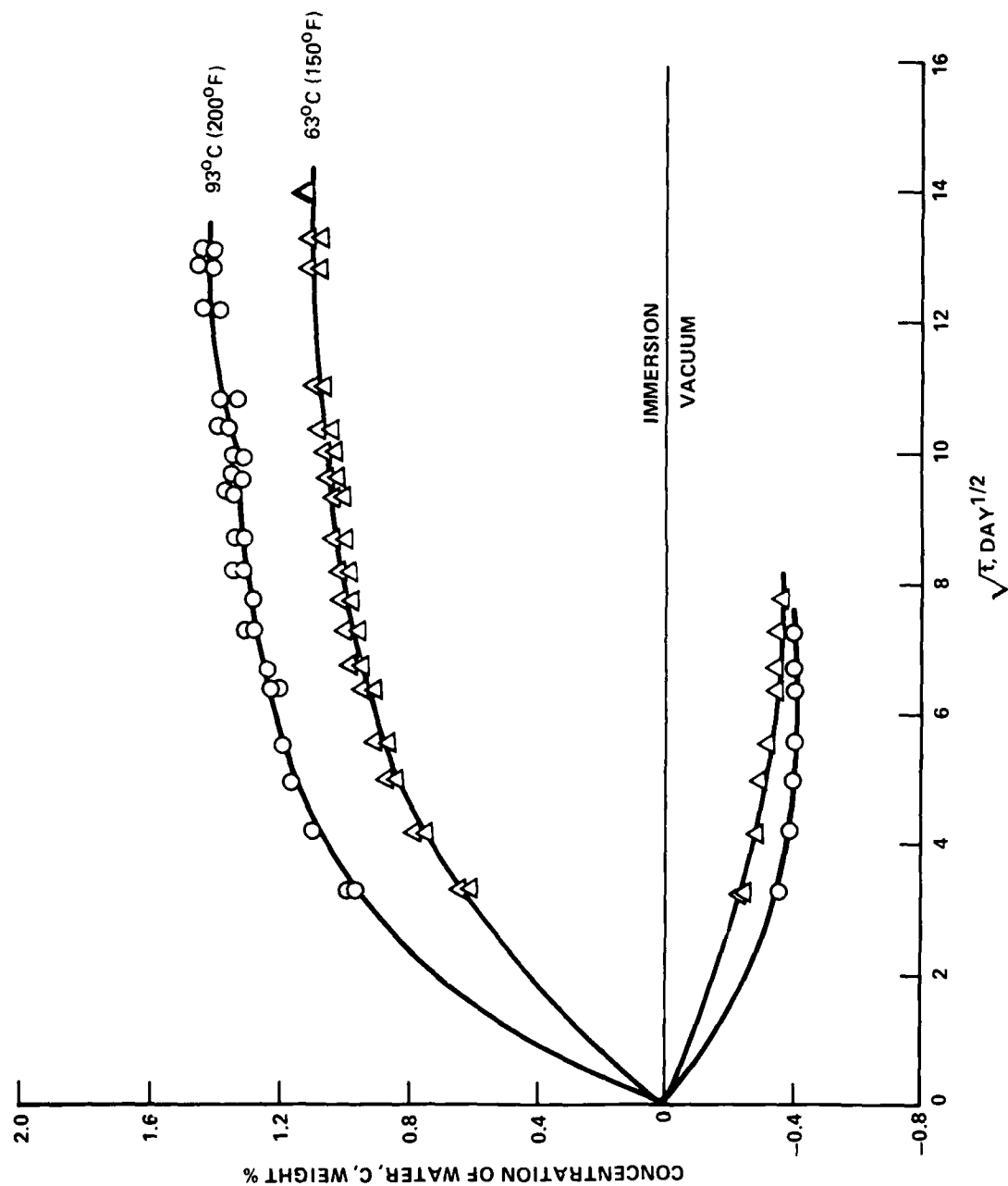


Figure 29. Preconditioning of 16-ply unidirectional laminate (1SV1136) for sorption and desorption studies.

AD-A088 439

LOCKHEED-CALIFORNIA CO BURBANK RYE CANYON RESEARCH LAB

F/6 11/4

EFFECT OF LOAD HISTORY ON FATIGUE LIFE.(U)

JUN 80 J T RYDER

F33615-78-C-5090

UNCLASSIFIED

LR-29586

AFWAL-TR-80-4044

NL

2 of 3

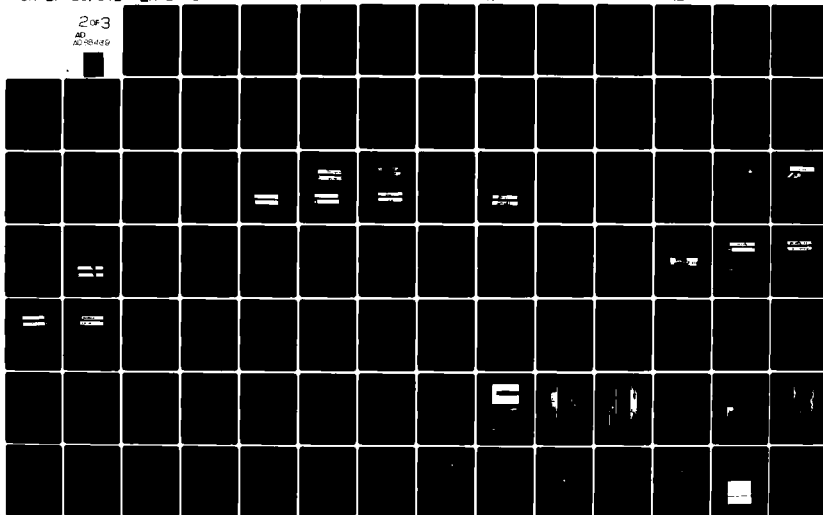
AD
AD-A088 439

TABLE 14
MOISTURE SORPTION TEST SCHEDULE - UNIDIRECTIONAL LAMINATE (1SV1136)

FIRST SORPTION								
Dried		Sorption		Moisture Content, C, Weight %				
°C	°F	°C	°F	0.3	0.6	0.8	1.0	
66	150	66	150		x			
		93	200		x			
93	200	49	120	x	xx			
		66	150	x	xx			
		82	180		x	x		x
		93	200		x			x
FIRST DESORPTION								
Immersion		Desorption		Moisture Content, C, Weight %				
°C	°F	°C	°F	0.3	0.6	0.8	1.2	
66	150	66	150	x	xx	x		x
93	200	66	150					x
		93	200					x
SECOND SORPTION								
Immersion		Desorption		Sorption		Moisture Content, C, Weight %		
°C	°F	°C	°F	°C	°F	0.8	1.0	1.4
66	200	93	150	66	150	x	x	x

Note: x = tests run.
x x = duplicate.

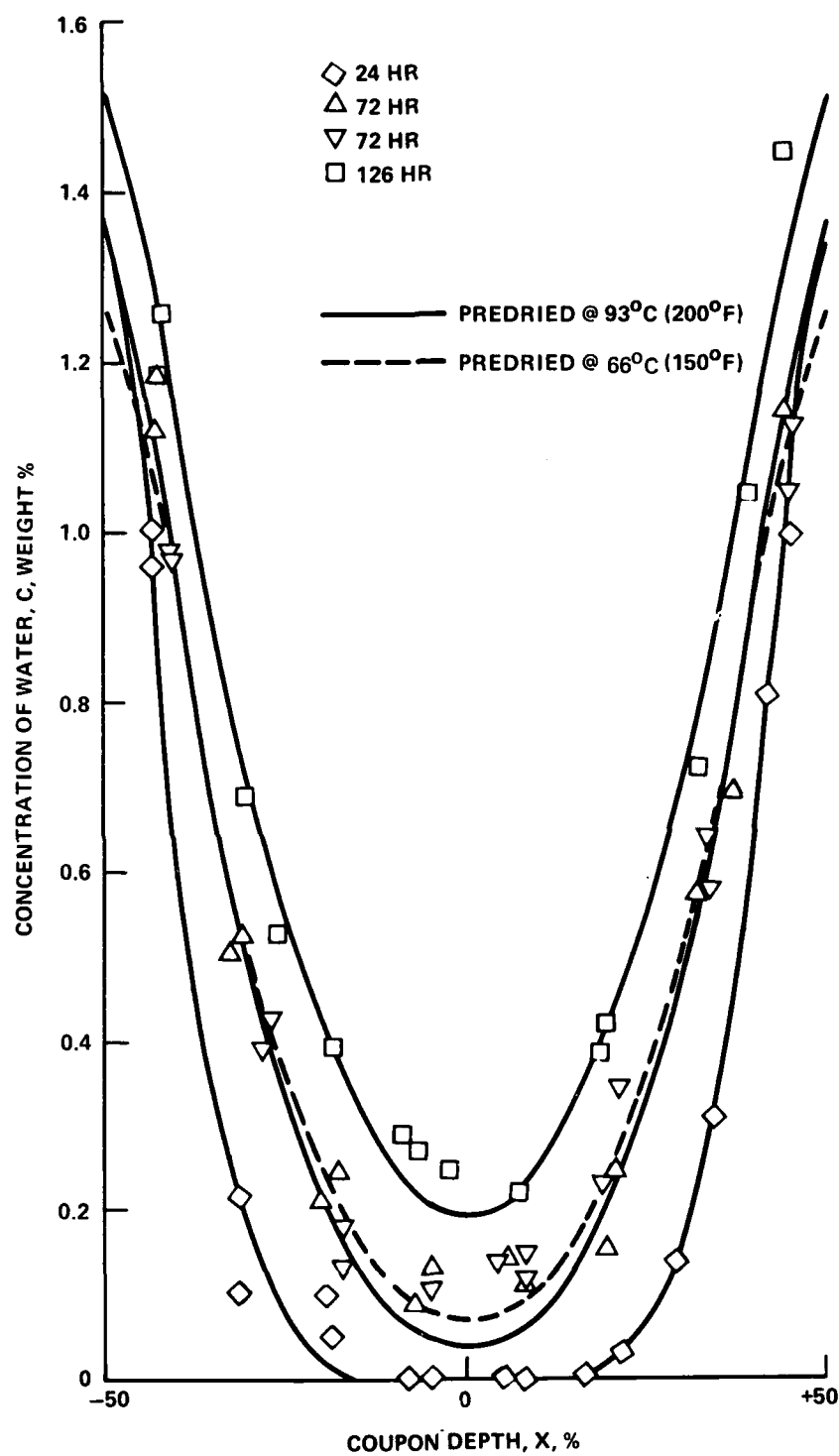


Figure 30. Moisture distributions in unidirectional test coupons following sorption at 66°C (150°F)/98% RH.

performed at 49°, 66°, 82°, and 93°C (120, 150, 180 and 200°F). The exposure time ranged from 6 to 720 hr and the moisture gain from 0.22 to 1.35 w%. The best fit to the sorption data was simple Fickian diffusion with constant diffusion coefficient. Typical calculated moisture distributions are presented in Figure 30. In this model,⁴² both the saturated concentration, C_s , and diffusion coefficient, D , are adjustable parameters. The values of C_s so calculated, Figure 31, appeared to increase initially with conditioning to a constant value of 1.409 ± 0.070 w% in this unidirectional laminate. This value is similar to that found for the VX material used in this program and described in Section 3.3.

The calculated value of C_s is seen to be equal to the moisture gain (M_t) at the first plateau of the sorption kinetics curve, Figure 32. However, the "equilibrium" moisture gain is greater than this value of C_s , which is evidence for the existence of a second diffusion mechanism or a physical change in the laminate. The diffusion coefficients were calculated for all exposure times; the calculated values of D are tabulated in Table 15. The value of D determined from the moisture distributions at 66°C (150°F) is somewhat higher [1.37×10^{-3} mm²/hr (2.12×10^{-6} in²/hr)] than that calculated by the sorption kinetics method [1.06×10^{-3} mm²/hr (1.65×10^{-6} in²/hr)]. The temperature relationship, Arrhenius equation, is shown in Figure 33. The activation energy agrees quite well with the values reported by Whitney and Browning for Hercules AS/3501-5.⁴³ Although the agreement may be fortuitous, the trend of the activation energy for this layup and also for others³⁷ suggests that the activated diffusion of moisture in graphite/epoxy laminates may vary intrinsically with fiber layup, and, in fact, may be less energetic in the more restricted matrices as shown in Table 16.

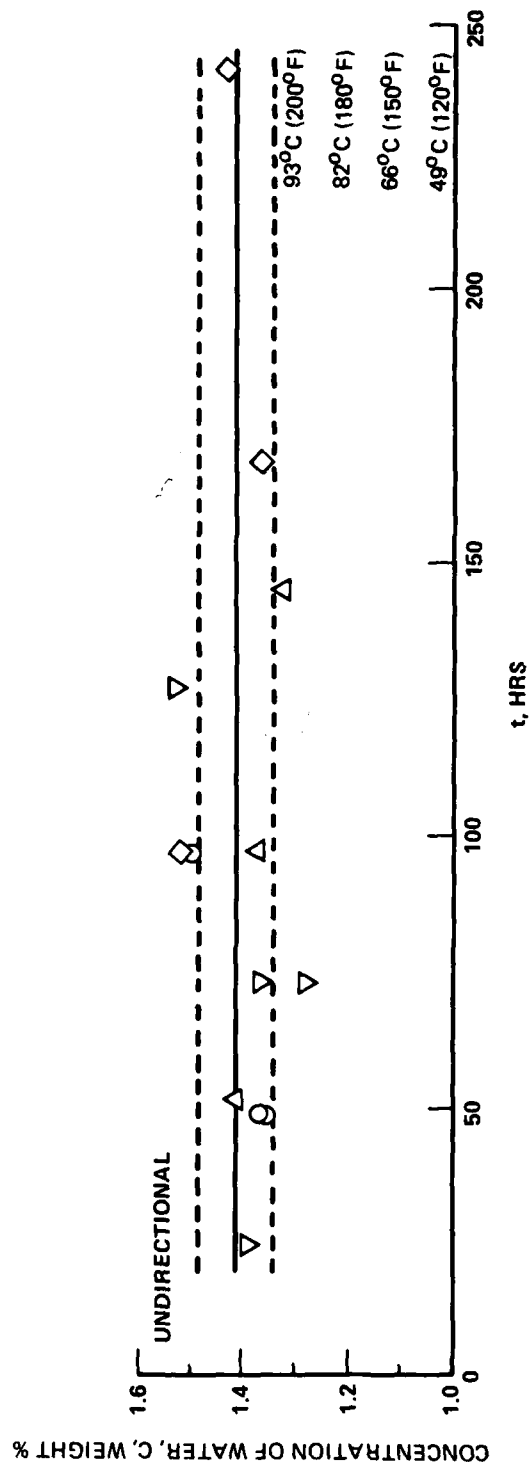


Figure 31. Saturated concentrations, C_s , calculated from moisture distributions in sorption experiments. Dashed lines represent error limits (one standard deviation).

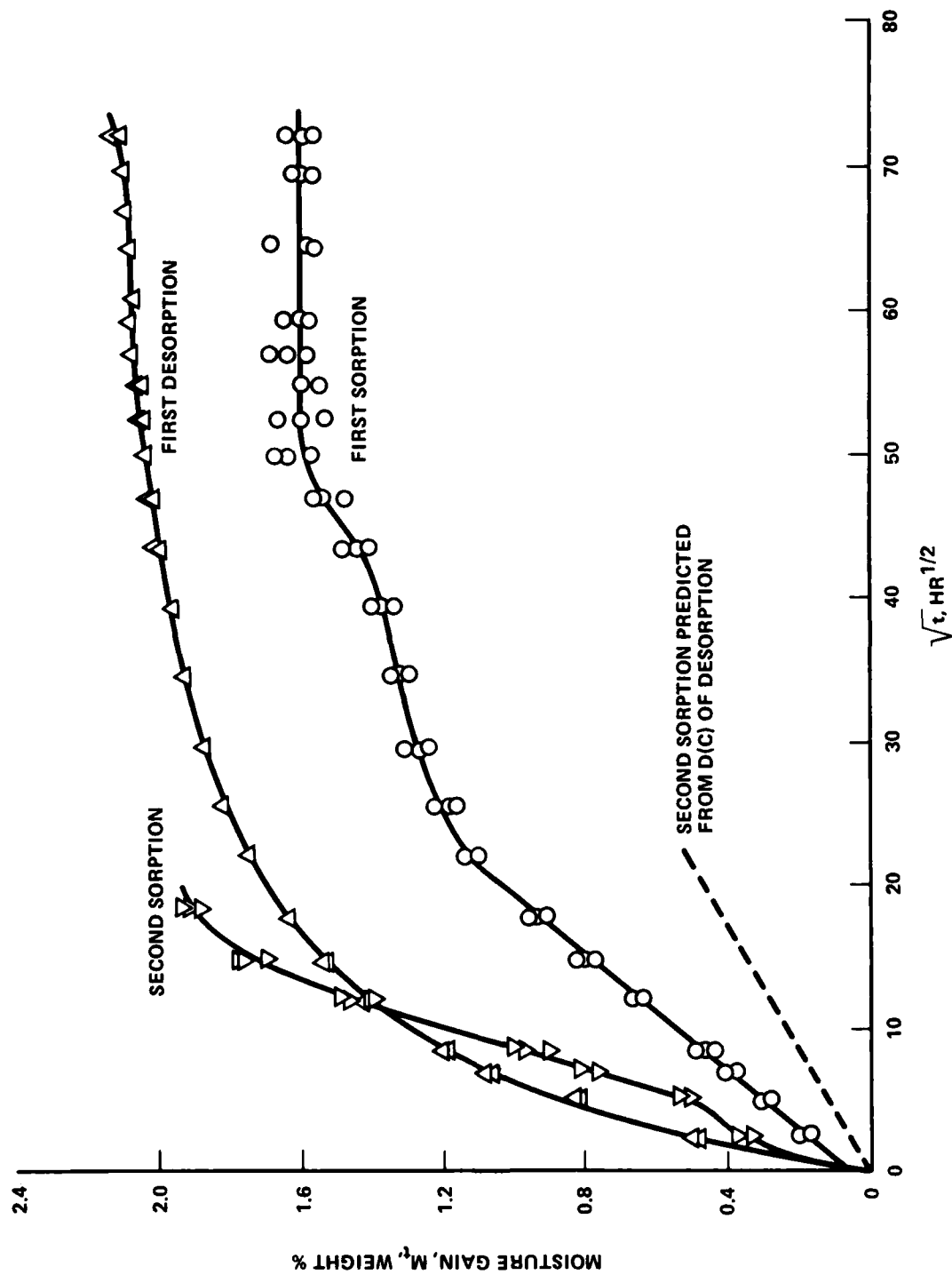


Figure 32. Sorption-desorption kinetic curves at 66°C (150°F) of unidirectional laminate. Desorption curve is for triplicate coupons previously saturated by immersion at 93°C (200°F).

TABLE 15
 DIFFUSION COEFFICIENT, D, AND SATURATED
 CONCENTRATION, C_s: UNIDIRECTIONAL PANEL
 1SV1136

Temperature		1/T 10 ⁻³ °C ⁻¹	Time hr	Saturated Concentration C _s w%	Diffusion Coefficient, D	
°F	°C				10 ⁻³ mm ² /hr	10 ⁻⁶ in ² /hr
200	93.3	2.729	48.0	1.351	4.4441	6.873
			48.0	1.365	4.454	6.892
			96.0	1.509	3.734	5.779
180	82.2	2.814	50.5	1.415	2.881	4.458
			96.0	1.376	2.516	3.894
			144.0	1.326	2.333	3.610
150	65.6	2.953	24.0	1.380	1.338	2.071
			72.0	1.355	1.316	2.037
			72.0	1.271	1.630	2.523
120	48.9	3.106	126.0	1.518	1.300	2.011
			96.0	1.518	0.655	1.013
			168.0	1.360	0.731	1.131
			240.0	1.429	0.688	1.065

Std. Dev., $\sigma = 16.2 \times 10^{-3} \text{ mm}^2/\text{hr}$ ($0.25 \times 10^{-6} \text{ in}^2/\text{hr}$)

$\sigma = 20.7 \times 10^{-3} \text{ mm}^2/\text{hr}$ ($0.32 \times 10^{-6} \text{ in}^2/\text{hr}$) expected (analysis of error)

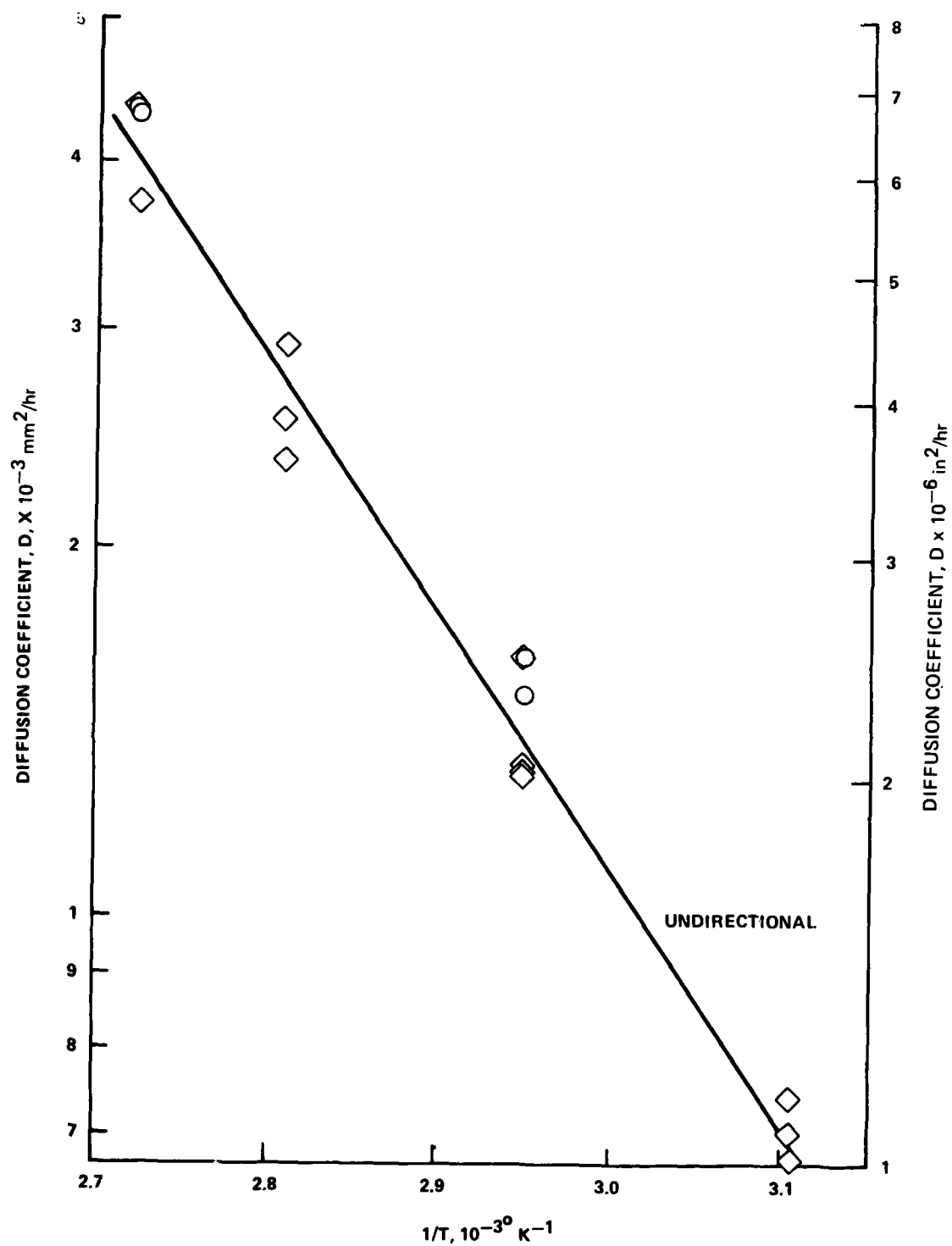


Figure 33. Arrhenius relationships of D and $1/T$ for sorption in 98% RH at 49, 66, 82, and 93°C (120, 150, 180, and 200°F)

TABLE 16
ACTIVATION ENERGIES FOR VARIOUS COMPOSITES

Composites	Ply Orientation	E, cal/g mole	Ref
3501-5	Neat resin	13,400	43
AS/3501-5	(0 ₄)t	9,470	43
T300/5208	(0 ₁₆)t	9,440	37
T300/5208	(±45/0/±45/0 ₃) _s	7,470	37
AS/3501-5	(0/90) ₅	6,980	43

First Desorption

Saturation by Immersion in Water. - Unidirectional coupons were saturated, prior to the desorption studies, by immersion in distilled water at 66°C or 93°C (150 or 200°F). Data taken during this preliminary conditioning permitted determination of C_s over a broad temperature range, by immersion, to compare with determinations at 98% RH, Table 17. The value of C_s was found to be higher in angle-ply than in unidirectional laminates.³⁷ This reflects the ease with which moisture diffuses into the laminate. The difference between 98% RH and immersion at 93°C (150°F) was statistically not significant. However, the value of C_s was markedly higher on immersion at 93°C (200°F). Since chemical thermodynamics dictates that saturated vapor and immersion should be equivalent with regard to solubility, Tajima hypothesized³⁷ that differences in the value of C_s were due to physical or mechanical differences between unidirectional and angle-ply laminates and to changes thereof with time and temperature of exposure.

Desorption following saturation at 66°C (150°F). - Moisture distributions following desorption at 66°C (150°F)/vacuo in coupons, which had been saturated by immersion at 66°C (150°F), are shown in Figure 34. Evidently, desorption is not simple Fickian diffusion. The moisture distributions were too flat near the mid plane and bowed out near the boundary layer.

TABLE 17
SATURATED CONCENTRATION, C_s , OF MOISTURE IN T300/5208
UNIDIRECTIONAL LAMINATE

C_x , w%	Method
1.409 ± 0.070	Moisture distributions at 49°, 66°, 83°, and 92°C (120, 150, 180 and 200°F) and 98% R.H.
1.601 ± 0.044	Saturation at 66°C (150°F)/98% RH, 5200 hrs.
1.484 ± 0.081	Immersion at 66°C (150°F), 4,700 hrs.
2.059 ± 0.050	Immersion at 92°C (200°F), 4,100 hrs.

Furthermore, analysis of the curves by simple Fickian diffusion theory did not lead to constant values for C_s or D .

The moisture distributions were analyzed using a number of models for concentration dependent diffusivity.³⁷ The best relationship appeared to be a linear function with second-order discontinuities, Figure 35. The functions, $D(C)$, for 66°C (150°F) were;

Unidirectional (1SV1136).

$$D = 1.284 \times 10^{-7} \text{ in}^2/\text{hr}, C \leq 0.162 \text{ w\%}$$

$$D = (3.981 \times 10^{-6})C - (5.169 \times 10^{-7})\text{in}^2/\text{hr}, 0.162 < C \leq 1.043 \text{ w\%}$$

$$D = (2.029 \times 10^{-4})C - (2.080 \times 10^{-4})\text{in}^2/\text{hr}, C > 1.043 \text{ w\%}$$

Note: multiply the above by 6.462×10^2 to convert to mm^2/hr

The calculated moisture distributions are shown in Figure 34. The standard deviations are 0.089 w%. The deviation is within the error expected from weighing and in-batch variations in thickness and permeability.

The concentration dependent diffusivity actually may be a more complex function. Although the above equation fits the experimental data quite well for the shorter and longer times, the calculated distributions are too concave for the intermediate times. The experimental distributions

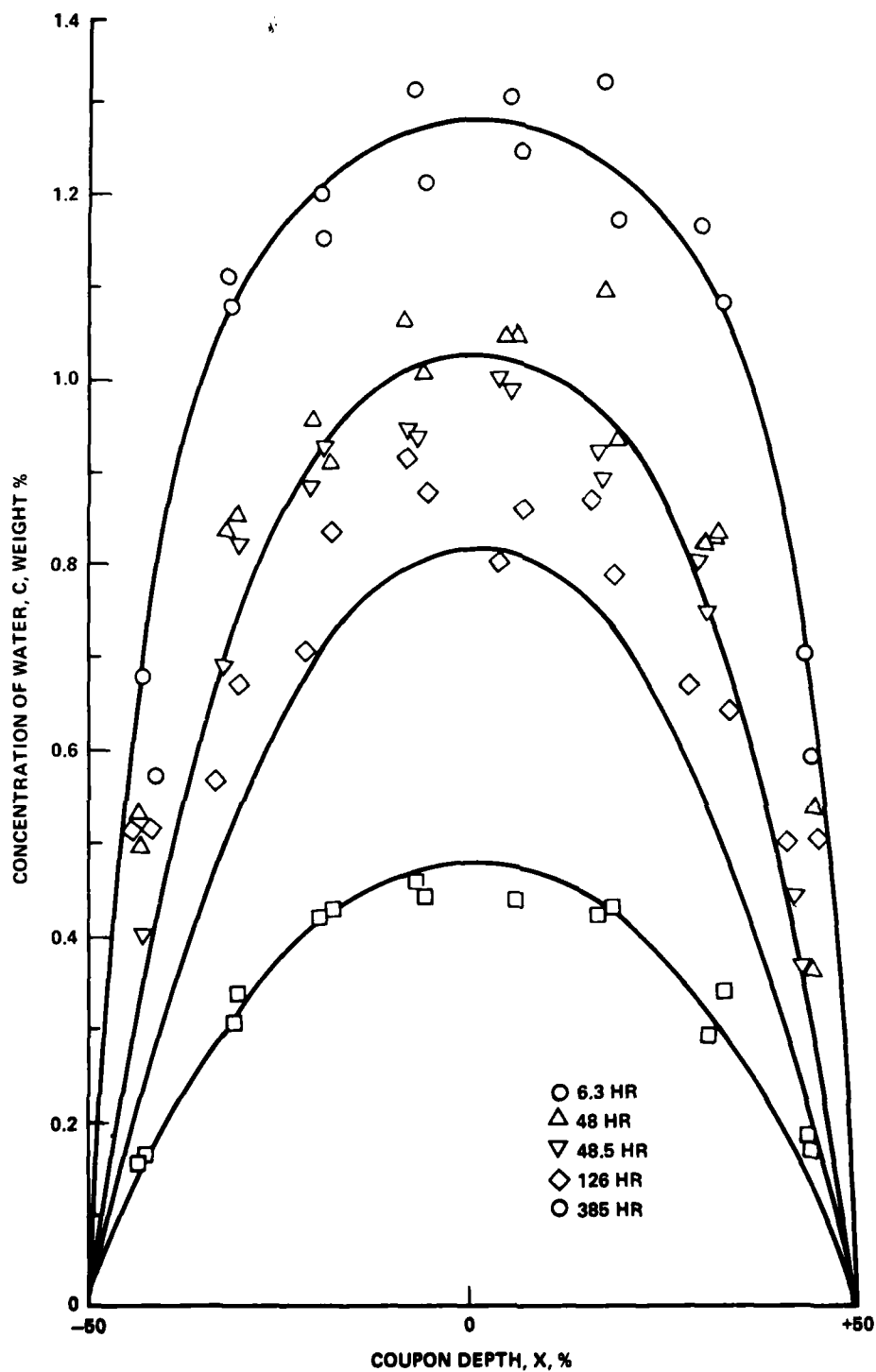


Figure 34. Moisture distributions in unidirectional test coupons after desorption in vacuo over Drierite at 66°C (150°F). Test coupons first saturated by immersion at 66°C (150°F).

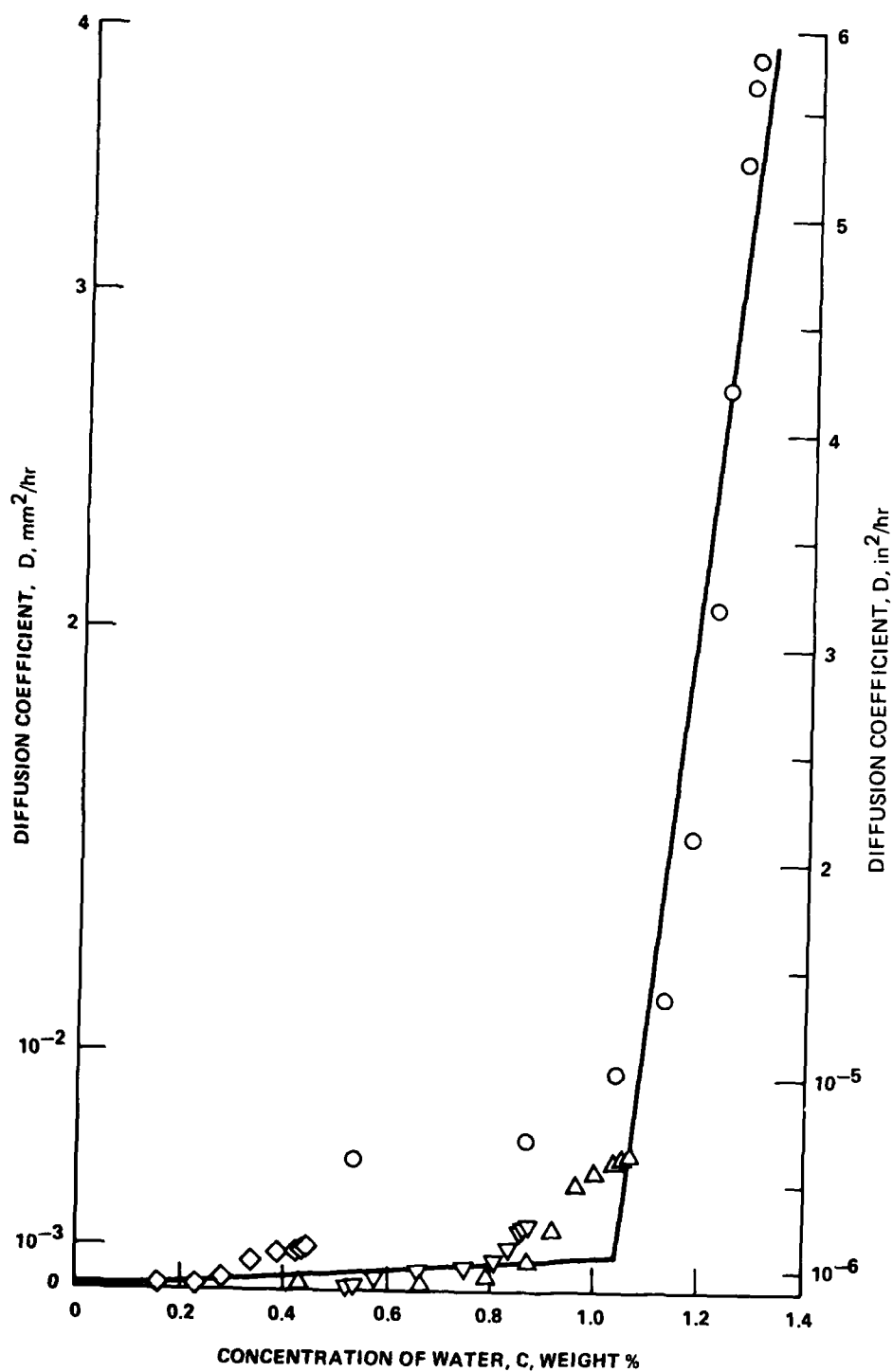


Figure 35. Function $D(C)$ for unidirectional laminate calculated from the moisture distributions shown in Figure 34 (desorption at 66°C (150°F)).

are flatter near the midplane and bow out more near both surfaces. The implication is that a step or another linear section should cut across the break at $C = 1.03 - 1.04$ w%. However, the important feature of $D(C)$ is not altered; i.e., D increases slightly with C until a critical concentration is reached, at which value D increases sharply with further increase of C . The desorption kinetics (moisture loss vs square root of time) were found to be almost exactly the same for unidirectional and angle ply laminates.³⁷ On the other hand, the diffusivity during sorption was higher in an angle-ply than in a unidirectional laminate.³⁷ The activation energy for sorption was found to be lower for angle-ply than for unidirectional laminates.³⁷ Thus, less energy was required to form a "hole" for a water molecule in the cross-ply laminate. The lower energy required may be due to greater residual tensile stresses in angle-ply laminates. The residual stresses are apparently relieved during hygrothermal conditioning so that the desorption kinetics become equal regardless of fiber orientation.

Desorption following saturation at 93°C (200°F). - The results of desorption experiments in vacuo over Drierite at 66° and 93°C (150° and 200°F) with coupons which were saturated by immersion at 93°C (200°F) are presented in this section. The moisture distributions in the unidirectional laminate appeared to be Fickian with concentration dependent diffusivity, $D(C)$, Figure 36. Moisture distributions in angle-ply laminates were found to be non-Fickian³⁷ as acceptable approximations to the moisture distributions could not be obtained assuming Fickian diffusion. The data suggested that the laminates may be damaged on prolonged immersion in water at 93°C (200°F) by the formation of a connected network of voids or capillary cracks.

Second Sorption

The sorption kinetics calculated by the function $D(C)$ derived from the desorption data, predict that the initial diffusion rate should decrease after one hygrothermal cycle, Figure 32. The first sorption curve was obtained for predried unidirectional specimens exposed to 98% RH at 66°C (150°F). The first desorption kinetic curve was obtained for specimens initially saturated with water at 93°C (200°F). The second kinetic curve was obtained for the

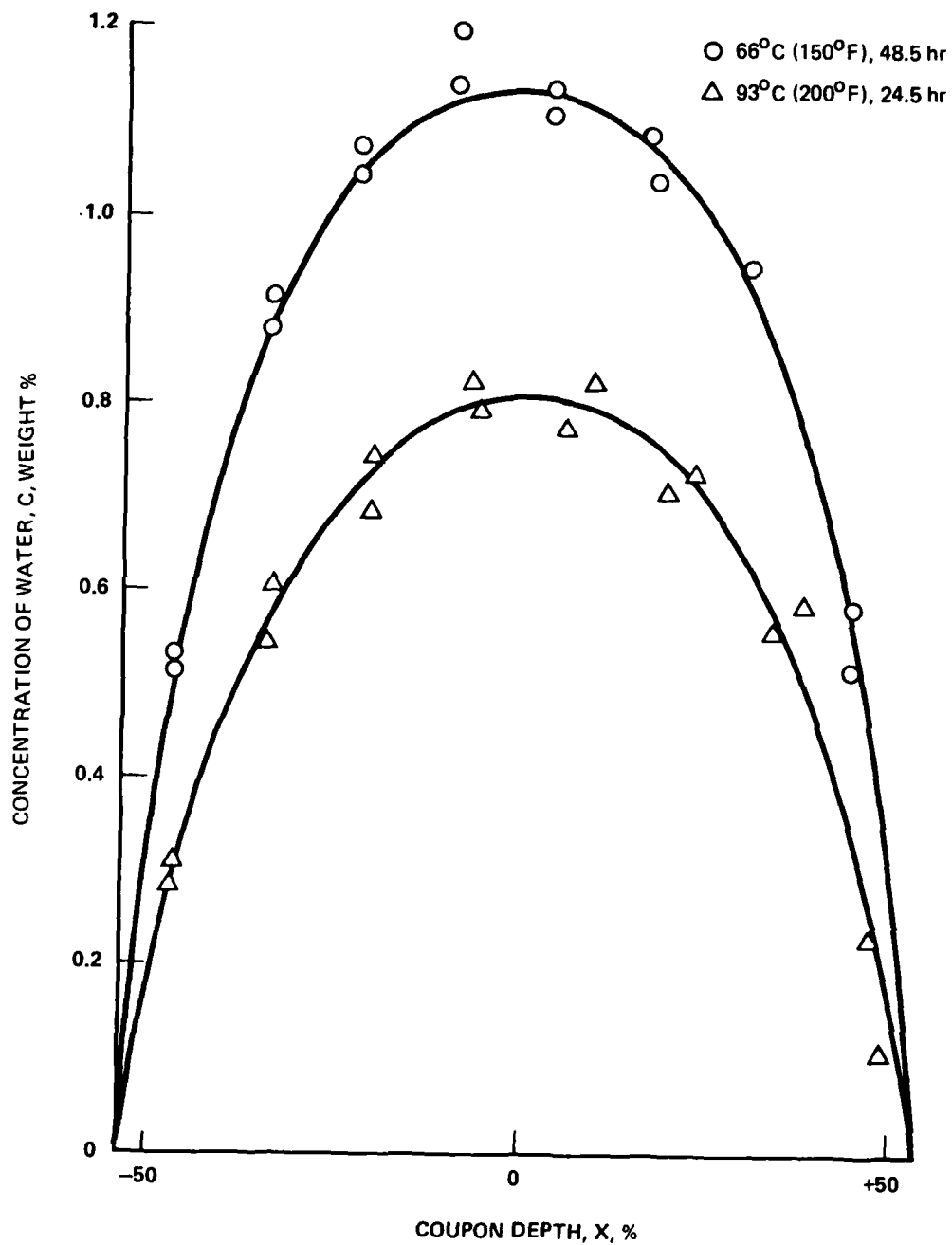


Figure 36. Moisture distributions in desorption of coupons first saturated by immersion at 93°C (200°F). Desorption in the unidirectional test coupons appear to be Fickian with concentration dependent diffusion coefficient.

latter specimens after the first desorption. The initial constant diffusion rate of the second sorption is much greater than predicted and almost equal to, but less than the initial diffusion rate of the first desorption. This observation has also been reported with 8-ply Hercules AS/3501-5 laminates.⁴⁴

The initial portion of the curves in Figure 32 are shown with expanded scales in Figure 37. For second sorption, the plot of M_t vs \sqrt{t} is almost linear to the equilibrium concentration. Moisture distributions determined during the second sorption cycle are presented in Figure 38. These indicate that the diffusion process is anomalous. The second sorption and first desorption curves of Figure 37 and the distributions of Figure 38 suggest Alfrey's Class II diffusion^{45,46}; that is, diffusion which is rate-controlled by polymer relaxation. In ideal Class II diffusion, the weight gain is linear with time until equilibrium saturation is established, and there is a discrete discontinuity or diffusate front between the near saturated swollen layer and the almost unpenetrated substrate ahead of the front. Shear is generated in the layer ahead of the front, and, as relaxation occurs, the diffusate rapidly diffuses into the expanded substrate. Crank⁴⁷ refined the analysis to include an instantaneous partial relaxation followed by a slower relaxation process. In this model, the concentration increases almost instantaneously to some value C_x at the moving boundary, then increases slowly to the final equilibrium concentration C_o behind this front. $D(C)$ is assumed to be a step-function with D increasing as C exceeds C_x . In this Class II diffusion, M_t increases almost linearly with \sqrt{t} to the equilibrium concentration. The moisture distributions are similar to those found for second sorption, Figure 38.

Effect of Hygrothermal Conditioning on Diffusivity

The conclusion that the first sorption of moisture in graphite/epoxy laminates is simple Fickian (constant diffusion coefficient) is consistent with the many reports in the literature. The evidence obtained by Tajima³⁷ indicated that subsequent (first) desorption is still Fickian but with concentration dependent diffusion coefficient.

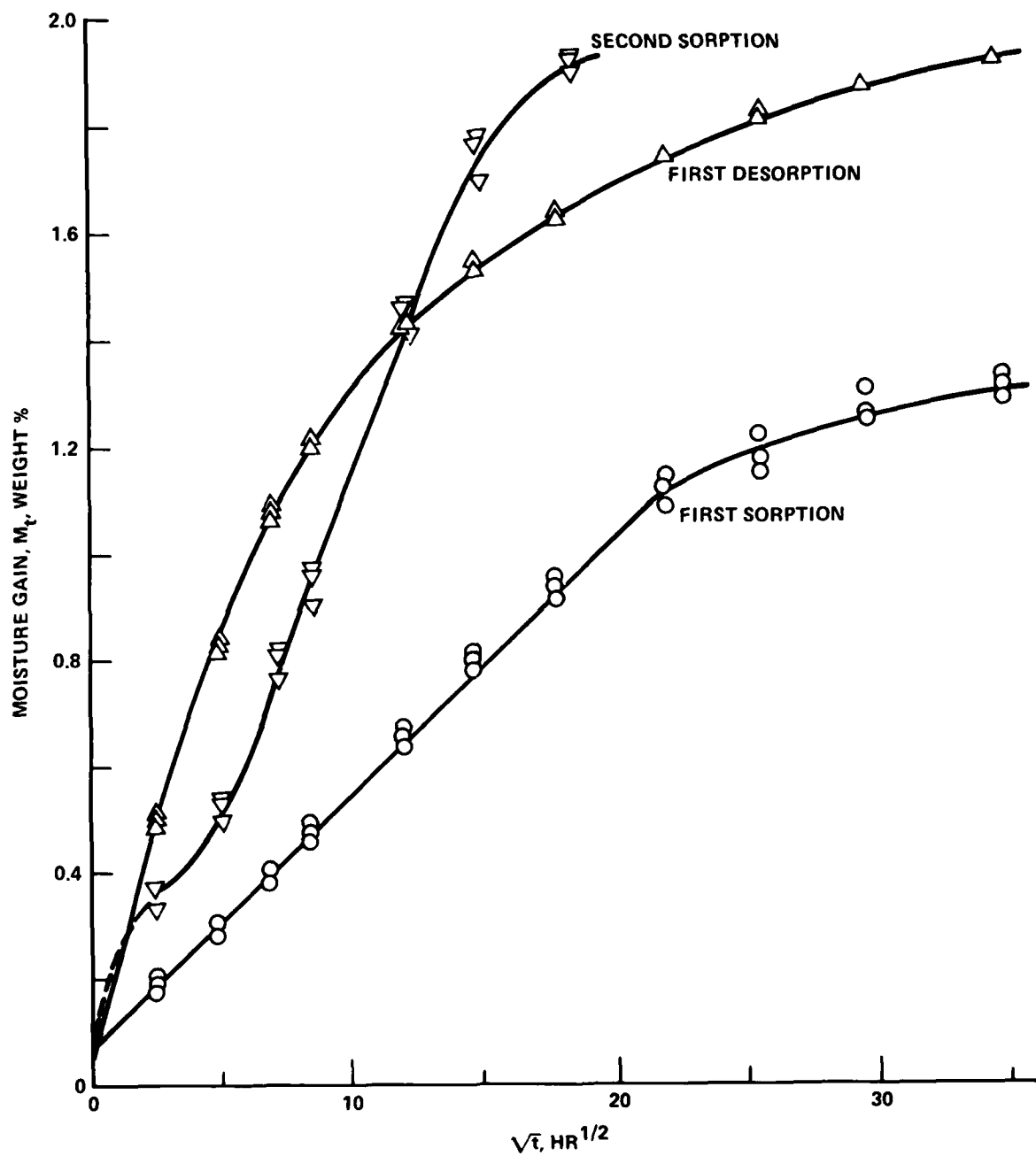


Figure 37. Sorption-desorption kinetic curves at 66°C (150°F) (See Figure 32). The almost linear s-shaped second sorption curve is characteristic of Crank's modified Class II diffusion.

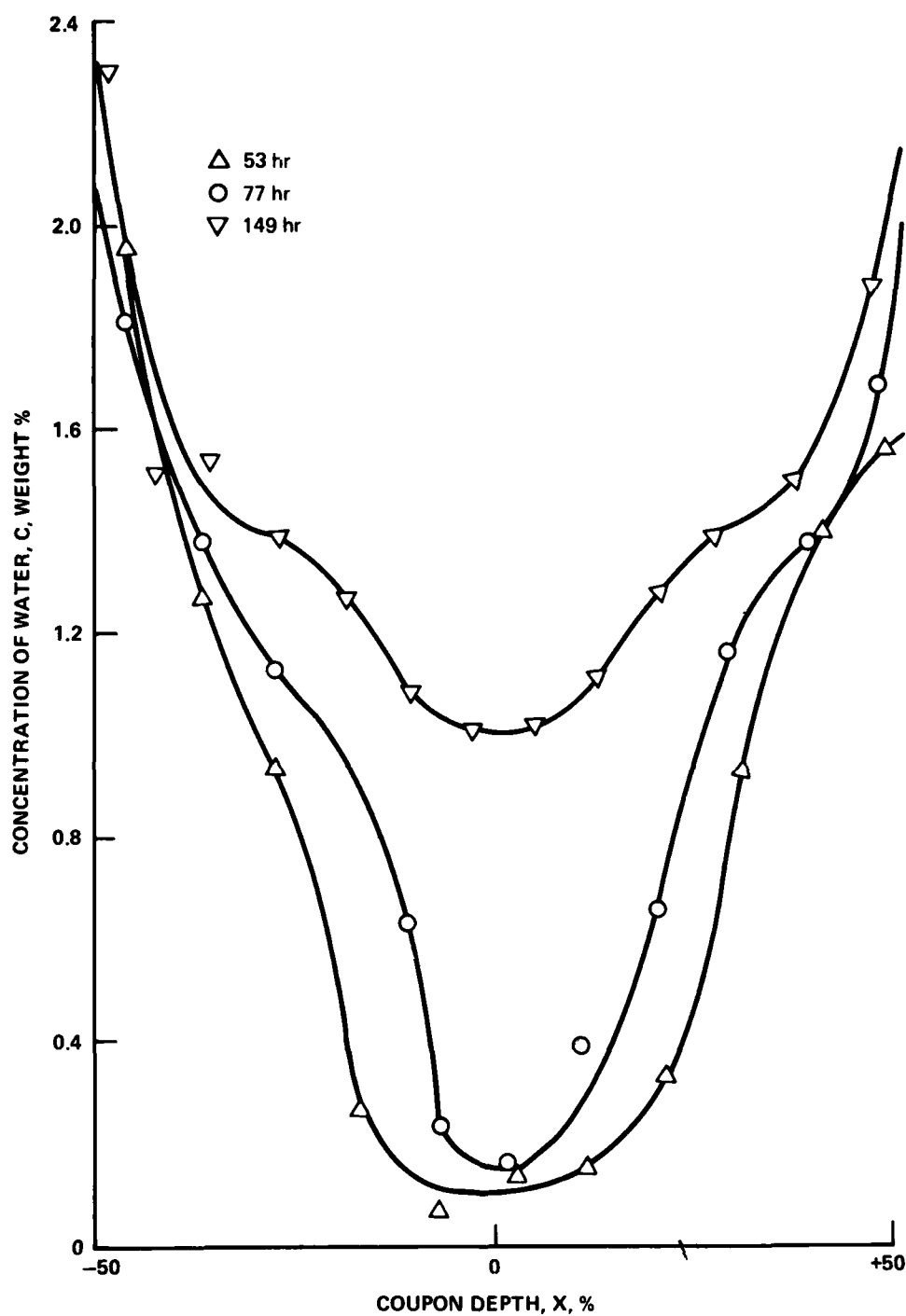


Figure 38. Moisture distributions in unidirectional coupons during second sorption of Figure 37. The distributions are characteristic of Crank's modified Class II diffusion.

Resorption (second sorption) appeared to be modified Class II diffusion. Swelling, at least initially, was rapid and without a noticeable induction period, and the diffusion rate was strain-dependent. Although the data was consistent with Crank's modified Class II diffusion, an alternative explanation was not ruled out by the data that were currently available.

Swelling and shrinking with attendant shear in the matrix may cause crazing and/or the formation of a connected network of microcracks^{43,44 48}. The implication is that diffusion may actually become Poiseuille flow after hygrothermal cycling. Fluid flow through a somewhat porous matrix with simultaneous Fickian diffusion could then conceivably account for the facts of Figures 37 and 38.

Shirrell, Leisler and Sandow⁴⁹ recently published scanning electron photomicrographs of T300/5208 coupons that had been conditioned over a range of temperatures, relative humidities and immersion in water. Microcracking was observed in the surface and exposed edges. The damage was found to increase with temperature, relative humidity and postcure, but was substantially less severe on immersion than on exposure to saturated water vapor. The authors attributed the microcracking not to the hygro- or hydrothermal conditioning per se, but to the cycling (inverted thermal spiking) imposed by the periodic removal of the coupons from the conditioning chambers to be weighed in order to follow moisture gain.

In the study by Tajima,³⁷ the samples showing anomalous diffusion on second sorption were conditioned by immersion at 93°C (200°F) which is higher than the upper limit investigated by Shirrell, et al.⁴⁹ On the other hand, the coupons were cycled to room temperature only twice; once when they were removed from the water bath to begin the desorption phase and again when they were transferred to the 93°C (150°F)/98% RH chamber for the second sorption study. Hence, one cannot conclude that the same type of surface damage occurred in the current investigation as was observed by Shirrell, et al.⁴⁹

3.4.2 Thermal Properties

Thermal expansion, thermal conductivity, thermal diffusivity and specific heat measurements were performed at Lockheed Missiles and Space Company under subcontract to Lockheed-California Company. All measurements were performed on 0° or 90° unidirectional specimens in the "as-received" condition (i.e., no pretreatment to control moisture content).

Thermal Expansion

A fused quartz dilatometer was used to measure thermal expansion of three 0° and three 90° specimens from panels 2VX1394 and 1VX1453. Each specimen was nominally 23.5 cm (9-1/4 in.) long by 2.54 cm (1 in.) wide, and the ends were polished to present flat and parallel surfaces for contact with the mating surfaces of the dilatometer pushrod and outer tube. Change in specimen length, referenced to the dilatometer outer tube, was measured with a crystal transducer having a least count of 2.54×10^{-5} mm (1×10^{-6} in.). The specimen was placed in the dilatometer and the assembly immersed into a temperature controlled tubular shaped chamber with only the supporting structure and transducer out of the variable temperature environment. The assembly was initially cooled, to -101°C (-150°F). Upon stabilization of specimen temperature and the transducer output, the assembly was heated at 1° - 2°C/min. (2° - 3°F/min.) to a maximum temperature of 121°C (250°F). Specimen temperature and transducer output were recorded at 1 min intervals during this temperature excursion. Thermal expansion was calculated from

$$\Delta L/L = (\Delta L/L)_T + (\Delta L/L)_D$$

where $(\Delta L/L)_T$ is the transducer dimensional change reading divided by the sample length at 19.4°C (67°F) and $(\Delta L/L)_D$ is the fused quartz dilatometer dimensional change per unit specimen length. This latter factor was determined from repeated calibration runs using NBS Standard Reference Material SRM 739; a fused silica standard obtained from NBS.

Typical results of the measurements on the six specimens are shown in Figures 39 and 40. The squares represent data points taken at 14°C (25°F)

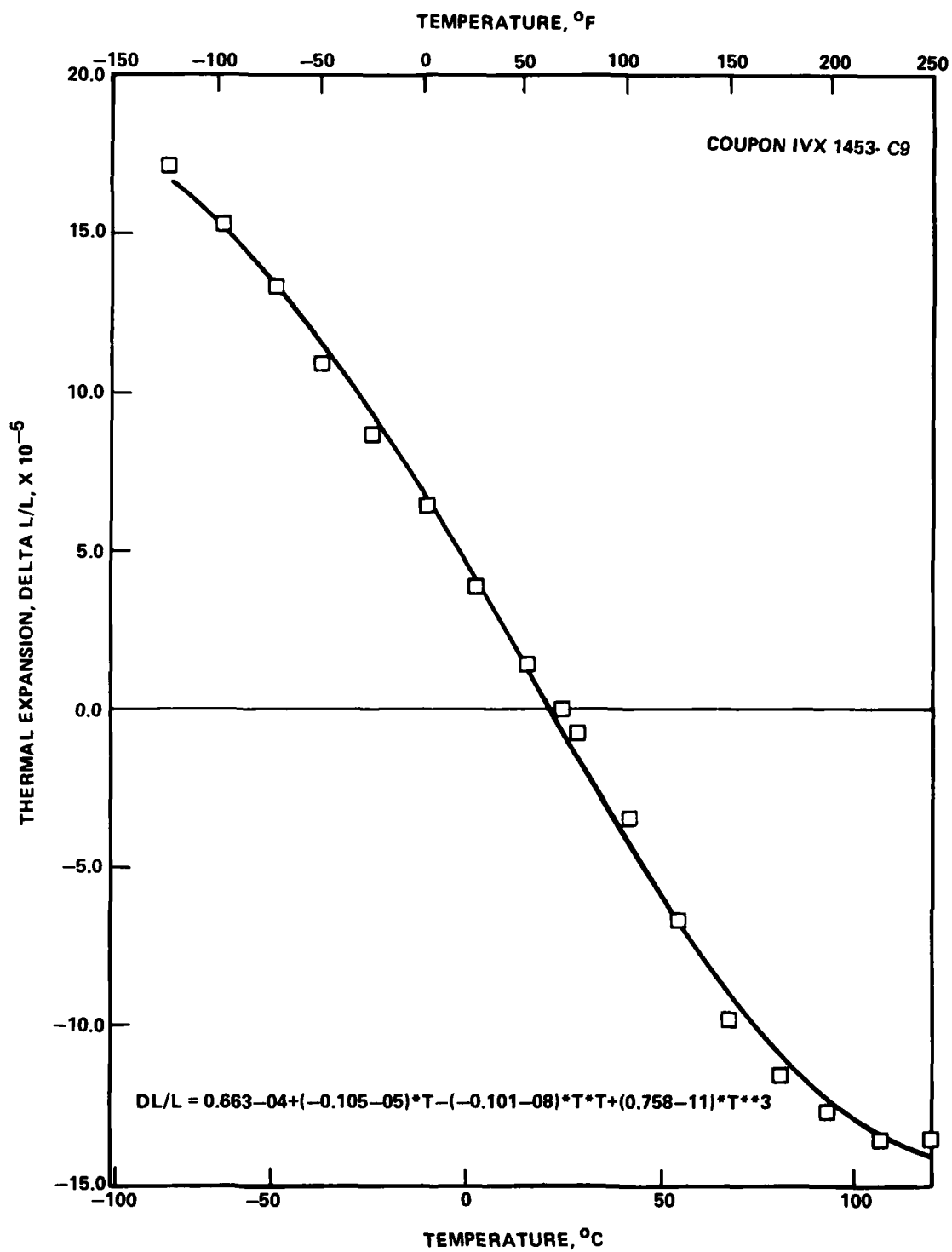


Figure 39. - Thermal expansion results for 0° unidirectional coupon IVX1453-C9.

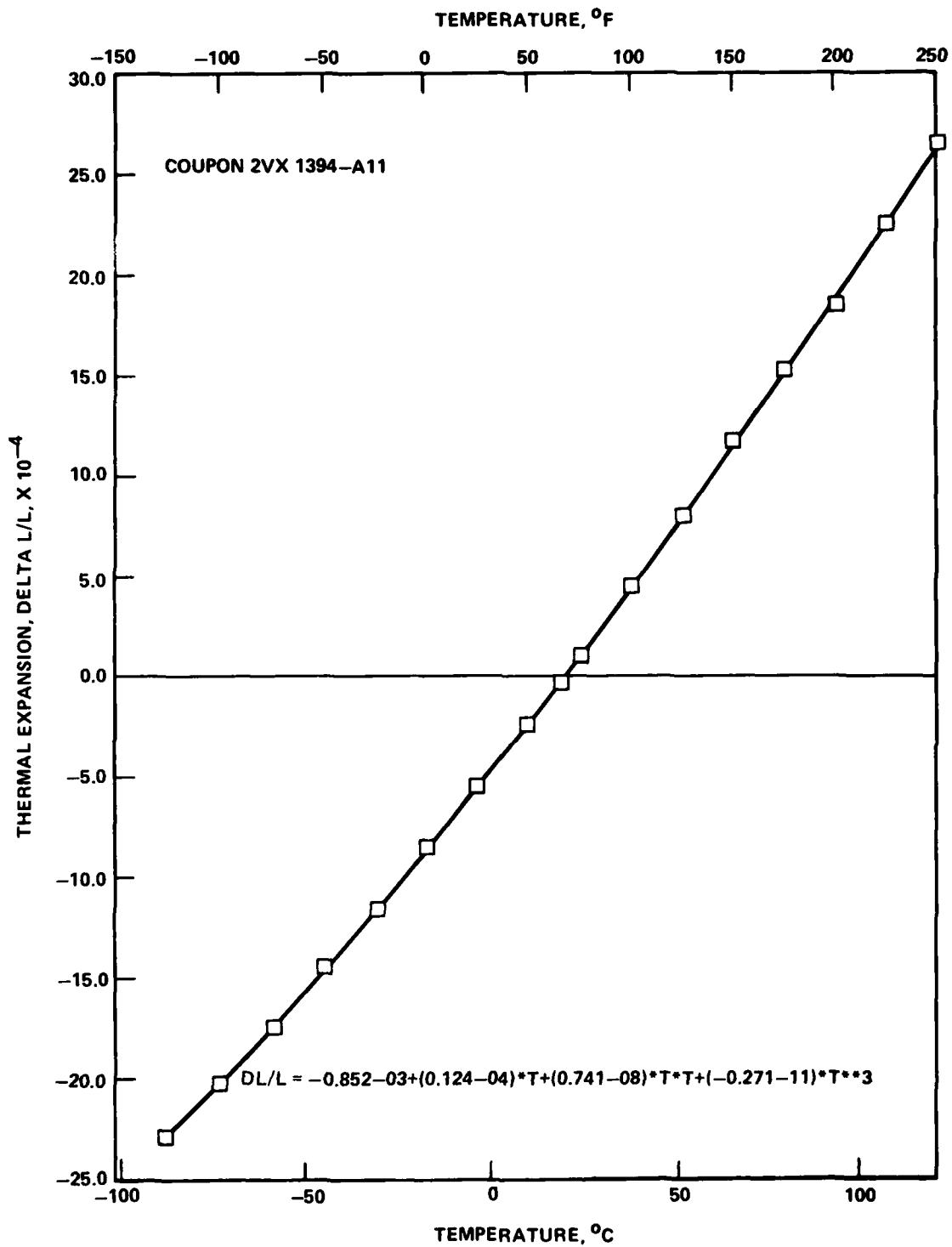


Figure 40. - Thermal expansion results for 90° unidirectional coupon 2XV1453-A11.

intervals. The curves represent the best fit of the experimental data to the third order polynomial equation shown on each figure as $DL/L =$. The maximum uncertainty in the experimental data, as $\Delta L/L$, is 1×10^{-5} . The experiments led to the following average, expansional strain results:

$$0^{\circ} \quad -1.76 \times 10^{-6} \text{ mm/mm/}^{\circ}\text{K} \quad (-0.82 \times 10^{-6} \text{ in/in/}^{\circ}\text{F})$$

$$90^{\circ} \quad 29.7 \times 10^{-6} \text{ mm/mm/}^{\circ}\text{K} \quad (13.7 \times 10^{-6} \text{ in/in/}^{\circ}\text{F})$$

Thermal Conductivity/Diffusivity

Thermal conductivity and thermal diffusivity measurements were made on specimens from Panel LVX1453. Direct measurements of thermal conductivity were made for the two orthogonal "in-plane" directions using a guarded strip technique. Figure 41 illustrates the apparatus, specimen configuration, and instrumentation. Data from these measurements are presented graphically in Figure 42. Maximum uncertainty for these data is 10 percent for C-8, D-10 and C-13 and 17 percent for AA1, AA2 and AA3.

For the thickness direction property, thermal diffusivity was measured using a pulse method.⁵⁰ These specimens were from panel LVX1453-AA. Thermal conductivity, k , was calculated from the relationship:

$$k = \alpha \rho C_p$$

where α is thermal diffusivity, ρ is bulk density and C_p is specific heat. Measured values of thermal diffusivity are presented in Figure 43. Calculated thermal conductivity values are shown in Figure 44. The maximum uncertainty in these values are 5 percent for diffusivity and 12 percent for conductivity.

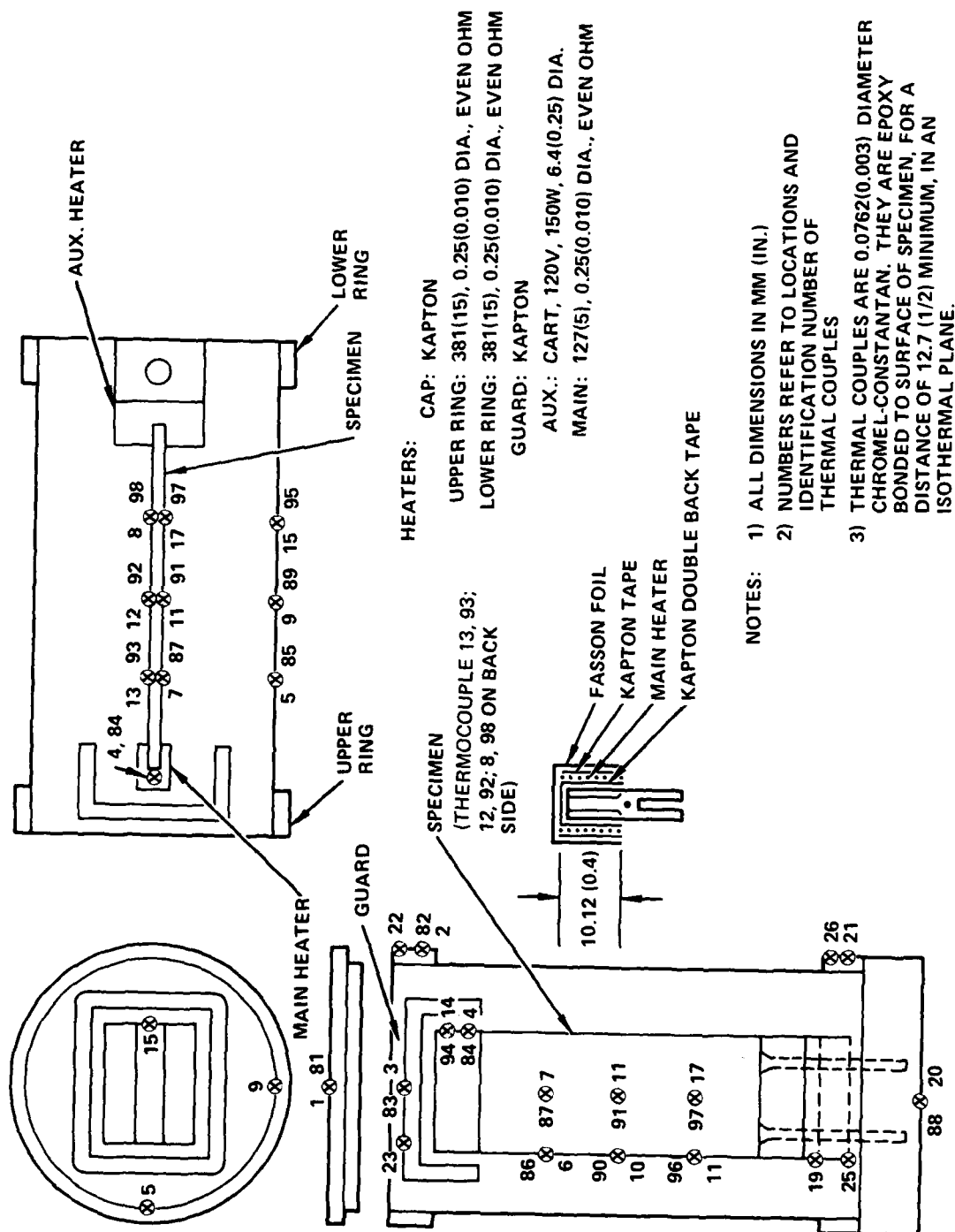


Figure 41. - Diagram of thermal conductivity experiment.

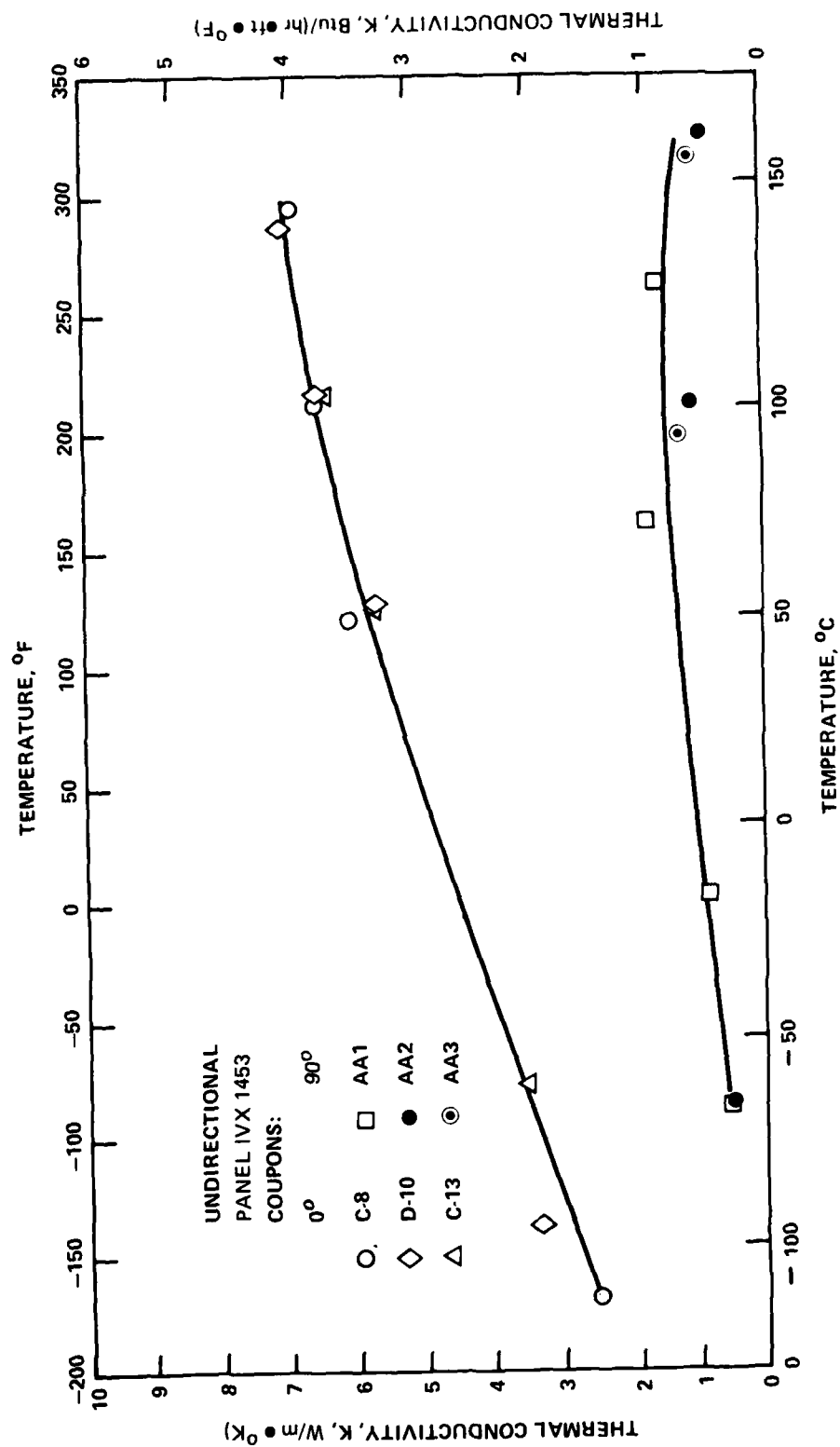


Figure 42. Thermal conductivity in 0° and 90° directions of unidirectional panel,

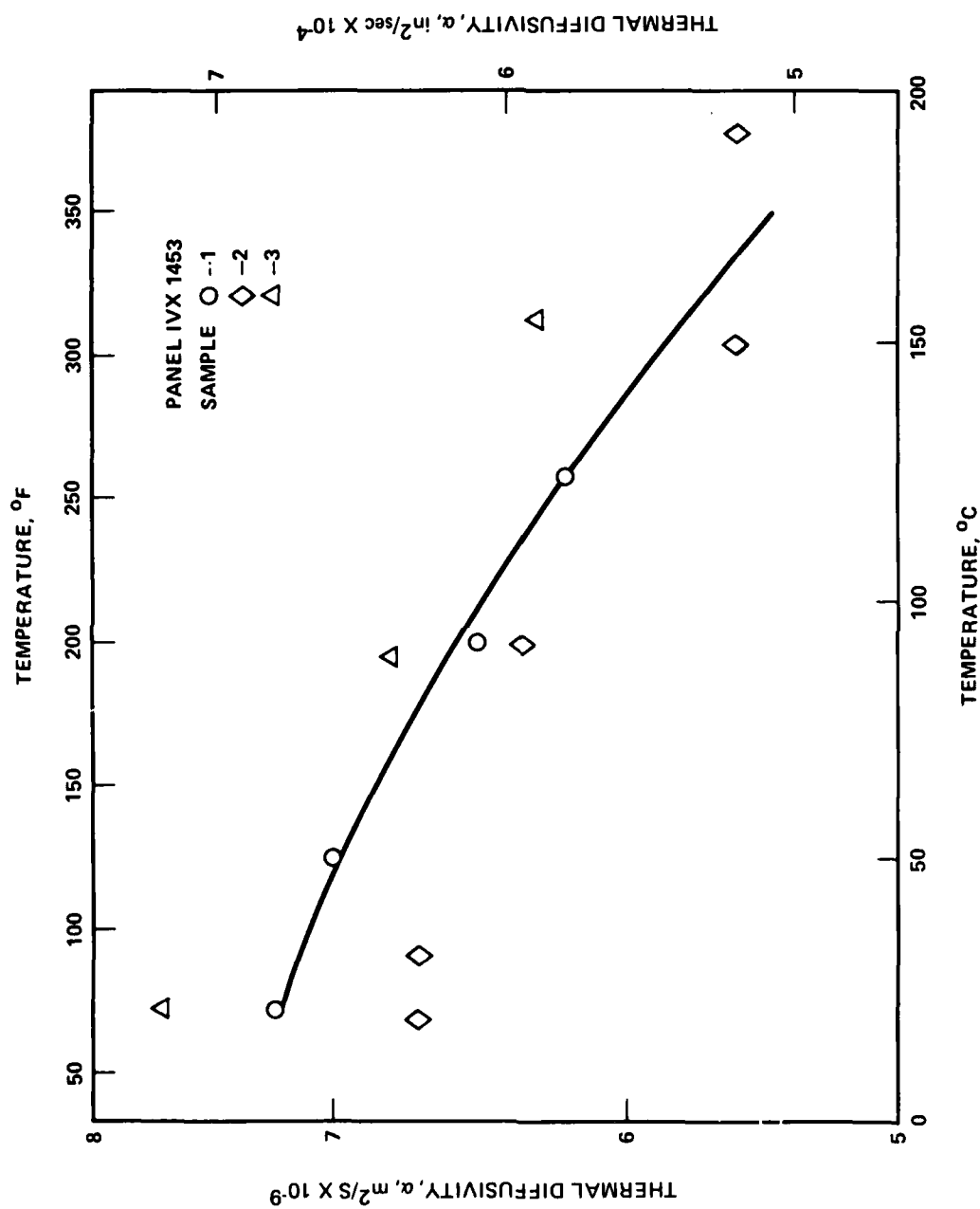


Figure 43. - Thermal diffusivity in thickness direction unidirectional panel.

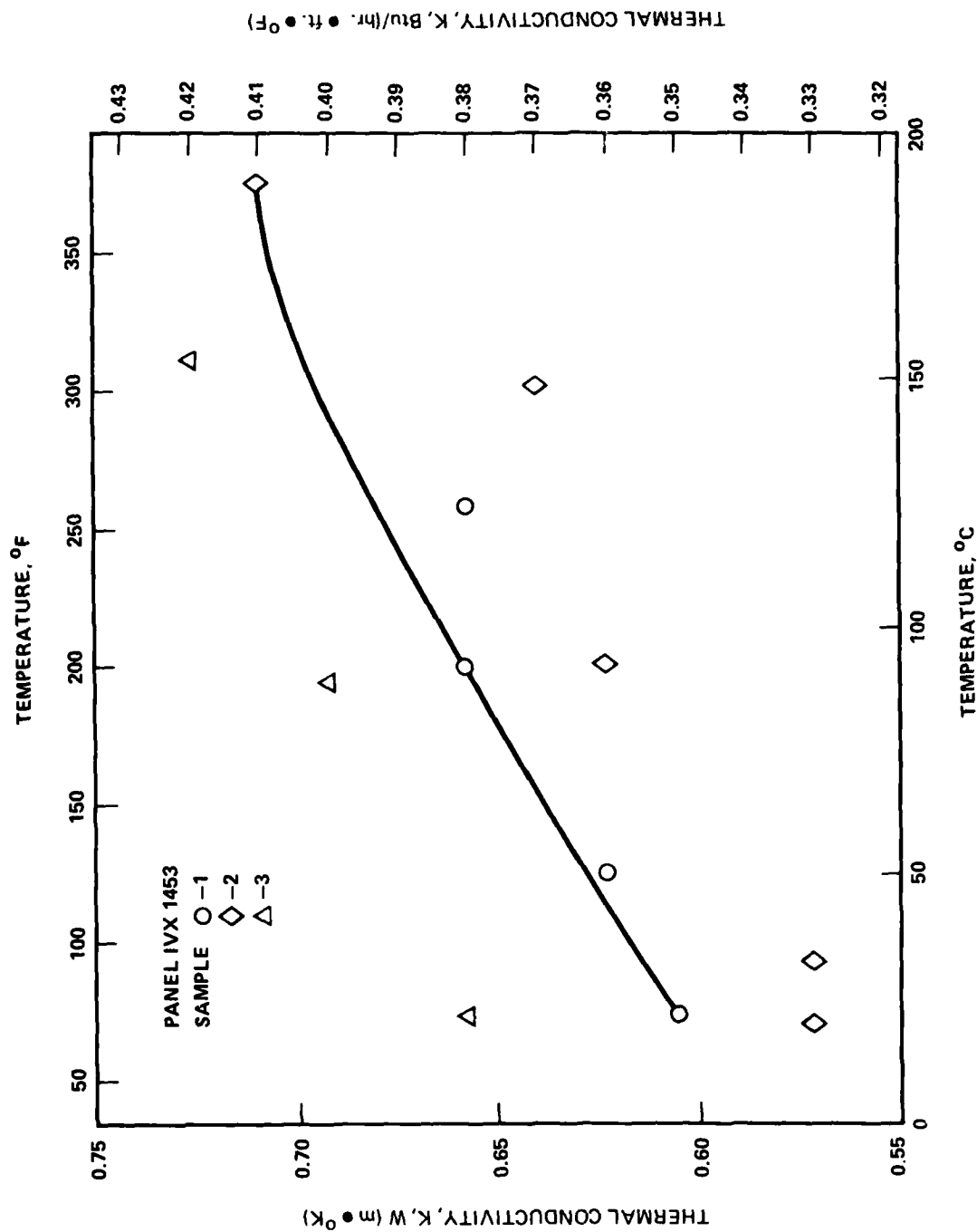


Figure 44, - Thermal conductivity in thickness direction of unidirectional panel.

Specific Heat. - A flooded ice-mantle drop-type calorimeter was used to measure enthalpy of the 1VX 1453 panel as a function of temperature. The enthalpy data, referenced to 0°C (32°F), were fit to the form

$$\Delta H_{0^{\circ}\text{C } (32^{\circ}\text{F})} = A_0 + A_1T + A_2T^2 + A_3T^{-1}$$

using a least squares routine (multiple regression). The resultant enthalpy equation was differentiated to give the equation of specific heat ($C_p = dH/dT$). The accuracy of the enthalpy measurement is 0.75 percent, based upon calibration with a NBS α - alumina standard. Maximum uncertainty for specific heat is estimated to be 5 percent, based upon the fit of the enthalpy data. The specific heat values are shown graphically in Figure 45 for the temperature range of -73° to 232°C (-100° to 450°F).

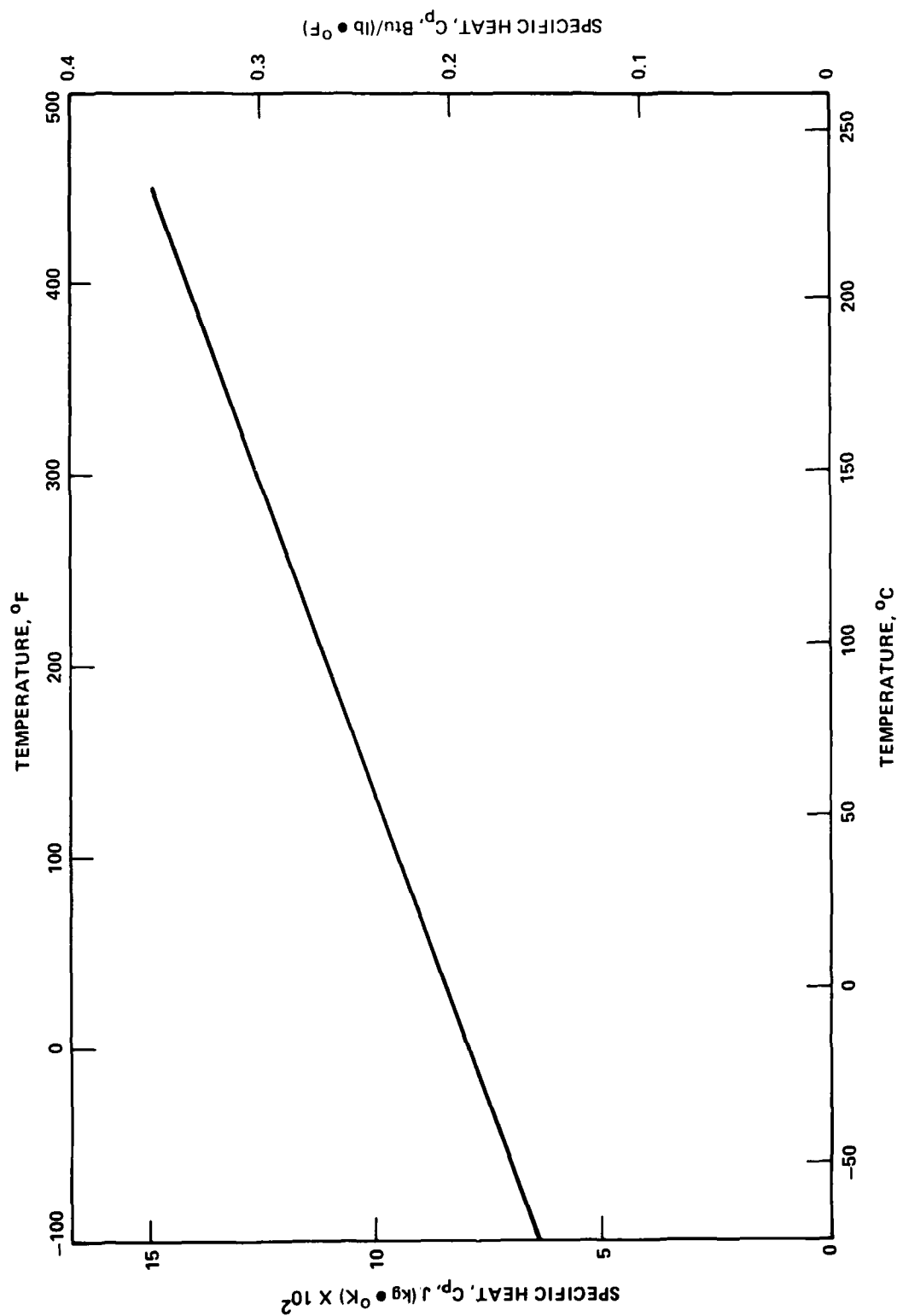


Figure 45. - Specific heat of unidirectional panel, 1VX1453.

SECTION 4

STATIC TENSION AND COMPRESSION RESULTS

Static testing included determination of both unidirectional and quasi-isotropic laminate properties. Lamina testing was conducted at three different environmental conditions: room temperature (RT), dry (as received); 82.2°C (180°F), dry (as received); and 82.2°C (180°F), wet. All laminate tests were conducted at the RT, dry condition. The detailed static test data is tabulated in Appendix B.

4.1 LAMINA PROPERTIES

Ten lamina coupons were tested at each of twelve conditions. The unidirectional lamina properties of this material are summarized in Tables 18 to 22. The compression results are for the fully-constrained column buckling mode as discussed in Section 2.4.1. The stress-strain curve of the 0° unidirectional tension tests had a slightly increasing curvature while that of the compression tests was slightly decreasing. Thus the moduli are really secant values. These slight nonlinear properties are consistent with other experimental observations.^{51,52} The nonlinear, increasing curvature properties under tension load are due to the non-Hookean, increasing curvature of fibers⁵² as reported by Curtis.⁵³ Van Druemel and Kemp⁵² hypothesized that the increasing modulus effect of the fibers would result in heavily stressed regions behaving stiffer, thus absorbing more load than would be expected. Possibly this would explain unexpected experimental results in cases where large stress variations occur in small volumes.⁵² For the 90° unidirectional coupons, tension stress-strain curves were linear while the compression curves slightly decreased. The ±45° curves were continuous decreasing curves as expected.

Typical failures in these lamina coupons are shown in Figures 46 to 50. The 0° unidirectional coupons exhibited a large amount of splintering when

TABLE 18. COMPARISON OF 0° UNIDIRECTIONAL LAMINA STATIC TEST RESULTS

Test Type	Test Environment	Average Ultimate Stress, σ_{ult}		Average Strain to Failure, ϵ_f	Average Secant Modulus at Failure, E_{sf}		Average Secant Modulus at 70 ksi, E_{S70}	
		MPa	ksi		GPa	psi x 10 ⁶	GPa	psi x 10 ⁶
Tension	RT, LA ^a	1645	238.6	0.0095	170.3	24.7	156.5	22.7
	82.2°C (180°F) Dry ^b	1736	251.8	0.0109	159.3	23.1	153.8	22.3
	82.2°C (180°F) Wet ^c	1629	236.3	0.0101	161.3	23.4	151.7	22.0
Compression	RT, LA	847	122.8	0.0066	128.2	18.6	140.0	20.3
	82.2°C (180°F), Dry	885	128.3	0.0067	132.4	19.2	142.7	20.7
	82.2°C (180°F), Wet	669	97.1	0.0070	95.8	13.9	103.4	15.0

^aRT – Room Temperature, LA – Laboratory Air^bDry – Coupons contains ~ 0.4% moisture by weight^cWet – Coupons contained ~ 1.7% moisture by weight

TABLE 19. SUMMARY OF WEIBULL PARAMETERS FOR 0° UNIDIRECTIONAL LAMINA STATIC TEST DATA

Test Type	Test Environment	Average Ultimate Stress, σ_{ult}		Weibull Coefficients			Correlation Coefficient, R
		MPa	ksi	k	e	v	
Tension	RT, LA ^a	1645	238.6	17.92	-0.330	243.3	0.99931
	82.2°C (180°F), Dry ^b	1736	251.8	18.44	-0.300	255.3	0.99931
	82.2°C (180°F), Wet ^c	1629	236.3	24.42	-0.289	236.8	0.99929
Compression	RT, LA ^a	847	122.8	14.82	-0.107	128.9	0.99957
	82.2°C (180°F), Dry ^b	885	128.3	8.34	-0.816	132.5	0.99637
	82.2°C (180°F), Wet	669	97.1	7.98	-0.448	98.5	0.99733

^aRT – Room Temperature, LA – Laboratory Air^bDry – Coupons contained ~ 0.4% moisture by weight^cWet – Coupons contained ~ 1.7% moisture by weight

TABLE 20. COMPARISON OF 90° UNIDIRECTIONAL LAMINA STATIC TEST RESULTS

Test Type	Test Environment	Average Ultimate Stress, σ_{ult}		Average Strain to Failure, ϵ_{sf}	Average Secant Modulus at Failure, E_{sf}		Average Secant Modulus at 70 ksi, E_{S70}	
		MPa	ksi		GPa	psi x 10 ⁶	GPa	psi x 10 ⁶
Tension	RT, LA ^a	34.1	4.95	0.0033	10.2	1.48	—	—
	82.2°C (180°F), Dry ^b	39.0	5.66	0.0047	8.3	1.21	—	—
	82.2°C (180°F), Wet ^c	15.5	2.25	0.0018	8.5	1.24	—	—
Compression	RT, LA	203	29.4	0.0232	8.8	1.28	9.7	1.40
	82.2°C (180°F), Dry	177	25.6	0.0243	7.5	1.09	8.8	1.27
	82.2°C (180°F), Wet	172	25.0	0.0471	3.7	0.54	4.6	0.67

^aRT — Room Temperature, LA — Laboratory Air^bDry — Coupons contained ~0.4% moisture by weight^cWet — Coupons contained ~1.5% moisture by weight

TABLE 21. SUMMARY OF WEIBULL PARAMETERS FOR 90° UNIDIRECTIONAL LAMINA STATIC TEST DATA

Test Type	Test Environment	Average Ultimate Stress, σ		Weibull Coefficients			Correlation Coefficient, R
		MPa	ksi	k	e	v	
Tension	RT, LA ^a	34.1	4.95	—	—	—	—
	82.2°C (180°F), Dry ^b	39.0	5.66	4.53	-0.229	5.63	0.98926
	82.2°C (180°F), Wet ^c	15.5	2.25	8.04	-0.026	2.32	0.99488
Compression	RT, LA ^a	203	29.4	8.06	-0.302	30.36	0.99569
	82.2°C (180°F), Dry ^b	177	25.6	8.74	-0.056	26.28	0.99897
	82.2°C (180°F), Wet ^c	172	25.0	19.89	-0.022	25.07	0.99946

^aRT — Room Temperature, LA — Laboratory Air^bDry — Coupons contained ~0.4% moisture by weight^cWet — Coupons contained ~1.7% moisture by weight

TABLE 22. COMPARISON OF $\pm 45^\circ$ UNIDIRECTIONAL LAMINA STATIC TENSION TEST RESULTS

Test Environment	Shear Stress at Failure, τ_{xy} ,		Shear Secant Modulus at 4 ksi, GS_4 ,	
	MPa	ksi	GPa	psi x 10^6
RT, LA ^a	89.6	13.0	5.3	0.77
82.2°C (180°F), Dry ^b	78.6	11.4	5.4	0.78
82.2°C (180°F), Wet ^c	73.1	10.6	4.5	0.65

^aRT - Room Temperature, LA - Laboratory Air

^bDry - Coupons contained ~0.4% moisture by weight

^cWet - Coupons contained ~1.7% moisture by weight

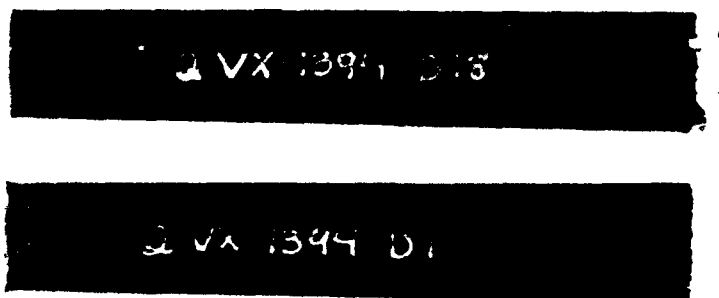


Figure 46. - Representative 0° unidirectional coupons which failed in static tension at room temperature in laboratory air.

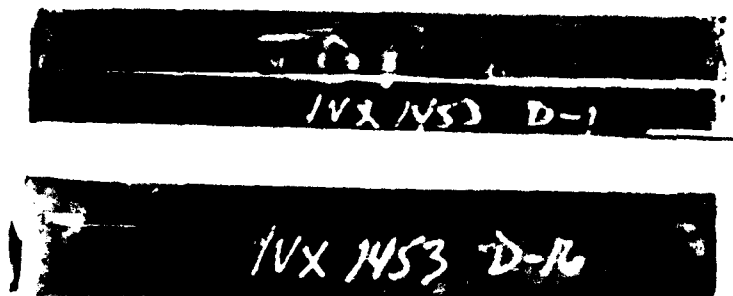


Figure 47. - Representative 0° unidirectional coupons which failed in static compression at room temperature in laboratory air.

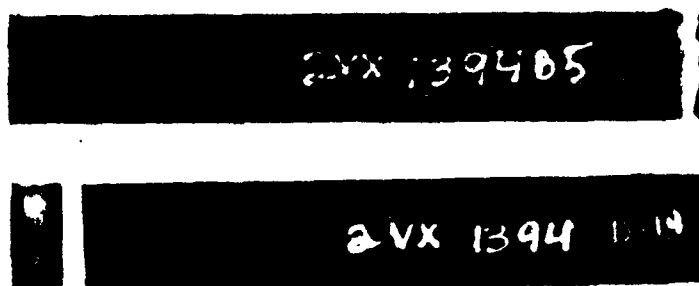


Figure 48. - Representation 90° unidirectional coupons which failed in static tension at room temperature in laboratory air.

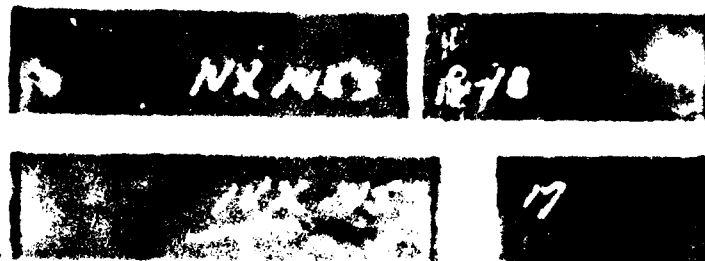


Figure 49. - Representative 90° unidirectional coupons which failed in static compression at room temperature in laboratory air.

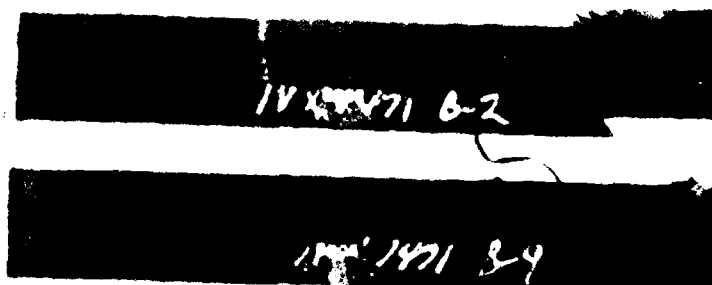


Figure 50. - Representative $\pm 45^\circ$ coupons which failed in static tension at room temperature in laboratory air.

failed under static tension loading, see Figure 46. The amount of splintering appeared to be unaffected by the high humidity and temperature environment. Similarly, the 0° coupons which failed under static compression suffered severe splintering, Figure 47, but this was significantly reduced at the 82.2°C (180°F), 95 percent RH, wet condition. Under tension loading, the 90° coupons failed straight across at or near the tabs without apparent variation due to environment, Figure 48. In contrast, these 90° coupons exhibited a 45° to the loading plane failure region within the gage length when under compression load, Figure 49, however environment again did not affect the degree of fracture severity. Lastly, the ± 45 coupons, Figure 50, exhibited a fracture region whose damage state became worse as the severity of the environment was increased.

4.2 LAMINATE PROPERTIES

4.2.1 Static Tension

Static tests on laminate coupons were conducted at two different strain rates, 0.01 mm/mm/min and 6.0 mm/mm/min. This allowed a comparison to be made between normal tension test results and those conducted at rates equivalent to a 10 Hz fatigue test. The tension failures at both strain rates were brittle-like with a discernible inelastic-like flow at the end of the high strain rate stress-strain curves. The stress-strain curves of the low-strain rate tensile coupons exhibited an initial linear, elastic portion with an apparent modulus of elasticity designated as E_1 . This straight portion was followed by a short, gradual, change to a second, inelastic, linear curve to failure with an apparent modulus designated E_2 . In contrast, stress-strain curves of high-strain rate coupons were linear without the dual slope characteristic at low rates. The stress-strain curves were similar to those previously observed for this layup.^{4,18}

All tensile failures were within the gauge length. Fracture regions were often within the region of 25 to 50 mm (1 to 2 in.) from a tab, but these did not differ in their failure strengths from those which failed near the center. The fracture region of high strain rate coupons was similar though apparently less extensive than those observed for the low strain rate coupons.

Typical static tension failures are shown in Figure 51. Only minor amounts of delamination occurred and was confined to the fracture region. Fibers in the outer 0° plies often failed along a $+45^\circ$ direction indicating a strong influence of the $+45^\circ$ plies on the fracture process. A secondary damage region due to compressive rebound usually occurred in the low strain rate coupons, but less often in the high strain rate specimens.

Tables 23 and 24 give summaries and comparisons of the laminate tension results. The detailed data are tabulated in Appendix B. To avoid the influence of line discontinuities (adjoining tape edges) which are known to increase the scatter in static and fatigue properties,^{4,23} panel layups were designed so that test coupons did not contain such discontinuities (see Section 2.2). This was expected to result in a coefficient of variation of less than 4 percent and a Weibull parameter, k , greater than 30 for the static tension results. This expectation was confirmed as shown in Tables 23 and 24. In addition, strain gauges on half of the coupons tested at each strain rate were placed at the 1/3 gauge length point and on the other half at the center. The strain gauge data at the two locations were compared and

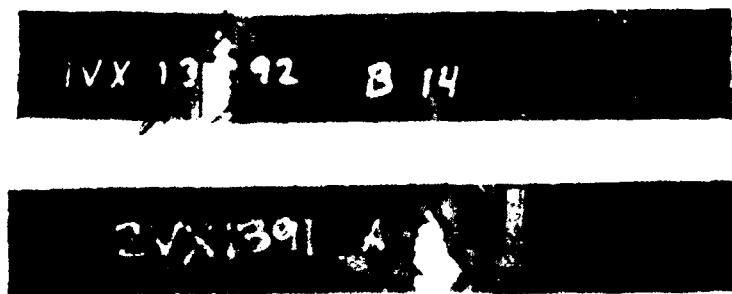


Figure 51. - Representative quasi-isotropic laminate coupons which failed in static tension at low strain rate in room temperature, laboratory air.

TABLE 23. SUMMARY OF QUASI-ISOTROPIC STATIC TENSION TEST RESULTS AT ROOM TEMPERATURE

Strain Rate, mm/mm/min	Failure Stress, σ_{ult}		Average Strain at Failure, ϵ_{ult} , mm/mm	Initial, Apparent Modulus of Elasticity, E_A	
	MPa	ksi		GPa	psi x 10 ⁶
0.01	547 ^a	79.3	0.0105	53.8 ^a	7.81
	19.1	2.77	0.00042	1.03	0.15
		3.49	4.03		1.96
6.0	507	73.6	0.0098	51.8	7.52
	17.9	2.60	0.00055	2.96	0.43
		3.53	6.66		5.68

a Average, standard deviation, and % coefficient of variability, respectively.

TABLE 24. SUMMARY OF WEIBULL PARAMETERS FOR QUASI-ISOTROPIC STATIC TENSION RESULTS AT ROOM TEMPERATURE

Strain Rate, mm/mm/min	Average Failure Stress, σ_{ult}		Weibull Coefficients			Correlation Coefficient, R
	MPa	ksi	k	e	v	
0.01	547	79.3	33.87	-0.061	80.30	0.99958
6.0	507	73.6	30.10	-0.040	74.64	0.99972

found to differ by less than 2 percent and thus to be statistically insignificant. This confirmed that at least the center 100 to 125 mm (4 to 5 inches) or the coupon gage length is experiencing the same strain field. Only thirteen high strain rate coupons are included in the data of Tables 23 and 24 because the others came from a damaged panel as discussed below.

Table 23 shows an approximately 8 percent drop in the static tensile strength at high strain rate compared to the low strain rate results. The cause of the strain rate effect is hypothesized to be due to the manner in which cracks propagate in the 0° layers. As the load on a coupon increases, transverse cracks appear first in the 90° layers followed by the -45° layers, after which, delamination starts and propagates. Load is increasingly transferred into the 0° plies further stressing the fibers and cracking the matrix.

At low strain rates, matrix cracks are postulated to grow to a fiber interface and then longitudinally because they do not have sufficient energy to drive across a fiber. Eventually, sufficient load is transferred into the 0° fibers resulting in the fracture of individual fibers or fiber bundles leading to the propagation of a macrosized, cross fiber crack or the coalescence of individual fiber bundle fractures or both.

At high strain rates the matrix cracks are hypothesized to have sufficient energy to cross fibers without generation of large amounts of longitudinal cracking causing early fracture and a lower strength. The entire concept is related to the ability of the material to dissipate energy. At low strain rates, energy tends to be dissipated over a large volume while at high strain rates energy dissipation tends to be concentrated in a narrow region. The important point is the postulation that at low strain rates, considerable energy is dissipated in the generation of inter and intra lamina longitudinal matrix cracks.

This concept was supported by examining the failure modes of coupons subjected to the low and high strain rates in this program. Of the twenty coupons tested at low strain rate, sixteen exhibited failure modes characterized by two damage regions. The first damage region was due to tensile

fracture of the coupon usually in the region of 2.5 to 5 cm (1 to 2 in.) from a tab. The second damage region occurred at the opposite end of the coupon, but in the same geometric region due to compressive buckling of the coupon caused by the rebound shock wave (see Figure 52). In contrast, of the coupons tested at high strain rate only two out of thirteen had two damage regions. The extent of longitudinal matrix cracking may explain the difference between the number of dual damage regions that occurred at low strain rates as compared to high strain rates. At low strain rates, a larger extent or more distributed longitudinal matrix cracking or both is hypothesized. This would leave relatively more of the 0^0 fiber ply unsupported and thus more susceptible to buckling failure under the compressive shock wave. In addition, the tensile fracture regions of the high strain rates coupons tended to be more contained than those at low strain rates and to have somewhat less longitudinal matrix cracking. These experimental observations, while in agreement with the energy dissipative hypothesis are by no means definitive, but do provide strong support.

An experimental verification of these suppositions could be obtained by first loading a coupon close to failure, but at a low strain rate. If after unloading, the coupon is reloaded to failure at a high strain rate, the strain rate effect should be reduced or eliminated. Essentially this experimental verification already exists in the many proof loading studies of unidirectional laminates.⁵⁻⁸ Similar support comes from the work of Crossman et al⁵⁴ where the observation was made that before consistent creep data could be obtained, coupons had to be load cycled several times.

The same type of observations have been made in that loading laminates with a high percentage of 0^0 fibers^{4,18} or 0^0 unidirectional laminates⁵⁵ to their maximum fatigue stress on the first cycle results in many premature failures. This indicates a strong strain rate effect which lowers strength. In addition, investigators have also observed that loading a laminate over several cycles up to the maximum fatigue load prevents the premature failures.^{4,18,55} This could be explained by the same hypothesis proposed to explain the strain rate effect. The low load cycling would tend to generate longitudinal cracks in the 0^0 plies due to the low energy.

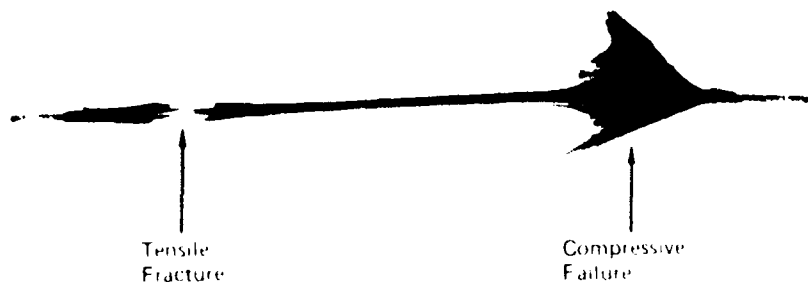


Figure 52. - Compression, shock wave, rebound failure of tensile, quasi-isotropic coupon 2VX1391-B13 tested in room temperature, laboratory air.

Subsequent cracking at higher loads would grow preferentially in the longitudinal direction thus reducing fiber breakage, premature failure, and increasing fatigue life. This latter concept is supported by well known observations that the "precracking" of manufactured parts reduces fatigue scatter and increases life.⁵⁶

During fatigue testing of coupons from panel 2VX1390, another source of strength reduction in static properties besides line discontinuity²³ and strain rate was discovered. A few coupons were found to have surface ply (top and bottom) "squiggles" (curved 0° fibers) of the type shown in Figure 53. These defects were not found by NDI C-scan since they do not result in an interface. Further they were missed in initial visual inspection since no corresponding disturbance in the panel peel ply occurred and they are difficult to see in untested coupons. Specimens found to have the "squiggle" defect only came from panel 2VX1390, therefore this panel was eliminated from further use in the experimental program. The cause of this

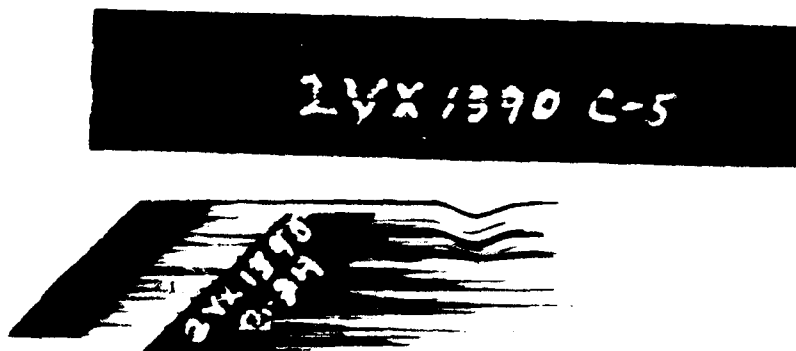


Figure 53. - Photograph of coupon 2VX1390-C5 with representative squiggles and subsequently sectioned top layers of specimen showing non-overlap of squiggles.

damage type and the associated effects on the static properties was investigated.

The "squiggle" defect is believed to be too large to have been missed by visual inspection during layup. They did not occur at foreign material accumulations. Since they occurred only on the outer 0° surface plies, they were probably not caused during layup. A second panel of the same layup was made in the same autoclave run which did not exhibit squiggles. The autoclave cure records state that the cure time, temperature, and pressure records are within tolerances except for a five minute, 8°C (15°F) overshoot of the controller at the dwell temperature of 135°C (275°F). Further facts concerning the presence of the squiggle defect are:

- The squiggles are believed to have been caused during pressurization in the pure cycle and appear only on the surfaces that contact the peel ply nylon.

- Since the panel made in the same autoclave run did not show squiggles, the temperature overshoot most likely did not cause the squiggles.
- Speculating only, wrinkles in the nylon peel ply could possibly account for the squiggles.
- Squiggles cannot be seen through the peel ply and inspection will have to be done after "C" scan and machining.
- "C" scan will not detect squiggles in surface plies.

Table 25 shows a comparison of the tension test results for specimens with and without squiggles. The average static tensile strength results for specimens containing significant, visually observable squiggles were reduced by 25 percent when compared to specimens containing no squiggles. Specimens containing a smaller amount of squiggles had an average tensile strength reduced by 10 percent as compared to those without squiggles. In addition, the scatter in strength was higher for the coupons containing the defect than for those without the defect. A number of coupons from panel 2VX1390 were tested at high strain rate prior to observing the squiggle defect. The results for these coupons is also shown in Table 25. The effect of strain rate is clearly shown for these coupons. Based on these results, observed severe strength degradation on panel 2VX1390 has been attributed to the presence of squiggles. However, the cause of the presence of the defect has not yet been determined.

4.2.2 Static Compression

Twenty compression tests were conducted at both 0.01 and 6.0 mm/mm/min using the procedure described in Section 2.4.1. Quasi-Isotropic coupons which failed in static compression, see Figure 54, exhibited no obvious damage prior to fracture although the stress-strain curve often was flat just prior to fracture indicating internal damage. Coupons usually failed at one location with the outer plies in the fracture region buckled out of plane. Extensive delamination usually occurred, but was limited over approximately 25 to 50-mm (1 to 2-in.) of the gage length in the vicinity

TABLE 25. EFFECT OF "SQUIGGLE" DEFECT ON STATIC TENSILE STRENGTH

Extent of Defect	Panel No's.	Strain Rate mm/mm/min	Failure Stress, σ_{ult}	
			MPa	ksi
None	2VX1391, 1VX1392	0.01	547 ^a	79.3
			19.1	2.77
Light	2VX1390	0.01	495	71.8
			27.4	3.98
Severe	2VX1390	0.01	414	60.1
			20.5	2.97
Light	2VX1390	6.0	409	59.3
			24.6	3.57

a -- Average, standard deviation, and percent coefficient of variability, respectively.

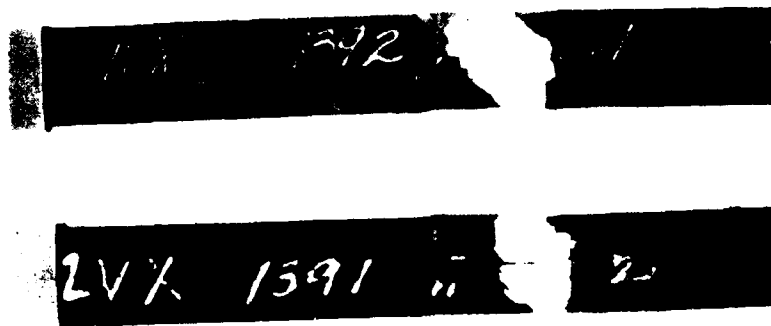


Figure 54. - Representative quasi-isotropic laminate coupons which failed in static compression at low strain rate in room temperature, laboratory air.

of the fracture region. Fractures appeared on the outer plies along an irregular line along either a $\pm 45^\circ$ or 90° angle to the loading direction. Failure modes did not appear to be affected by the strain rate.

Tabulated static compression test results are listed in Appendix B. In these tables, the moduli are secant values since the stress-strain curves are continuous decreasing slopes. None of the coupons exhibited crushing prior to failure. Compression tests results are summarized in Tables 26 and 27. The quasi-isotropic laminate showed essentially the same compression strength using this test method as in tension. Table 26 shows that strain rate had no significant effect on the quasi-isotropic compression properties.

TABLE 26. SUMMARY OF QUASI-ISOTROPIC STATIC COMPRESSION TEST RESULTS AT ROOM TEMPERATURE

Strain Rate, mm/mm/min	Stress at Failure		Average Strain at Failure mm/mm	Secant Modulus of Elasticity at Failure, E_{SF} ,	
	MPa	ksi		GPa	psi x 10^6
0.01	562 ^a	81.5	0.0115	48.2 ^a	6.99
	22.3	3.23	0.00075	1.65	0.24
	3.96		6.47	3.48	
6.0	546	79.2	0.0121	46.8	6.79
	51.6	7.48	0.0012	1.65	0.24
	9.44		10.5	3.5	

a - Average, standard deviation, and percent coefficient of variation, respectively.

TABLE 27. SUMMARY OF WEIBULL PARAMETERS FOR QUASI-ISOTROPIC STATIC COMPRESSION RESULTS AT ROOM TEMPERATURE

Strain Rate, mm/mm/min	Average Failure Stress,		Weibull Coefficients			Correlation Coefficient, R
	MPa	ksi	k	e	v	
0.01	562	81.5	27.75	-0.076	82.6	0.99950
6.0	546	79.2	11.96	-0.235	81.7	0.99884

SECTION 5

FATIGUE RESULTS

Fatigue tests were conducted in this task for two reasons. First, to provide stress-life data to serve as a baseline for the Task II study of load history effects. Second, as an aid for selecting state-of-the-art NDI procedures for detecting and monitoring damage growth and initiation during the fatigue experiments of Tasks II and III. These two goals were met by conducting at least five constant amplitude fatigue tests at each of six stress levels per stress-life curve of interest. Five coupons per stress level was sufficient to determine the average life at an acceptable level of accuracy.¹⁸ Life distributions at selected stress levels will be determined during Task II experimentation.

Stress-life curves were obtained at four stress ratios, R , (+0.5, 0.0, -0.5, and -1.0) as per RFP requirements. Exploring the effect of various R ratios on fatigue life brings up two separate, but necessarily related questions: 1) whether the range of stress or maximum level or both determine fatigue life; and 2) the effect of constraint type on fatigue life under tension-compression loading. Both of these questions are pertinent to an understanding of the load history effects to be obtained in Tasks II and III. Previous investigation of this laminate showed that at maximum stress levels above the -45° ply static tension failure stress, the fatigue life is dependent on maximum stress rather than stress range.¹⁸ However, at lower maximum stresses, the stress range appeared to determine fatigue life. These results were true not only for tension-tension fatigue loading, but also for tension-compression loading using the particular form of constraint employed in that investigation.¹⁸

The data being obtained at various R ratios in this investigation, when combined with data previously available^{4,18}, potentially allow the effects of

maximum stress and stress range to be separable. The success of this endeavor depends, to a large extent, upon the effect of constraint on fatigue life under tension-compression (T-C) loading. A coupon under tension-tension (T-T) loading, such as at $R = 0$ or $+0.5$, is not constrained within the coupon gage length. However, under T-C loading, coupons need to have either a low slenderness ratio or be mechanically constrained to prevent excessive out-of-plane buckling. Without one or the other of these conditions, compression loads are limited to the instability load. The use of thick laminates to reduce the slenderness ratio is usually not employed for reasons of fiscal economy. Therefore, the problem is often solved by reducing the coupon gage length. This necessitates different coupon geometries for tension and compression loading, and thus may introduce a nuisance variable. In addition, the question arises as to whether or not a strain field region within the gage length is actually established which is not influenced by the load introduction. To avoid these potential problems, a coupon geometry was used for T-C fatigue identical to that used in T-T fatigue.

The choice of coupon geometry for T-C fatigue loading required consideration of the constraint type. Such constraints can vary from local buckling guides of various geometries to a fully constrained condition using complete face plates. The type of constraint selected will influence the form of damage initiation and growth and thus require definition of fatigue failure, hence, influencing fatigue life. In Task I, fully supported constraint fixtures were selected, but the large number of cutouts required for the NDI monitoring apparatus influenced the fatigue life and damage growth in a manner that cannot be easily analyzed. This problem of analysis is a principal difficulty in T-C fatigue loading. The T-C fatigue results must be analyzable in such a manner that results can be applied to other constraint conditions, thus allowing for an understanding of the material response. Therefore, based upon previous experience^{4,18} and that gained in Task I, a multiple bay constraint system was selected for T-C fatigue loading during Tasks II and III. Such a constraint can be analyzed relatively simply for a coupon under static loading^{24,51} and this appears to also be true for fatigue loading.

A schematic diagram of the type of T-C fatigue constraint selected for Tasks II and III is shown in Figure 55. The detailed geometry of the fixture is being developed during Task II. The selected constraint system will allow the delamination damage mode to occur which is restrained by a fully supported constraint fixture. Thus the effect of load history on the development of all of the different types of damage modes under tension-compression loading can be investigated.

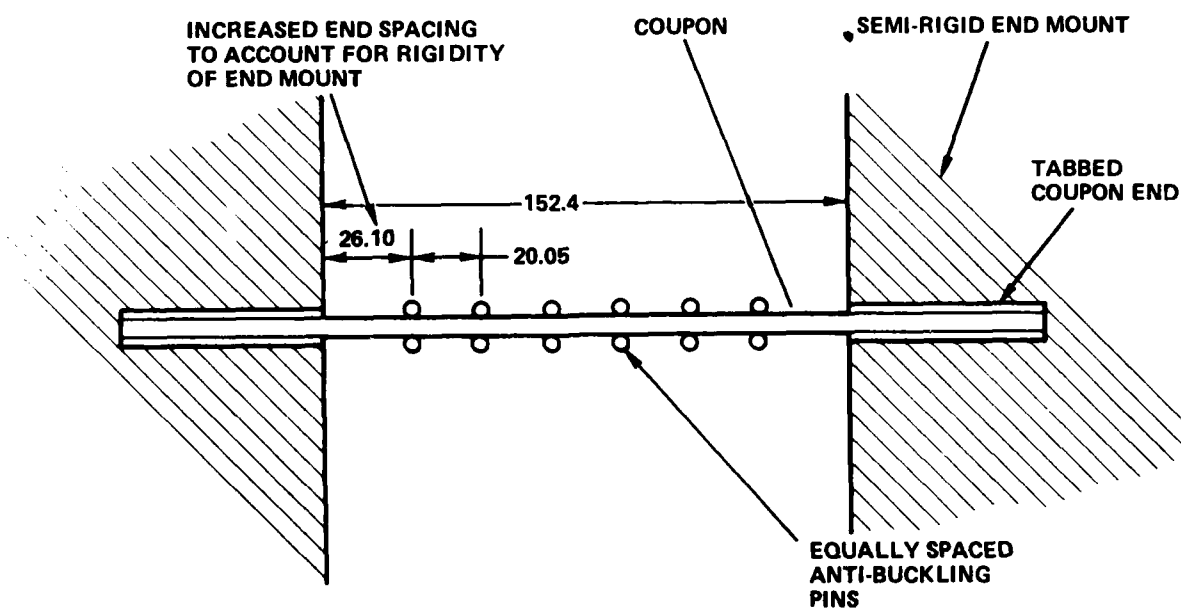
5.1 FATIGUE TEST RESULTS

Constant amplitude fatigue tests were conducted at four R ratios (+0.5, 0.0, -0.5, -1.0) using the experimental procedures and apparatus described in Section 2.4.2. At least five data points were obtained at each stress level. However, coupons from panel 2VX1390 were found to have significantly different properties than those from other panels due to the "squiggle" type defect found in this panel and discussed in Section 4. Therefore, within the restraints of time and funding, additional coupons were fatigue cycled to replace those from panel 2VX1390. The data is tabulated in Appendix C and graphically displayed in Figures 56 to 59. The triangular symbols denote coupons from panel 2VX1390 while the open circles denote those from other panels.

The distinct effect of the "squiggle" defect on fatigue life is apparent in these figures. The defect caused major damage to occur up to 2.5 orders of magnitude earlier in life than in coupons without the defect. The total fatigue life was reduced by 1 to 3 orders of magnitude depending on the R ratio and stress level. Figure 60 shows a typical, large defect region which delaminated early in fatigue life.

The fatigue data obtained under T-C loading does not appear to be directly relatable to the T-T data. The T-C data shows the fatigue response of this material subjected to the particular constraint system selected. During Task II, the $R = -1.0$ data will be repeated using the six bay buckling guide so a more easily analyzable and relatable data base can be developed.

Representative examples of coupons which failed in constant amplitude fatigue at the various R ratios are shown in Figures 61 to 64. Differences



DIMENSIONS IN MILLIMETERS

Figure 55. - Schematic diagram of tension - compression fatigue restraint system.

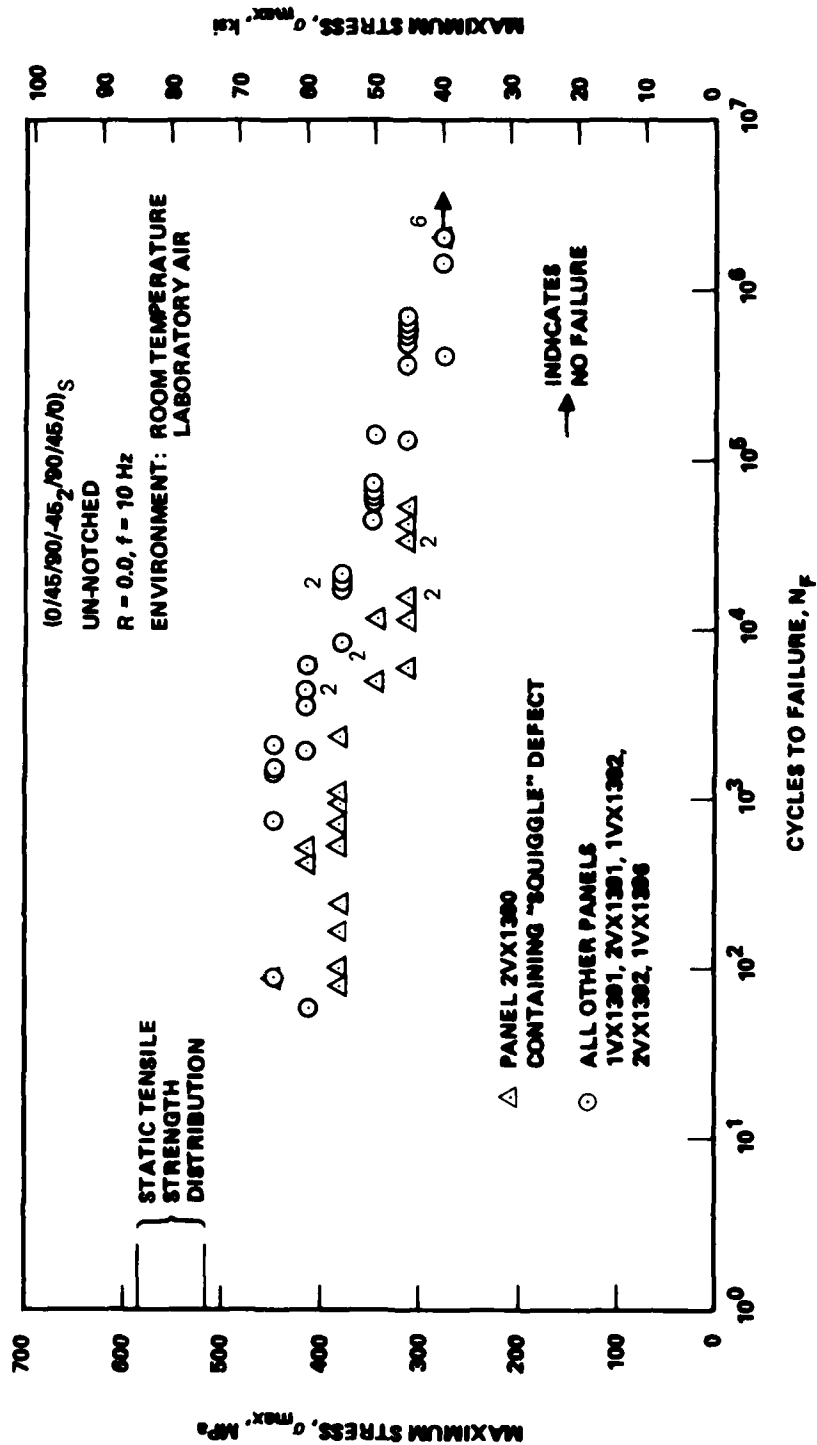


Figure 57. - Quasi-isotropic, fatigue stress-life scan results at R = +0.0 (room temperature, laboratory air).

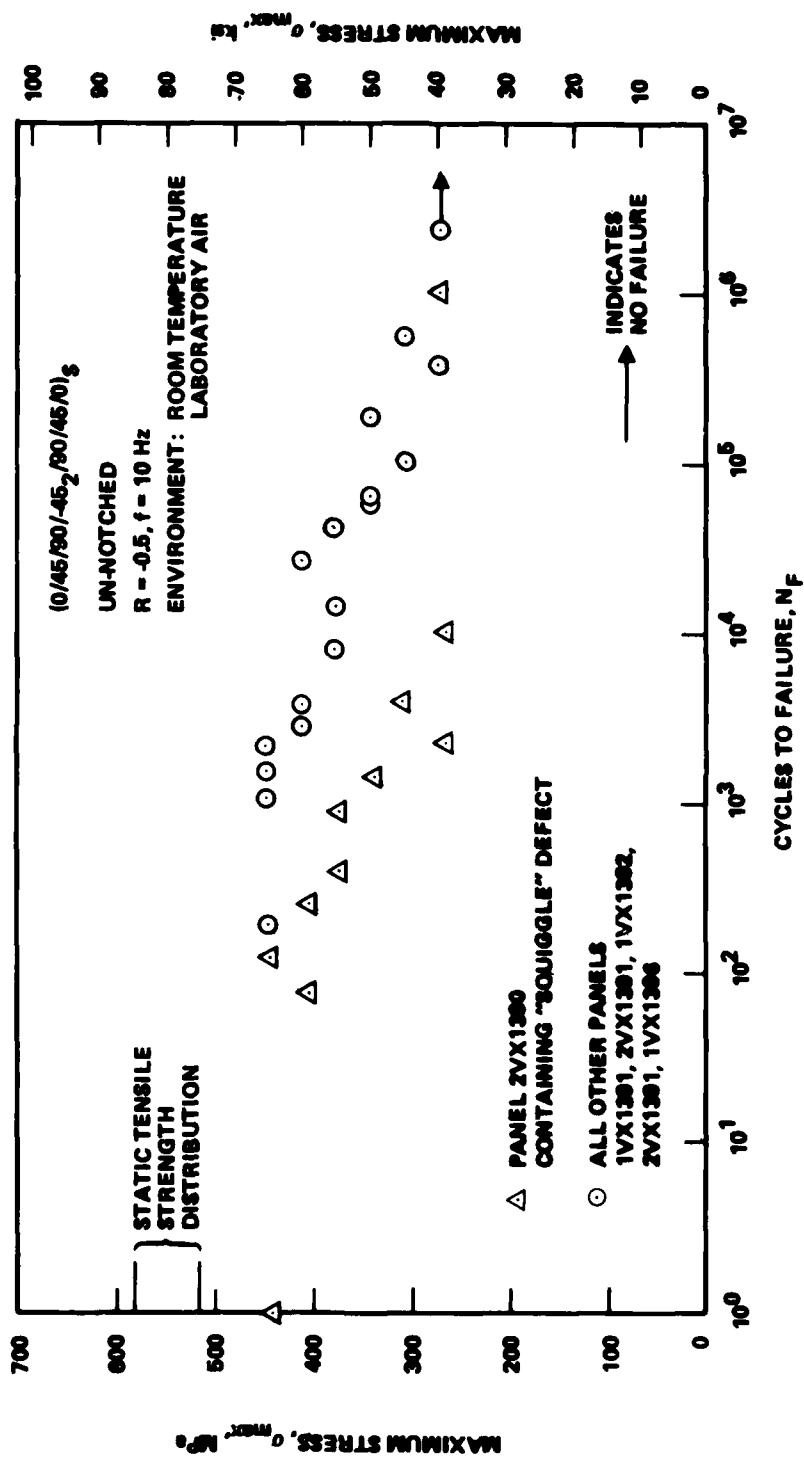


Figure 58. - Quasi-isotropic, fatigue stress-life scan results at $R = -0.5$ (room temperature, laboratory air).

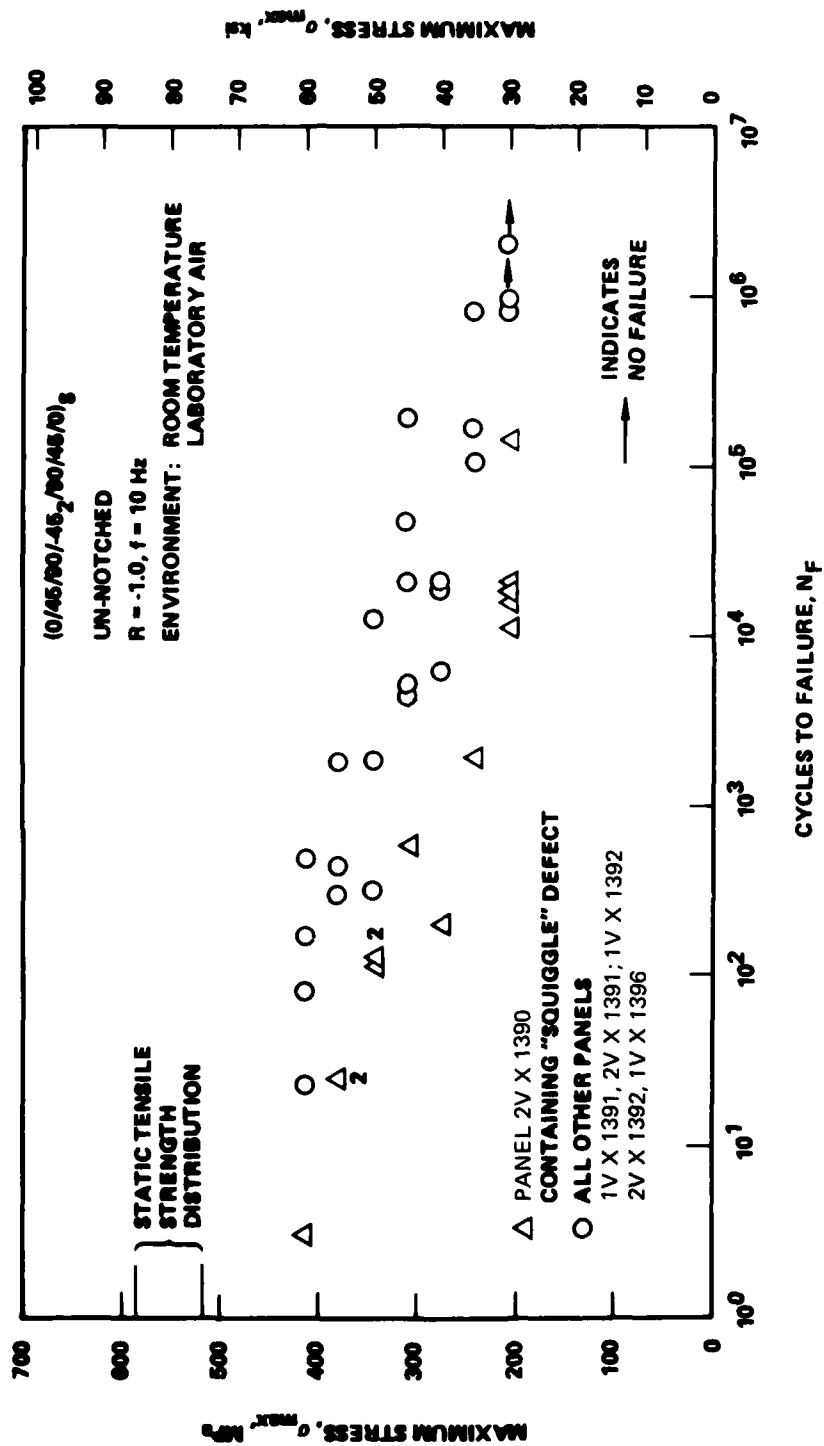


Figure 59. - Quasi-isotropic, fatigue stress-life scan results at $R = 0.0$ (room temperature, laboratory air).

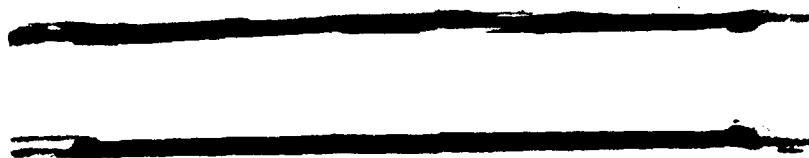


Figure 60. - Delamination of "squiggle" defect during initial fatigue cycling.

2VX1391 B 26

NF 2VX1391 B1

167 8594



167 8594

Figure 61. - Face and edge views of coupons fatigue tested at $R = +0.5$ (top, 2VX1391-B26, 414 MPa (60 ksi), $N_F=267,700$; bottom, 2VX1391-B1, 379 MPa (55 ksi), NF at (2×10^6)).

1VX 1396 A5

2VX 1391 D-20

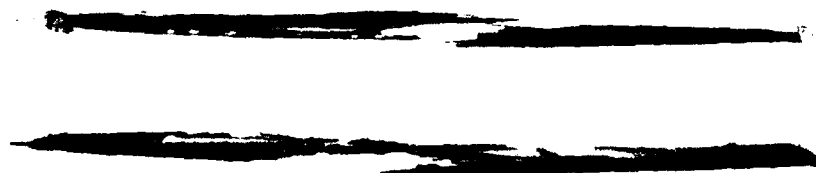


Figure 62. - Face and edge views of coupons fatigue tested at $R = 0.0$
(Top, 1VX1396-A5, 379 MPa (55 ksi), $N_F = 18740$; bottom,
2VX1391-D20 310 MPa (45 ksi), $N_F = 476,020$).

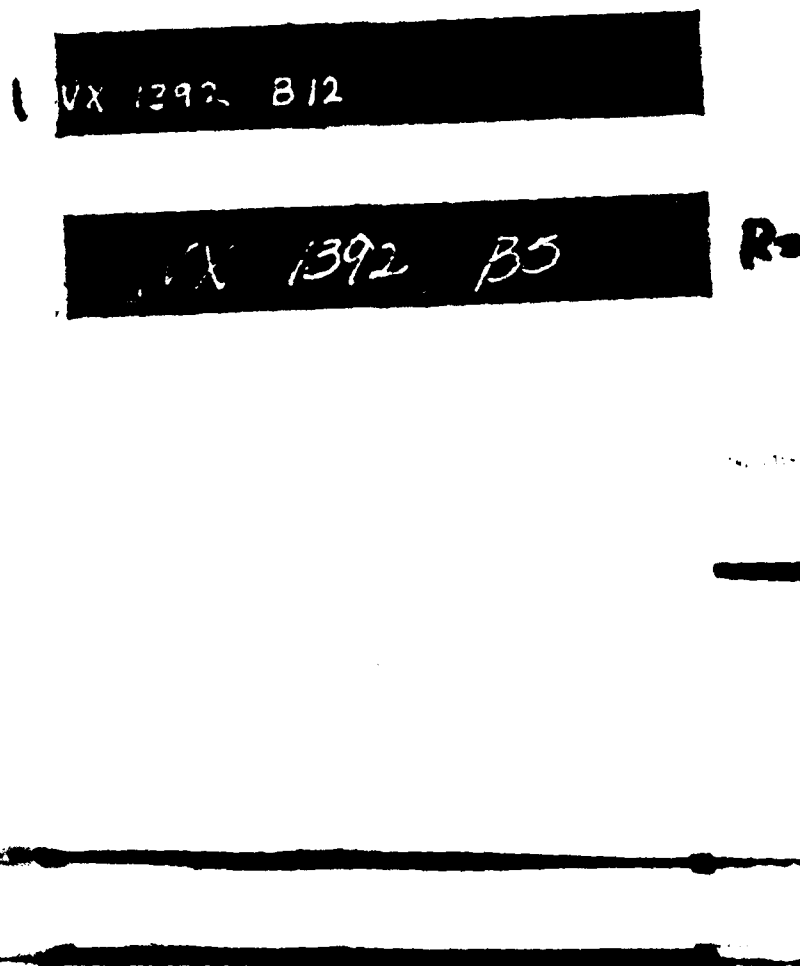


Figure 63. - Face and edge views of coupons fatigue tested at $R = -0.5$
(Top, 1VX1392-B12, 379 MPa (55 ksi), $N_F = 13937$; bottom
1VX1392-B5, 414 MPa (60 ksi), $N_F = 26,350$).

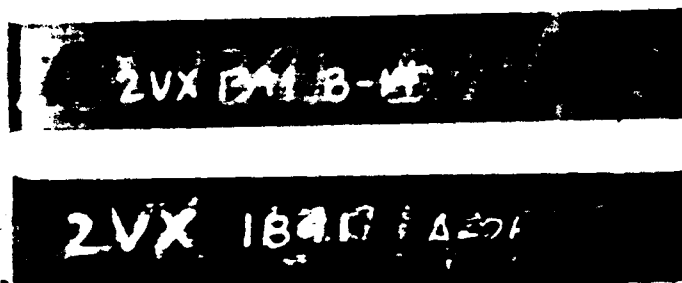


Figure 64. - Face and edge views of coupons fatigue tested at $R = -1.0$
(Top, 2VX1391-B14, 276 MPa (40 ksi), $N_F = 18400$; bottom,
2VX1391-A26, 207 MPa (30 ksi), $N_F = 802,709$).

between the failure modes of coupons tested at $R = +0.5$ or 0.0 were not observed, Figures 60 and 61. Those coupons which were tested at $R = -0.5$ or -1.0 displayed failure modes which were primarily influenced by the holes in the constraint fixture. This problem of the constraint fixture influencing fatigue life and failure mode cannot be avoided, but, hopefully, will be more easily analyzable using the fixture type to be employed in Tasks II and III.

The $R = 0$, T-T fatigue data for this quasi-isotropic laminate was compared to the similar room temperature, laboratory air, previously obtained data⁴ for T300/934 material. The results of the comparison are shown in Figure 65. As can be observed in Figure 65, the fatigue results for this laminate were essentially the same regardless of the type of epoxy matrix. A previous investigation showed that batch to batch effects on fatigue life were negligible.⁴ Therefore, an experimental basis has been established for concluding that the fatigue properties of a laminate are not significantly influenced at room temperature by the epoxy type or by batch properties.

5.2 RESIDUAL STRENGTH RESULTS

Coupons which did fail in fatigue were loaded to failure, half in tension and half in compression, as per RFP requirements. The test results of those coupons which could be loaded are shown in Tables 28 and 29. The data is too limited to make any definitive statements. In general, however, both the fatigue data and the residual strength data indicate that the $R = +0.5$ fatigue loading is less damaging at equivalent maximum stresses than the $R = 0.0$ loading. This suggests that fatigue cycling, not just maximum load, causes damage growth, a conclusion of importance for the Task II investigation.

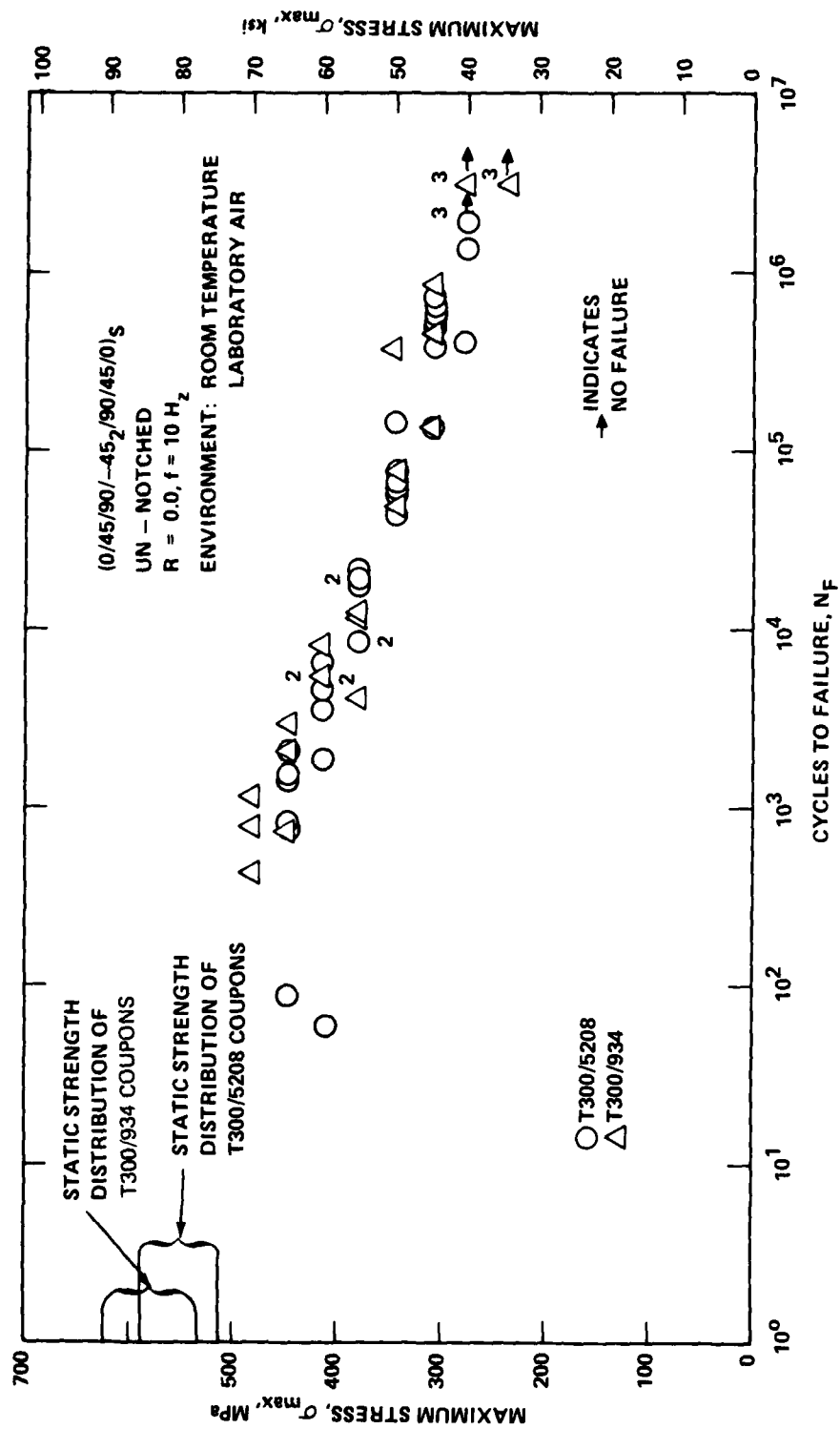


Figure 65. - Comparison of tension-tension fatigue data of laminated composites of T300/5208 and T300/934 in room temperature, laboratory at $R = 0.0$.

TABLE 28. - TENSION RESIDUAL STRENGTH TESTS OF UNFAILED FATIGUE COUPONS

R Ratio	Coupon ID	Average Area,		Ultimate Stress,		Strain to Failure, mm/mm in 254mm	Apparent Modulus of Elasticity,		Extent of Damage	Fatigue Stress Level	
		mm ²	in. ²	MPa	ksi		G Pa	psi x 10 ⁶		MPa	ksi
+0.5	2VX1341										
	-A15	52.5	0.0814	580	84.2	0.0107	54.3	7.87	None visible	345	50
	-A20	52.3	0.0811	572	83.0	0.0108	53.0	7.68	None visible	310	45
	-A23	52.6	0.0815	462	67.0	0.0095	48.6	7.05	Severe	379	55
	-B28	52.2	0.0809	531	77.0	0.0102	52.1	7.55	None visible	379	55
	-C24	52.2	0.0809	566	82.1	0.0096	59.0	8.55	None visible	276	40
	1VX1396										
	-A30	51.9	0.0804	579	84.0	0.0104	55.7	8.08	None visible	310	45
0.0	2VX1390										
	-C16	53.4	0.0828	364	52.8	0.0089	40.9	5.93	Severe	310	45
	2VX1391										
	-D9	51.9	0.0805	476	69.0	0.0107	44.5	6.45	Severe	276	40
0.0	-D19	52.3	0.0810	486	70.5	0.0100	48.6	7.05	Severe	276	40
	1VX1396										
	-A4	51.7	0.0802	496	72.0	0.0094	52.8	7.66	Medium	276	40

TABLE 29. COMPRESSION RESIDUAL STRENGTH TEST RESULTS OF UN-FAILED FATIGUE COUPONS

R Ratio	Coupon ID	Average Area,		Ultimate Stress,		Strain to Failure, mm/mm in 254mm	Secant Modulus at 35 ksi,		Extent of Damage	Fatigue Stress Level,	
		mm ²	in. ²	MPa	ksi		G Pa	psi x 10 ⁶		MPa	ksi
+0.5	2VX1391										
	-B1	52.7	0.0817	364	52.8	0.0087	47.2	6.86	Severe	379	55
	-B5	52.1	0.0807	509	73.8	0.0106	51.4	7.45	None visible	310	45
	-B24	Coupon damaged during Static Testing							None visible	276	40
	-D3	49.9	0.0774	547	79.3	0.0101	57.4	8.33	None visible	310	45
	2VX1390										
	-A30	54.5	0.0845	405	58.8	0.0084	51.9	7.53	Light	276	40
	-B14	53.9	0.0835	343	49.8	0.0075	49.2	7.14	None visible	310	45
0.0	-B18	53.4	0.0827	310	45.0	0.0077	46.4	6.73	Severe	345	50
	1VX1396										
	-A24	52.1	0.0808	343	49.8	0.0075	50.3	7.29	Severe	276	40
	2VX1390										
	-A17	53.4	0.0827	279	40.5	--- ^a	---	---	Severe	276	40

^a Stress-strain curve extremely irregular due to presence of "squiggle" defect

SECTION 6

EVALUATION AND SELECTION OF NDI METHODS FOR DAMAGE MONITORING

In this subtask, several nondestructive investigational techniques were evaluated as to their usefulness for providing reproducible and clear detection of damage mechanics, such as matrix cracking and ply delamination, in the graphite/epoxy coupons used in this program. The ease of use, time required, and cost of each technique were considered. The technique evaluation process began with a survey of those NDI techniques available at the inception of this program. Several techniques were selected from the survey for further investigation and evaluation. These selected techniques were used to detect damage in coupons loaded in static tension and in tension-tension fatigue. The capabilities of the techniques were evaluated and specific techniques selected for use in Tasks II and III. The selected techniques will be used to detect and monitor damage which results from the fatigue loading histories used in those tasks.

In general, the criteria used to select NDI techniques were determined by program objectives. The technique selection criteria of a quality control or in-site inspection program differs from those of a damage mechanism research investigation in terms of the type of damage being detected, the size of the material part being inspected, the allowable operational time, and the cost requirements. While an ideal situation might be to select the same technique for use in both types of programs, this may not be possible due to the differences in technique criteria. The techniques considered in this program were evaluated only with respect to the limited program objectives. The evaluation and selection of the techniques is detailed below.

Based upon the discussion in Sections 1.2 and 1.3, an inference was drawn which affected the choice of NDI techniques to be evaluated. The inference is that there exist three principal damage mechanisms in graphite/epoxy composite materials: microcracks, delamination, and fiber breakage. An ideal NDI procedure for laboratory use must meet several criteria based upon the expected type of damage. Specifically, the method must: 1) be reproducible; 2) locate damage sites; 3) differentiate among mechanisms; and 4) indicate expected failure locations.

6.1 SELECTION OF TECHNIQUES

At the inception of this program, the methods most commonly used for the inspection of composites were ultrasonic C-scan, x-ray, Moiré, brittle lacquer, acoustic imaging, photoelastic casting, penetrant, thermography, acoustic emission, and laser holography. In addition, some methods were being used to measure specific parameters, such as ultrasonics to measure moisture level, eddy current to monitor fiber volume^{57,58}, and radiography and thermal neutron mass absorption to determine resin content⁵⁹. A review of the literature showed that of the variety of NDI methods available, few provided detailed information on the type of damage present.

One class of methods provided information on the extent of surface distortion by monitoring displacements in the thickness direction. These methods included laser holography and Moiré. While some investigators reported limited success using these methods⁶⁰⁻⁶³, no quantitative correlation between strength and the holographic indications had been found, for example, necessitating a refined definition of the specific type of damage which resulted in the NDI indication. Laser holographic techniques^{64,65} had been examined by Sendeckyj, Maddux, and Tracy⁶⁶. They concluded that the technique had potential, but that much work needed to be done, particularly in determining which type of loading (thermal, acoustic, or mechanical) would give the most useful fringe patterns and in interpreting the fringe pattern anomalies. Thus, this technique was not a state-of-the-art procedure available at the beginning of this program.

X-ray methods were being successfully used for NDI⁶⁷⁻⁷³. An opaque additive dye, normally TBE (tetrabromoethane), was usually necessary to enhance the resulting x-ray. This method had the potential of being able to define the actual types of damage, particularly when a microfocus x-ray source was used. The enhanced x-ray NDI procedure was able to clearly show matrix cracking. Information covering the number of delaminations which lay above one another has been obtained by carefully varying the exposures and the x-ray angle on multiple shots and comparing the results.⁷⁴ Photos resulting from this method provided a great deal of information on damage type and extent, and had been used as input for computer enhancement analysis, which could identify damage patterns not readily visible to the eye.

On the negative side, in addition to the inherent dangers of using x-ray sources, TBE was known to be a biologically hazardous material. The compound was extremely toxic and constituted a health hazard due to inhalation and skin contact. Thus the likelihood of using TBE outside of a controlled laboratory situation was reduced. More importantly, serious questions existed as to the potential effects of TBE on subsequent material behavior.^{57,23} From a chemical viewpoint, the penetrant had the potential to seriously change the behavior of the epoxy and graphite,^{68,75} but this has not been observed experimentally.^{76,77} Alternatives to TBE had been investigated. Renografin, a medical radio-opaque dye, had been found to be ineffective while two other compounds of low toxicity were of possible interest: DIB (1, 4 diiodobutane); and trimethyl bismuthine.⁶⁸ The DIB material was found to have similar radio-opaqueness to TBE, was less toxic, and appeared not to degrade graphite/epoxy as recently evaluated.⁷⁹ Therefore, this enhancer was selected for use in this program.

A major problem with the enhanced x-ray NDI procedure is that only those damage areas that intersected a surface where the radio-opaque penetrant could infiltrate the damage zone would be seen.^{79,80} Damage limited to the inside region with no path to the free surface could not be observed. Hence, while the method provided excellent detail (assuming all damage areas were wetted and penetrated by the penetrant), the serious question of effectiveness for inspecting unnotched coupons remained to be resolved in this program.

Application of acoustic imaging methods had recently been shown to have the potential to detect and define the type and extent of damage in composite materials.^{81,82} Acoustic images of an object are formed in a manner analogous to that in optical imaging. In general, these acoustic images consist of amplitude and phase variations of an ultrasonic field in an image plane - this field having interacted with a material undergoing non-destructive testing. Ultrasonic sensors are used to detect the acoustic signal variations, and sensor output is displayed photographically, on a conventional television, and/or recorded on video tape. Unlike radiography, any small inclusion or discontinuity in a material scatters acoustic energy;

hence, cracks and minute defects produce substantial acoustic signal variations. This high sensitivity was an important factor in the success of acoustic imaging in displaying interior voids, delaminations, and other anomalies in graphite/epoxy composites.

Advantages of acoustic imaging for interior inspection of graphite/epoxy materials include: presentation in real time of a two-dimensional display representing interior structural variations and discontinuities, high sensitivity and resolution, and tomographic (cross-sectional) viewing capability by acoustic focusing. In addition, by precision focusing, the structure at various levels can be examined, thus providing added information as to the relative location of various damage through the thickness. One disadvantage of this method is that an acoustic transfer medium (water) has to be in contact with the specimen. This is the same disadvantage as for normal C-scan ultrasonics. In situ inspection is, therefore, not possible. The main disadvantage was that this experimental system was essentially not available at the inception of this program and required a large expenditure (approximately \$100,000) in order to be made operation.

Simple ultrasonic C-scan^{60,66} has been used in the past with generally poor results. The "go no-go" type of instrument normally used gives only an indication of a loss of energy being transmitted through the specimen and no detail of the damage type or depth. Several researchers have found that the method gives quick and clear indications of a general damage region.^{83,84} A variation of using ultrasonics for inspection was ultrasonic spectroscopy, where a spectrum analyzer was used to display an amplitude versus frequency plot for a returned signal. This procedure is considered to have a potential for locating damage regions by essentially an acoustic signature identification procedure.⁸³ Much more research was needed to develop this procedure. In general, a simple potential for identifying damage size in any quantifiable manner was lacking.

A pulse-echo type of ultrasonic system, sometimes called acoustic imaging, involves the use of both C-scan and B-scans. This system appeared to have a large potential for identifying preload manufacturing defects (voids, damaged fibers, etc.), matrix delamination and, to some extent,

matrix and fiber cracking. The method, developed by Holosonics, Inc. uses their Holoscan ultrasonic unit to display damage. The system being used at the Lockheed-California Company on AFFDL Contract F-33615-77-C-3084⁷⁷ permitted a large selection of transducers. The system has an analog memory and real-time display processor interfaced with other electronics to produce a digital memory storage unit capable of retention and display of data in C or B-scan format as well as in 3-D isometric. This provides a major tool to examine composite damage characteristics in that the measurement of the ply level at which damage occurred, as well as the extent of damage at each level, could be determined. The scanner system can be used on coupons mounted in the test frame as water immersion is not required. A hand-held transducer allows quick location of damage regions for subsequent detailed scan. More details on this procedure are reported elsewhere.^{77,85}

Acoustic Emission (AE) is an NDI procedure that has been introduced for the inspection for, and location of, damage in composites.^{58,86-92} The AE procedure has the potential of detecting fiber breakage. At the time (1978), the procedure gave only a general level of activity type of information and limited definition of source type and location. For static strength and stress-rupture testing, the AE count rate had been shown to correlate well with increasing load, to be relatively quiet during a load hold, and to increase again just prior to failure.⁹³ In the case of fatigue, the problem was much more complex in that, possibly, the rising portion of the load profile was the most important for AE monitoring.^{86,89} For a boron/epoxy composite, reasonable correlation had been shown between the normalized total AE count and compliance (inverse stiffness) of a coupon tested in fatigue.⁸⁶ Acoustic emission had also been used to locate the flaw source with an acceptable degree of reliability.⁸⁰ In general, the AE damage detection procedure appeared to have greatest value for continuous in situ detection and location of damage and some limited use for determination of damage type. The ultimate usefulness of the technique may lie in using AE in conjunction with other NDI techniques.

Another technique considered of value for the detection of damage initiation and growth in composites was the plastic-casting of specimen edges for

the detection of cracks.^{93,94} This technique was borrowed from photoelastic casting techniques used in the analysis of failures in metallic components and the green-out of visual observations of edge cracks.⁹⁵ The edge-replication technique can detect early cracks in the specimen matrix and could be especially valuable for unnotched coupons where the expected major damage location was not known with precision prior to the test. Edge-replication appeared to have a distinct advantage over direct visual observations in that the entire edge was recorded, not just a small portion as would be photographed through a microscope.⁹⁴ Like enhanced x-ray, internal damage cannot be detected.

Damage initiation in composites could also be detected by thermographic recording of hot spots, which were indicative of localized damage.^{86,93,96,97} Essentially, the thermographic camera records the distribution of temperature. The technique had been shown to be effective for both locating and tracking damage, particularly that caused by delamination. The inspection procedure is used primarily for fatigue, since little heat is generated during static loading. Even in fatigue, the technique had greatest utility for boron-epoxy laminates since they generated a fair amount of heat under cyclic loading. To be applicable to graphite/epoxy composites, significant development work remained to be undertaken.^{98,99} The procedure could be modified for use under static loading or during hold periods of fatigue loading by ultrasonically vibrating the specimen being inspected at high frequencies (approximately 20 kHz).^{94,100} This vibrothermographic technique also required further development.⁹⁵ Even though correlation between the thermographic records and thermal predictions had been achieved^{93,98}, the heat patterns did not conform directly to the actual damage size and shape.^{98,99} The question as to the feasibility of determining the level of ply information with this technique had not been answered.

Temperature has also been used as a general NDI inspection technique by simple monitoring of the temperature rise in a coupon.^{18,101} The primary value of this technique is monitoring the change in overall coupon temperature, which appears to be primarily related to the onset of delamination or severe

matrix cracking. The technique might have more value for tension-tension fatigue than for tension-compression fatigue monitoring, where the temperature rises quickly after initial loading and does not significantly change until failure.¹⁸ The procedure is considered to be primarily valuable as a qualitative indication of damage.

Another monitoring procedure of interest was that for recording laminate stiffness changes during fatigue. Stiffness is known to change due to fatigue loading.^{18,101,102-104} Stiffness has been proposed as a criteria for fatigue damage¹⁰³ because stiffness changes appeared to be directly relatable to delamination, dimensional change, acoustic emission, stress state variations as monitored by heat emission¹⁰⁵⁻¹⁰⁷, and microscopic internal damage.¹⁰⁸

Fluorescent penetrants have also been used to detect damage¹⁰⁹ in graphite/epoxy composites. This procedure detected delamination along edges and around holes, but, like x-ray radiographic techniques using opaque penetrants, no damage could be detected that did not intersect outside surfaces. The question of damage to the composite itself was unknown. In general, the use of simple penetrants for detection of delamination might eventually prove useful for a quick, overall detection procedure, however, the procedure did not, at the time, offer the versatility or precision of other NDI techniques.

Selected NDI Procedures

Based upon the above discussion of the state-of-the-art of NDI techniques as applied to composites, the following procedures were selected for further evaluation in Task I of this program:

- 1) Enhanced x-ray radiography
- 2) Ultrasonic pulse-echo using a Holoscan unit
- 3) Acoustic emission
- 4) Plastic-cast edge replication
- 5) Monitoring of stiffness change
- 6) Monitoring of thermal temperature rise

Both the enhanced x-ray radiography and the ultrasonic pulse-echo techniques had the potential to detect internal composite coupon damage, such as matrix cracking and ply delamination. The acoustic emission method was a real-time monitoring technique which had the potential of detecting damage location and differentiating among damage types. However, the level of ply damage at a particular location would not be identifiable. Plastic-cast edge replication enabled the making of permanent records of the matrix cracking and delamination that had occurred along coupon edges. The recording of changes in coupon temperature and stiffness was undertaken as per the requirements of the RFP. Coupon temperature monitoring was retained mainly to ensure that overall coupon temperature change was not excessive. Coupon stiffness is related to the damage state, but the sensitivity of the procedure is dependent on layup configuration. Layups with a high percentage of 0° fibers (>50%) in the loading direction can withstand severe damage without significant tensile stiffness changes.¹⁸ This fact reduces the general efficacy of stiffness monitoring.

Thermography was not included because of the large effort which remained to make the technique available for general use on graphite/epoxy laminates. Acoustic imaging was not selected because no system was presently available at that time in the form required and similar information could be obtained using the Holosonics ultrasonic system. Other possible ultrasonic systems were also not included for they did not seem to add any different or additional information to that obtainable from the selected NDI techniques. Simple penetrant inspection was eliminated because of the lack of definitiveness of damage detection and lack of knowledge as to the potential damage to the graphite/epoxy composite material.

6.2 NDI: EXPERIMENTAL PROCEDURES

Enhanced X-Ray Radiography

A Norelco MG 150 constant potential radiographic x-ray system with a 150 kV Beryllium window tube was used in conjunction with the radio-opaque penetrant DIB (1,4, diiodobutane). The DIB was applied to the specimen edges, and the surface residue was removed after soaking for 15 minutes.

A microfocus x-ray tube with a 0.7 mm focal spot was used to produce the x-rays on Kodak Type M film. The exposures were made at 25 kVp, 5 ma for 70 sec. (350 Mas), and focal distance of 183 cm (72 in.)

Ultrasonic Inspection

Two types of ultrasonic inspection systems were used in the program: a reflected through transmission "go, no-go" Immerscope 725 Ultrasonic Unit with a SR150 C-scanned bridge and a Horisonic 5 MHz long focus transducer; and a pulse-echo Holosonic System 400. "Go, no-go" C-scans of the entire 15.2 cm (6 in.) gage length of the specimen were made. Coupons showing damage within the center 5.1 cm (2 in.) of the gage length were inspected with the pulse-echo system, and B and C-scans were made. The scan length of the pulse-echo unit was limited by the size of the scanner mount and the size of the acoustic transducer foot. A fixture was designed to enable the pulse echo unit to scan the 2.54 cm (1 in.) wide coupons.

Acoustic Emission

Acoustic emission experimental procedures and test equipment will be described in greater detail than those used with the other NDI techniques. The description is lengthy because eventually acoustic emission was rejected for use in Tasks II and III. The reasons for rejection cannot be understood without a clear perception of the test equipment and experimental procedures.

An acoustic emission is defined as a packet of energy that is rapidly released from a stressed material. In graphite/epoxy composites these emissions, or events, are thought to be caused by matrix cracking, ply delamination or fiber breakage. The acoustic emission technique consisted of monitoring in real time the events which occurred during a material test and characterizing the event waveforms in terms of count, amplitude and location parameters, Figure 66. A count was defined as each crossing of the event waveform above a selected threshold voltage. The amplitude was the peak voltage of the event waveform, and the location was the position of event origin. The total counts, count rate distribution of event amplitudes,

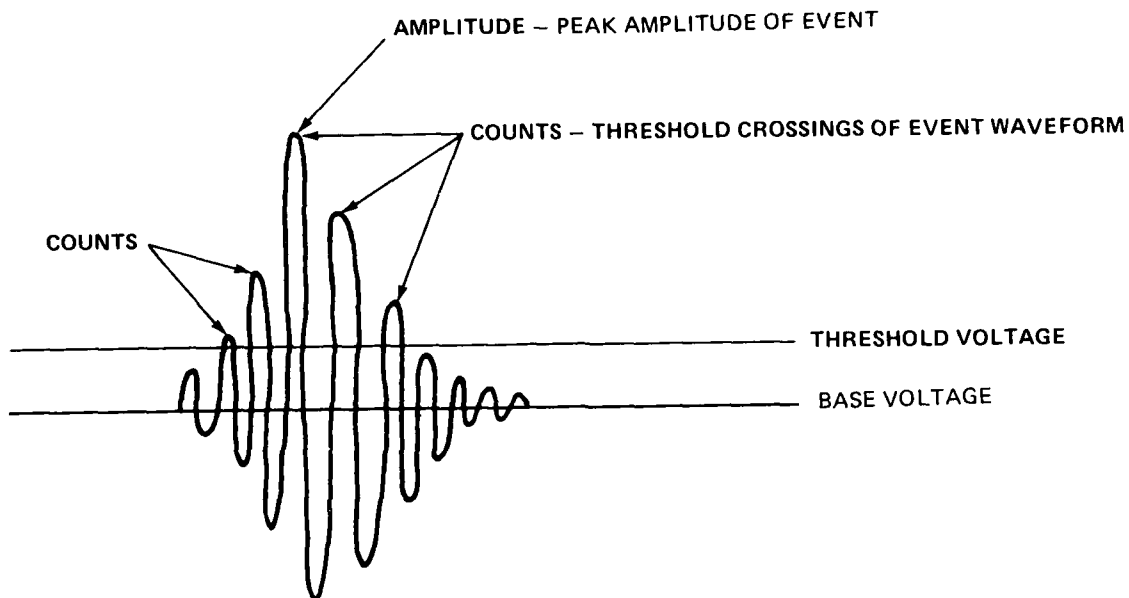


Figure 66. - Schematic of Acoustic Emission Event

and distribution of event locations were recorded for each experiment. The information was evaluated to determine whether reproducible "signature patterns" of emission history existed for each parameter, and if so, whether the parameter data could be correlated with the occurrence of composite matrix cracking, ply delamination or fiber breakage.

The Series 3000 Acoustic Emission Instrumentation System by Dunegan/Endevco was selected for evaluation in this program. The capabilities of this system represented the basic state-of-the-art capabilities for the acoustic emission (AE) technique that were available at the inception of this program. The acoustic emission process for graphite/epoxy was intended to be investigated using the Series 3000 System before a more complex, but characteristically similar, computer system was to be considered for use in Tasks II and III. Figure 67 is a schematic diagram of the acoustic emission experimental equipment.

Two 7.6 mm (0.3 in.) diameter miniature transducers (Model S1000BM) were placed at each end of the 15.2 cm (6 in.) coupon gage length, resulting in a center-to-center transducer separation of approximately 11.7 cm (4.6 in.). Acoustic emissions from the test specimen were received by the two data transducers, amplified a fixed 40 dB by preamplifiers (Model 1801), and amplified a selected 40 dB by a Dual Signal Conditioner (Model 302A) to filter out noise from the test machine. The counts of the event waveforms were determined by the signal conditioner and the total number of counts and the count rate values or both were tallied by a Dual Counter (Model 303). For static tests, the count rate and total count values were plotted in real time versus the load being applied to the specimen or versus a time base provided by a Ramp Generator (Model 502). For fatigue tests, these values were plotted in real time versus the number of applied load cycles. The number of cycles was provided by a Voltage Control Gate (Model 906A), a module which also allowed selection of the portion of the load cycle which was monitored for acoustic emission activity. The positive slope portion of each cycle was monitored during the fatigue experiments.

The 11.7 cm (4.6 in.) length between the two data transducers was divided into a 0 to 100% scale. The location scale was calibrated by introducing pulses to the test specimen via a pulse transducer (Model S140B) with an attached waveguide and by calibrating the pulse locations with a Distribution Analyzer (Model 920 A). The event origin locations were determined by the Distribution Analyzer and processed as the number of events per location (event location distribution). An amplitude threshold of 40 dB was selected to eliminate noise from the testing machine. Event amplitudes greater than the threshold were determined by an Amplitude Detector (Model 921) and the values were processed by an External Memory (Model 922) to give the number of events per amplitude (event amplitude distribution). Log and linear plots of the amplitude and location distributions were viewed on an oscilloscope (Display Model 118) and on an x-y plotter. Guard transducers, one placed between each data transducer and test machine grip, and a Spatial Discriminator (Model 420) locked out intermittent transient noise from the testing machine grips.

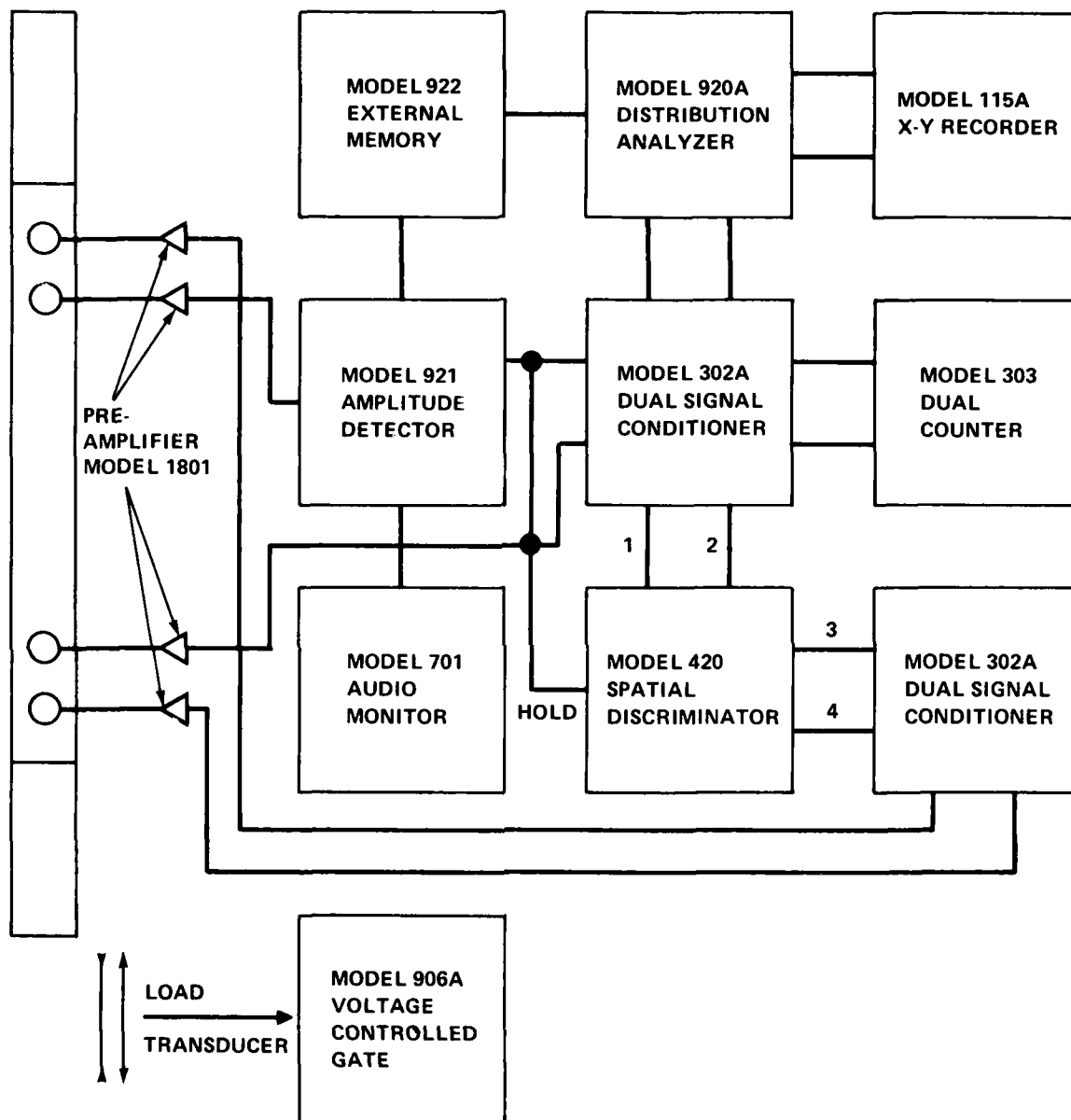


Figure 67. - Schematic Diagram of Acoustic Emission System

Edge Replication

The plastic-cast edge replication technique used in this program was developed and modified from the original method of Stalnaker and Stinchcomb.⁹⁴ A strip of acetate tape, 5 mil thick was softened by acetone and placed on the edge of a specimen being held under load. A fresh acetate strip was placed over the first tape and pressed firmly to ensure good contact of the tape with the specimen edge and to remove air bubbles from between the two tapes. After drying for fifteen minutes, the replica was removed from the specimen edge and placed between two glass slides to keep it flat. To make photographs of selected portions of a replica, the replica were first used as a negative in a photographic enlarger. Later, a microfisch reader was found to be an improvement.¹¹⁰ Prints up to 30 times magnification were made and examined for signs of cracking.

Monitoring of Stiffness Change

The stiffness of the coupons loaded in tension-tension fatigue was monitored by taking the initial and final static tensile moduli, and the initial and final dynamic tensile moduli. Axial strain gages measured the strain for the static and dynamic moduli. As a precaution for the potential fatigue failure of the strain gages, a clip gage was also used to obtain the static moduli. The clip gage was not used to obtain the dynamic moduli because the type used was not capable of measuring strain during a dynamic test.

Monitoring of Thermal Temperature Rise

The temperature monitoring of coupons under tension-tension fatigue loading was accomplished by attaching two thermocouples to the coupon and exposing one control thermocouple to the air. The testing machine grips, coupon, and thermocouple wires were enclosed in a shield to reduce deviations in temperature due to air currents.

6.3 NDI EXPERIMENTAL TEST MATRIX

Experimental

The NDI studies were conducted on laminate coupons tested in static tension to selected load levels and in tension-tension fatigue to selected cycle intervals. Only tension load excursion experimentation was conducted because the state-of-the-art of some of the procedures was found to be less adequate than expected. Since the objective was to select NDI procedures for Tasks II and III, more emphasis was placed upon developing sound techniques than simply on obtaining test data. Difficulties encountered with the NDI procedures during the selection process necessitated restricting experimentation to tension load excursions.

The test matrices were selected to provide opportunities for the monitoring of different damage mechanisms. Coupons tested in static tension were loaded at a strain rate of 0.01 mm/mm/min to 20, 40, 60, 80 and 100 percent of the average ultimate load. The coupons were monitored during the tests by acoustic emission and after the tests by edge replication, enhanced x-ray radiography, and by reflected through transmission and pulse-echo ultrasonic inspection, Table 30. To provide an indication of the capability of the acoustic emission technique, laminate coupons loaded in static tension at a strain rate of 6 mm/mm/min were also monitored by the technique. This high strain rate approximated the rate of the fatigue tests, which were run at 10 Hz.

The tension-tension fatigue maximum stress levels and cycle intervals were selected after inspection of the $R = 0.0$ stress-life curve developed in Task I. These tests were run at maximum stresses of 310 and 379 MPa (45 and 55 ksi). The 310 MPa (45 ksi) test coupons were inspected at 100, 1000, 5000, 10 000, 20 000, 30 000, and 40 000 cycles. The 379 MPa (55 ksi) test coupons were inspected at 50, 100, 400, 700, 1000, 13 000, and 16 000 cycles. The two fatigue stress levels provided examples of damage occurring at two different rates. The 310 MPa (45 ksi) test coupons were inspected by acoustic emission, enhanced x-ray, radiography, ultrasonic inspection, temperature monitoring and stiffness monitoring, Table 31. After the

TABLE 30. NDI TEST MATRIX FOR STATIC TENSION TESTS
STRAIN RATE = 0.01 mm/mm/min

	Percentage of Average Ultimate Load				
	20%	40%	60%	80%	100%
Total Coupons Tested	6	3	3	3	3
Coupons Tested Per NDI Technique:					
Enhanced X-Ray Radiography	6	3	3	2 ^a	--
Acoustic Emission	6	3	3	3	3
Ultrasonic Inspection					
"Go-No-Go"	6	3	3	2 ^a	--
Pulse-Echo	5	--	1	--	--
Edge Replication	3	3	3	3	--

a One coupon failed

TABLE 31. NDI TEST MATRIX FOR TENSION-TENSION FATIGUE TESTS
 σ_{\max} = 310 MPa (45 ksi), R = 0.0

	Number of Cycles						
	100	1000	5000	10 000	20 000	30 000	40 000
Total Coupons Tested	2	2	2	2	2	2	2
Number of Coupons Tested Per NDI Techniques:							
Enhanced X-Ray Radiography	2	2	2	2	2	2	2
Acoustic Emission	2	1	1	1	--	--	--
Ultrasonic Inspection							
"Go, No-Go"	2	2	2	2	2	1	2
Pulse-Echo	--	1	--	1	--	--	2
Thermal Monitoring	1	1	1	1	2	2	1
Stiffness Monitoring							
Static Modulus — Initial Axial							
Strain Gage	2	2	2	2	2	2	1
Clip Gage	2	2	2	2	1	2	--
Final Axial							
Strain Gage	2	2	1	--	--	--	--
Clip Gage	2	2	2	1	1	2	2
Dynamic Modulus — Initial Axial							
Strain Gage	2	2	2	2	2	2	2
Final Axial							
Strain Gage	1	1	1	1	--	--	--

evaluation and elimination of several NDI techniques, the 379 MPa (55 ksi) test coupons were monitored for temperature changes and inspected with enhanced x-ray radiography, Table 32. The capabilities of each NDI technique to detect the type and location of the damage present in the tested composite coupons was evaluated.

6.4 NDI EXPERIMENTAL RESULTS

6.4.1 DIB Enhanced X-Ray Radiography

Using the DIB enhanced x-ray radiography technique, interply matrix cracks were detected, as expected, in 90°, -45°, +45°, and 0° plies. Interply delamination was also easily detected. Matrix cracking in the 90° plies was, however, clearly visible only after the -45° plies had cracked.

In the static tests, no cracking was detectable at 20% of the average ultimate tensile strength. This is consistent with a general ply analysis, which indicates fracture of the 90° plies at approximately 25% of the ultimate strength. However, this result is different from that of other investigations¹ where cracking of these plies is seen earlier than the analytically derived ply failure load. Possibly, and perhaps most likely, this is caused by the inability of the DIB enhancer to penetrate the extremely fine, low load, transverse 90° cracking, or that the amount of DIB is so small that improved x-ray techniques are required. Similarly, at 40% of the average ultimate strength, the 90° transverse cracks, though visible, were difficult to detect, again apparently due to the extreme fineness of the cracks. In contrast, at

TABLE 32. NDI TEST MATRIX FOR TENSION-TENSION FATIGUE TESTS
 $\sigma_{\max} = 379 \text{ MPa (55 ksi)}$, $R = 0.0$

	Number of Cycles						
	50	100	400	700	1000	1300	1600
Total Coupons Tested	3	2	2	2	2	2	2
Coupons tested per NDI techniques:							
Enhanced X-ray radiography	3	2	2	2	2	2	2
Thermal monitoring	3	2	2	2	2	2	2

60% of the average ultimate strength, both 90° and -45° ply matrix cracks were easily detectable, although the -45° ply cracks were more pronounced. This result was expected because the -45° plies crack at about 55% of the ultimate strength. That the 90° ply cracks were more easily observed is presumably due to their increased width. In many cases, the -45° ply cracks were not detected as extending from edge to edge, which is similar to other experimental results.³ Finally, the coupons loaded to 80% of the average ultimate strength showed a crack pattern similar to that observed at 60%. The 90° and -45° ply cracking appeared to be more extensive, but no $+45^{\circ}$ ply crack was observed, nor was interply delamination detected. At each load level, the amount of cracking detected varied considerably from coupon to coupon, which is consistent with variability in the static failure data.

In order to confirm the cracking detected in these coupons by enhanced x-ray radiography, a photomicrographic section was taken in the 0° direction from the center of a coupon loaded to 60% of the average ultimate tensile strength. Figure 68 shows portions of that section. Matrix cracks in the 90° and -45° plies are clearly visible. The spacing of these matrix cracks appears to be regular.

Coupons were fatigue cycled at 310 and 329 MPa (45 and 55 ksi) for the purpose of interrupting them at various cycle counts to monitor damage growth. Of those cycled at 310 MPa (45 ksi), no damage could be detected by x-ray after 100 cycles. At 1000 cycles, 90° ply matrix cracks were evident, as were a few -45° cracks which emanated from the coupon edge, but did not transverse more than a quarter of the coupon width. At 2000, 5000, 10 000, 20 000, and 30 000 cycle intervals, the 90° ply cracks became more evident, while the -45° ply cracks increased in number, and eventually transversed the coupon by 30 000 cycles, see Figure 69.

Matrix cracks in the $+45^{\circ}$ began to appear in some coupons between 30 000 and 40 000 cycles, see Figure 70a. These $+45^{\circ}$ matrix cracks appeared to be much less in number than the 90° or -45° cracks. Delamination began at various regions on the coupon edges, apparently after cracking began in the $+45^{\circ}$ plies, grew in the longitudinal and width direction, and coalesced at

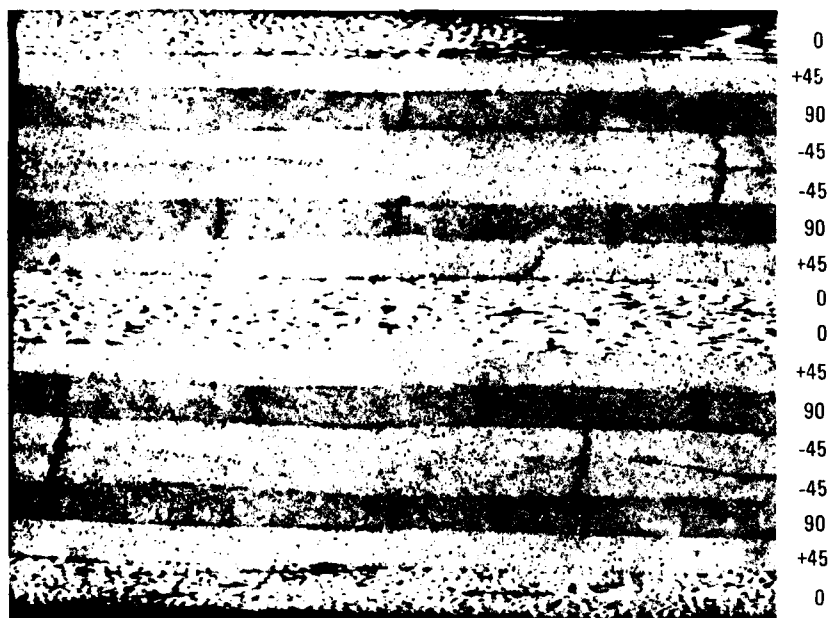
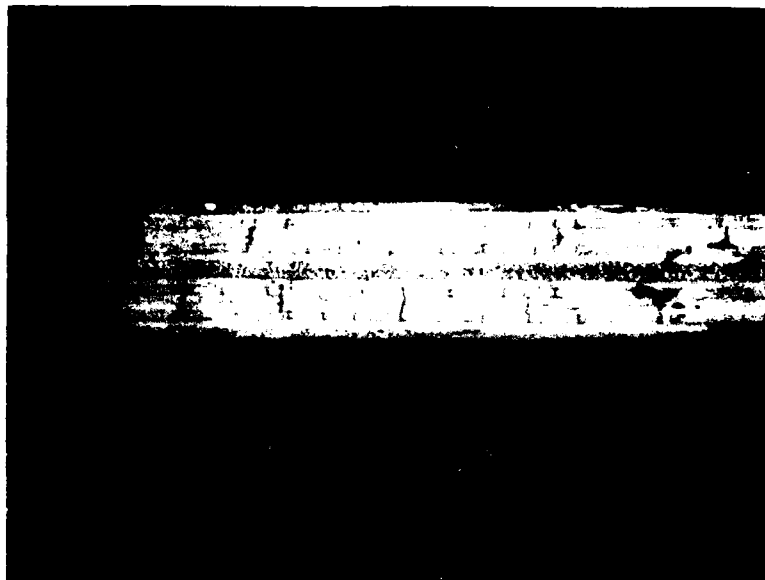


Figure 68. - Cross section in the 0° direction of a coupon loaded statically to 60% of the average ultimate tensile strength.

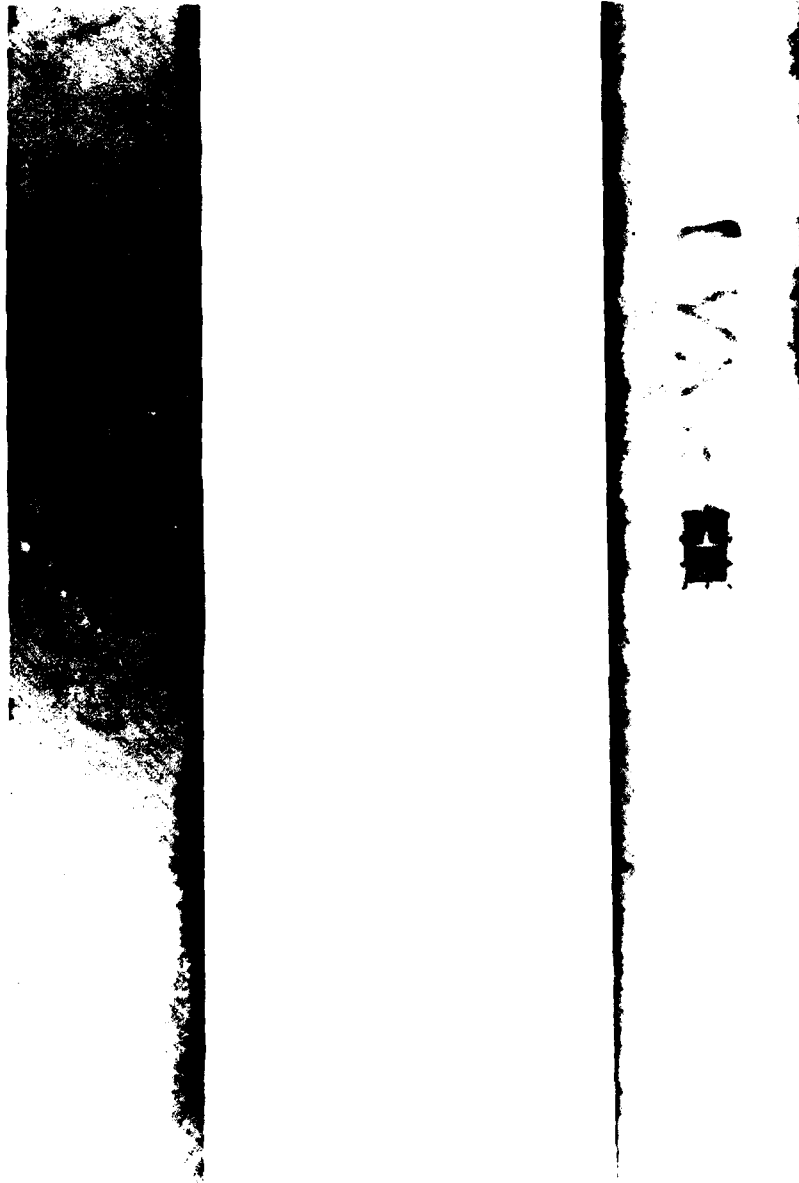


Figure 69. - Enhanced x-ray photographs of coupons fatigue cycled at 310 MPa (45 ksi), $R = 0.0$, showing 90° and -45° ply matrix cracking. (90° cracks were difficult to reproduce for this report).

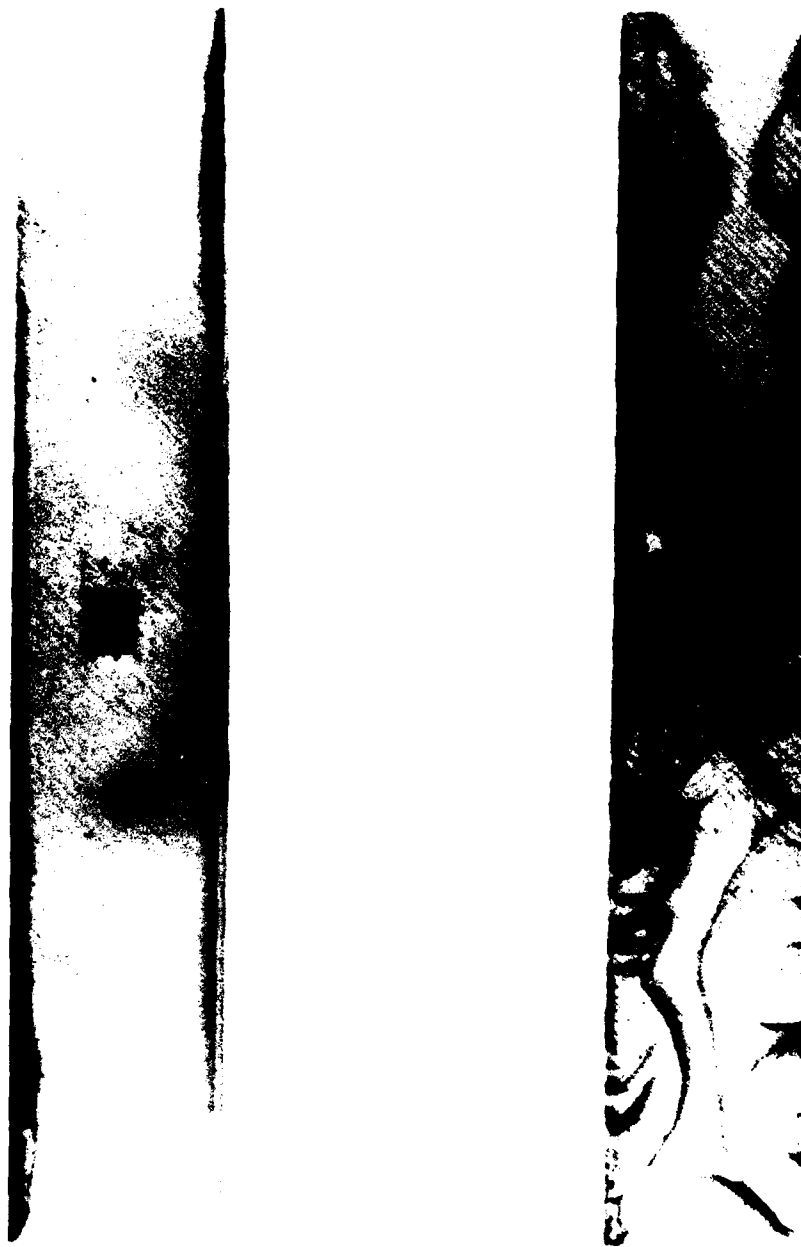


Figure 70. - Enhanced x-ray photographs of coupons fatigue cycled at 310 MPa (45 ksi), $R = 0.0$, showing $+45^\circ$ cracking and delamination and 0° longitudinal cracking.

some region, see Figure 70b. In the delamination regions, matrix cracks were detected in the 0° longitudinal plies. These 0° cracks were not observed in undelaminated regions, except for a short distance where they ran partially out of these regions. Unlike the transverse ply cracking, 0° ply cracking generally had a regular spacing of about a fiber tow width.

Coupons fatigue loaded at 349 MPa (55 ksi) at $R = 0.0$ were found to have cracked in both the 90° and -45° plies after 50 cycles, see Figure 71. This is consistent with the static data which indicated that 349 MPa (55 ksi) is considerably above -45° ply failure. The number of -45° ply cracks varied in each coupon, being quite extensive in some, while restricted to less than 30 in others. Many -45° cracks did not extend across the coupon width. Similar to the coupons cycled at 310 MPa (45 ksi), these coupons exhibited more -45° ply cracks, more of which crossed the coupon width as the number of cycles increased, Figure 71. Edge delamination was found to be clearly visible and to begin in some coupons by 700 cycles, see Figure 72. Matrix cracking in the $+45^\circ$ plies were observed to develop at the free edge, but they were never found to be as numerous as the -45° ply cracks. As cycles were increased, delamination growth was easily detected, as were 0° ply cracks, which developed in the delamination regions, see Figure 72. As in the coupons tested at 310 MPa (45 ksi), the 0° ply cracks were confined to the delamination regions. Hence, though 0° ply cracks were observed extending from tab to tab, they were found only near the free edge in the delaminated regions.

The above described observations showed the viability of using enhanced x-ray radiography as a damage detection and monitoring technique. The only detail not determined by the procedure used was the ply level in which delamination occurred. This question will be discussed in Section 6.4.4 on plastic-cast edge replication. The damage details observed in the enhanced radiographs, though necessarily limited due to the purpose of Task I, nonetheless allow inferences as to the nature of damage initiation and growth in this quasi-isotropic laminate. These inferences provide a firm base for the detailed NDI investigation to be undertaken in Tasks II and III.



Figure 71. - Enhanced x-ray photographs of coupons fatigue cycled at 379 MPa (55 ksi), $R = 0.0$, showing 90° and -45° ply matrix cracking. (90° cracks were difficult to reproduce for this report).



Figure 72. - Enhanced x-ray photographs of coupons fatigue cycled at 379 MPa (55 ksi), $R = 0.0$, showing $+45^\circ$ ply cracks, delamination initiation and growth, and 0° ply cracks.

Under a tensile load to failure, at low strain rate, this laminate first sustains matrix cracks in the 90° plies, followed by cracking in the -45° plies at higher load. Whether the 90° and -45° ply crack densities reach a characteristic spacing is yet to be determined. At loads in excess of 80% of the coupon strength, $+45^\circ$ ply matrix cracks occur. At higher loads, delamination apparently occurs predominately between the outer 90° and -45° ply, but also to some extent, between the outer 90° and $+45^\circ$ plies. The hypothesis is made, to be confirmed in Task II, that 0° ply matrix cracks now occur in the delaminated regions, and, because of the high load, 0° fibers fracture in small bundles in the region across the open space of the underlying $+45^\circ$ ply. This results in the growth of a cross-fiber crack in an outer 0° ply in a direction perpendicular to the loading direction. The growing transverse crack will be along a $+45^\circ$ direction, as is observed in fractured coupons. The growing 0° ply crack may not transverse the coupon at a $+45^\circ$ angle before the other 0° plies fracture, resulting in a final fracture region exhibiting 0° ply fracture partially at $+45^\circ$ starting from the edge and partially at 90° . In these low strain rate static tests, the longitudinal growth of 0° matrix cracks followed by fracture of 0° fiber bundles in a small delaminated region is believed to occur coincident with, or soon after, delamination. This sequence of events results in coupon fracture without significant delamination in other regions.

At high strain rates, similar damage growth is believed to take place as at low strain rates. However, in this case, the matrix cracks which form in the 0° plies have sufficient energy per unit time, in many cases, to fracture the fibers without significant longitudinal growth resulting in a lower strength.

In the case of tension-tension fatigue, damage growth appears to be the same as under tensile static loading up to the onset of delamination. This delamination also occurs primarily between the outer 90° and -45° plies and also often between outer 90° and $+45^\circ$ plies. Under fatigue loading, sufficient time occurs allowing delamination to initiate and grow in many regions because of the lower rate of energy expenditure. In these delaminated regions, matrix cracks initiate and are forced to grow longitudinally.

Eventually, in some regions, the delaminations extending from opposite edges coalesce and overlap. In coalesced region, 0° fiber fracture begins to occur at the open space of a $+45^{\circ}$ ply crack resulting in coupon fracture with the outer 0° ply fracture usually exhibiting a dominant $+45^{\circ}$ fracture. The damage state of the entire coupon at fracture is observed to be quite different than for one fractured under static tension loading due to differences in the extent of delamination.

When the fatigue loading of a coupon is interrupted and the coupon is loaded to failure under tension load, a new and different damage state is developed. At the point of fatigue loading interruption, un-notched coupons of this laminate are usually delaminated along the edges. If the coupon is now tensile loaded to failure, delamination will probably extend differently than if fatigue cycling had continued. Matrix cracking in the 0° plies in the delaminated regions will result in fiber fracture, transverse crack growth usually predominated by a $+45^{\circ}$ crack, and coupon fracture. The overall coupon damage state at fracture will be different than either under static or fatigue loading. Though the coupon may have lower strength after fatigue cycling than without, the damage state will be different than if cycled to failure. This hypothesis, though well supported by data^{4,18} needs to be documented by NDI in Task II.

The conclusion, from the above described observations and hypotheses, is drawn that, at least, from the point of onset of delamination, the final fracture state is path dependent in this laminate. This is consistent with the concepts discussed in Sections 1.2 and 1.3 and results previously reported. The correctness of the hypothesis will be investigated in Task II. Regardless of the results of Task II, the value of the enhanced radiographic technique for this program has been demonstrated in Task I.

A further question was investigated concerning the x-ray technique; that of whether or not the DIB enhancer was retained within the coupons. This investigation was related to whether or not the enhancer effects material properties. An informal study showed that DIB was retained by a specimen for at least three days after the initial exposure even when subjected to a 82.2°C (180°F) environment for six hours. Comparisons of gas

chromatograms and x-rays of a control specimen and a DIB exposed specimen were used to detect the presence of the DIB. Later studies showed the presence of the DIB 10 days after exposure. The effect of retained DIB on the future behavior of composite specimens is unknown. As previously discussed, no effect has been observed in limited studies conducted at room temperature.⁷⁸ However, the long-term retention of the DIB enhancer is contrary to much industry speculation. The question of whether DIB may affect the material at higher temperatures remains unanswered.

6.4.2 Ultrasonic Inspection

Two ultrasonic inspection systems were evaluated in this program: reflected through transmission, go, no-go system and the pulse-echo system produced by Holosonics. Delaminations and matrix ply cracking that had been detected by the DIB enhanced x-ray radiography technique were not clearly or reliably detected from C-scans of the go, no-go system. Therefore, this technique was not selected for further use in this program. The pulse-echo Holosonics system was able to distinguish ply delamination, but not the fine matrix ply cracking. Unfortunately, this system was also geometrically restricted to monitoring only the center of the 5 cm (2 in.) of the 15 cm (6 in.) gage length coupons due to technical restrictions on the size of the acoustic transducer foot. Due to the geometrical scanning restriction and the inability to detect matrix ply cracking, the pulse echo system was not selected for use in Tasks II and III.

6.4.3 Acoustic Emission

An investigation of the ability of state-of-the-art acoustic emission (AE) equipment to detect and monitor damage was conducted in the manner described in Section 6.2. The technique was evaluated because this procedure is one of the few, if only, available ones which could potentially detect and monitor all three types of damage in real time (matrix cracking, delamination, fiber breakage).

A preliminary study, parts of which were conducted on contract funds and part on internal Lockheed funding, was undertaken to evaluate the feasibility of the technique.¹¹¹ The preliminary investigation was

conducted using the Fiberite system HY-E-1034C (Thornel T300/Fiberite 934 Resin). The same quasi-isotropic laminate was chosen for investigation as used in the rest of this program. These specimens were identical to those on which data are given in AFML-TR-76-241,¹⁸ and thus are also similar to those used in Task I.

Two different closed-loop electrohydraulic servo-controlled test machines were used in this phase of the AE evaluation. The first was a 22 kN (50 kip) capacity Lockheed-designed test frame controlled by a CGS, Inc. control system. The second was a 44 kN (100 kip) MTS, Inc. test frame and control system. Neither system was modified in any manner to reduce the background noise. The fatigue tests were conducted at an R ratio (minimum load/maximum load) of 0 and at maximum stress levels of approximately 345 MPa (50 ksi) to result in fatigue lives of 50 000 to 300 000 cycles.

Ten fatigue tests were monitored, only three of which are reported here in detail. The others were used to aid in developing the experiments reported here. The first coupon was fatigue tested in the Lockheed-designed frame. No guard transducers were used in this first test. The threshold level could not be lowered below 60 dB at a 5-Hz test frequency or below 70 dB at 10 Hz. During the 10-Hz frequency test, no event data was obtained until the last few cycles of fatigue life. The events were few in number and between 70 and 90 dB. They occurred without prior warning in the last few seconds before fracture. The test results indicated that the matrix degradation and delamination had not been detected.

The second experiment was conducted in the 44 kN (100 kip) MTS, Inc. system. At a 10-Hz test frequency, the threshold appeared to be at or just below 60 dB without guard transducers being used. The test without guard transducers again showed few significant events above the 60 dB threshold, although they did occur somewhat earlier than the previous experiment. This test confirmed the previous result in apparently recording only fiber breakage events near the end of fatigue life. These tests showed, as expected, that if matrix degradation and delamination were to be detected, the dB threshold needed to be reduced.

The use of guard transducers reduced the threshold from 60 dB to 30 dB. This improvement allowed for the feasibility of detecting matrix damage and delamination which was suspected to occur between 30 and 60 dB. Therefore, a third coupon was tested using "guard" transducers in the 44 kN (100 kip) MTS, Inc. test machine. The selected coupon was tested in tension-tension constant amplitude fatigue at a maximum stress of 310 MPa (45 ksi). Fatigue life of the coupon was 125 000 cycles. The data collected from this experiment indicated that the acoustic emission system detected the expected information.

Early in the coupon fatigue life, amplitude data were generally between 30 and 50 dB, Figure 73, later a region between 45 and about 60 dB was observed, Figure 74, and finally one above 65 dB was displayed, Figure 75. The lower dB data (30 to 40) was believed to be related to general matrix degradation; that between approximately 45 to about 60 dB to matrix delamination; and that above 65 dB to fiber breakage. These conclusions were supported by the fact that no matrix delamination was observed at less than 45 000 cycles and correspondingly, no activity was recorded above 50 dB, see Figure 73. However, when delamination was observed, amplitude data above 50 dB was detected, Figure 74. In fact, this region of acoustic emission activity was observed prior to fracture of the coupon, Figure 75, indicating that they might be associated with fiber breakage.

Although the fatigue investigation appeared to successfully meet program objectives, the amplitude plots showed a large number of events below the threshold, Figures 75 and 76. In addition, the statistical validity of the data needed to be evaluated. These questions were investigated using the quasi-isotropic laminate coupons tested statically to various percentages of the average tensile ultimate strength.

In Figure 77, the acoustic emission count rate versus load is displayed for a typical static tension test conducted at 0.01 mm/mm/min. The peaks at 7.6 and 12.0 kN (1700 and 2700 lb) correspond, respectively, to the 90° and -45° ply failures. The peaks at higher loads correspond to +45° ply failures, followed by general cracking and coupon fracture. At failure,

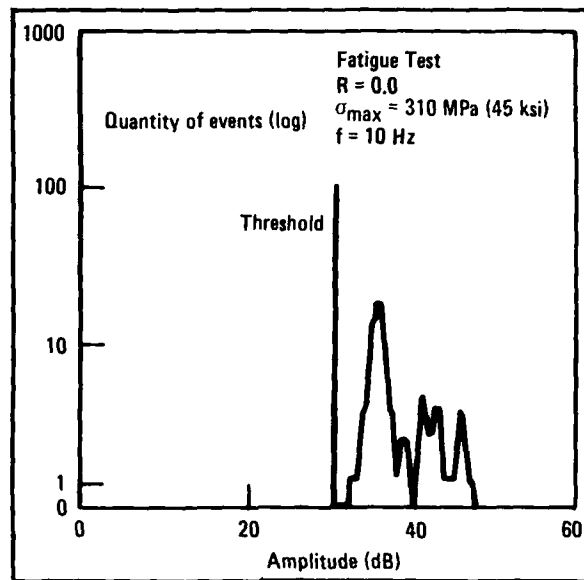


Figure 73. - Differential amplitude distribution, 0-40,000 cycles.

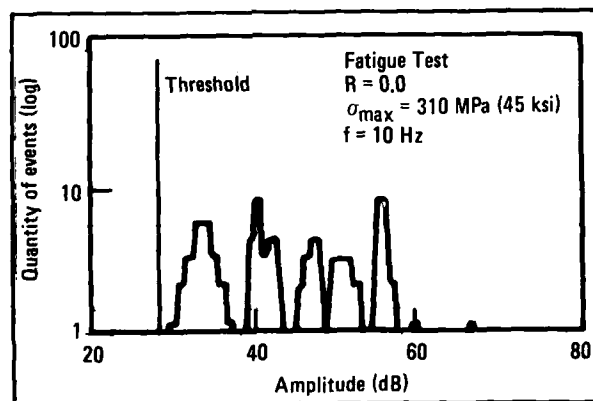


Figure 74. - Differential amplitude distribution, 40,000-63,000 cycles.

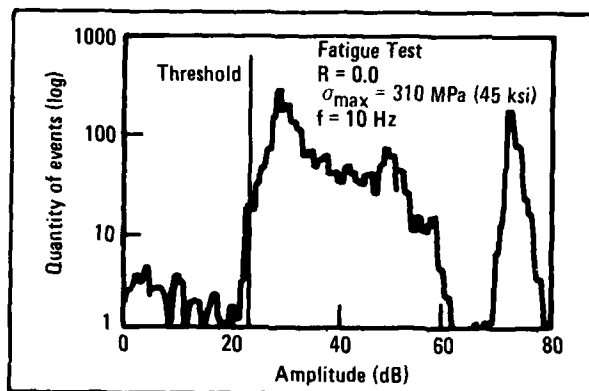


Figure 75. - Differential amplitude distribution,
117,000-125,000 cycles.

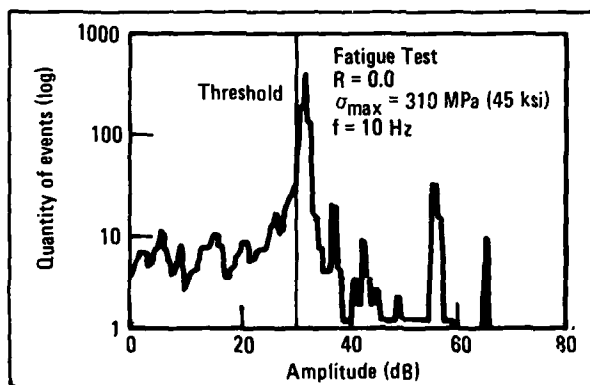


Figure 76. - Differential amplitude distribution,
82,000-92,000 cycles.

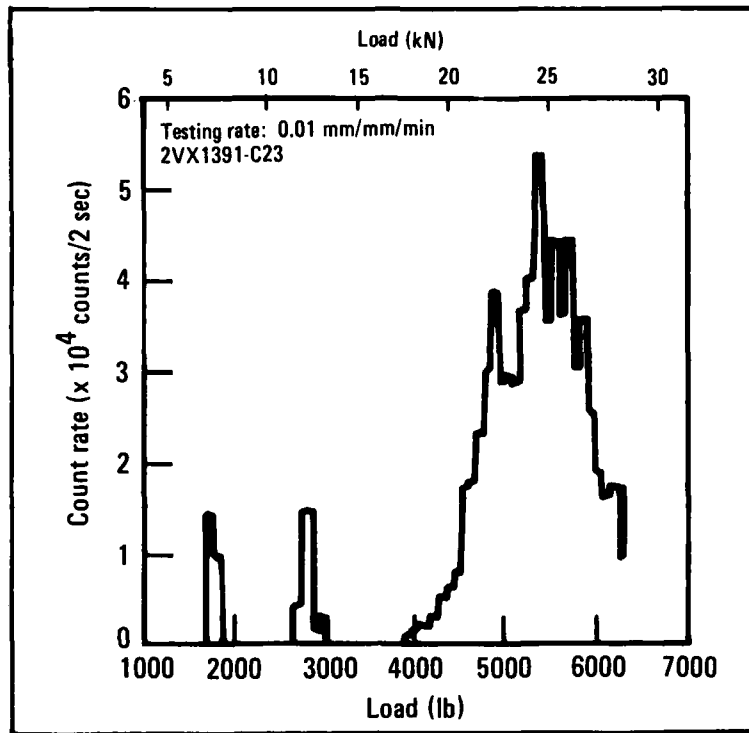


Figure 77. - Count rate vs load, static tension test.

typical amplitude plots appeared like that shown in Figure 78, and at 60 percent of the failure load, as in Figure 79. Although ply failures were properly detected by count rate, the amplitude plots brought to mind the question of the actual meaning of the amplitudes. This was due to the fact that, as Figures 78 and 79 show, many events were recorded below the threshold. In addition, during the static tests loaded to various percentages of the average failure load, the shape of the amplitude distribution plot did not appear to change. Therefore, the manner in which the amplitude plot is obtained by the recording equipment was investigated by Dunnegan/Endevco personnel.

Amplitudes recorded below the threshold were found to occur for two reasons. First, as indicated in diagram A of Figure 80, they are due to a splitting action. Many competitive acoustic emission systems presently available operate similarly as in Figure 80A. An acoustic event crosses the trigger threshold, activating the peak follower, followed by a ramp

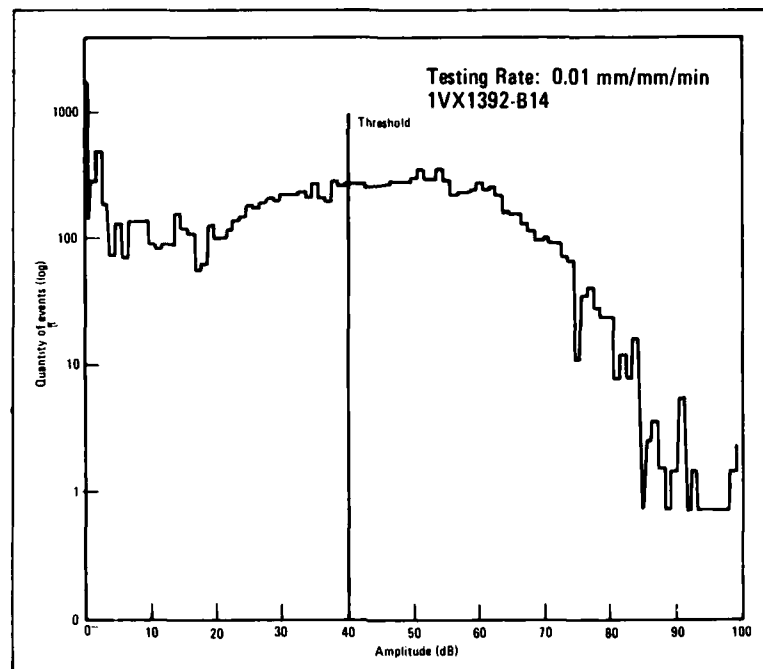


Figure 78. - Amplitude distribution diagram for static tension test to failure.

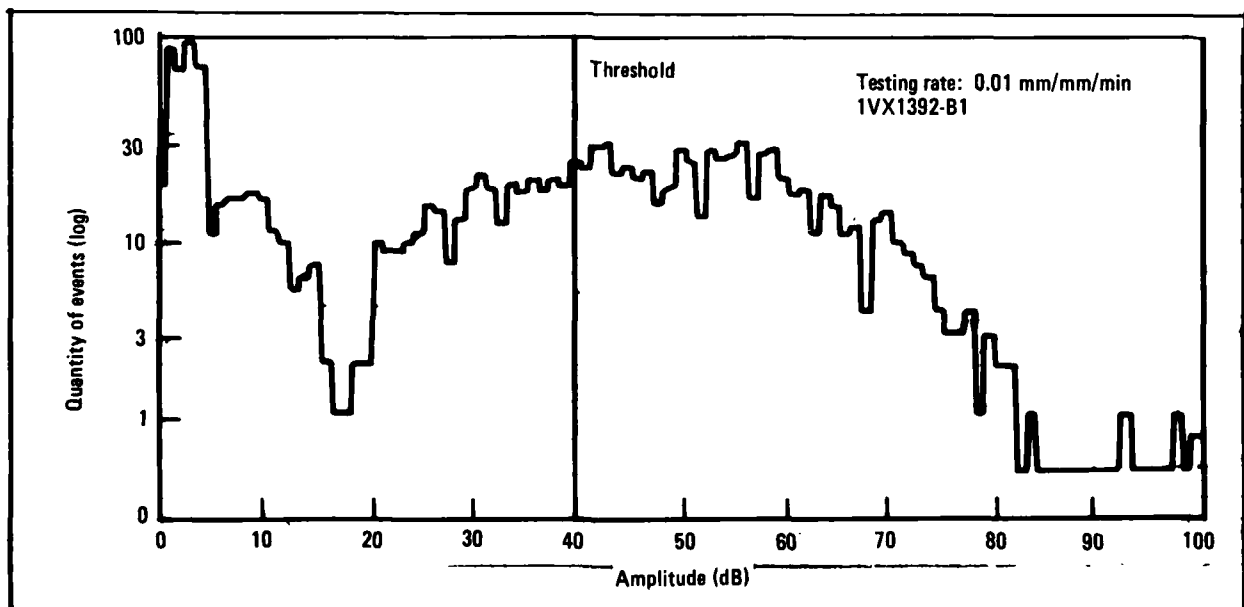


Figure 79. - Amplitude distribution diagram for static tension test, 0 to 60% average ultimate stress.

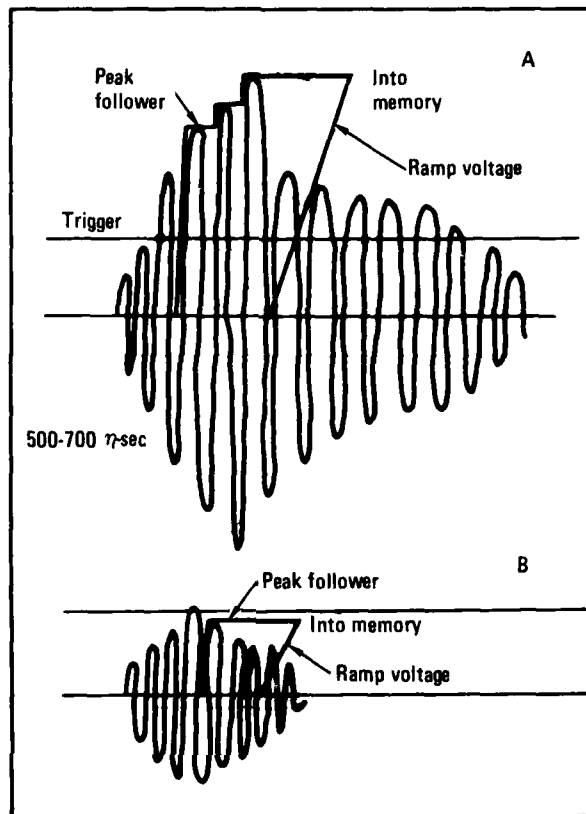


Figure 80. - Acoustic emission event.

voltage increase after a time delay. The ramp voltage converts amplitude to voltage. If the event time above the threshold is less than the time duration for the ramp voltage to intersect the peak follower voltage, the amplitude of the event is recorded as a split event (such as 80 dB recorded as 50 and 30 dB) whose magnitudes are dependent on the time differences. This problem was successfully reduced by equipment modifications which increased ramp rise time and decreased delay time between triggering the peak follower and the ramp voltage. Such a problem may also possibly be negated by use of a computer storage system. The second cause of amplitudes recorded below the threshold was due to noise, as shown in Figure 80B. If a low level event triggers the threshold and then decreases, a low-amplitude event will be recorded. This type of problem can only be solved by a

system which simply does not hold such events. However, such spurious events do not bias the data since they can be ignored provided the other reason for low amplitude events is eliminated. A potential third problem concerning amplitude distribution is whether an event duration can be less than the memory storage time. If so, multiple events could be recorded as one summed event, thus multiple low-amplitude events would be stored as one high-amplitude event. This potential difficulty has not been investigated.

These three-potential and real difficulties have led to three concerns with regard to the initial success of using acoustic emission to monitor fatigue tests. First, do high-amplitude displays correspond to high-amplitude events or to summed events? This has not yet been answered. Second, do low-amplitude displays correspond to low-amplitude events or to split down high amplitude events? This is known to occur, but the extent of the problem, though reduced by equipment modifications, remains unclear. These two questions raise the third question as to what mechanisms the presently recorded amplitude distributions actually correspond. At present, no reliable conclusion can be made that the apparent separation of the amplitude distribution into different mechanisms actually conforms to physical reality.

The use of acoustic emission for detecting and monitoring fatigue-induced damage in graphite/epoxy composites was dependent on obtaining a statistically valid sampling of data during the times when the guard transducers were not blocking data storage. Therefore, an experiment was performed to determine the amplitude distribution of a coupon tested to failure in one cycle at a rate (6 mm/mm/min) equivalent to a 10-Hz fatigue loading frequency. The results are shown in Figure 81. Only two events were recorded above the threshold. The conclusion was reached that little information is actually obtained on each fatigue cycle.

To further evaluate the statistical validity of the data, additional fatigue tests of this 5208/T300, quasi-isotropic laminate were conducted at 310 and 345 MPa (45 and 50 Ksi), at $R = 0.0$. The modified AE system with the increased amplitude processing rate was employed. The system was set

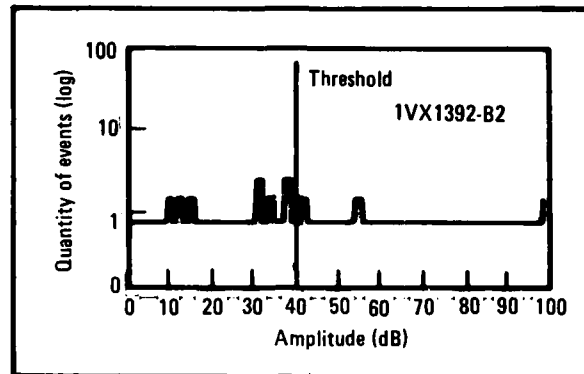


Figure 81. - Amplitude distribution diagram for static tension test to failure conducted at 6 mm/mm/min.

up to process the location and amplitude at each event whose amplitude was greater than 40 dB. Thus, there was to be a one-to-one correspondence between the number of amplitude and location values recorded. In several fatigue tests, however, the amount of amplitude values greatly exceeded the amount of location values. In one case, approximately twenty-three amplitude values were recorded for each location value. This data also indicated the need for further development of the technique. Such development lay outside the scope of this program.

The state-of-the-art AE technique evaluated in this program clearly needed further investigation and development before the systems potential capabilities to distinguish composite damage mechanisms and locations could be properly realized. Therefore, this technique was not selected for use in Tasks II and III because, at the time of this evaluation, the system was not yet capable of fulfilling the needs of this program. One

alternative to monitoring the amplitudes and locations of acoustic emission events has been to monitor the time signature and frequency spectra of the events. Initial studies by Henneka¹¹² have shown the potential of distinguishing matrix cracking from fiber breakage by these event characteristics. The suggestion is made that this concept also be pursued.

6.4.4 Edge Replication

Initial efforts at obtaining high quality edge replications using a plastic-cast technique resulted in poor quality photographs. This was due to the unexpected roughness of the coupon edge surface in the as-manufactured state. Therefore, with the advice of Dr. W. Stinchcomb,¹¹³ an extensive study was made to determine the best procedure for edge polishing, selection of the proper acetone tape type, and development of a successful pressure application technique. Typical results of this study are shown in Figure 82. Matrix cracks in the 90° and -45° plies are clearly visible as are short interply cracks.

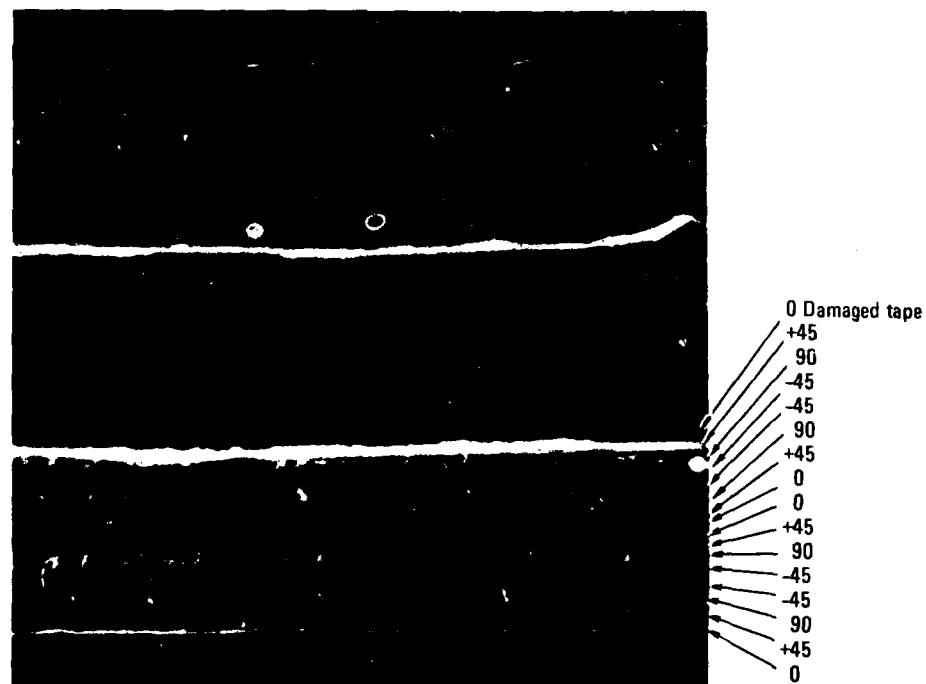


Figure 82. - Plastic-cast edge replications of quasi-isotropic laminate coupon loaded in static tension to approximately 60% of the average ultimate strength.

Because of early difficulties with this procedure, no well documented set of high quality replicates was obtained from the various coupons used for the NDI investigation. However, the proper technique for these coupons was developed and has been used to demonstrate the capability to detect where damage occurs with respect to ply level. Thus the technique is available for use as a complement to enhanced radiography.

Originally, plastic-cast edge replication was used as an attempt to ameliorate the problems encountered with direct microscopic photography of the coupon edges. Such photography is difficult to perform while a coupon is underload in a test machine.⁹⁴ In addition, many photographs are needed and contrast is poor.⁹⁴ At Lockheed, Sandifer¹¹⁴ attempted to solve some of these problems. In his procedure, a fine, high contrast powder, such as chalk, is quickly rubbed into the coupon. The coupon is subsequently placed in a photographic set up, visually scanned, and photographs of 10X - 25X taken as needed. The technique appears to reveal detail equivalent to or better than plastic-casting with less time and with no difficulty incurred such as damaging or storing of replicates. Typical results obtained using this technique are shown in Figure 83. This technique may be used in Tasks II and III instead of plastic-casts.

6.4.5 Stiffness Monitoring

Strain gages are not considered to be a particularly good method for monitoring stiffness changes. First, they give a strain measurement only over a short length. Second, stiffness monitoring using commercially available strain gages was demonstrated to be unsatisfactory since their characteristics change too rapidly when the number of cycles exceeds 5000 at the strain levels required. Strain gages commercially available for use in fatigue loading, for instance those from Micro-Measurements, have a fatigue life of approximately 10^5 cycles at a strain range of 0 to 5400 $\mu\epsilon$. However, the measurement error is as much as 10 percent.¹¹⁵ This strain range of 0 - 5400 $\mu\epsilon$ is approximately that required to give lives between 10^5 and 10^6 cycles for the quasi-isotropic laminate of this program. Shorter lives for this layup require a much higher strain range (>0 to 6000

AD-A088 439

LOCKHEED-CALIFORNIA CO BURBANK RYE CANYON RESEARCH LAB

F/6 11/4

EFFECT OF LOAD HISTORY ON FATIGUE LIFE.(U)

JUN 80 J T RYDER

F33615-78-C-5090

UNCLASSIFIED

LR-29586

AFWAL-TR-80-4044

NL

3 of 3

AD
A088-439

END

DATE

FILED

DTIC



Figure 83. - Matrix cracking revealed on a coupon edge by using chalk and standard photography. Coupon loaded in static tension to approximately 85% of average ultimate strength.

or 7000 $\mu\epsilon$). Presently available strain gages are inadequate for such conditions. Thus, the use of strain gages for obtaining static and dynamic stiffness over the entire cycle life range of interest in Tasks II and III of program is not proposed.

Axial strain gages were, however, used to compare static and dynamic stiffness on the first and second fatigue loading cycle of coupons tested at 310 MPa (45 ksi) at $R = 0.0$. The dynamic stiffness was found to be within 4% of the static stiffness and usually to be identical. This is consistent with the static test data reported in section 4.2.

Stiffness variations due to fatigue loading were studied using coupons fatigue cycled at $R = 0.0$ and at 310 MPa (45 ksi). The procedure used was a clip gage mounted on aluminum tabs bonded to the coupons. The repeatable accuracy of removing and reattaching the 2.54 cm (1 in.) gage length clip gage was found to give stiffness readings which varied by less than $\pm 0.5\%$. Stiffness monitoring was undertaken strictly to evaluate the technique as an NDI procedure. Results are shown in Table 33. The test results clearly showed that stiffness monitoring is not sensitive enough to detect accurately and consistently early matrix cracking in the 90° and -45° plies. As damage progressed, stiffness changes were evident, but did not allow inferences as to damage details.

Based on the results of stiffness monitoring, the technique was not selected for use in Tasks II and III due to insensitivity to damage details. The collection of stiffness change data may, however, be found to be useful for certain types of proposed cumulative damage laws.

6.4.6 Temperature Monitoring

Simple thermal monitoring of coupon temperature changes can be useful for two reasons. First, at the test frequencies of interest, temperature rise must not be excessive to avoid matrix degradation. Second, general temperature perturbations may occur which correspond to specific types of damage initiation. In view of these two considerations, overall thermal changes were monitored on coupons fatigue cycled at 310 and 379 MPa (45 and 55 ksi) at $R = 0.0$ and at $R = -1.0$ at several stress levels.

TABLE 33. EFFECT OF FATIGUE LIFE ON TENSILE STIFFNESS
AT 310 MPa (45 ksi) AT R = 0.0

Coupon ID	No. of Fatigue Cycles	Percent Modulus Change from 0 Cycles	Damage State from Enhanced X-ray
2VX1391-D18	100	0	90° ply cracks
2VX1391-A5	1000	0	90° ply cracks, partial -45° cracks
2VX1391-B19	1000	-1.8	90° ply cracks, partial -45° cracks
2VX1391-A14	5000	-1.2	90° ply cracks, partial -45° cracks
2VX1391-C29	5000	-0.8	90° ply cracks, partial -45° cracks
2VX1391-B21	10 000	+1.5	90° ply cracks, partial -45° cracks, more extensive
1VX1391-B20	20 000	-4.0	90° and -45° ply cracks, edge to edge
2VX1391-B10	30 000	-1.6	90° and -45° ply cracks, edge to edge
1VX1392-B23	30 000	-3.3	90° and -45° ply cracks, edge to edge
1VX1392-B28	40 000	-3.7	90°, -45° cracks, some + 45°
2VX1390-D18	40 000	-6.7	extensive delamination near failure

Coupons fatigue cycled at 310 MPa (45 ksi) at R = 0.0 were found to continuously increase in temperature until reaching a plateau of about 4°C (8°F) increase at 20 000 cycles, see Table 34. No further temperature rise was seen until near failure when delamination was excessive. At that point, temperature increased by approximately 5°C (10°F). At 379 MPa (55 ksi), coupons cycled at R = 0.0 were found to exhibit a continuous thermal rise of up to 6°C (11°F) followed by a thermal spike at failure of up to 1°C (2°F). These results are similar to those found previously.¹⁸ They demonstrated that this form of simple temperature monitoring is not adequately sensitive to damage states, but also indicated that thermal changes are not of concern on these tension-tension fatigue tests at 10 Hz.

The first coupons subjected to R = -1.0 fatigue cycling exhibited thermal temperature increases of up to 40°C (70°F). This was due to frictional heat generated by coupon and support rubbing. The problem was easily reduced, for coupons used for data collection, to a thermal rise of less than 11°C (20°F) by forced air cooling of the test fixture. In Tasks II and III, the problem will not be of great concern because full support fixtures will be replaced by a pin loaded fixture as discussed in Section 5.1.

TABLE 34. THERMAL TEMPERATURE DATA FOR COUPONS FATIGUE CYCLED
AT 310 MPa (45 ksi) AT R = 0.0

Coupon ID	No. of Fatigue Cycles	Maximum Temperature Change, °C (°F)	Damage State
2VX1391-D18	100	None	90° ply cracks
1VX1392-A29	100	None	90° ply cracks
1VX1391-A5	1 000	2(4)	90° cracks, partial -45° cracks
2VX1391-A14	5 000	4(7)	90° cracks, partial -45° cracks
2VX1391-E21	10 000	3(6)	90° cracks, more extensive -45° cracks
2VX1391-B10	20 000	4(8)	90° and -45° cracks, edge to edge
1VX1392-B17	20 000	3(6)	90° and -45° cracks, edge to edge
2VX1391-A6	30 000	4(7)	90° and -45° cracks, edge to edge
2VX1391-B23	30 000	5(9)	90° and -45° cracks, edge to edge
1VX1392-B28	40 000	4(8)	90°, -45° cracks, some +45°

Based upon previous experience,¹⁸ the open bay fixture is not expected to generate a thermal problem.

6.5 SELECTION OF NDI TECHNIQUES FOR TASKS II AND III

The capabilities of the NDI techniques discussed in Section 6.4 are summarized in Table 35. The DIB enhanced x-ray radiography technique was selected for use in Tasks II and III of this program. With this technique, matrix cracking in the 90°, -45°, +45°, and 0° plies as well as interply delamination was detected. The edge replication technique was selected because the procedure compliments the radiography procedure by allowing observation of the level of delamination. The damage that is detectable by either of these techniques is limited to only that which intersects the edges of the coupon. Pulse-echo ultrasonic inspection could distinguish ply delaminations isolated from the specimen edges, but the technique was not selected for further use because of the geometric scanning restriction and insensitivity to intraply matrix cracking. The NDI techniques of acoustic emission, "go, no-go" ultrasonic inspection, temperature and stiffness monitoring were not selected for further use because these techniques were not able to reliably and reproducibly indicate the composite damage mechanisms of interest in this program. The NDI selection process conducted in

TABLE 35. DAMAGE DETECTION CAPABILITIES OF EVALUATED NDI TECHNIQUES

NDI Techniques	Ply Direction in Which Matrix Cracks Were Detected				Delamination		Comments
	90°	-45°	+45°	0°	Detected	Ply Level	
DIB Enhanced X-Ray Radiography	Y ^a	Y	Y	Y	Y	N	90° ply matrix cracking clearly visible only on unprinted pictures
Acoustic Emission	Capabilities Undefined at This Time						
Ultrasonic Inspection							
Go, No-go "	N	N	N	N	Y	N	Not definitive
Pulse-Echo	N	N	N	N	Y	N	Geometrically restricted scanning area
Edge Replication	Y	Y	Y	N	Y	Y	Can not detect interior damage extent
Thermal Monitoring	N	N	N	N	Y	N	
Stiffness Monitoring	N	N	N	N	Y	N	

^a Y = Yes
N = No

this task is outlined in Table 36. Selected coupons in Tasks II and III will be sectioned for photomicrography in order to verify the damage detected by enhanced radiography and edge replication.

TABLE 36. SUMMARY OF NDI TECHNIQUE EVALUATION PROCESS

Initial Survey	Techniques Evaluated in Task I	Techniques Chosen For Tasks II and III
Moire Methods Laser Holography X-Ray Acoustic Imaging Ultrasonic Inspection Acoustic Emission Edge Replication Thermography Temperature Monitoring Stiffness Monitoring	DIB Enhanced X-Ray Radiography Acoustic Emission Ultrasonic Inspection Edge Replication Temperature Monitoring Stiffness Monitoring	DIB Enhanced X-Ray Radiography Edge Replication

SECTION 7

SUMMARY AND CONCLUSIONS

This section summarizes specific experimental observations and conclusions obtained in Task I which are considered to be of special importance. Statements concerning the experimental results pertain to narrow width, unnotched coupons of a type similar to that used in the research program. The numbers in parenthesis at the end of each item reference the particular subsection of the report which provides support for the statement.

INTRODUCTION

- This report had four purposes:
 - give a program overview
 - explain the relationship of experimental data to development of an understanding of load history effects
 - provide a discussion of the analytic approach
 - report the results of the work conducted in Task I. (1.0)
- The experimental research effort of Task I was restricted to two types:
 - obtain baseline data for Tasks II and III
 - select diagnostic inspection techniques for detecting and monitoring damage initiation and growth. (1.1)
- An attitude or concept as to the nature of damage initiation and growth in laminated composites was formulated. The formulation of a conceptual attitude provides a context for investigating the effects of load history on fatigue and for an analytical approach to life prediction. (1.2)

Considerations were determined, upon which analytical attention will be placed, which are expected to be helpful in expanding formulations of fatigue life prediction methodologies. (1.3)

- A detailed description of the rationale for material and laminate selection, of the Task I experimental test matrix, and of the experimental test procedures is given in Section 2.

MATERIAL CHARACTERIZATION

- The selected material, Narmco Rigidite T300/5208, was found to meet all requirements of the Quality Control Plan. (3.1)
- The fiber properties of individual batches of material vary by as much as 25% from one another. (3.1)
- Average manufactured panel properties were: weight percent resin content, 26.8; volume percent fiber content, 66.1; percent void content <1 ; average density, 1.583 gm/cm^3 . (3.2)
- The estimated average moisture content within the coupons tested in each environmental condition was: 0° and 90° unidirectional, 0.4% at 22°C (72°F) and 82.2°C (180°F) and 1.5% at 82.2°C (180°F) in the wet condition; $\pm 45^\circ$, 0.5% at 22°C (72°F) and 82.2°C (180°F) and 1.7% at 82.2°C (180°F) in the wet condition; quasi-isotropic, 0.6% at 22°C (72°F) in the as received condition. (3.3)
- Moisture diffusivity, thermal expansion, and thermal conductivity/diffusivity were obtained for the unidirectional coupons. (3.4)
- A type of previously unobserved defect was found in one quasi-isotropic panel and termed "squiggle" defect. The cause of the defect was undetermined, but static, and later, fatigue properties were found to be drastically reduced by the defect. The only NDI technique believed to be able to detect the defect, at this time, is extremely careful, direct visual inspection of the panel surface. (4.2.1)

STATIC LOADING RESULTS

- As expected, 0° unidirectional tensile properties were found not to be significantly affected by environment. Compressive properties

decreased by ~20% in the presence of high temperature, but only when coupon moisture content was high. (4.1)

- The stress-strain curves of tensile loaded 0° coupons were non-linear displaying a non-Hookean, increasing curvature consistent with other experimental observations.^{51,52} (4.1)
- High temperature was found only to affect the tensile properties of those 90° unidirectional coupons which had a high moisture content. The 90° unidirectional compression properties decreased by ~15% due to high temperature, but were not further affected by high moisture content. (4.1)
- Shear stress properties were affected by both temperature and coupon moisture content. (4.1)
- Static tension data of quasi-isotropic laminates obtained at a loading rate of 0.01 mm/mm/min displayed a low coefficient of variation (3.5%) and high Weibull exponent (34) indicative of low scatter. This was due to the elimination from the data set of those coupons containing adjoining tape edges called line discontinuities. (4.2.1)
- The average tensile strength of quasi-isotropic coupons tested at a loading rate of 6 mm/mm/min was ~8% lower than those tested at 0.01 mm/mm/min. The cause of the reduction was hypothesized to be due to the manner in which matrix cracks propagate at the different strain rates. (4.2.1)
- High strain rate compression test results for quasi-isotropic coupons were not significantly different than low strain rate results except that data dispersion was greatly increased. (4.2.2)

FATIGUE RESULTS FOR QUASI-ISOTROPIC COUPONS

- The fatigue properties of this laminate are not significantly affected, at room temperature, by epoxy resin type or by batch fiber properties. (5.1)

- Fatigue lives of coupons cycled at $R = +0.5$ were one to two orders of magnitude longer than those at $R = 0.0$ when compared on the basis of σ_{\max} . This indicated that both the maximum stress and stress range significantly affect fatigue life. (5.1)
- Based upon the tension-compression results and analytical concepts, a different type of constraint fixture will be used in Tasks II and III. (5.1)
- A limited residual strength experimental study of unfailed fatigue coupons supported the conclusion reached on the basis of fatigue data results that damage is extended by fatigue cycling and not just by a creep mechanism occurring at maximum load. (5.2)

NDI TECHNIQUE EVALUATION

- NDI techniques were considered and evaluated based upon four criteria that a selected procedure was expected to meet: 1) be reproducible; 2) locate damage regions; 3) differentiate among the three damage mechanisms of matrix cracking, ply delamination and fiber breakage; 4) indicate expected failure locations. (6.0)
- Based upon a literature review and RFP requirements, six NDI techniques were selected for evaluation: 1) enhanced radiography; 2) ultrasonic pulse echo; 3) acoustic emission; 4) plastic-cast edge replication; 5) stiffness monitoring; 6) temperature monitoring. (6.1)
- The experimental procedures of the selected NDI techniques were described in detail. (6.2)
- The selected NDI techniques were evaluated using quasi-isotropic coupons statically loaded to various percentages of their average ultimate tensile strength and by coupons fatigue loaded at $R = 0.0$ to various cycle lines. (6.3)
- Two NDI techniques were selected for Tasks II and III based upon the experimental evaluation: enhanced radiography and edge replication. These two techniques are complementary and together meet all of the

criteria established for NDI evaluation except for detection of fiber breakage. No simple, non-labor intensive, and inexpensive technique for detecting details of fiber breakage is presently available. (6.4 and 6.5)

- Evaluation of the data obtained by enhanced radiography strongly supported the hypothesized proposed in Section 1.2 that the fracture process, and thus coupon strength, in laminated coupons is path dependent after the onset of delamination. (6.4.1)

REFERENCES

1. Reifsnider, K.L. and Talug, A. "Analysis of Fatigue Damage in Composite Materials," Int. J. Fatigue, January 1980, pp. 3-11.
2. Wang, A.S.D. and Crossman, F.W. "Initiation and Growth of Transverse Cracks and Edge Delamination in Composite Laminates - Part I An Energy Method," J. Composite Materials, June 1980, also Drexel U. Report, October 1979.
3. Crossman, F.W., Warren, W.J., Wang, A.S.D. and Law, G.L. "Initiation and Growth of Transverse Cracks and Edge Delamination in Composite Laminates - Part II - Experimental Correlation," J. Composite Materials, June 1980, also Drexel U. Report, October 1979.
4. Ryder, J.T. and Walker, E.K., "The Effect of Compressive Loading on the Fatigue Lifetime of Graphite/Epoxy Laminates," AFML-TR-79-4128, October 1979.
5. Hahn, H.T. and Kim, R.Y., "Proof Testing of Composite Materials," J. Composite Materials, Volume 9, July 1975, pp. 297-311.
6. Chow, P.C. and Croman, R., "Degradation and Sudden-Death Models of Fatigue of Graphite/Epoxy Composites," Composite Materials: Testing and Design (Fifth Conference), ASTM STP 674, S.W. Tsai, Ed., American Society for Testing and Materials, 1979, pp. 431-454.
7. Yang, J.N. and Liu, M.D., "Residual Strength Degradation Model and Theory of Periodic Proof Tests for Graphite/Epoxy Laminates," J. Composite Materials, Volume 11, April 1977, pp. 176-203.
8. Yang, J.N. and Jones, D.L., "Load Sequence Effects on Statistical Fatigue of Composite Materials," Presented at the ASTM Symposium on the Fatigue of Fibrous Composite Materials, San Francisco, CA, May 22-23, 1979, to be published in forthcoming ASTM STP 731.
9. Hahn, H.T., "Fatigue Behavior and Life Prediction of Composite Laminates," Composite Materials: Testing and Design (Fifth Conference), ASTM STP 674, S.W. Tsai, Ed., American Society for Testing and Materials, 1979, pp. 383-417.
10. Halpin, J.C., Waddoups, M.E., and Johnson, T.A., "Kinetic Fracture Models and Fracture Stability," Int. J. Fracture Mechanics, Volume 8, 1972, pp. 465-468.

11. Reifsnider, K.L., Stinchcomb, W.W., and O'Brien, T.K., "Frequency Effects on a Stiffness Based Fatigue Failure Criterion in Flawed Composite Specimens," ASTM STP 636, K.L. Reifsnider and K.N. Lauraitis, Eds., American Society for Testing and Materials, 1977, pp. 171-184.
12. Kulkarni, S.V., McLaughlin, P.V., Pipes, R.B., and Rosen, B.W., "Fatigue of Notched Fiber Composite Laminates: Analytical and Experimental Evaluation," Composite Materials: Testing and Design (Fourth Conference), ASTM STP 617, American Society for Testing and Materials, 1977, pp. 70-92.
13. Ratwani, M.M. and Kan, H.P., "Compression Fatigue Analysis of Fiber Composites," NADC-78049-60, September 1979.
14. Grimes, G.C., "Structural Design Significance of Tension - Tension Fatigue Data on Composites," Composite Materials: Testing and Design (Fourth Conference), ASTM STP 617, American Society for Testing and Materials, 1977, pp. 106-119.
15. Phoenix, S.L., "Statistical Aspects of Failure of Fibrous Materials," Composite Materials: Testing and Design (Fifth Conference), ASTM STP 674, S.W. Tsai, Ed., American Society for Testing and Materials, 1979, pp. 455-483.
16. Harlow, D.G., "Properties of the Strength Distribution for Composite Materials," Composite Materials: Testing and Design (Fifth Conference), ASTM STP 674, S.W. Tsai, Ed., American Society for Testing and Materials, 1979, pp. 484-501.
17. Kitagawa, H., Fujita, T., and Miyazawa, K., "Small Randomly Distributed Cracks in Corrosion Fatigue," Proc. 2nd Intl. Conf. on Mech. Behavior of Materials, Boston, 1976.
18. Ryder, J.T., and Walker, E.K., "Ascertainment of the Effect of Compressive Loading on the Fatigue Lifetime of Graphite Epoxy Laminates for Structural Applications," AFML-TR-76-241, December 1976.
19. Sandifer, J.P., "Effects of Specimen Width on Fatigue Life of Graphite/Epoxy Composites," Lockheed Report, LR 27976, January 1977, to be presented at the Third International Conference on Composite Materials, 26-29 August 1980, Paris, France, to be published in the conference proceedings.
20. Pagano, N.J. and Pipes, R.B., "Some Observations on the Interlaminar Strength of Composite Laminates," Int. J. Mech. Sci., Vol. 15, 1973.
21. Pipes, R.B. and Pagano, J.J., "Interlaminar Stresses in Composite Laminates Under Uniform Axial Extension," J. Comp. Materials, Vol. 4, 1970.

22. Wang, A.S.D., and Crossman, F.W., "Some New Results on Edge Effect in Symmetric Composite Laminates," J. Comp. Materials, Vol. 11, 1977, p. 92.
23. Pettit, D.E., Ryder, J.T., and Lauraitis, K.N., "Effects of Line Discontinuity in Composite Laminates on Static and Fatigue Strength Distribution," Presented at the 24th National Sampe Symposium, San Francisco, California, May 8-10, 1979, published in the Conference Proceedings.
24. Sandorff, P.E., Ryder, J.T. and Lauraitis, K.N., "Experimental Evaluation of Compression and Column Buckling Properties of Graphite/Epoxy Composites," accepted for publication in ASTM Journal of Testing and Evaluation, JTEVA; to be published in 1980.
25. Ryder, J.T. and Black, E.D., "Compression Testing of Large Gage Length Composite Coupons," Composite Materials: Testing and Design (4th Conference), ASTM STP 617, American Society for Testing and Materials, 1977, pp. 170-189.
26. Sandorff, P.E. and Dillon, R.N., "Compression Stress-Strain Properties of Some Aircraft Materials," Proceedings of the American Society for Testing and Materials, Vol. 46, 1946, p. 1039.
27. Bowie, G.E., Pettit, D.E., Ryder, J.T. and Krupp, W.E., "NDI Life Analysis Interface," Lockheed-California Co. Report LR 27013, September 1974.
28. Gumbell, E.J., Statistics of Extremes, Columbia University Press, New York, 1958.
29. Talreja, R., "Estimation of Weibull Parameters for Composite Material Strength and Fatigue Life Data," to be published by American Society for Testing and Materials in ASTM STP 723, Fatigue of Fibrous Composite Materials, Fall 1980.
30. Weibull, W. and Weibull, G.W., "New Aspects and Methods of Statistical Analysis of Test Data with Special Reference to the Normal, the Log Normal and the Weibull Distributions," Part I and II, FOA Report D20045-DB, Defense Research Institute, Stockholm, Denmark, June, 1977.
31. Antle, C.E. and Klimko, L.A., "Choice of Model for Reliability Studies and Related Topics II," ARL-73-0121, AD 772775, 1973.
32. Harter, H.L. and Moore, A.H., "Maximum Likelihood Estimation of the Parameters of Gamma and Weibull Populations from Complete and Censored Data," Technometrics, Vol. 1, No. 4, 1965, pp. 639-643.
33. Bowie, G.E., Besari, M.S. and Trapp, W.J., "Experimental Mechanics: Development of Methods for Numerical Analysis of Composite Fatigue Data," Lockheed-California Co. Report LR 27981, January, 1977.
34. Lieblein, J., "On Moments of Order Statistics from the Weibull Distribution," Annals of Math. Statistics, V.26, 1955, pp. 330-333.

35. Sandorff, P.E., and Tajima, Y.A., "A Practical Method for Determination of Moisture Distribution, Solubility, and Diffusion Coefficient for Composite Laminate," Lockheed-California Company Report, LR 28047, April 28, 1978.
36. Tajima, Y.A., Private Communication, January 1980.
37. Tajima, Y.A., "The Effect of Hydrothermal Conditioning on the Diffusion of Moisture in Graphite Fiber Reinforced Epoxy Laminates," Lockheed-California Company Report, LR 29356, January 9, 1980.
38. Tajima, Y.A. and Sandorff, P.E., "Experimental Determination of Moisture Distribution and Diffusion Parameters in Graphite-Epoxy Laminates," Annual Convention, Amer. Soc. of Civil Engineers, 10/16-20/78, Chicago, Ill.
39. Gurtin, M.E. and Yatomi, C., "On a Model for Two Phase Diffusion in Composite Materials," J. Composite Materials, Vol. 13, April 1979, pp. 126-130.
40. Sandorff, P.E. and Tajima, Y.A., "A Practical Method for Determination of Moisture Distribution, Solubility, and Diffusion Coefficient of Composite Laminate," SAMPE Quarterly, Vol. 10, 1979, p. 21.
41. Sandorff, P.E. and Tajima, Y.A., "The Experimental Determination of Moisture Distribution in Carbon/Epoxy Laminates," Composites, Vol. 10, 1979, pp. 37-38.
42. Loos, A.C. and Springer, G.S., "Moisture Absorption of Graphite-Epoxy Composites Immersed in Liquids and Humid Air," J. Composite Materials, Vol. 13, April 1979, pp. 131-148.
43. Whitney, J.M. and Browning, C.E., "Some Anomalies Associated with Moisture Diffusion in Epoxy Matrix Composite Materials," Advanced Composite Materials - Environmental Effects ASTM STP 658, J.R. Vinson Ed., Amer. Soc. for Testing and Materials, 1978, pp. 43-60.
44. Hahn, H. T. and Kim, R.Y., "Swelling of Composite Laminates," Advanced Composite Materials - Environmental Effects. ASTM STP 658, J.R. Vinson, Ed., Amer. Soc. for Testing & Materials, 1978, pp. 98-120.
45. Alfrey, T., Jr., Gurney, E.F., and Lloyd, W.G., "Diffusion in Glass Polymers," J. Polymer Science, Pt. C. No. 12, pp. 249-261, 1966.
46. Haward, R.N., Ed., The Physics of Glassy Polymers, John Wiley & Sons, New York, 1973.
47. Crank, J. "A Theoretical Investigation of the Influence of Molecular Relaxation and Internal Stress on Diffusion in Polymers," J. Polymer Science, Vol. 11, 1953, pp. 151-163.

48. Shirrell, C.D., "Diffusion of Water Vapor in Graphite/Epoxy Composites," Advanced Composite Materials - Environmental Effects, ASTM STP 658, J.R. Vinson, Ed., Amer. Soc. for Testing and Materials, 1978, pp. 21-42.
49. Shirrell, C.D., Leisler, W.H., and Sandow, F.A., "Moisture Induced Surface Damage in T300/5208 Graphite/Epoxy Laminates," Nondestructive Evaluation and Flaw Criticality for Composite Materials, ASTM STP, 696, R.B. Pipes, Ed., Amer. Soc. for Testing and Materials, 1979, pp. 209-222.
50. Cunningham, Jr., G.R., Smith, R., and Bradshaw, C., "Thermal Diffusivity Measurements of Graphite and Chars," Progress in Astronautics and Aeronautics, Vol. 18, Academic Press, 1964.
51. Lauraitis, K.N., and Sandorff, P.E., "The Effect of Environment on the Compressive Strengths of Laminated Epoxy Matrix Composites," AFML-TR-79-4179, December 1979.
52. Von Dreumel, WIM H.M., and Kamp, John L.H., "Non Hookeon Behavior in the Fibre Direction of Carbon-Fibre Composites and the Influence of Fibre Waviness on the Tensile Properties," J. Comp. Matls., Vol. 11, October 1977, pp. 461-469.
53. Curtis, G.J., Milne, "Non-Hookeon Behavior of Strong Carbon Fibres," Nature, Vol. 220, December 1968.
54. Crossman, F.W., Private Communication, April 1980.
55. Awerbuch, J. and Hahn, H.T., "Fatigue and Proof-Testing of Unidirectional Graphite/Epoxy Composite," Fatigue of Filamentary Composite Materials, ASTM STP 636, K.L. Reifsnider and K.N. Lauraitis, Eds, American Society for Testing and Materials, 1977, pp. 248-266.
56. Lauraitis, K.N., Private Communication, Spring 1979.
57. Altman, J., Konicki, D., Burroughs, B., Nodler, M., "Advanced Composites Servicibility Quarterly Progress Report," Rockwell International Corp., NA-76-783-1, January 1977.
58. Olvston, C.N., "Eddy Current Methods for Examination of Carbon Fiber Reinforced Epoxy Resin," Materials Evaluation, Vol. 34, 1976.
59. Martin, B.G., "An Analysis of Radiographic Techniques for Measuring Resin Content in Graphite Fiber Reinforced Epoxy Resin Composites," Materials Evaluation, September 1977, pp. 65-68.
60. Nevadunsky, J.J., Lucas, J.J., and Salkind, M.J., "Early Fatigue Damage Detection in Composite Materials," J.Comp. Materials, Vol. 9, 1975, p. 394.

61. Burchett, D.J., and Irwin, J.L., "Laser Holography of Carbon Composite Structures," Carbon Composite Technology, Proceedings of the 10th Annual Conference, ASME, 1970, p. 237.
62. McCaughey, W.A., Grant, R.M., and Brown, G.M., "Holographic Non-destructive Testing of Aircraft Materials," Proc. 156th National SAMPE Symposium and Exhibition, SAMPE Publication, Vol. 15, p. 913.
63. Aas, H., Erf, R., and Waters, J., "Investigation to Determine the Feasibility of Employing Laser Beam Holography for the Detection of Characterization of Bond Defects in Composite Material Structures," United Aircraft Research Labs, NASA CR-111836, February 1971.
64. Grubinskas, R.C., State of the Art Survey on Holography and Microwaves in Nondestructive Testing, AMMRC MS 72-9, September 1972.
65. Erf, R.K., ed., Holographic Nondestructive Testing, Academic Press, 1974.
66. Sendekyj, G.P., Maddux, G.E., and Tracy, N.A., "Comparison of Holographic, Radiographic, and Ultrasonic Techniques for Damage Detection in Composite Materials," Proceedings, 2nd International Conference on Composite Materials, B. Norton, R. Signorelli, K. Street, and L. Phillips, Eds., American Institute of Mining, Metallurgical, and Petroleum Engineers, 1978, pp. 1037-1056.
67. Sendekyj, G.P., Stalnaker, H.D., Kleismet, R.A., "Effect of Temperature on Fatigue Response of Surface Notched $[(0/\pm 45/0)_S]_3$ Graphite/Epoxy Laminate," Fatigue of Filamentary Composite Materials, ASTM STP 636, American Society for Testing and Materials, 1977, pp. 123-140.
68. Chang, F.H., Gordon, D.E., and Gardner, A.H., "A Study of Fatigue Damage in Composites by Nondestructive Testing Techniques," Fatigue of Filamentary Composite Materials, ASTM STP 636, American Society for Testing and Materials, 1977, pp. 57-72.
69. Roderick, G.L., and Whitcomb, J.D., "Fatigue Damage of Notched Boron/Epoxy Laminates Under Constant Amplitude Loading," Fatigue of Filamentary Composite Materials, ASTM STP 636, American Society for Testing and Materials, 1977, pp. 73-78.
70. Rose, J.L., and Shelton, W., "Damage Analysis in Composite Materials," Composite Reliability, ASTM STP 580, American Society for Testing and Materials, 1975, pp. 215-226.
71. Chang, F.H., Couchman, J.C., Eisenmann, J.R., and Yee, B.G.W., "Application of a Special X-Ray Nondestructive Testing Technique for Monitoring Damage Zone Growth in Composite Laminates," Composite Reliability, ASTM STP 580, American Society for Testing and Materials, 1975, pp. 176-190.

72. Chang, F.H., Gordon, D.W., Rodini, B.T., and McDaniel, R.H., "Real-Time Characterization of Damage Growth in Graphite/Epoxy Laminates," J. Comp. Materials, Vol. 10, July 1976, pp. 182-192.
73. Audience questions to discussion following presentation of paper on Reference 68.
74. Knollman, G.C., Lockheed Missiles and Space Company, Private Communication, March 1978.
75. Warner, S.B., Peebles, L.H., and Uhlmann, O.R., "Plasticization of Carbon Fibre," Carbon Fibres; Their Place in Modern Technology, Plastics and Polymers Conference Supplement No. 6, The Plastics Institute, London, 1974, pp. 16-19.
76. Sendeckyj, G.P., "The Effect of Tetrabromoethane - Enhanced X-Ray Inspection on Fatigue Life of Resin-Matrix Composites," Composites Technology Review, Vol. 1, No. 1, Winter 1980, pp. 9-10.
77. Lauraitis, K.N., and Pettit, D.E., "Residual Strength Degradation for Advanced Composites; Task I Final Report," AFFDL-TR-79-3095, May 1980, Lockheed Report LR 28360-16 to AFFDL on Contract F33615-77-C-3084, May 1980.
78. Ratwani, M.M., "Influence of Penetrants Used in X-Ray Radiography on Compression Fatigue Life of Graphite/Epoxy Laminates," Composites Technology Review, Vol. 2, No. 1, Winter 1980, pp. 10-12.
79. Kettering, D., and Mostik, E., "Development of a Radio-Opaque Penetrant for Use in Composite Material Radiography," Inter-Office Memo, Grumman Aircraft Corporation, Long-Island, N.Y., September 28, 1977.
80. Bailey, C.D., Freeman, S.M., and Hamilton, J.M., "Detection and Evaluation of Impact Damage in Graphite/Epoxy Composites," Materials and Processes-in Service Performance, 9th National SAMPE Technical Conference, Vol. 9, Society for the Advancement of Material and Process Engineering, October 1977, pp. 491-503.
81. Knollman, G.C., et al, "Acoustic Imaging Techniques for Real-Time Non-destructive Testing," Acoustical Holography (Plenum Press), New York Vol. 6, 1975, p. 637.
82. Knollman, G.C., Weaver, J.L., Hartog, J.J., and Bellin, J.L., "Real Time Ultrasonic Imaging Methodology in Nondestructive Testing," J. Acoust. Soc. Amer. Vol. 58, 1975, p. 455.
83. Rose, J.L., Carson, J.M., and Leidel, D.J., "Ultrasonic Procedures for Inspecting Composite Tubes," Analysis of the Test Methods for High Modulus Fibers and Composites, ASTM STP 521, American Society for Testing and Materials, 1973, pp. 311-325.

84. Porter, T.R., "Evaluation of Flawed Composite Structure Under Static and Cyclic Loading," Fatigue of Filamentary Composite Materials, ASTM STP 636, K.L. Reifsnider and K.N. Lauraitis, Eds., American Society for Testing and Materials, 1977, pp. 152-170.
85. Sheldon, W.H., "Comparative Evaluation of Potential NDE Techniques for Inspection of Advanced Composite Structures," Materials Evaluation, February, 1978, pp. 41-46.
86. Williams, R.S. and Reifsnider, K.L., "Real-Time Nondestructive Evaluation of Composite Materials During Fatigue Loading," Materials Evaluation, August 1977, pp. 50-54.
87. Wadin, J.R., and Pollock, A.A., "Periodic Proof Testing of Fiberglass Booms through the Use of Non-Kaiser Acoustic Emission Responses," Materials and Processes - In Service Performance, 9th National SAMPE Technical Conference, Vol. 9, Society for the Advancement of Material and Process Engineering, October 1977, pp. 419-560.
88. Awerbuch, J., and Hahn, H.T., "Fatigue and Proof Testing of Unidirectional Graphite/Epoxy Composites," Fatigue of Filamentary Composite Materials, ASTM 636, K.L. Reifsnider and K.N. Lauraitis, Eds., American Society for Testing and Materials, 1977, pp. 248-266.
89. Williams, R.J. and Reifsnider, K.L., "Investigation of Acoustic Emission During Fatigue Loading of Composite Materials," J. Comp. Materials, Vol. 8, October 1974, pp. 340-355.
90. Hamsted, M.A., and Chiao, T.T., "Acoustic Emission from Stress Rupture and Fatigue of an Organic Fiber Composite," Composite Reliability, ASTM STP 580, American Society for Testing and Materials, 1975, pp. 191-301.
91. Henneke, E.G., II, and Hering, H.W., "Spectrum Analysis of Acoustic Emissions from Boron - Aluminum Composites," Composite Reliability, ASTM STP 580, American Society for Testing and Materials, 1975, pp. 202-214.
92. Hahn, H.T., and Kim, R.Y., "Proof Testing of Composite Materials," J. Composite Materials, Vol. 9, July 1975, pp. 297-311.
93. Henneke, E.G., II, Reifsnider, K.L., and Stinchcomb, W.W., "Defect-Property Relationships in Composite Materials," presented at AFML, AFOSR, and AFFDL Mechanics of Composites Review, Bergamo Center, Dayton, Ohio, 25-27 October, 1977, pp. 150-162.
94. Stalnaker, D.O., and Stinchcomb, W.W., "An Investigation of Edge Damage Development in Quasi-Isotropic Graphite Epoxy Laminates," Interim Report, AFML Contract F33615-75-C-5119, Virginia Polytechnic Institute and State University Report VPI-E-77-24, September 1977.

95. Reifsnider, K.L., Henneke, E.G., II, and Stinchcomb, W.W., "Delamination in Quasi-Isotropic Graphite-Epoxy Laminates," Composite Materials: Testing and Design (Fourth Conference), ASTM STP 617, American Society for Testing and Materials, 1977, pp. 93-105.
96. Reifsnider, K.L., and Williams, R.S., "Determination of Fatigue Related Heat Emission in Composite Materials," Experimental Mech. Vol. 14, No. 12, 1974, pp. 479-485.
97. Marcus, L.A., and Stinchcomb, W.W., "Measurement of Fatigue Damage in Composite Materials," Paper No. S2544 Society for Experimental Stress Analysis Fall Meeting, Indianapolis, Indiana, 16-19 October 1973.
98. Whitcomb, J.D., Private Communication, April 1977.
99. Reifsnider, K.L., Private Communication, April 1977.
100. Jones, T.S., "Thermographically Detecting Damaged Regions in Fiber Reinforced Composite Materials," M.S. Thesis, Virginia Polytechnic Institute and State University, Blacksburg, Virginia, 1977.
101. Hahn, H.T., and Kim, R.Y., "Fatigue Behavior of Composite Laminates," J. Composite Materials, Vol. 10, April 1976, pp. 156-180.
102. Reifsnider, K.L., Stinchcomb, W.W., Williams, R.S., and Turgey, H.M., "Frequency Effects on Flawed-Composite Fatigue Reliability," Composite Reliability, ASTM STP 580, American Society for Testing and Materials, 1975, pp. 425-442.
103. Reifsnider, K.L., Stinchcomb, W.W., and O'Brian, T.K., "Frequency Effects on a Stiffness-Based Fatigue Failure Criterion in Flawed Composite Specimens," Fatigue of Filamentary Composite Materials, ASTM STP 636, American Society for Testing and Materials, 1977, pp. 171-184.
104. Stinchcomb, W.W., Reifsnider, K.L., Marcus, L.A. and Williams, R.S., "Effects of Frequency on the Mechanical Response of Two Composite Materials to Fatigue Loads," Fatigue of Composite Materials, ASTM STP 569, American Society for Testing and Materials, 1975, pp. 115-129.
105. Reifsnider, K.L., and Stinchcomb, W.W., "Investigation of Dynamic Heat Emission Patterns in Mechanical and Chemical Systems," Proceedings, Second Biennial Infrared Information Exchange, August 1974, pp. 45-58.
106. Reifsnider, K.L., and Williams, R.S., Experimental Mechanics, December 1974, pp. 479-486.
107. Marcus, L.A., and Stinchcomb, W.W., Experimental Mechanics, Vol. 15, No. 2, February 1975, pp. 55-60.

108. O'Brian T.K., and Reifsnider, K.L., "Fatigue Damage Stiffness/Strength Comparisons for Composite Materials," Journal of Testing and Evaluation, Vol. 5, No. 5, September 1977.
109. Wood, R.E., "Graphite Composite Hole Quality," Lockheed-California Company Report LR 28385, December 21, 1977.
110. Stinchcomb, W.W., Private Communication, September 1979.
111. Ryder, J.T. and Wadin, J.R., "Acoustic Emission Monitoring of a Quasi-Isotropic Graphite/Epoxy Laminate under Fatigue Loading," presented at the ASNT Spring Conference, April 2-5, 1979, San Diego, Ca., published in the conference proceedings and to appear in 1980 in the ASNT journal.
112. Henneke II, E.G., "Signature Analysis of Acoustic Emissions from Composites," NASA Report NASA-CR-145373, May 19, 1978.
113. Stinchcomb, W.W., Private Communication, January 1980.
114. Sandifer, J.P., Private Communication, June 1980.
115. Micro-Measurements, "Tech-Note, Fatigue of Strain Gages," TN-130-3, 1974, and private communication, April 1980.

APPENDIX A

T300/5208 GRAPHITE/EPOXY LAMINATE
AND TEST SPECIMEN FABRICATION
QUALITY CONTROL PLAN

for

EFFECT OF LOAD HISTORY ON FATIGUE LIFE

AFML CONTRACT F33615-78-C-5090

QUALITY CONTROL PLAN

Manufacturing and quality assurance procedures will be applied to material and laminates, as described below, to ensure quality, uniformity and traceability of test specimens.

1. Material Acquisition

Narmco T300/5208 graphite/epoxy prepreg material conforming to Lockheed Material Specification C-22-1379/111 will be acquired for this program in one procurement. Other materials required for the fabrication of test laminates will be purchased to the requirements given in the Lockheed Engineering Purchasing Specification (EPS) Manual, to the extent indicated in section 3. Fiberglass for the specimen tabs will be acquired to Lockheed Material Specification LCM C-22-1032/141.

2. Material Acceptance

The prepreg material supplier will be required to provide a certificate of conformance, including test data, resin/catalyst age, and date of mixing with each delivery. Lockheed Quality Assurance laboratories will then conduct acceptance tests on the delivered material in confirmation of supplier data. These tests will include:

- Uncured Properties
 - Fiber orientation
 - Resin content
 - Volatiles content
 - Resin flow
 - Gel time
 - Infrared Analysis
 - Areal Weight

- Mechanical and Physical Properties of Cured Material

- Void Content
- Specific Gravity
- Cured Resin Content or Fiber Volume
- Interlaminar Shear
- Longitudinal Tensile Strength and Modulus
- Longitudinal Flexural Strength and Modulus
- Cured Ply Thickness

The test methods and acceptance limits shall be as specified in the applicable material specifications, C-22-1379/111 and C-22-1379A. Materials not conforming to the requirements of the Specifications will be rejected.

Material specifications further stipulate preparation-for-delivery provisions covering date of shipment, allowable time and temperature in transit, and vapor-tight packaging required for supplier and transporter conformance. Materials requiring refrigerated storage will be placed in Quality Assurance approved refrigerators immediately upon receipt. Pending acceptance by the Quality Assurance laboratory, all materials will be kept segregated and withheld from use. After acceptance, each container, roll, or spool of material will be stamped or otherwise approved by Quality Assurance and controlling labels will be attached.

3. Material Processing

This section establishes the requirements and procedures for the lamination of graphite/epoxy (T300/5208) test panels, fabrication of glass/epoxy tab stock and bonding of tabs to coupons.

3.1 Applicable Documents and Materials

The following documents form a part of this procedure to the extent specified herein.

3.1.1 Lockheed Materials Specifications

Lockheed Material Specification, C-22-1379A Graphite Fiber Non-Woven Tape and Sheet, Resin Impregnated, General Specification for.

Lockheed Material Specification C-22-1379/111 Graphite Fiber Non-Woven Tape and Sheet, 2410 MPa (350 ksi) Strength, 228 GPa (33 Msi Modulus, 177°C (350°F) Curing, Epoxy Preimpregnated.

Lockheed Material Specification LCM C-22-1032/141 Glass Fabric/Epoxy Preimpregnated, 177°C (350°F) Cure.

3.1.2 Commercial Materials

3.1.2.1 The following commercial materials, covered by the Lockheed Engineering Purchasing Specification (EPS) Manual, form a part of this procedure to the extent specified herein.

<u>Material</u>	<u>EPS Item No.</u>
Vacuum Bag Nylon Film	22.9001
Parting Agent Film	22.9004
Porous Release Cloth	22.9030
Peel Ply	25.5910
Stick Contact Adhesive	30.0650

3.1.2.2 The following commercial materials not covered by the Engineering Purchasing Specification Manual are required for use in this procedure.

American Cyanamid Co.	FM-400 Epoxy Adhesive Film, 3.35 Pa (0.07 lb/ft ²), 177°C (350°F) Cure
Air Tech International Inc.	Flashbreaker 5 Pressure Sensitive Tape

3.2 Material Control

All materials shall conform to the applicable specifications.

3.2.1 Storage and control requirements shall be as specified in Table 37. Refrigerated material shall be stored in sealed, moisture vapor proof containers.

3.2.2 Refrigerated materials shall be thawed until moisture no longer condenses on the moisture-proof containers.

3.2.3 All perishable materials shall have had validation tests performed within 30 days of use, if initial storage time limit has been exceeded. Validation tests are the same as those shown in table 37.

3.2.4 A manufacturer's identified defects (MID's) record is furnished with each roll of Gr/Ep by the material supplier. This record shall be furnished to the Composites Laboratory with each roll of Gr/Ep.

3.2.5 Stored perishable material in which visible water is observed in the bag shall be rejected.

TABLE 37. MATERIAL CONTROL

Material	Max. Storage Temp.	Maximum Storage Time Before Retesting, Days		Minimum Required Tests	Max. Allowed Out Time During Proc. @ 23°C (75°F) & 55% R.H.
		Initial	Subsequent		
Gr/ep Prepreg	18°C (0°F)	180	60	△ △	14 days
Adhesive Film	18°C (0°F)	180	90	---	10 days
△ Flow and gel time, room temp, flexural and short beam shear, specific gravity and resin content.					
△ See applicable Material Specifications for test methods and requirements.					

3.3 Environmental Control

3.3.1 All work shall be done in controlled areas to avoid degradation of the materials and laminates. Temperature shall be between 18-27°C (65-80°F) and relative humidity shall not exceed 55%.

3.3.2 All incoming air into controlled areas shall be filtered by at least a 3.7 cm (1-1/2 in.) thick throw-away type or permanent washable type filter or by an equivalent method. Inspect and clean filters monthly.

3.4 Tooling

3.4.1 All tools shall be designed and coordinated to produce parts that meet all requirements of this specification and the Engineering drawing. Tools shall have the minimum mass necessary for dimensional and thermal control.

3.4.2 All tool plates used for curing laminates shall be aluminum. Thickness of the caul plate shall be 12.7 mm (0.500 in.) with a tolerance of ± 0.08 mm (± 0.003 in.), flat and parallel. Caul plates used on top surface of laminate under the vacuum bag shall be aluminum sheet 1.62 mm (0.064 in.) standard thickness.

3.4.3 Tooling parting agents and cleaners shall not contaminate the laminates or interfere with subsequent bonding, finishing and inspection.

3.5 Material Preparation

3.5.1 Templates or patterns shall be placed on the prepreg in such a way as to ensure that the fiber direction is in accordance with Engineering drawing requirements and does not include any MID's flagged by the supplier (see 3.2.4).

3.5.2 Panels will be laid-up such that the edges of tape are parallel or perpendicular to the required fiber direction within 1°.

3.5.3 All areas from which material will be cut shall be checked prior to cutting for the defects defined in C-22-1379, Quality and Condition Requirements, which may not have been flagged by the manufacturer. Material containing unacceptable defects will not be used. Patch plies are not permitted.

3.5.4 Plies shall be cut with sufficient care so as not to disorient fibers. Cutting tools shall be cleaned prior to use on prepregs.

3.5.5 No ply end butt splices are permitted in the laminate assembly.

3.6 Tool Preparation

3.6.1 The tool molding surfaces shall be solvent wiped and all resin removed prior to layup.

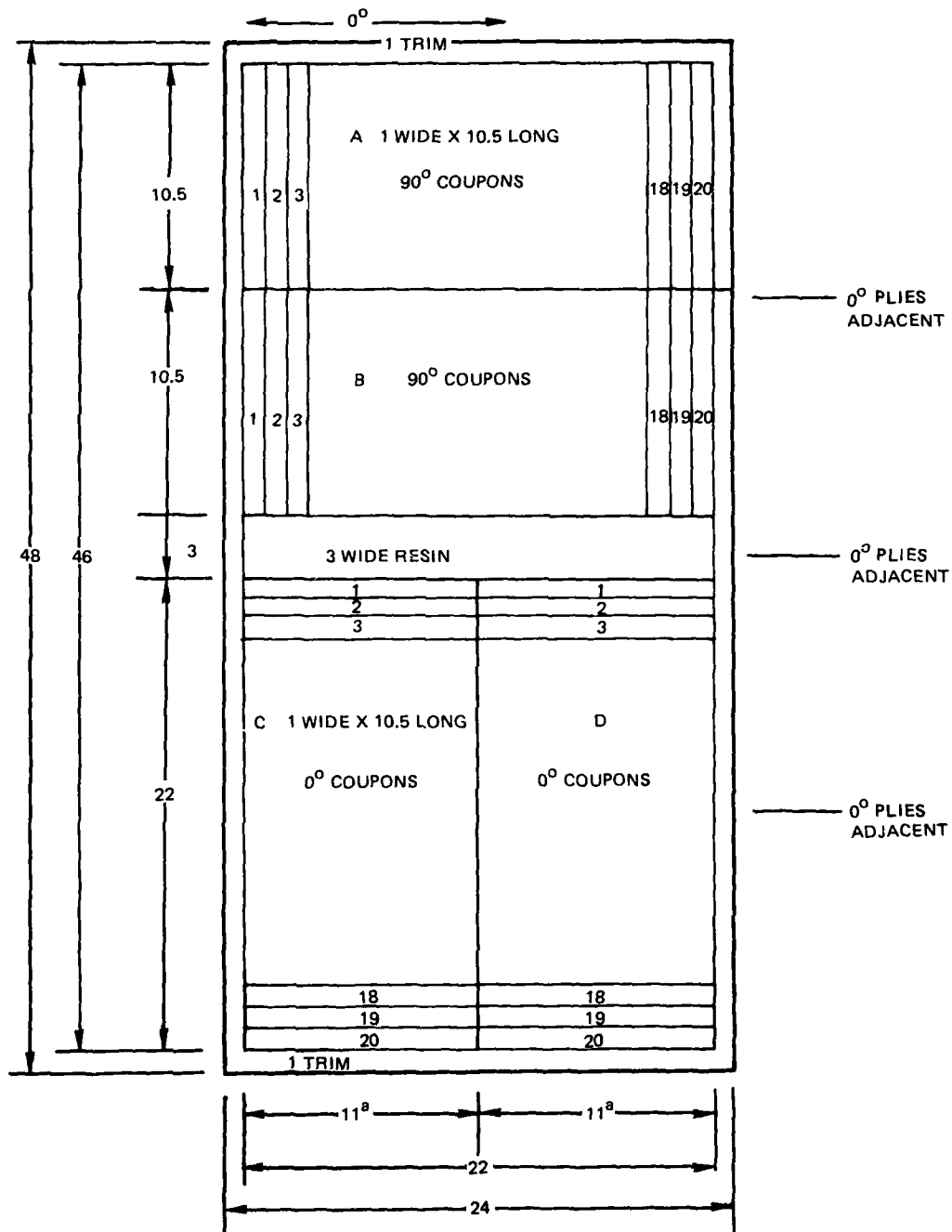
3.7 Panel Lay-up

3.7.1 The preimpregnated graphite tape shall be placed on the tool in the sequence and orientation specified on the Engineering drawing or Engineering Test Request. As each ply is placed on the assembly, it shall be checked for the defects defined in C-22-1379 prior to applying the ply firmly in place. A check-off system shall be used to assure proper orientation and stacking sequence of each ply.

3.7.2 The surface of each ply shall be wiped with a teflon, polyethylene or equivalent device to give maximum adhesion to the previous ply. Wiping shall be done only in the direction of the fibers to prevent fiber separation and distortion. Wiping the surface should be done only when the orientation of the tape edge has been verified to be within $\pm 1^\circ$ of the drawing requirement. Excessive pressure shall not be applied during wiping and wiping shall be kept to a minimum.

3.7.3 Panels shall be layed up as shown in figures 84 to 86. Parallel $+45^\circ$ or -45° plies shall be laid up so that edge splices are staggered a minimum of 5.08 cm (2.0 in.) in adjacent plies and shall not coincide from one to the next.

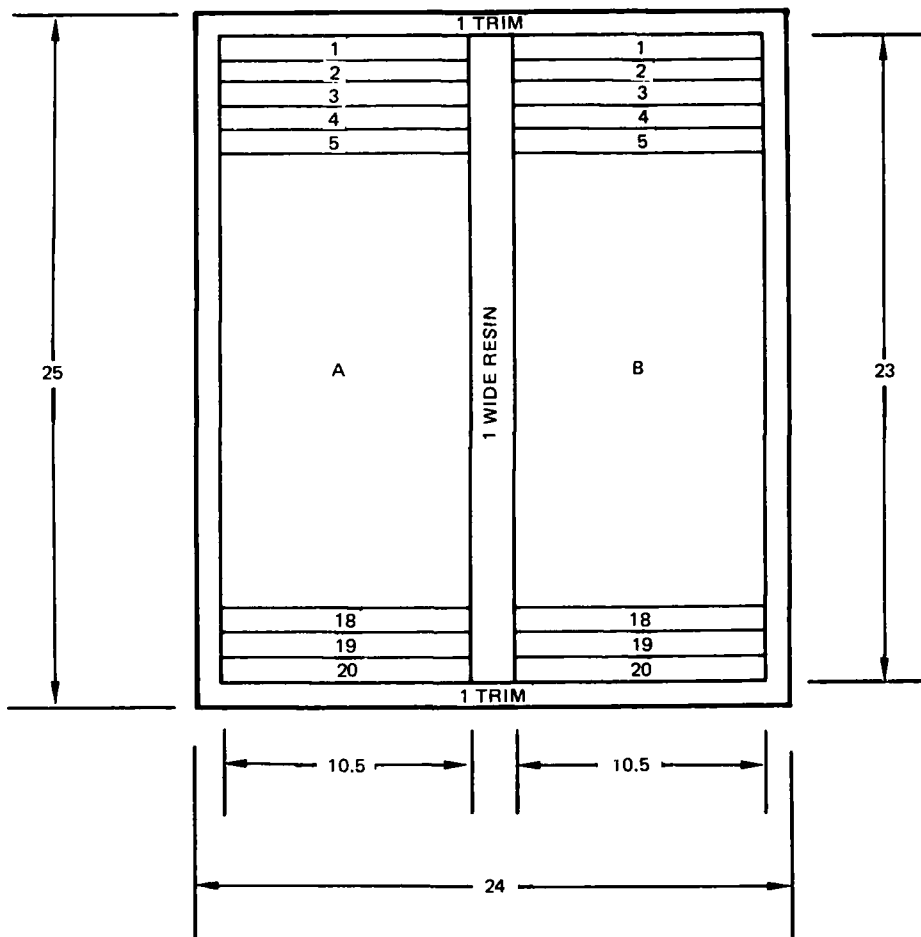
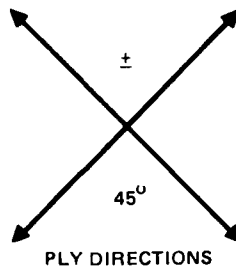
ALL DIMENSIONS IN in.



NOTE: ALL 0° TAPE JOINTS ARE LINED UP THROUGHOUT PANEL

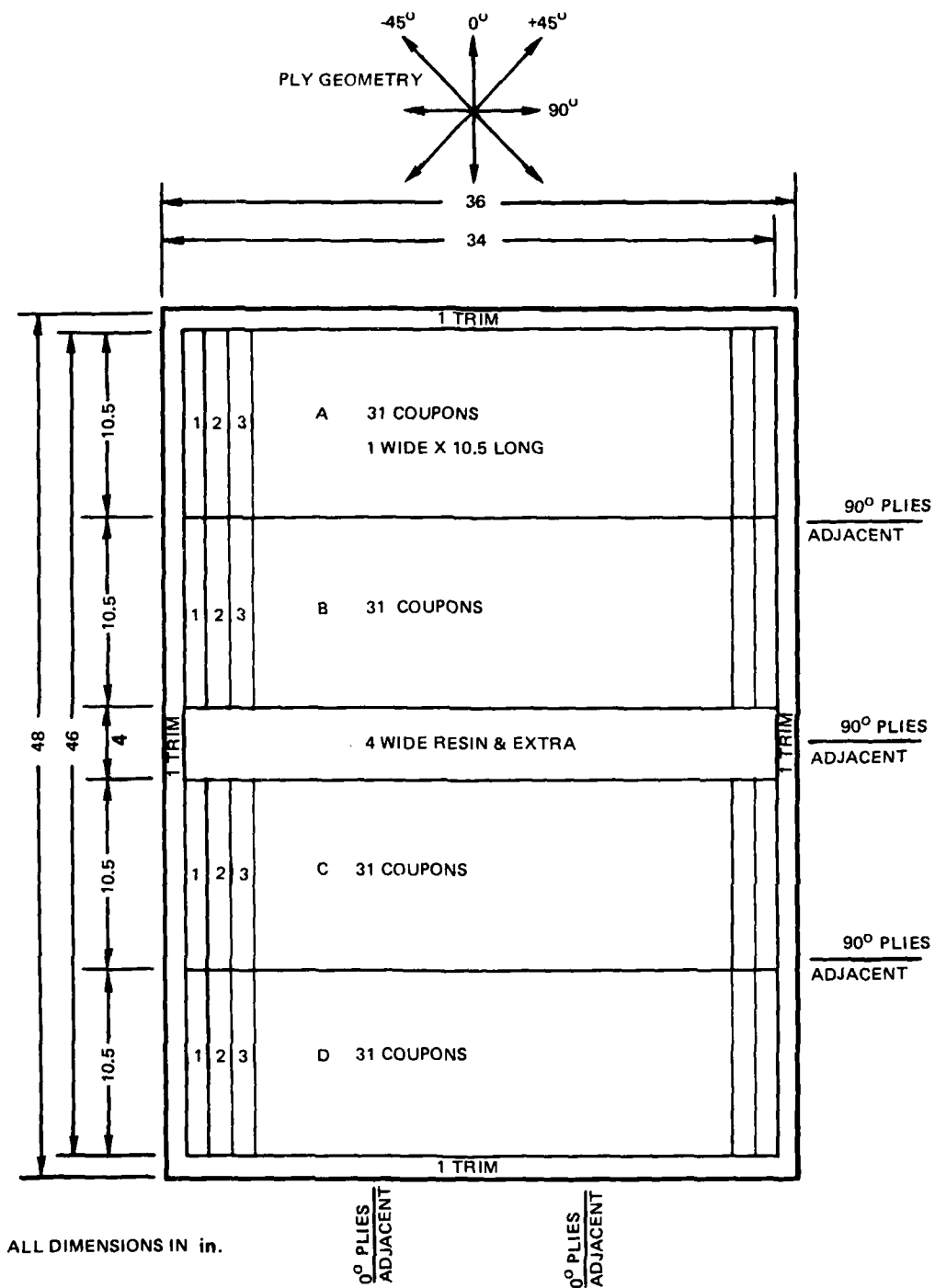
^aTRIM TO 10.5

Figure 84. - Layup of Laminuate U1 16 Ply (0°)₁₆



NOTE: NO TAPE JOINTS ARE LINED UP THROUGH THE PANEL THICKNESS.
ALL DIMENSIONS IN in.

Figure 85. - Layup of Laminuate U2 16 Ply ($\pm 45^\circ$)_{4S}.



NOTE: 0° AND 90° TAPE JOINTS ARE LINED UP THROUGH PANEL THICKNESS,
45° JOINTS ARE NOT LINED UP

Figure 86. - Layup of Laminuate L1 16 Ply (0/45/90/-45₂/90/45/0)_S.

3.7.4 Edge splices shall be butted flush ± 0.8 mm (± 0.03 in.).

3.7.5 Entrapped air in blisters that cannot be wiped out without distorting fibers shall be removed by puncturing the blister with a needle or pointed sharp blade as often as needed and wiping in the direction of the fibers toward the puncture. Care shall be taken not to damage the under ply fibers.

3.7.6 Where permanent edge steps or dams are not incorporated in the tool for edge thickness control, an edge dam shall be built around the perimeter of the laminate. The dam shall not be more than 1.52 mm (0.06 in.) from the laminate edge and shall be of sufficient height to enclose the laminate. The bleeder may not extend over the dam surface. Joints in the dam shall be kept to a minimum. Dam joint gaps shall not exceed 0.8 mm (0.03 in.).

3.7.7 A dry peel ply of fabric (EPS 25.5910) or equivalent shall be placed on both sides of the layup and wiped smooth.

3.7.8 A bleeding and bagging system of the following construction shall be used.

- (a) Cure plate
- (b) Separator film - perforated parting agent film or porous release cloth.
- (c) Mochburg CW1850 bleeder paper (1 ply for 4 plies of prepreg.)
- (d) One ply of porous Teflon-coated glass cloth (DuPont Armalon)
- (e) Nylon peel ply
- (f) Graphite/epoxy laminate
- (g) Nylon peel ply
- (h) One ply Armalon
- (i) Mochburg CW1850 bleeder paper (4:1 ratio)
- (j) Release film
- (k) Caul plate (aluminum)

- (l) One ply Mochburg CW1850
- (m) Release film
- (n) Glass breather
- (o) Nylon film vacuum bag placed over the laminate and sealed to the tool face.

3.7.9 Curing - Pressure and cure cycle should be within the limits given in Table 38.

3.8 Laminate Control Specimens

Each panel will be laid up to contain an excess strip at least 2.5 cm (1.0 in.) wide and running either the width of the panel.

3.8.1 Laminate control coupons will be cut from this strip for the determination of resin content, specific gravity and average ply thickness. Test requirements are given in Table 39.

3.8.1.1 Void volume fraction will be obtained from laminate control coupons from selected panels using standard metallographic techniques. This method will be used to confirm results calculated from the acid digestion and density measurement values for each panel. Void content shall not exceed 1.0% maximum by volume.

TABLE 38. CURE CYCLE

1.	Apply full vacuum.
2.	Heat to $135^{\circ} \pm 3^{\circ}\text{C}$ ($275^{\circ} \pm 5^{\circ}\text{F}$) @ $1 - 2^{\circ}\text{C}$ ($2 - 3^{\circ}\text{F}$)/min.
*3.	Dwell @ 135°C ($275^{\circ} \pm 5^{\circ}\text{F}$) for 30 ± 1 minutes.
4.	Apply 0.69 ± 0.04 M Pa (100 ± 5 psi) vent vacuum to air @ 0.14 M Pa (20 psi).
5.	Heat to $177^{\circ} \pm 3^{\circ}\text{C}$ ($350 \pm 5^{\circ}\text{F}$) @ $1 - 2^{\circ}\text{C}$ ($2 - 3^{\circ}\text{F}$)/min.
6.	Cure for 120 ± 10 min. @ $177^{\circ} \pm 3^{\circ}\text{C}$ ($350 \pm 5^{\circ}\text{F}$).
7.	Cool to $60^{\circ} \pm 3^{\circ}\text{C}$ ($140 \pm 5^{\circ}\text{F}$) under pressure @ less than 2.5°C (4°F)/min.
8.	Cool to room temperature.
*NOTE: Dwell time started when temperature reaches 130°C (265°F).	

TABLE 39. TEST REQUIREMENTS

Test	Requirements
Fiber Volume	66 ± 2%
Specific Gravity	1.56 - 1.60
Thickness/Ply	0.117 - 0.135 mm (.0046 - .0053 in.) (Report for information only)

3.9 Workmanship

All laminated details and bonded assemblies shall be of highest quality. Conditions in excess of the following shall be cause for rejection.

3.9.1 There shall be no evidence of surface cracking, uncoated fibers, excess resin, pits, tackiness or other indications of defective resin characteristics or distribution.

3.9.2 No visual delaminations are allowed.

3.9.3 No wrinkles containing graphite fibers are permitted. Resin wrinkles caused by peel ply gathering or by the bleeder system shall not be cause for rejection if the resin ridge can be removed without damaging the graphite fibers using 320 grit or finer sandpaper.

3.9.4 The presence of foreign material, e.g., separator film, masking tape, etc., in the part is not acceptable.

3.9.5 There shall be no sharp or frayed edges, nor edge delaminations resulting from trimming and routing operations.

3.10 Cleanup

Chemical strippers shall not be used in any way to remove excess resin or adhesive. If removal is necessary, it shall be done with an abrasive, and shall not damage any surface graphite fibers.

3.11 Records

The following records are required for permanent retention and traceability.

1. Temperature-pressure-vent-time profile record for each cure cycle.
2. Thermocouple locations.
3. Material batch and roll number, acceptance laboratory report number and cumulative out-time up to the time of vacuum application.
4. A completed autoclave record sheet as shown in figure 87.

3.12 Machining of Test Specimens

Specimens are to be machined to the dimension shown in figures 88 and 89. Specimen cuts will be made parallel to the panel edge to ± 1 degree. Cutting rates will be chosen to minimize edge damage.

3.13 Fabrication and Bonding of Glass Fabric/Epoxy Grip Tabs

3.13.1 Grip tab sheet material shall be fabricated by laminating the required number of plies of Style 181, 1581, or 7581 glass fabric/epoxy prepreg. For most standard coupons, the laminate consists of 6 plies or 3 plies in thickness depending on the type of coupon. Thicknesses and other dimensions shall be in accordance with figures 88 and 89. Tab dimensions shall be as specified on specimen drawing.

3.13.2 The material used for grip tab stock shall be glass/epoxy prepreg conforming to Lockheed Material Spec. LCM C-22-1032/141. This material shall be cured at 177°C (350°F) for one hour under a pressure of 0.24 M Pa (35 psi) plus vacuum. A caul sheet shall be used under a vacuum bag for pressure application.

3.13.3 The adhesive used for bonding tabs to coupons shall be American Cyanamid Co. FM-400, 3.35 Pa (0.07 lbs/ft^2). Aluminum caul plates 0.63 to 1.27 mm (0.25 to 0.5 in.) thick shall be used to apply bonding pressure on tabs.

Run # _____

ETR/Dwg.# _____ Panel I.D. _____ Matl. Code _____

Q.A. Lab. Report # _____ Made for _____ Date _____

I. Description of Materials

Designation _____ Batch# _____ Roll# _____ Date _____
Mfd. _____

No. of Plies _____ Orientation _____

CURE CYCLE (NARMCO)

- II. Cure Press. _____ psi
Cure Temp _____ °F
Cure Time _____ min.
Vac. Bag _____ inch-Hg
- III. Autoclave Pressurization
Time @ start _____
Time @ press. _____
Delta Time min. _____
- IV. Temp _____ °F
- V. Temp _____ °F @ lay-up
1. Apply fuel vacuum
2. Heat to 275° ± 5°F @ 2-3°F/min.
*3. Dwell @ 275° ± 5°F for 30 ± 1 min.
4. Apply 100 ± 5 psi & vent vac to air @ 20 psi.
5. Heat to 355 ± 5°F @ 2-3°F/min.
6. Cure 120 ± 10 min. @ 355 ± 5°F
7. Cool to 140 ± 5°F under press. @ <4°F/min.
8. Cool to R.T.
- * NOTE: dwell time starts when temp reaches 265°F.
- V. %R.H. _____ @ lay-up

VI. TIME RECORD

	1	2	3	4	5
Temp Time	Temp Time	Temp Time	Temp Time	Temp Time	Temp Time
Start heat					
At temp.					
Time to temp min.					
Time @ temp min.					OFF _____
Heat-up rate °F/min.					
Cool-down rate °F/min.					

VI. Panels

I.D.	Size(in.)	No.	Meas.
	x	Plies	Thick

IX. Comments

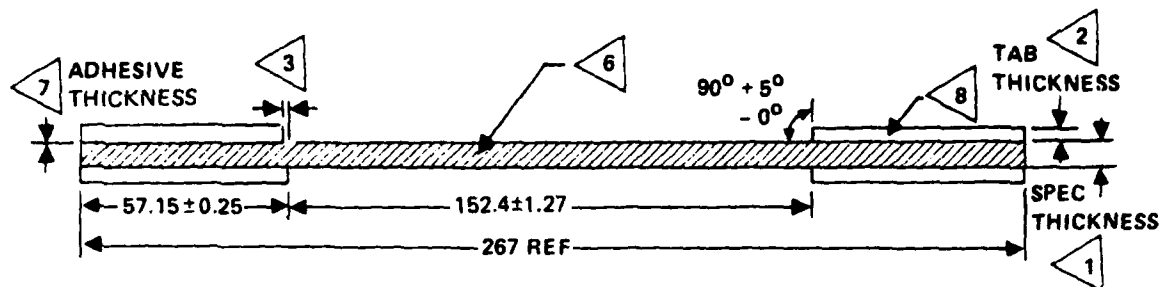
VIII. Bleeding & Bagging

- _____ nylon bag
_____ 181 glass breather
_____ vac pac
_____ Mochburg (1 ply)
_____ caul plate
_____ vac pac
_____ Mochburg (4:1 ratio)
_____ armalon
_____ nylon peel ply
_____ LAMINATE
_____ nylon peel ply
_____ armalon
_____ Mochburg
_____ vac pac
_____ cure plate

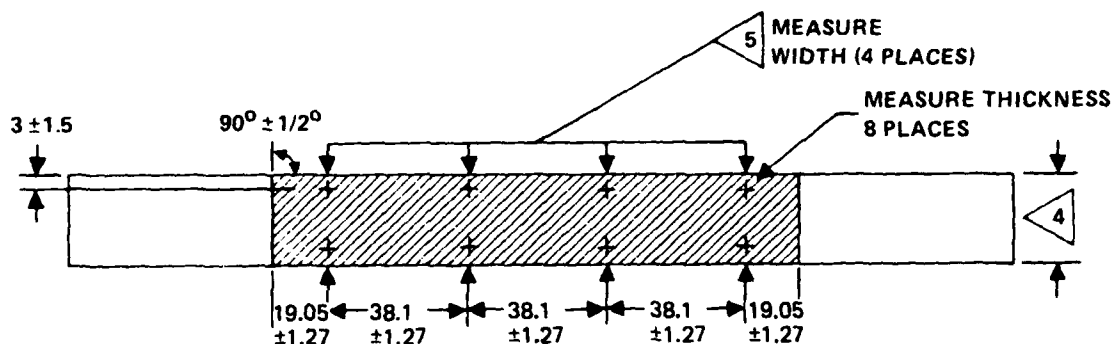
Signature of Inspecting Engineer _____

NOTE: Laminate completely damaged
perforated vac pac taped to dam.

Figure 87. - Sample Autoclave Record.

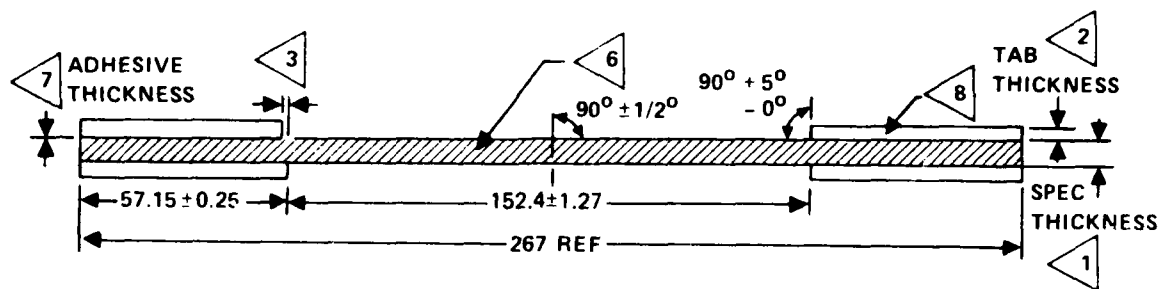


ALL DIMENSIONS IN MILLIMETERS

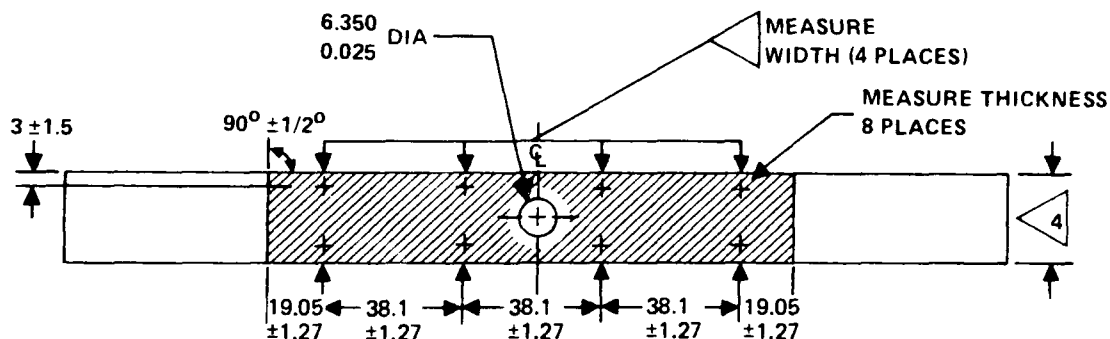


- <9> SPECIMENS TO BE FLAT OVER THE ENTIRE 267 mm (10.5 in.) LENGTH WITHIN 0.25 mm (0.01 in.)
- <8> TAB EDGES TO BE PARALLEL TO SIDES OF SPECIMEN WITHIN 0.025 mm (0.001 in.) OVERHANG NOT TO EXCEED 3.8 mm (0.003 in.)
- <7> THE TAB AND SPECIMEN BONDING SURFACES TO BE THOROUGHLY SOLVENT CLEANED USING METHYL-ETHYL-KETONE PRIOR TO BONDING. A 177°C (350°F) CURING ADHESIVE IS TO BE USED AND MUST COVER ENTIRE SURFACE UNIFORMLY.
- <6> SPECIMENS TO BE CUT DRY. MACHINED SURFACES TO BE r_{ms} 50 OR BETTER. NO EDGE DAMAGE OR FIBER SEPARATION SHOULD BE VISIBLE UNDER 10X MAGNIFICATION.
- <5> MEASURE SPECIMEN WIDTH 4 PLACES. WIDTH MUST NOT VARY BY MORE THAN 0.102 mm (0.004 in.)
- <4> SPECIMEN WIDTH TO BE 22.225 ± 0.127 mm (0.875 ± 0.005 in.)
- <3> MISMATCH OF TABS FROM SIDE TO SIDE NOT TO EXCEED 0.25 mm (0.01 in.)
- <2> TABS TO BE CUT FROM AN 6 PLY LAMINATE FABRICATED FROM PREPREG OF 1581 GLASS FABRIC IN A 177°C (350°F) CURING EPOXY.
- <1> SPECIMEN THICKNESS TO BE WITHIN ± 0.08 mm (± 0.003 in.) OF THE AVERAGE OF 8 THICKNESS MEASUREMENTS.

Figure 88. - Un-Notched Composite Test Specimen



ALL DIMENSIONS IN MILLIMETERS



- ◀ 9 SPECIMENS TO BE FLAT OVER THE ENTIRE 267 mm (10.5 in.) LENGTH WITHIN 0.25 mm (0.01 in.)
- ◀ 8 TAB EDGES TO BE PARALLEL TO SIDES OF SPECIMEN WITHIN 0.025 mm (0.001 in.) OVERHANG NOT TO EXCEED 3.8 mm (0.003 in.)
- ◀ 7 THE TAB AND SPECIMEN BONDING SURFACES TO BE THOROUGHLY SOLVENT CLEANED USING METHYL-ETHYL-KETONE PRIOR TO BONDING. A 177°C (350°F) CURING ADHESIVE IS TO BE USED AND MUST COVER ENTIRE SURFACE UNIFORMLY.
- ◀ 6 SPECIMENS TO BE CUT DRY. MACHINED SURFACES TO BE rms 50 OR BETTER. NO EDGE DAMAGE OR FIBER SEPARATION SHOULD BE VISIBLE UNDER 10X MAGNIFICATION.
- ◀ 5 MEASURE SPECIMEN WIDTH 4 PLACES. WIDTH MUST NOT VARY BY MORE THAN 0.102 mm (0.004 in.)
- ◀ 4 SPECIMEN WIDTH TO BE 22.225 ± 0.127 mm (0.875 ± 0.005 in.)
- ◀ 3 MISMATCH OF TABS FROM SIDE TO SIDE NOT TO EXCEED 0.25 mm (0.01 in.)
- ◀ 2 TABS TO BE CUT FROM AN 6 PLY LAMINATE FABRICATED FROM PREPREG OF 1581 GLASS FABRIC IN A 177°C (350°F) CURING EPOXY
- ◀ 1 SPECIMEN THICKNESS TO BE WITHIN ± 0.08 mm (± 0.003 in.) OF THE AVERAGE OF 8 THICKNESS MEASUREMENTS.

Figure 89. - Notched Composite Test Specimen.

Cure adhesive at $177^{\circ} \pm 3^{\circ}\text{C}$ ($350^{\circ}\text{F} \pm 5^{\circ}\text{F}$) for 60 to 70 minutes using 0.10 ± 0.01 M Pa (15 ± 1 psi) positive pressure on bondline (no vacuum). Cool to 27°C (170°F) under pressure.

4. QUALITY ASSURANCE PROVISIONS

To produce test panels of consistent quality, strict adherence to all the minimum Engineering requirements of section 3 is vital. The requirements of section 4 are intended to outline the minimum amount of inspection and surveillance before, during, and after processing testing to confirm that adherence has been achieved.

4.1 Material

Verification shall be made that only adhesives and prepreg materials are used that are approved to the material specifications specified.

4.1.1 Adhesive or prepreg material which is stored below room temperature shall be wrapped in a closed impermeable bag at all times. Evidence of material cracking or moisture condensation on the material is cause for rejection. Exposure to ambient temperature shall be minimized.

4.1.1.1 Adhesive or prepreg material which is withdrawn from storage and left out 30 minutes or more before returning to the box, shall have the out-time marked on an appropriate tag attached to the roll. Material for which accumulated out-time at ambient temperature exceeds the allowable out-time given in table A, shall not be used.

4.1.2 All adhesive and prepreg materials shall be controlled as to batch, lot, and roll numbers for traceability.

4.1.2.1 Material which has exceeded the allowable storage shall not be used unless tested within one week prior to use.

4.1.2.2 All refrigerated materials shall be checked for compliance to 3.2.2 prior to use.

4.2 Panels and coupons shall be clearly marked before and after application of tabs to indicate the bag side of the graphite/epoxy laminate as originally cured. Panels shall be identified with a number including material code and autoclave run number. Coupons shall be identified with panel number from which cut and a dash number indicating location.

Example: 1VX1391-A7

Coupons shall be numbered consecutively as they are cut from panels to indicate relative location of the panel (see figures 84, 85 and 86).

4.3 Equipment and Facilities Control

Equipment and facilities used for materials storage, processing, and inspection shall be controlled in accordance with LCP79-1053.

4.4 An effective quality control system shall be provided to ensure compliance with the requirements of this procedure as specified in the following sections.

4.4.1 Material Acceptance testing will be performed by Lockheed Quality Assurance Laboratories.

4.4.2 Panel and tab fabricating and tab bonding will be accomplished by personnel of the Composites Laboratory at Rye Canyon Research Laboratories. Layup and cure of each panel will be witnessed and inspected by Engineering.

4.4.3 Dimensional inspection of specimens will be the responsibility of the machining company.

4.4.4 The principal investigator will have final acceptance/rejection authority for material, panels and specimens.

4.4.5 An engineering approved autoclave record will be maintained for each panel.

4.5 Non-Destructive Inspection

4.5.1 All test panels shall be non-destructively inspected for internal defects by ultrasonic "C" Scan procedure. Standard reference 0.005 mm (0.002 in.) thick teflon pads of 3.175 and 12.37 mm (0.125 and 0.500 in.) diameter will be placed at one corner of each panel. A permanent record of the C-Scan results shall be retained with the records required in 3.11.

4.5.1.1 Specimens will not be cut from areas in the panels which show indications comparable to the standards.

APPENDIX B
SUMMARY OF STATIC
TESTS RESULTS

TABLE 40
TENSION TEST RESULTS OF LAMINA U1, 0° UNIDIRECTIONAL COUPONS
AT ROOM TEMPERATURE IN LABORATORY AIR

Coupon ID	Average Area, in. ²		Ultimate Stress, σ_{ult} , ksi		Strain to Failure, ϵ_f , mm/mm in 25.4 mm	Secant Modulus at Failure, E_{sf} , psiX10 ⁶		Secant Modulus at 70 ksi, E_{s70} , psiX10 ⁶	
	mm ²		MPa			GPa		GPa	
2VX1394-C5	47.9	0.0742	1571	227.8	a	-	-	146.2	21.2
C6	48.5	0.0752	1746	253.3	a	-	-	166.2	24.1
C7	48.5	0.0752	1715	248.7	0.0094	182.4	26.5	151.0	21.9
C18	50.4	0.0782	1578	228.9	0.0091	173.4	25.2	166.2	24.1
D1	50.3	0.0780	1644	238.5	a	-	-	155.8	22.6
D3	50.4	0.0781	1448	210.0	0.0083	174.4	25.3	142.0	20.6
D7	51.0	0.0791	1713	248.4	0.0105	163.1	23.7	166.2	24.1
D10	49.1	0.0761	1649	239.2	0.0099	166.6	24.2	146.2	21.2
D15	50.4	0.0781	1642	238.2	0.0092	178.5	25.9	178.6	25.9
D18	51.1	0.0792	1746	253.2	0.0115	151.8	22.0	146.2	21.2
Average	49.7	0.0771	1645	238.6	0.0095	170.3	24.7	156.5	22.7
Std. Der.	1.2	0.0018	93.8	13.6	0.0011	10.3	1.5	12.1	1.8
Coef. of Var. %	2.3		5.4		11.2	6.1		7.8	

a = Stress-Strain Plot Damaged During Test

TABLE 41. TENSION TEST RESULTS OF LAMINA U1, 0° UNIDIRECTIONAL COUPONS
AT 82.2°C (180°F), DRY, IN LABORATORY AIR

Coupon ID	Average Area, mm^2 in. 2		Ultimate Stress, σ_{ult} , MPa ksi		Strain to Failure, ϵ_f , mm/mm in 25.4 mm	Secant Modulus at Failure, E_{sf} , GPa $\text{psi} \times 10^6$		Secant Modulus at 70 ksi, E_{s70} , GPa $\text{psi} \times 10^6$	
	mm^2	in. 2	MPa	ksi		GPa	$\text{psi} \times 10^6$	GPa	$\text{psi} \times 10^6$
2VX1394-C2	49.8	0.0772	1724	250.0	0.0104	165.5	24.0	153.8	22.3
C8	48.4	0.0750	1917	278.0	0.0117	164.1	23.8	160.6	23.3
C14	50.7	0.0786	1807	262.1	0.0114	162.7	23.6	151.0	21.9
C16	50.1	0.0777	1859	269.6	0.0116	160.0	23.2	151.0	21.9
C19	50.2	0.0778	1799	260.9	0.0111	162.0	23.5	151.0	21.9
D12	50.1	0.0776	1595	231.3	0.0098	163.4	23.7	160.6	23.3
D13	50.7	0.0786	1693	245.5	0.0111	152.4	22.1	151.0	21.9
D16	50.2	0.0778	1595	231.4	0.0105	151.7	22.0	156.5	22.7
D17	50.4	0.0781	1722	249.7	0.0112	153.8	22.3	146.2	21.2
D19	50.7	0.0786	1653	239.8	0.0104	159.3	23.1	155.8	22.6
Average	50.1	0.0777	1736	251.8	0.0109	159.3	23.1	153.8	22.3
Std. Dev.	0.70	0.0011	108	15.7	0.0006	4.8	0.7	4.8	0.7
Coef. of Var. %	1.4		6.2		5.6	3.2		3.0	

TABLE 42
TENSION TEST RESULTS OF LAMINA U1-1, 0° UNIDIRECTIONAL COUPONS
AT 82.2°C (180°F), WET, IN LABORATORY AIR

Coupon ID	Average Area, 2		Ultimate Stress, σ_{ult} , ksi	Strain to Failure, ϵ_f , mm/mm in 25.4 mm	Secant Modulus at Failure, E_{sf} , psiX10 ⁶		Secant Modulus at 70 ksi, E_{s70} , psiX10 ⁶	
	mm ²	in. ²	MPa		GPa		GPa	
2VX1394-C1	48.6	0.0753	1524	0.0093	164.1	23.8	166.2	24.1
C4	47.7	0.0739	1586	0.0096	165.5	24.0	157.2	22.8
C11	48.6	0.0754	1651	-a	-	-	162.0	23.5
C12	50.0	0.0775	1619	0.0103	157.2	22.8	160.0	21.9
C13	50.5	0.0783	1729	0.0101	171.0	24.8	155.8	22.6
C15	50.6	0.0784	1517	0.0095	160.0	23.2	147.5	21.4
C17	50.8	0.0788	1881	0.0117	160.6	23.3	142.0	20.6
D2	50.9	0.0789	1643	0.0104	157.9	22.9	142.7	20.7
D4	50.2	0.0778	1578	0.0100	157.9	22.9	142.7	20.7
D11	49.2	0.0763	1563	0.0098	159.3	23.1	160.0	21.9
Average	49.7	0.0771	1629	0.0101	161.3	23.4	151.7	22.0
Std Dev	1.10	0.0017	109	0.0007	4.8	0.7	8.3	1.2
Coef of Var %	2.2		6.7	7.0	2.8		5.5	

a = Stress-Strain Plot Damaged During Test

TABLE 43
COMPRESSION TEST RESULTS OF LAMINA U1, 0° UNIDIRECTIONAL COUPONS
AT ROOM TEMPERATURE IN LABORATORY AIR

Coupon ID	Average Area, 2		Ultimate Stress, σ_{ult} , ksi		Strain to Failure, ϵ_f , mm/mm in 50.8 mm	Secant Modulus at Failure, E_{sf} , psiX10 ⁶		Secant Modulus at 70 ksi, E_{s70} , psiX10 ⁶	
	mm ²	in. ²	MPa	ksi		GPa	psiX10 ⁶	GPa	psiX10 ⁶
IVX1453-C3	50.7	0.0786	1019	147.8	0.0080	127.6	18.5	146.2	21.2
C4	51.2	0.0783	880	127.6	0.0067	131.0	19.0	142.0	20.6
C6	49.9	0.0774	855	124.0	0.0067	127.6	18.5	133.8	19.4
C10	49.5	0.0767	793	115.0	0.0059	130.3	18.9	146.2	21.2
C11	51.7	0.0802	892	129.4	0.0071	125.5	18.2	137.9	20.0
C12	50.8	0.0787	729	105.7	0.0056	130.3	18.9	153.1	22.2
C16	50.5	0.0783	778	112.9	0.0062	125.5	18.2	137.9	20.0
D1	50.8	0.0787	883	128.1	0.0065	135.8	19.7	133.8	19.4
D11	50.8	0.0788	824	119.5	0.0068	121.3	17.6	137.9	20.0
D16	50.6	0.0785	815	118.2	0.0065	125.5	18.2	133.8	19.4
Average	50.6	0.0785	847	122.8	0.0066	128.2	18.6	140.0	20.3
Std Der	0.61	0.0010	80	11.6	0.0007	4.0	0.6	6.5	0.9
Coef of Var %	1.2		9.4		10.0	3.1		4.6	

TABLE 44
COMPRESSION TEST RESULTS OF LAMINA U1, 0° UNIDIRECTIONAL COUPONS
AT 82.2°C (180°F), DRY, IN LABORATORY AIR

Coupon ID	Average Area,		Ultimate Stress, σ_{ult} , ksi	Strain to Failure, ϵ_f , mm/mm in 50.8 mm	Secant Modulus at Failure, E_{sf} , psi $\times 10^6$		Secant Modulus at 70 ksi, E_{s70} , psi $\times 10^6$	
	mm ²	in. ²	MPa		GPa		GPa	
1XVI453-C20	51.9	0.0805	774	0.0057	135.8	19.7	146.2	21.2
C21	49.2	0.0762	851	0.0064	131.7	19.1	141.3	20.5
D3	52.3	0.0811	893	a	a	a	146.2	21.2
D5	50.6	0.0785	1006	0.0080	126.9	18.4	133.8	19.4
D9	51.6	0.0800	822	0.0063	130.3	18.9	146.2	21.2
D12	50.8	0.0788	926	0.0074	126.2	18.3	133.8	19.4
D13	51.5	0.0798	1018	0.0080	128.2	18.6	141.3	20.5
D14	51.2	0.0794	1058	0.0078	135.8	19.7	146.2	21.2
D17	50.7	0.0786	738	0.0054	136.5	19.8	146.2	21.2
D19	51.9	0.0805	760	0.0055	138.6	20.1	146.2	21.2
Average	51.2	0.0793	885	0.0067	132.4	19.2	142.7	20.7
Std Dev	0.9	0.0014	114	0.0011	4.8	0.7	4.8	0.7
Coef of Var %	1.9		13.0	16.0		3.5		3.6

a = Stress-Strain Plot Damaged During Test

TABLE 45
COMPRESSION TEST RESULTS OF LAMINA U1, 0° UNIDIRECTIONAL COUPONS
AT 82.2°C (180°F), WET, IN LABORATORY AIR

Coupon ID	Average Area, in.^2		Ultimate Stress, σ_{ult} , ksi		Strain to Failure, ϵ_f , mm/mm in 50.8 mm	Secant Modulus at Failure, E_{sf} , $\text{psi} \times 10^6$		Secant Modulus at 70 ksi, E_{s70} , $\text{psi} \times 10^6$	
	mm^2	in.^2	MPa	ksi		GPa	$\text{psi} \times 10^6$	GPa	$\text{psi} \times 10^6$
IVX1453-C1	50.0	0.0775	583	84.6	0.0063	92.4	13.4	104.1	15.1
C2	51.3	0.0795	659	95.6	0.0072	91.7	13.3	99.3	14.4
C5	50.7	0.0786	723	104.8	0.0073	99.3	14.4	107.8	15.6
C14	51.2	0.0794	652	94.5	0.0069	94.5	13.7	104.8	15.2
C19	51.3	0.0795	912	132.3	0.0096	95.0	13.8	104.8	15.2
D2	52.6	0.0815	519	75.3	0.0052	100.0	14.5	100.7	14.6
D4	52.0	0.0806	681	98.8	a	a	a	100.7	14.6
D7	51.4	0.0796	594	86.2	0.0060	99.3	14.4	102.7	14.9
D8	52.0	0.0806	728	112.9	0.0079	98.6	14.3	17.8	15.6
D15	51.3	0.0795	593	86.0	0.0065	91.0	13.2	98.6	14.3
Average	51.4	0.0796	669	97.1	0.0070	95.8	13.9	103.4	15.0
Std Dev	0.71	0.0011	113	16.4	0.0013	3.6	0.5	3.6	0.5
Coef of Var %	1.4		16.9		18.0	3.7		3.1	

a = Stress-Strain Plot Damaged During Test

TABLE 46. TENSION TEST RESULTS OF LAMINA U1, 90° UNIDIRECTIONAL COUPONS
AT ROOM TEMPERATURE IN LABORATORY AIR

Coupon ID	Average Area,		Ultimate Stress,		Strain to Failure, ϵ_f , mm/mm in 25.4 mm	Secant Modulus at Failure, E_{sf} , psi X 10 ⁶	
	mm ²	in. ²	MPa	ksi		GPa	
2VX1394-A2	50.6	0.0785	32.3	4.69	0.0029	11.2	1.62
A8	50.9	0.0789	- ^a	-	-	-	-
A13	51.0	0.0790	30.5	4.43	0.0032	9.5	1.38
A19	50.4	0.0781	39.0	5.66	0.0032	12.1	1.75
B4	50.4	0.0788	35.7	5.18	0.0036	9.4	1.36
B5	50.7	0.0786	31.9	4.63	0.0032	10.0	1.45
B7	51.0	0.0790	34.7	5.04	0.0036	9.6	1.40
B14	50.1	0.0776	15.3 ^b	2.22 ^b	0.0014 ^b	11.0 ^b	1.59 ^b
B16	49.8	0.0772	33.9	4.92	0.0032	10.3	1.49
B17	51.4	0.0796	34.6	5.02	0.0036	9.6	1.40
Average	50.6	0.0785	34.1	4.95	0.0033	10.2	1.48
Std. Dev.	0.5	0.0007	2.6	0.38	0.0003	1.0	0.14
Coef. of Var. %	0.9		7.7		9.1	9.2	

a = No Data, Coupon Damaged During Testing

b = Reason For Low Value Unknown, Not Included in Averages

TABLE 47. TENSION TEST RESULTS OF LAMINA U1, 90° UNIDIRECTIONAL COUPONS
AT 82.2°C (180°F), DRY, IN LABORATORY AIR

Coupon ID	Average Area,		Ultimate Stress,		Strain to Failure, ϵ_f , mm/mm in 25.4 mm	Secant Modulus at Failure, E_{sf} , psi X 10 ⁶	
	mm ²	in. ²	MPa	σ_{ult} , ksi		MPa	psi
2VX1394-A4	51.2	0.0793	30.2	4.39	0.0034	8.9	1.29
A7	51.3	0.0795	- ^a	-	-	-	-
A10	51.0	0.0791	37.6	5.46	0.0042	9.0	1.30
A15	50.0	0.0775	45.9	6.66	0.0053	8.6	1.25
B1	50.4	0.0781	34.2	4.97	0.0040	8.6	1.24
B3	51.0	0.0791	41.3	5.99	0.0064	6.5	0.94
B8	51.0	0.0791	44.1	6.40	0.0054	8.1	1.18
B10	50.8	0.0788	19.6 ^b	2.84 ^b	0.0021	9.3	1.35
B13	50.8	0.0787	- ^a	-	-	-	-
B19	50.7	0.0786	39.5	5.72	0.0044	9.0	1.30
Average	50.8	.0788	39.0	5.66	0.0047	8.3	1.21
Std. Dev.	0.4	.0006	5.5	0.80	0.0010	0.9	0.13
Coef. of Var. %	0.8		14.1		21.3	10.7	

a = No Data, Coupon Damaged During Testing

b = Reason For Low Value Unknown, Not Included In Averages

TABLE 48. TENSION TEST RESULTS OF LAMINA U1, 90° UNIDIRECTIONAL COUPONS
AT 82.2°C (180°F), WET, IN LABORATORY AIR

Coupon ID	Average Area, in. ²		Ultimate Stress, σ_{ult} , ksi		Strain to Failure, ϵ_f , mm/mm in 25.4 mm	Secant Modulus at Failure, E_{sf} , psi X 10 ⁶	
	mm ²		MPa			GPa	
2VX1394-A3	50.7	0.0786	18.3	2.65	0.0021	8.1	1.26
A12	51.2	0.0794	15.8	2.29	0.0018	8.8	1.27
A16	50.3	0.0780	14.6	2.12	0.0019	7.7	1.12
A17	50.1	0.0776	14.8	2.15	0.0017	8.7	1.26
A18	50.4	0.0781	- ^a	-	-	-	-
B6	50.6	0.0785	- ^a	-	-	-	-
B9	50.6	0.0785	15.7	2.27	0.0019	8.2	1.19
B11	49.2	0.0763	16.3	2.37	0.0019	8.6	1.25
B12	50.5	0.0783	11.4	1.65	0.0013	8.8	1.27
B18	50.7	0.0786	17.4	2.53	0.0020	8.1	1.26
Average	50.5	0.0782	15.5	2.25	0.0018	8.5	1.24
Std. Dev.	0.5	0.0008	2.1	0.30	0.0002	0.3	0.05
Coef. of Var. %	1.0		13.4		13.3		4.3

a = No Data, Coupon Damaged During Testing

TABLE 49. COMPRESSION TEST RESULTS OF LAMINA U1, 90° UNIDIRECTIONAL COUPONS
AT ROOM TEMPERATURE IN LABORATORY AIR

Coupon ID	Average Area, in. ²		Ultimate Stress, σ_{ult} , ksi		Strain to Failure, ϵ_f , mm/mm in 50.8 mm	Secant Modulus at Failure, E_{sf} , psiX10 ⁶		Secant Modulus at 17 ksi, E_{s17} , psiX10 ⁶	
	mm ²	in. ²	MPa	ksi		GPa	psiX10 ⁶	GPa	psiX10 ⁶
1VX1453-A17	51.5	0.0799	208	30.2	0.0237	8.7	1.27	9.3	1.35
A19	51.4	0.0796	180	26.1	0.0204	8.8	1.28	9.3	1.35
B3	51.0	0.0791	214	31.0	0.0246	8.7	1.26	9.8	1.42
B4	51.4	0.0797	193	28.0	0.0215	9.0	1.30	9.8	1.42
B7	51.7	0.0801	245	35.6	0.0297	8.3	1.20	9.5	1.38
B13	51.2	0.0783	223	32.3	0.0251	8.9	1.29	9.8	1.42
B16	50.6	0.0785	152	22.0	0.0162	9.4	1.36	9.9	1.44
B18	51.2	0.0794	208	30.2	0.0243	8.5	1.24	10.0	1.45
Average	51.2	0.0794	203	29.4	0.0232	8.8	1.28	9.7	1.40
Std Dev	0.3	0.0005	28	4.1	0.0040	0.3	0.05	0.3	0.04
Coef of Var %	6.3		14.0		17.0	3.6		2.8	

TABLE 50. COMPRESSION TEST RESULTS OF LAMINA U1, 90° UNIDIRECTIONAL COUPONS
AT 82.2°C (180°F), DRY, IN LABORATORY AIR

Coupon ID	Average Area, mm ² in. ²		Ultimate Stress, σ_{ult} , ksi MPa		Strain to Failure, ϵ_f , mm/mm in 50.8 mm	Secant Modulus at Failure, E_{sf} , GPa psiX10 ⁶		Secant Modulus at 17 ksi E_{s17} , GPa psiX10 ⁶	
	mm ²	in. ²	MPa	ksi		GPa	psiX10 ⁶	GPa	psiX10 ⁶
1VX1453-A18	51.7	0.0801	170	24.7	0.0222	7.7	1.11	8.3	1.21
A20	51.2	0.0793	172	25.0	0.0216	8.0	1.16	9.0	1.31
B1	51.7	0.0802	141	20.4	a	a	a	8.9	1.29
B2	51.2	0.0793	197	28.6	0.0258	7.7	1.11	9.1	1.32
B8	51.4	0.0796	190	27.5	0.0258	7.4	1.07	8.7	1.26
B9	51.3	0.0795	204	29.6	0.0294	7.0	1.01	8.7	1.26
B12	51.7	0.0802	177	25.6	0.0240	7.4	1.07	8.7	1.26
B17	51.8	0.0803	160	23.2	0.0210	7.6	1.10	8.5	1.24
Average	51.5	0.0798	177	25.6	0.0243	7.5	1.09	8.8	1.27
Std Dev	0.3	0.0004	21	3.0	0.0030	0.3	0.05	0.3	0.04
Coef of Var %	5.4		11.7		12.3	4.3		2.9	

a = Stress-Strain Record Damaged During Test

TABLE 51. COMPRESSION TEST RESULTS OF LAMINA U1, 90° UNIDIRECTIONAL COUPONS
AT 82.2°C (180°F), WET, AT ROOM TEMPERATURE

Coupon ID	Average Area, in.^2		Ultimate Stress		Strain to Failure, ϵ_f , mm/mm in 50.8 mm	Secant Modulus at Failure, E_{sf} , $\text{psi} \times 10^6$		Secant Modulus at 17 ksi, E_{s17} , $\text{psi} \times 10^6$	
	mm ²	in. ²	MPa	ksi		GPa	$\text{psi} \times 10^6$	GPa	
LVX1453-B5	51.7	0.0802	167	24.4	0.0482	3.5	0.51	3.9	0.56
B6	51.7	0.0802	- ^a	-	-	-	-	-	-
B10	51.4	0.0796	160	23.2	- ^b	-	-	4.8	0.70
B11	51.3	0.0795	176	25.5	0.0469	3.7	0.54	4.8	0.70
B14	51.4	0.0796	161	23.4	0.0414	4.0	0.58	4.6	0.67
B15	51.7	0.0801	194	28.2	0.0558	3.5	0.51	4.6	0.67
B19	51.3	0.0795	180	26.2	0.0487	3.7	0.54	4.7	0.68
B20	51.2	0.0794	168	24.3	0.0414	4.1	0.59	5.0	0.72
Average	51.5	0.0798	172	25.0	0.0471	3.7	0.54	4.6	0.67
Std Dev	0.2	0.0003	12	1.8	0.0054	0.2	0.03	0.3	0.05
Coef of Var %	0.4		7.0		11.4	6.2		7.8	

a = No Data, Coupon Damaged During Test

b = Stress-Strain Record Damaged During Test

TABLE 52.
TENSION TEST RESULTS OF LAMINA U2, +45° LAMINA COUPONS AT
ROOM TEMPERATURE IN LABORATORY AIR

Coupon ID	Average Area,		Ultimate Stress, σ_{ult}	Axial Strain at 10 ksi, ϵ_{x10}	Lateral Strain at 10 ksi, ϵ_{y10}	Poisson's Ratio at 10 ksi, $ \epsilon_y/\epsilon_x $	Shear Stress at Failure, $\tau_{xy max}$		Shear Strain at Failure, $\gamma_{xy max}$	Shear Secant Modulus at 4 ksi, G_{S4}	
	mm ²	in. ²	MPa	mm/mm	mm/mm		MPa	ksi	mm/mm	GPa	psi x 10 ⁶
1VX1471-A4	52.8	0.0818	177	0.0036	0.0028	0.78	88.2	12.8	0.0347	5.5	0.80
A5	52.8	0.0818	177	0.0037	0.0029	0.78	88.9	12.9	0.0352	5.5	0.80
A6	52.7	0.0817	181	0.0036	0.0028	0.78	90.3	13.1	0.0371	5.6	0.82
A8	52.8	0.0818	181	0.0037	0.0028	0.76	90.3	13.1	0.0352	5.5	0.80
A11	52.8	0.0818	179	0.0038	0.0030	0.79	89.6	13.0	0.0370	5.0	0.73
A12	52.7	0.0817	181	0.0037	0.0029	0.78	90.3	13.1	0.0356	5.4	0.79
B2	53.4	0.0828	181	0.0038	0.0030	0.79	91.0	13.2	0.0382	5.0	0.73
B3	52.7	0.0817	179	0.0037	0.0029	0.78	89.6	13.0	0.0366	5.5	0.80
B4	53.4	0.0828	177	0.0038	0.0030	0.79	88.2	12.8	^a	5.0	0.73
B9	53.4	0.0827	179	0.0039	0.0029	0.74	88.9	12.9	^a	5.0	0.73
Average	53.0	0.0821	179	0.0037	0.0029	0.78	89.6	13.0	0.0368	5.3	0.77
Std. Dev.	0.3	0.0005	1	0.0001	0.0001	0.02	0.7	0.1	0.0017	2.8	0.04
Coef. of Var. %	0.6		0.7	2.6	2.8	2.0	1.1		4.5	4.9	

^a Strain exceeded systems strain measurement limits

TABLE 53. TENSION TEST RESULTS OF LAMINA U2, $\pm 45^\circ$ LAMINA COUPONS AT 82.2°C (180°F), DRY, IN LABORATORY AIR

Coupon ID	Average Area,		Ultimate Stress σ_{ult}	Axial Strain ^a 10 ksi, $\epsilon_x \times 10$, mm/mm	Lateral Strain at 10 ksi, $\epsilon_y \times 10$, mm/mm	Poissons Ratio at 10 ksi, $ \epsilon_y/\epsilon_x $	Shear Stress at Failure, τ_{xy} max,		Shear Strain at Failure, γ_{xy} max, mm/mm	Shear Secant Modulus at 4 ksi G_{SL} ,	
	mm ²	in ²	MPa	ksi	mm/mm	mm/mm	MPa	ksi		GPa	psi $\times 10^6$
1VX1471-B7	52.8	0.0818	154	22.4	0.0035	0.88	77.2	11.2	- ^a	5.0	0.73
B8	52.7	0.0817	158	22.9	0.0029	0.83	79.3	11.5	- ^a	5.8	0.84
B10	52.7	0.0817	156	22.6	0.0034	0.85	77.9	11.3	- ^a	5.8	0.84
B12	52.8	0.0818	157	22.7	0.0041	0.76	78.6	11.4	- ^a	5.0	0.73
B13	52.7	0.0817	153	22.2	0.0039	0.79	76.5	11.1	- ^a	5.2	0.76
B15	53.3	0.0826	152	22.1	0.0036	0.81	76.5	11.1	- ^a	5.5	0.80
B16	52.7	0.0817	158	22.9	0.0040	0.75	79.3	11.5	- ^a	4.8	0.70
B17	52.6	0.0816	164	23.8	0.0038	0.76	82.0	11.9	- ^a	5.5	0.80
B18	52.7	0.0817	157	22.7	0.0034	0.85	78.6	11.4	- ^a	5.8	0.84
B19	52.7	0.0817	157	22.8	0.0036	0.81	78.6	11.4	- ^a	5.5	0.80
Average	52.8	0.0818	157	22.7	0.0037	0.81	78.6	11.4		5.4	0.78
Std. Dev.	0.2	0.0003	3	0.5	0.0002	0.04	1.4	0.2		0.3	0.05
Coef. of Var. %	3.5		2.1		6.4	5.4	2.0			6.6	

^a Strain exceeded systems strain measurement limits

TABLE 54. TENSION TEST RESULTS OF LAMINA U2, $\pm 45^\circ$ LAMINA COUPONS AT
82.2°C (180°F), WET, IN LABORATORY AIR

Coupon ID	Average Area,		Ultimate Stress, σ_{ult}	Axial Strain at 10 ksi, ϵ_{x10}	Lateral Strain at 10 ksi, ϵ_{y10}	Poissons Ratio at 10 ksi $ \epsilon_y/\epsilon_x $	Shear Stress at Failure, $\tau_{xy max}$		Shear Strain at Failure, $\gamma_{xy max}$	Shear Secant Modulus at 4 ksi G_{S4}	
	mm ²	in ²	MPa	ksi	mm/mm		MPa	ksi	mm/mm	GPa	psi x 10 ⁶
1VX1471-A1	52.8	0.0818	139	20.2	0.0045	0.84	69.6	10.1	- ^a	5.0	0.73
A2	53.4	0.0828	156	22.6	0.0043	0.90	77.9	11.3	- ^a	4.6	0.67
A7	52.8	0.0818	148	21.4	0.0048	0.90	73.8	10.7	- ^a	4.6	0.67
A10	52.8	0.0818	148	21.5	0.0045	0.85	74.5	10.8	- ^a	3.9	0.57
A13	53.4	0.0828	141	20.5	0.0045	0.78	71.0	10.3	- ^a	3.8	0.55
A16	52.7	0.0817	145	21.1	0.0051	0.84	73.1	10.6	- ^a	3.9	0.57
A18	52.8	0.0818	150	21.7	0.0043	0.81	75.2	10.9	- ^a	5.0	0.73
A20	53.3	0.0826	142	20.6	0.0045	0.78	71.0	10.3	- ^a	4.6	0.67
B1	52.7	0.0817	142	20.6	0.0045	0.84	71.0	10.3	- ^a	4.6	0.67
B5	52.8	0.0818	143	20.7	0.0045	0.78	71.7	10.4	- ^a	4.6	0.67
Average	53.0	0.0821	145	21.1	0.0048	0.83	73.1	10.6		4.5	0.65
Std. Dev.	0.3	0.0005	5	0.7	0.0004	0.05	2.8	0.4		0.4	0.06
Coef. of Var. %		0.6	3.3	9.7	10.5	5.4	3.4				9.9

^a Strain exceeded systems strain measurement limits

TABLE 55. RESULTS OF TENSION TESTS OF QUASI-ISOTROPIC LAMINATE CONDUCTED AT ~ 0.01 in./in./min
ENVIRONMENT: ROOM TEMPERATURE LABORATORY AIR

Compon ID	Area, in. ²	Ultimate Stress, ksi	Longitudinal Ultimate Strain, in./in. X	Transverse Ultimate Strain, in./in. Y	Poisson's Ratio at Failure	Slope Deviation Stress, ksi	Slope Deviation Longitudinal Strain, X	Slope Deviation Transverse Strain, Y	Poisson's Ratio at Slope Deviation	Initial Apparent Modulus of Elasticity, psi $\times 10^6$	Final Apparent Modulus of Elasticity, psi $\times 10^6$	Remarks, Gage Location
1VX1392												
B40	0.0826	78.5	.0106	-.0034	0.320	52.1	.0067	.0022	.328	7.78	6.77	1/3
B76	0.0816	76.6	.0100	-.0031	0.310	56.5	.0071	.0023	.323	7.76	6.93	1/2
C8	0.0817	81.0	.0109	-.0035	0.321	62.4	.0082	.0027	.329	7.61	6.89	1/2
C20	0.0808	83.9	.0111	-.0036	0.324	56.5	.0072	.0023	.319	7.85	7.03	1/2
D2	0.0823	75.7	.0096	-.0030	0.313	58.2	.0072	.0023	.319	8.08	7.29	1/3
D4	0.0818	76.9	.0104	-.0032	0.308	57.4	.0074	.0023	.311	7.76	6.50	1/2
2VX1391												
A29	0.0815	79.9	.0106	-.0034	0.321	61.8	.0081	.0026	.321	7.63	7.24	1/2
B8	0.0807	81.0	.0107	-.0033	0.308	62.4	.0078	.0025	.321	8.00	6.43	1/3
B13	0.0818	82.6	.0110	-.0034	0.309	56.5	.0072	.0023	.319	7.85	6.86	1/3
B18	0.0808	84.6	.0112	-.0034	0.304	58.5	.0076	.0023	.303	7.70	6.69	1/2
B25	0.0828	79.9	.0107	-.0035	0.327	55.9	.0072	.0024	.333	7.76	6.86	1/2
B31	0.0794	76.7	.0106	-.0031	0.292	52.4	.0070	.0021	.300	7.49	6.75	1/3
C7	0.0811	78.5	.0103	-.0033	0.320	55.3	.0071	.0024	.338	7.79	7.25	1/3
C16	0.0814	81.6	.0108	-.0037	0.343	61.2	.0078	.0025	.359	7.85	6.80	1/3
C30	0.0815	80.5	.0103	-.0033	0.320	62.9	.0078	.0025	.359	8.06	7.04	1/2
D5	0.0805	80.2	.0105	-.0033	0.314	54.1	.0069	.0022	.319	7.96	7.25	1/2
D7	0.0814	75.1	.0099	-.0033	0.333	58.2	.0074	.0024	.324	7.86	6.76	1/3
D19	0.0815	79.8	.0108	-.0033	0.306	58.8	.0077	.0024	.312	7.64	6.87	1/2
D25	0.0811	74.9	.0099	-.0037	0.374	56.6	.0070	.0023	.329	7.94	6.66	1/3
D29	0.0816	78.7	.0105	-.0032	0.305	60.0	.0077	.0024	.312	7.79	6.68	1/2
Avg.	0.0814	79.3	.0105			57.8	.0074	.0024	.324	7.81	6.88	
Std. Dev.	0.00076	2.77	.00042			3.23	.0041	.00014	.015	.15	0.25	
Var. %	0.93	3.93	4.03			5.58	5.57	5.98	4.69	1.96	3.57	

TABLE 56. RESULTS OF STATIC TENSION TESTS OF QUASI-ISOTROPIC LAMINATE CONDUCTED AT ~6 in./in./min LOADING RATE ENVIRONMENT: ROOM TEMPERATURE, LABORATORY AIR

Coupon ID	Area, in. ²	Ultimate Stress, ksi	Longitudinal Ultimate Strain, in./in.	Transverse Ultimate Strain, in./in.	Poisson's Ratio At Failure	Average Modulus of Elasticity, E , $\times 10^6$ psi	Remarks: Gage Location
1VX 1392							
A10	0.0812	71.6	0.0099	-0.0030	0.303	7.23	1/2
A14	0.0811	70.0	0.0089	-0.0028	0.315	7.87	1/2
A19	0.0817	73.0	0.0100	-0.0030	0.300	7.30	1/2
A27	0.0812	77.1	0.0108	-0.0030	0.278	7.14	1/2
B2	0.0823	74.6	0.0090	-0.0029	0.322	8.29	1/2
B7	0.0809	75.4	0.0096	-0.0030	0.313	7.86	1/2
B15	0.0818	68.8	0.0095	-0.0028	0.295	7.28	1/3
C7	0.0818	76.2	0.0108	-0.0032	0.296	7.06	1/3
2VX 1391							
A7	0.0812	70.8	0.0098	-0.0027	0.276	7.22	1/2
A8	0.0809	75.9	0.0104	-0.0035	0.336	7.30	1/3
A13	0.0814	75.4	0.0104	-0.0031	0.298	7.25	1/3
B17	0.0814	74.6	0.0090	-0.0029	0.322	8.29	1/2
D1	0.0814	73.9	0.0097	-0.0030	0.309	7.62	1/3
Avg.		73.6	0.0098		0.305	7.52	
Std. Dev.		2.60	0.00059		0.017	0.43	
Coef. of Var. %		3.53	6.66		5.64	5.68	

TABLE 57. RESULTS OF TENSION TESTS OF QUASI-ISOTROPIC LAMINATE PANEL CONTAINING MINIMAL AMOUNT OF "SQUIGGLE" DEFECTS, CONDUCTED AT -0.01 in./in./min LOADING RATE ENVIRONMENT ROOM TEMPERATURE, LABORATORY AIR

Specimen Number	Average Area, in. ²	Ultimate Stress, σ_{max} , ksi	Ultimate Strain, ϵ_{max} , in/in in 1 in.	Slope Deviation Stress, σ_{xl} , ksi	Strain At Slope Deviation, ϵ_{xl} , in/in in 1 in.	Initial Apparent Modulus of Elasticity, E_{xl} , psi $\times 10^6$	Final Apparent Modulus of Elasticity, E_{xf} , psi $\times 10^6$
2VX 1390-D1	0.084	66.6	0.0084				
D3	0.080	73.0	0.0092	48.8	0.0063	7.75	7.00
D7	0.080	69.3	0.0090	50.0	0.0061	8.20	7.20
D14	0.080	77.0					
D19	0.080	73.0	0.0094	51.3	0.0062	8.27	6.10
Mean		71.8	0.0090	50.0	0.0062	8.07	6.20
Std. Dev.		3.98	0.00043	1.25	0.0001	0.282	0.200
Coef. of Var. \bar{z}		5.54	4.80	2.50	1.61	3.50	11.50

TABLE 58. RESULTS OF TENSION TESTS OF QUASI-ISOTROPIC LAMINATE PANEL CONTAINING MAJOR AMOUNT OF "SQUIGGLE" DEFECTS, CONDUCTED AT ~0.01in./in./min LOADING RATE ENVIRONMENT, ROOM TEMPERATURE, LABORATORY AIR

Specimen Number	Average Area, in. ²	Ultimate Stress, 'max, ksi	Ultimate Strain, 'max, in./in. in 1 in.	Slope Deviation Stress, 's, ksi	Strain Deviation At Slope 's, in./in. in 1 in.	Initial Apparent Modulus of Elasticity, E ₁ , psi X 10 ⁶	Final Apparent Modulus of Elasticity, E ₂ , psi X 10 ⁶
2VX 1390-C22	0.084	54.3	0.0070	39.3	0.0046	8.54	5.00
C23	0.084	63.0	0.0077	39.3	0.0046	8.54	6.25
C24	0.085	57.2	0.0082	48.2	0.0067	7.19	5.00
C25	0.084	56.9	0.0078	47.6	0.0063	7.56	5.00
C26	0.083	62.7	0.0084	50.6	0.0066	7.67	5.71
C28	0.083	60.5	0.0082	48.2	0.0063	7.65	5.56
C29	0.084	60.4	0.0083	47.6	0.0064	7.44	6.25
C30	0.085	62.5	0.0088	48.2	0.0065	7.42	5.26
C31	0.083	60.5	0.0084	48.2	0.0066	7.30	5.26
D31	0.083	62.5	0.0088	47.0	0.0064	7.34	5.26
Mean		60.1	0.0082	46.4	0.0061	7.67	5.46
Std. Dev.		2.97	0.00054	3.87	0.00080	0.485	0.480
Coeff. of Var. %		4.95	6.61	8.34	13.14	6.32	8.79

TABLE 59. RESULTS OF STATIC TENSION TESTS OF QUASI-ISOTROPIC LAMINATE PANEL CONTAINING "SQUIGGLE" DEFECT, CONDUCTED AT .6 in./in./min LOADING RATE

Coupon ID	Area, in. ²	Ultimate Stress, max, psi	Longitudinal Ultimate Strain, x mm/mm	Transverse Ultimate Strain, y mm/mm	Poisson's Ratio at Failure	Average of Elasticity, psi X 10 ⁶	Remarks, Gage Location
1VX1590-A3	0.0814	59.6	0.0079	-0.0021	0.266	7.54	1/2
A4	0.0845	61.8	0.0084	-0.0022	0.262	7.36	1/2
A15	0.0841	59.9	0.0080	-0.0022	0.275	7.49	1/2
A26	0.0856	62.6	0.0006	-0.0024	0.279	7.29	1/3
A28	0.0841	52.5	0.0072	-0.0021	0.292	7.29	1/2
B4	0.0836	59.4	0.0078	-0.0023	0.295	7.62	1/2
Avg.		59.3	0.0080			7.43	
Std. Dev.		3.57	0.0005			0.14	
Coeff. of Var. %		6.02	6.16			1.86	

TABLE 60. RESULTS OF COMPRESSION TESTS OF QUASI-ISOTROPIC LAMINATE CONDUCTED AT 0.01 in./in./min
LOADING RATE ENVIRONMENT: ROOM TEMPERATURE LABORATORY AIR

Coupon ID	Area, in. ²	Ultimate Stress, ksi	Longitudinal Ultimate Strain, %	Transverse Ultimate Strain, %	Poisson's Ratio at Failure, ν	Secant Modulus at Failure, psi $\times 10^6$	Longitudinal Strain at 35 ksi, in./in.	Transverse Strain at 35 ksi, in./in.	Poisson's Ratio at Failure, ν
1VX1392									
B9	0.0813	85.8	-0.0123	0.0037	0.401	6.98	-0.0045	0.0014	0.401
B18	0.0823	84.7	-0.0118	0.0036	0.405	7.15	-0.0045	0.0014	0.405
B24	0.0818	80.5	-0.0110	0.0035	0.418	7.32	-0.0044	0.0014	0.418
C5	0.0813	78.7	-0.0109	0.0034	0.411	7.22	-0.0046	0.0015	0.411
C9	0.0812	85.3	-0.0122	0.0038	0.417	6.99	-0.0046	0.0014	0.417
C19	0.0818	75.4	-0.0107	0.0031	0.290	7.05	-0.0045	0.0013	0.290
C23	0.0813	83.2	-0.0117	0.0038	0.325	7.11	-0.0046	0.0015	0.325
2VX1391									
A2	0.0811	80.8	-0.0113	0.0033	0.292	7.15	-0.0044	0.0014	0.292
A4	0.0808	67.9	-0.0097	0.0028	0.289	7.00	-0.0046	0.0014	0.289
A9	0.0813	79.5	-0.0117	0.0036	0.308	6.79	-0.0048	0.0015	0.308
B15	0.0814	84.2	-0.0129	0.0038	0.295	6.52	-0.0049	0.0014	0.295
B29	0.0811	78.1	-0.0119	0.0034	0.286	6.56	-0.0049	0.0014	0.286
C8	0.0816	79.6	-0.0117	0.0038	0.325	6.80	-0.0048	0.0014	0.325
C26	0.0810	83.3	-0.0121	0.0037	0.306	6.88	-0.0044	0.0013	0.306
D24	0.0804	78.0	-0.0113	0.0033	0.292	6.90	-0.0047	0.0014	0.292
D30	0.0814	84.9	-0.0115	0.0038	0.330	7.18	-0.0044	0.0014	0.330
Avg.	0.0813	80.4	-0.0115	0.0035	0.306	6.99	-0.0046	0.0014	0.306
Std Dev	0.00044	4.61	0.00075	0.00029	0.014	0.24	0.00018	0.00006	0.014
Coef of Var %	0.54	5.71	6.47	8.32	4.68	3.48	3.81	4.5	4.68

TABLE 61. RESULTS OF TENSION TESTS OF QUASI-ISOTROPIC LAMINATE CONDUCTED AT 6 in./in./min
LOADING RATE ENVIRONMENT: ROOM TEMPERATURE, LABORATORY AIR

Coupon ID	Area, in. ²	Ultimate Stress, ksi	Longitudinal Ultimate Strain, in./in.	Transverse Ultimate Strain, in./in.	Poisson's Ratio at Failure, ϵ_y/ϵ_x	Secant Modulus at Failure, E_{sf} , psi x 10 ⁶	Longitudinal Strain at 35 ksi, ϵ_{35} , in./in.	Transverse Strain at 35 ksi, ϵ_{35} , in./in.	Poisson's Ratio at 35 ksi, $\epsilon_{y35}/\epsilon_{x35}$	Secant Modulus at 35 ksi, E_{s35} , psi x 10 ⁶
1VX1392										
A16	0.0812	72.1	-0.0103	0.0030	0.291	7.00	*	*	*	*
A17	0.0815	90.9	-0.0129	0.0038	0.295	7.05	-0.0046	0.0014	0.304	7.61
A24	0.0813	76.8	Stress - Strain Plot Not Available							
B10	0.0814	67.5	-0.0098	0.0027	0.276	6.89	*	*	*	*
B16	0.0814	81.4	-0.0122	0.0035	0.287	6.67	*	*	*	*
B29	0.0815	88.2	-0.0126	0.0039	0.310	7.00	-0.0046	0.0014	0.304	7.61
C6	0.0812	81.5	-0.0124	0.0038	0.306	6.57	-0.0048	0.0014	0.292	7.29
C16	0.0813	81.2	-0.0112	0.0034	0.304	7.25	-0.0046	0.0014	0.304	7.61
2VX1391										
A12	0.0813	81.3	-0.0124	0.0034	0.274	6.56	*	*	*	*
B2	0.0816	83.8	-0.0122	0.0034	0.279	6.87	*	*	*	*
B9	0.0809	76.0	-0.0116	0.0029	0.250	6.56	*	*	*	*
B16	0.0817	86.3	-0.0134	0.0036	0.269	6.44	*	*	*	*
C13	0.0815	84.2	-0.0124	0.0035	0.283	6.79	*	*	*	*
C22	0.0811	65.2	-0.0094	0.0029	0.309	6.94	*	*	*	*
D14	0.0813	80.8	-0.0108	0.0030	0.278	7.48	Tab Failure	*	*	*
D26	0.0809	66.8	-0.0097	0.0026	0.268	6.89	Tab Failure	*	*	*
D31	0.0784	73.4	-0.0113	0.0031	0.274	6.49	Tab Failure	*	*	*
Avg.	0.0812	79.7	-0.0118	0.0034	0.287	6.81				7.53
Std Dev	0.00074	7.48	0.0012	0.00038	0.018	0.24				0.16
Coeff of Var %	0.91	9.4	10.5	11.4	6.2	3.5				2.12

*Value is not included because the validity of the initial portion of the stress-strain curve is doubtful.

APPENDIX C
SUMMARY OF FATIGUE TEST RESULTS

TABLE 62. - STRESS-LIFE SCAN RESULTS OF FATIGUE TESTS AT R = +0.5 FOR
UN-NOTCHED QUASI-ISOTROPIC LAMINATE ENVIRONMENT: ROOM
TEMPERATURE, LABORATORY AIR

Maximum Stress Level MPa (ksi)	Coupon ID	Average Area		Cycles to Failure, N _F
		mm ²	in. ²	
483 (70)	1VX1391 - D21	51.7	0.0802	2,127
	2VX1392 - A25	52.4	0.0813	1,562
	- C5	52.6	0.0815	1,237
448 (65)	2VX1390 - B2 ^a	53.8	0.0834	78
	- B3 ^a	53.4	0.0827	12
	- B7 ^a	53.2	0.0824	1
	- C12 ^a	54.0	0.0837	2
	- C18 ^a	54.0	0.0837	70
	1VX1391 - B3	51.7	0.0802	14,820
	- D8	51.9	0.0805	38,320
	2VX1391 - B30	52.6	0.0815	45,921
	- C14	51.7	0.0802	34,170
	2VX1392 - B29	52.4	0.0812	15,534
414 (60)	2VX1390 - B13 ^a	53.5	0.0830	563
	- B30 ^a	54.2	0.0840	2
	1VX1391 - A29	51.7	0.0801	1,175,286
	- A31	51.5	0.0798	144,439
	2VX1391 - B26	52.8	0.0818	267,700
	2VX1392 - A6	52.4	0.0812	280,640
	1VX1396 - A13	52.5	0.0813	380,430
379 (55)	2VX1390 - B5 ^a	54.6	0.0847	13,795
	2VX1390 - B16 ^a	53.0	0.0821	1,562,180
	2VX1391 - A23	52.8	0.0818	NF ^b
	- B1	52.7	0.0817	NF
	- D15	52.1	0.0807	1.968620 x 10 ⁶ NF
345 (50)	2VX1390 - B18 ^a	53.4	0.0827	NF
	- C3 ^a	54.6	0.0847	7,820
	- C8 ^a	54.0	0.0837	14,840
	2VX1391 - A15	52.8	0.0818	NF
	- B28	52.3	0.0810	NF
310 (45)	2VX1390 - B14 ^a	53.9	0.0835	NF
	- C4 ^a	53.9	0.0835	1,756,875
	2VX1391 - A20	51.7	0.0802	NF
	- B5	52.3	0.0811	NF
	- D3	49.9	0.0774	NF
	1VX1396 - A30	51.9	0.0804	NF
276 (40)	2VX1390 - A30 ^a	54.5	0.0845	NF
	2VX1391 - B7	52.6	0.0816	NF
	- B24	52.4	0.0812	NF
	- C24	52.2	0.0809	NF
a - Coupon not included in data analysis due to "squiggle" damage in this panel				
b - NF indicates no failure at 2 x 10 ⁶ cycles				

TABLE 63. - STRESS-LIFE SCAN RESULTS OF FATIGUE TESTS AT R = 0.0 FOR
UN-NOTCHED QUASI-ISOTROPIC LAMINATE ENVIRONMENT: ROOM
TEMPERATURE, LABORATORY AIR $f = 10$ Hz

Maximum Stress Level MPa (ksi)	Coupon ID	Average Area		Cycles to Failure, N_F
		mm ²	in. ²	
448 (65)	2VX1390 - A18 ^a	53.4	0.0827	87
	1VX1391 - B4	53.2	0.0825	83
	- C10	51.7	0.0801	2,049
	2VX1391 - B27	51.8	0.0803	1,416
	1VX1392 - A15	52.4	0.0812	756
	2VX1392 - A27	51.4	0.0797	805
	1VX1396 - A27	52.5	0.0813	1,519
414 (60)	2VX1390 - A12 ^a	53.0	0.0822	415
	- B17 ^a	54.0	0.0837	513
	1VX1391 - A25	53.0	0.0821	4,620
	2VX1391 - D2	51.9	0.0805	6,200
	1VX1392 - B3	52.1	0.0807	4,420
	2VX1392 - B13	53.7	0.0832	1,820
	- C3	53.4	0.0827	3,580
	1VX1396 - A26	52.1	0.0807	60
379 (55)	2VX1390 - A6 ^a	54.1	0.0839	2,396
	- A14 ^a	54.2	0.0840	1,084
	- D10 ^a	53.9	0.0836	98
	- D23 ^a	54.1	0.0840	77
	1VX1391 - C30	52.3	0.0811	21,450
	- D17	52.4	0.0812	18,400
	1VX1392 - A13	52.3	0.0810	17,945
	- A28	52.3	0.0811	8,276
	2VX1392 - D27	52.7	0.0817	8,660
	1VX1396 - A5	52.6	0.0816	18,740
345 (50)	2VX1390 - A5 ^a	53.5	0.0830	11,800
	- A24 ^a	57.5	0.0892	5,203
	1VX1391 - B31	52.6	0.0816	62,240
	2VX1391 - C5	52.2	0.0809	68,028
	1VX1392 - A20	52.7	0.0817	58,364
	2VX1392 - A26	53.4	0.0827	58,300
	- B15	54.0	0.0837	46,900
	1VX1396 - A10	52.5	0.0813	140,013
310 (45)	2VX1390 - A29 ^a	54.6	0.0847	33,850
	- B10 ^a	52.8	0.0818	42,949
	- C7 ^a	54.6	0.0847	15,653
	- C19 ^a	53.0	0.0822	15,762
	- C27 ^a	53.0	0.0821	11,130
	- C28 ^a	53.3	0.0826	36,561
	- D28 ^a	54.3	0.0841	57,690
	- D30 ^a	54.8	0.0850	6,179
	1VX1391 - A20	52.6	0.0816	695,000
	- D31	51.8	0.0803	548,370
	2VX1391 - D16	51.7	0.0802	708,917
	- D22	51.9	0.0804	32,677
	2VX1392 - C6	52.8	0.0818	380,267
	- D20	51.5	0.0798	616,025

TABLE 63. - STRESS-LIFE SCAN RESULTS OF FATIGUE TESTS AT R = 0.0 FOR
UN-NOTCHED QUASI-ISOTROPIC LAMINATE ENVIRONMENT: ROOM
TEMPERATURE, LABORATORY AIR $f = 10$ Hz (Continued)

Maximum Stress Level MPa (ksi)	Coupon ID	Average Area		Cycles to Failure, N_F
		mm ²	in. ²	
276 (40)	2VX1390 - A17 ^a	53.4	0.0827	NF ^b
	- B12 ^a	52.5	0.0813	NF
	- C16 ^a	53.4	0.0827	NF
	2VX1391 - D9	51.9	0.0805	NF
	- D23	52.3	0.0810	408,900
	1VX1392 - A12	52.4	0.0812	1,435,755
	1VX1396 - A4	51.7	0.0802	NF
	- A24	52.1	0.0808	NF
<p>a - Coupon not included in data analysis due to "squiggles" damage in this panel</p> <p>b - NF indicates no failure at 2×10^6 cycles</p>				

TABLE 64. - STRESS-LIFE SCAN RESULTS OF FATIGUE TESTS AT
R = -0.5 FOR UN-NOTCHED QUASI-ISOTROPIC
LAMINATE ENVIRONMENT: ROOM TEMPERATURE,
LABORATORY AIR f = 10 Hz

Maximum Stress Level MPa (ksi)	Coupon ID	Average Area		Cycles to Failure, N _F
		mm ²	in. ²	
408 (65)	2VX1390 - A13 ^a	53.5	0.0829	130
	- B23 ^a	53.4	0.0827	1
	1VX1391 - A7	51.9	0.0805	215
	2VX1391 - C3	52.8	0.0818	1,522
	1VX1392 - B4	52.1	0.0807	1,036
414 (60)	2VX1390 - B24 ^a	53.7	0.0833	400
	- C21 ^a	52.6	0.0815	270
	2VX1391 - C4	52.8	0.0818	3,853
	1VX1392 - D10	51.8	0.0803	2,776
	- B5	52.7	0.0817	26,530
379 (55)	1VX1390 - A10 ^a	51.6	0.0800	7,955
	- A25 ^a	54.4	0.0843	852
	2VX1391 - A17	52.1	0.0808	39,022
	1VX1392 - B12	52.8	0.0818	13,937
	2VX1391 - C10	52.1	0.0808	8,240
345 (50)	2VX1390 - B27 ^a	53.8	0.0834	1,447
	1VX1392 - A30	52.5	0.0813	151,810
	2VX1391 - A16	52.1	0.0808	57,969
	- C17	52.1	0.0807	61,850
310 (45)	2VX1390 - B22 ^a	53.4	0.0828	3,959
	1VX1391 - A15	53.7	0.0832	95,955
	2VX1391 - C18	51.8	0.0803	549,700
276 (40)	2VX1390 - A9 ^a	54.3	0.0842	676,600
	- A20 ^a	53.8	0.0834	12,000
	- C5 ^a	54.3	0.0842	2,000
	1VX1391 - A12	53.0	0.0821	992,570
	- A14	53.1	0.0823	462,170
	2VX1391 - B4	51.8	0.0803	NF ^b
	- A25	52.8	0.0818	NF
a - Coupon not included in data analysis due to "squiggle" defect in this panel				
b - NF indicates no failure at 2 x 10 ⁶ cycles				

TABLE 65. - STRESS-LIFE SCAN RESULTS OF FATIGUE TESTS AT R = -1.0 FOR UN-NOTCHED QUASI-ISOTROPIC LAMINATE ENVIRONMENT: ROOM TEMPERATURE, LABORATORY AIR f = 10 Hz

Maximum Stress Level MPa (ksi)	Coupon ID	Average Area		Cycles to Failure, N_F
		mm ²	in. ²	
414 (60)	2VX1390 - A1 ^a	53.5	0.0830	23
	- C13 ^a	54.0	0.0837	3
	1VX1391 - A4	51.9	0.0805	82
	2VX1391 - A27	52.6	0.0815	174
	- C28	51.9	0.0805	496
379 (55)	2VX1390 - C14	52.9	0.0820	25
	- D27	54.3	0.0841	25
	2VX1391 - A28	51.7	0.0802	1,883
	1VX1392 - A26	52.1	0.0807	305
345 (50)	2VX1390 - A19 ^a	54.0	0.0837	117
	- C15 ^a	54.0	0.0837	129
	1VX1391 - A3	52.7	0.0817	319
	- B6	52.6	0.0816	1,862
	2VX1391 - D4	51.9	0.0804	435
310 (45)	2VX1390 - C17 ^a	54.0	0.0837	582
	1VX1391 - A9	51.9	0.0805	4,765
	2VX1391 - B12	52.1	0.0807	189,326
	1VX1392 - D8	52.1	0.0808	20,162
276 (40)	2VX1390 - C2 ^a	54.6	0.0847	202
	2VX1391 - B14	52.1	0.0808	18,400
	- D10	51.4	0.0796	4,309
	1VX1396 - A10	51.7	0.0802	6,270
241 (35)	2VX1390 - B1 ^a	53.9	0.0836	1,919
	1VX1391 - A8	53.0	0.0821	NF ^b
	2VX1391 - D2	51.7	0.0801	162,574
	1VX1396 - A15	51.9	0.0805	103,060
207 (30)	2VX1390 - A7 ^a	54.6	0.0847	16,375
	- A23 ^a	55.2	0.0855	22,200
	- C6 ^a	50.0	0.0775	139,299
	- C10 ^a	53.1	0.0823	19,317
	- D16 ^a	51.3	0.0795	11,324
	2VX1391 - C25	52.5	0.0813	NF
	- A26	52.3	0.0810	802,709
	1VX1396 - A3	51.9	0.0805	10 ⁶ NF
a - Coupon not included in data analysis due to "squiggle" defect in this panel				
b - NF indicates no failure at 2×10^6 cycles				

DATE
FILMED

—8